A Thesis for the Degree of Ph.D. in Science

Chemistry and biology of novel androgen receptor antagonist antarlides from microbial origin

March 2017

Graduate School of Science and Technology

Keio University

Shun Saito

Contents

Abbreviations

AC_2O	acetic anhydride
cDNA	complementary DNA
COSY	correlated spectroscopy
DNA	deoxyribonucleic acid
EtOAc	ethyl acetate
GAPDH	glyceraldehyde-3-phosphate dehydrogenase
GFP	green fluorescent protein
HDAC	histone deacetylase
HMBC	heteronuclear multiple bond correlation
HMQC	heteronuclear multiple quantum coherence
HPLC	high performance liquid chromatography
HR-ESITOFMS	high resolution-electrospray ionization time-of-flight mass spectrometry
HSQC	heteronuclear single quantum coherence
IC_{50}	half maximal inhibitory concentration
IR	infrared absorption
kDa	kilodalton
LC-MS	liquid chromatography-mass spectrometry
MeCN	acetonitrile
MeOH	methanol
mRNA	messenger RNA
NADH	nicotinamide adenine dinucleotide
NaOMe	sodium methoxide
NMR	nuclear magnetic resonance
NOESY	NOE correlated spectroscopy
PCR	polymerase chain reaction
RNA	ribonucleic acid
RPMI	Roswell Park memorial institute medium
rRNA	ribosomal RNA
TMS	tetramethylsilane
TOCSY	totally correlated spectroscopy
UV	ultraviolet
WT	wild type

Chapter 1

General Introduction

1.1 Chemical biology

In recent years, since the responsible molecules of various diseases have become clear, these molecular-targeted drugs are high potency and mainstream in drug discovery. In the development of this molecular-targeted drug, it is important how the researchers find the novel responsible molecule and obtain drug-lead effectively. On the other hand, chemical biology is a research method that regulates the function of biomolecules and elucidates cellular functions using diverse small molecules. Therefore, in chemical biology studies, it is necessary to discover the small molecules that have diverse functions. The molecular-targets of these small molecules have potential to become the novel responsible molecule for drug development. Moreover, these small molecules have potential to become drug-leads. Thus, chemical biology is expected to be potent method for drug discovery. To develop a potent drug-lead, it is essential to (1) secure a unique screening source, (2) construct unique screening system, (3) identify targeted-molecule and analyze the mechanism.

1.1.1. Screening source

Natural Products have been widely used as potent screening source of small molecule in chemical biology study. However, screening for drug-leads has shifted from natural product-derived compound to synthetic compound. This is because, natural product-derived compound has a following problem, (1) Low rate of obtaining novel compound, (2) Spending long period for isolation and structure elucidation of active compound, (3) Difficulty of derivative synthesis. On the other hand, high throughput screening (HTS) using synthetic compound library has become mainstream with developing the combinatorial chemistry. However, the structural diversity of combinatorial synthetic compounds is limited, and could not obtain the structural diversity [1]. The advantage of natural product-derived compounds is having complex chemical

structure, and interacting with targeted-molecule specifically. Therefore, natural product-derived compound is expected to attract attention as a potent screening source again. In this study, the author tries to search for the drug-seed of prostate cancer from natural products.

1.1.2. Screening system

The screening system is categorized into forward screening system and reverse screening system. The forward screening system is the method, which searches for the compound that induces changing phenotype of cell. On the other hand, reverse screening system is the method, which searches for the compound that interacts with specific molecule directly. Since the responsible molecules of various diseases have become clear, reverse screening system is mainstream in pharmaceutical company. In this study, the author focused on androgen receptor (AR), that plays a central role in the malignancy of prostate cancers as a targeted-molecule.

1.1.3. Identification of targeted-molecule

If the researchers could obtain a potent compound from a unique screening source, it is necessary to analyze the mechanism of this compound for expanding chemical biology study. In particular, identification of targeted-molecule is necessary and difficulty. Identification methods of targeted-molecule are also categorized into direct method and indirect method [2]. In direct method, for example, targeted-molecule is identified from cell lysate using biotin-labeled compound. On the other hand, in indirect method, targeted-molecule is identified by applying biological activity of the compound to known signaling cascade. However, identification of targeted-molecule by these methods is not easy resulted in various reasons. For this, identification methods of targeted-molecule are progressing daily, desiring a novel method. In recent years, identification of targeted-molecule is performed by metabolome analysis [3] and bioinformatics method [4] in our laboratory. Previously, our laboratory have screened for small molecules that bind to AR by bioinformatics method.

1.2 Natural products drug discovery

The secondary metabolites from microbial origin, such as actinomycetes and fungi, are especially used as source of small molecule for natural products drug discovery. Since antibacterial activity of penicillin was discovered [5], small molecules, that have diverse bioactivity, have become searched from secondary metabolites from microbial origin. For example, streptomycin isolated from *streptomyces griseus* was used for the antibiotics [6]. Moreover, mitomycin C isolated from *streptomyces caespitosus* was used for the anti-cancer drug [7]. In addition, FK506 (Tacrolimus) isolated from *streptomyces tsukubaensis* was used for immunesuppressant [8]. These compounds demonstrated a great potential of secondary metabolites from microbial origin (Figure 1a).

The small molecules from microbial origin have complex structures and rigid conformation generated by many chiral centers and diverse of ring structure differed from synthetic compounds. In addition, small molecules from microbial origin include many oxygen atoms in comparison with synthetic compounds [9]. This feature indicates that small molecule from microbial origin has functional moiety that can be donor/acceptor of hydrogen bond for interaction with biomolecules. Therefore, small molecules from microbial origin are superior to synthetic compounds as screening source. In fact, it is reported that small molecules from microbial origin have many bioactivities, and natural product-derived compounds are covering about 60% clinical drug in past 30 years [10]. In recent years, halicondrin B, isolated from the marine sponge *Harichondria okadai*, was total synthesized and its partial structure was approved as eribulin for metastatic breast cancer (Figure 1b) [11]. In addition, ivermectin, synthesized from avermectin isolated from *Streptomyces avermitilis*, have been widely used for intestinal strongyloidiasis all over the world (Figure 1c) [12]. Moreover, Dr. Satoshi Omura who

discovered avermectin received the Nobel Prize in 2015. This glory broke a ray of light to the potential of natural products drug discovery.

However, as above described, the development of natural products drug discovery is not becoming mainstream. Today, the various efforts are making progress to re-establish natural products drug discovery. In Japan, natural product-derived compound library is constructed and drug discovery support is progressing as the national project. In this project, the researchers of industry and academia can utilize this natural product-derived compound library mutually. On the other hand, many methodologies to obtain novel natural product-derived compound are developing. These methods are categorized into artificial method and not artificial method. In artificial method, for example, biosynthetic gene of secondary metabolite is edited, and natural unnatural product is generated [13]. It is characteristic that microorganism oneself couldn't produce the product generated by this method. On the other hand, recent study revealed that some biosynthetic genes of secondary metabolites are not used, and their products are not produced in normal condition. In not artificial method, unused biosynthetic gene is awoken by any method. For example, unused biosynthetic gene is awoken by adding HDAC inhibitor into culture medium [14]. This is speculated that HDAC inhibitor regulates the gene expression that is essential for secondary metabolism in microorganism. Today, it is reported that the number of cultivable microorganism is about 1% [15]. From now, if novel microorganism source is developed, and unused biosynthetic gene is awoken by above methods, it is speculated that many novel natural products-derived compounds are discovered.

a)

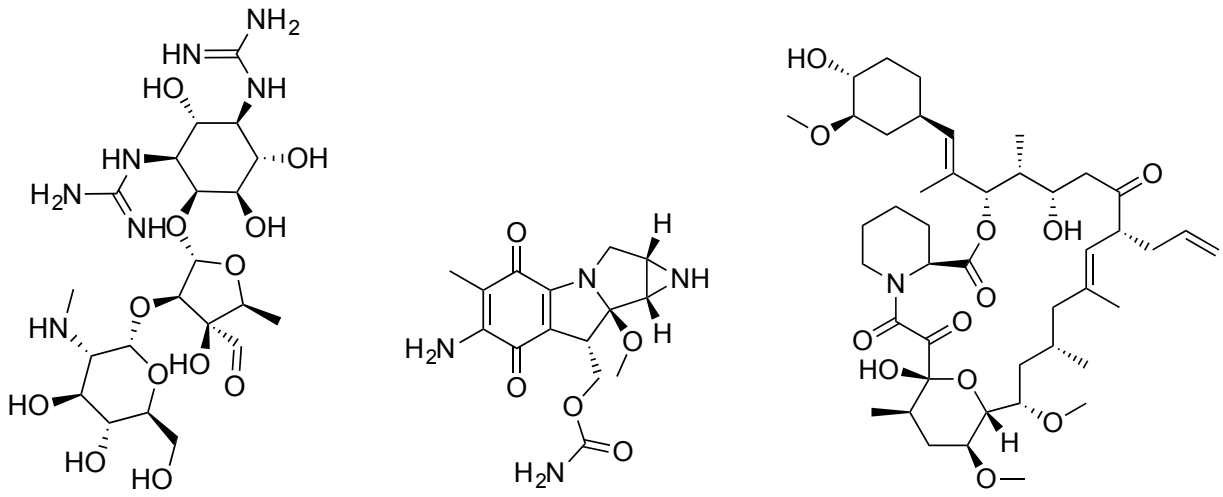

b)

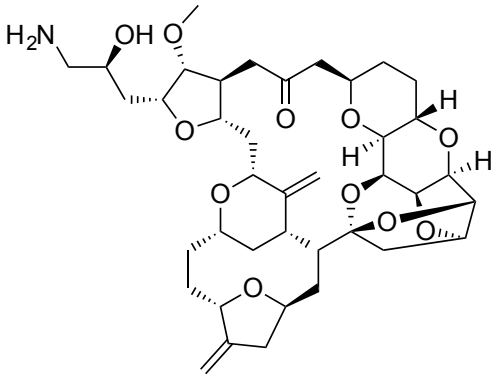

c)

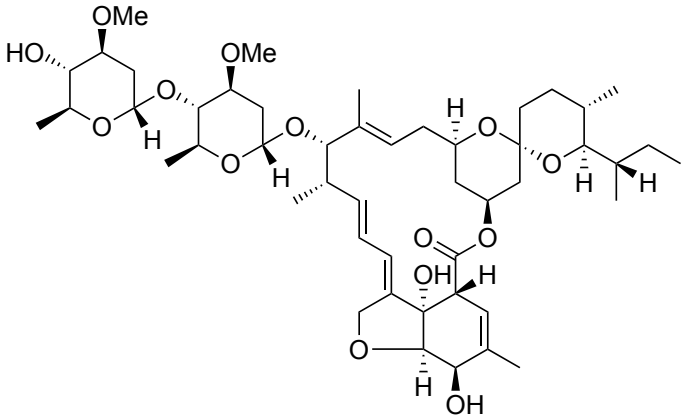

Figure 1. (a) The structure of streptomycin (left), mitomycin C (middle) and FK506 (right). (b) The structure of eribulin. (c) The structure of ivermectin.

1.3 Prostate cancer

Prostate cancer is one of the most commonly diagnosed cancers among men worldwide [16]. In recent years, the number of prostate cancer patients has been increasing rapidly in Japan. In fact, the morbidity of prostate cancer is increasing, and predicted to become the first in 2020 [17].

Androgen receptor (AR) signaling plays a central role in the malignancy of prostate cancer [18]. AR is a member of the nuclear receptor superfamily, and activated by androgens (a male hormone), such as testosterone and dihydrotestosterone (DHT). AR contains 919 amino acids and consists of the N-terminal domain (NTD; 1-555), the DNA-binding domain (DBD; 556-623), hinge region (624-665), and the C-terminal ligand binding domain (LBD; 666-919) [19]. The androgen deprivation by medical or surgical castration is the standard first line treatment for men with advanced prostate cancer. Over time, most men will progress to a more aggressive form of the disease called castration-resistant prostate cancer (CRPC). CRPC is commonly associated with sustained activity of AR-signaling through AR gene overexpression or amplification [20][21]. The continued reliance on AR signaling in CRPC has led to the development of AR antagonists that compete with androgens for binding to the AR as second line treatment.

AR antagonists are classified into two structural types, steroidal and anilide-type compounds. Steroidal-type AR antagonist such as chlormadinone acetate often develops side effects because of cross-reactivity with other steroid hormone nuclear receptors, such as estrogen receptor (ER) [22]. Therefore, anilide-type AR antagonists, such as flutamide and bicalutamide (First generation AR antagonists) have been commonly used (Figure 2a) [23][24]. However, these first generation AR antagonists have a low affinity for the AR and, as a result, insufficiently block AR signaling [25]. Moreover, long-term treatment with these AR antagonists can lead to AR point mutations which link to the development of resistance (T877A for flutamide resistance [26],

W741C for bicalutamide resistance [27]). A second generation AR antagonist, Enzalutamide (MDV3100), has evolved from the need for more effective and long-term AR inhibition and has been recently approved by the U.S. Food and Drug Administration (Figure 2b) [28]. Enzalutamide shows antagonist activities to wild type AR and mutant ARs (T877A and W741C), and overcomes these resistances. Moreover, enzalutamide inhibits not only the translocation of AR to the nucleus but also the bond of AR to DNA [28]. However, despite the initial response to enzalutamide, resistance also develops in most patients with metastatic CRPC. The recent studies have revealed that a F876L mutation in the AR confers resistance to enzalutamide [29]. This reason is speculated that enzalutamide is also anilide-type compound.

Apalutamide (ARN-509) is currently in phase III clinical trials for CRPC, however, it does not show antagonist activity against mutant AR (F876L), possibly due to structural similarity with enzalutamide (Figure 2c) [30]. Since the diversity of chemical scaffolds of clinically used AR antagonists has thus far been narrow, new structures are of interest as they might have properties that differ from current AR antagonists. Darolutamide (ODM-201) is a synthetic AR antagonist presently in a phase III study, and it is both novel and structurally distinct from any known AR antagonist, including the enzalutamide (Figure 2c) [31]. Darolutamide has been shown to be a full antagonist of mutant AR (F876L), AR (W741L for bicalutamide resistance), and AR (T877A). In addition, FL442 and SC97 derivative, that are reported recently, have been shown to be antagonists of mutant AR (F876L) respectively, and structurally distinct from any known AR antagonist (Figure 2d) [32][33]. Therefore, the unique structure may be important for developing AR antagonists that can overcome resistance to AR-targeted therapy.

From these backgrounds, the author chose the secondary metabolites from microbial origin as a screening source, because the secondary metabolites from microbial origin include many unique structural compounds.

a)

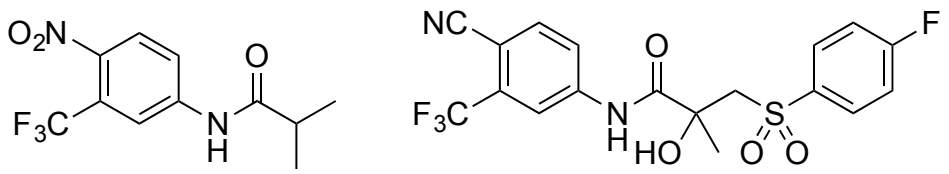

b)

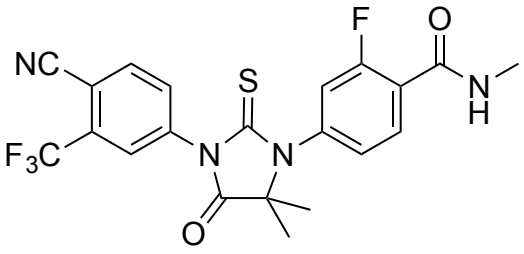

c)

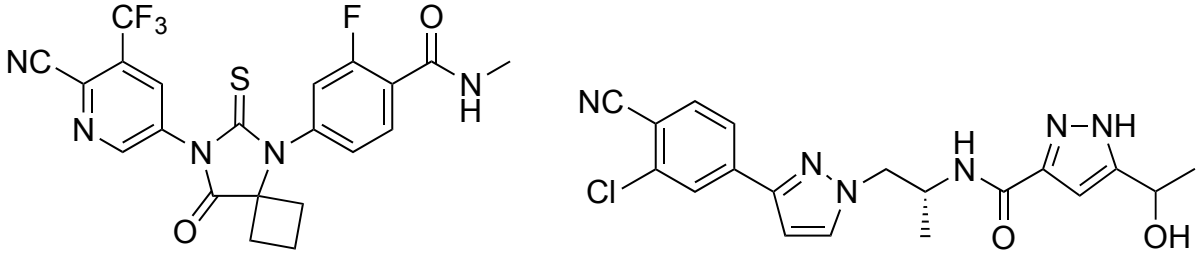

d)

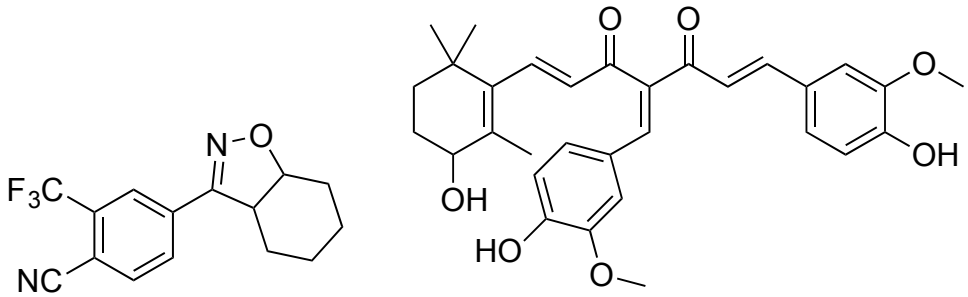

Figure 2. (a) The structure of first generation AR antagonists (flutamide (left) and bicalutamide (right)). (b) The structure of a second generation AR antagonist (enzalutamide). (c) The structure of new generation AR antagonists (apalutamide (left) and darolutamide (right)). (d) The structure of new generation AR antagonists (FL442 (left) and SC97 derivative (right)).

Chapter 2

Antarlides: A New Type of Androgen Receptor (AR) Antagonist that Overcomes Resistance to AR-Targeted Therapy

2.1 Introduction

To obtain a new type-AR antagonist, our laboratory have conducted *in silico* screening and natural products screening. From both screening system, our laboratory have obtained some new type-AR antagonists.

T5853872 obtained by *in silico* screening is a synthetic compound, and not steroidal and anilide-type compound (Figure 3a). In fact, T5853872 is structurally distinct from any known AR antagonist, as judged from the chemical space based on E-Dragon [34]. However, it is a problem that T5853872 has a low AR antagonist activity to prostate cancer cells, and shows cytotoxic effect. Arabilin is isolated from secondary metabolites of *Streptomyces* sp. MK756-CF1 as a new type-AR antagonist (Figure 3b) [35]. Arabilin is a novel polypropionate-derived metabolite with a *p*-nitrophenyl group and a substituted γ-pyrone ring, and also distinct from any known AR antagonist, as judged from the chemical space based on E-Dragon [36]. Moreover, arabilin shows a high AR antagonist activity to prostate cancer cells, and this activity is equal to flutamide, which is clinically used for the treatment of prostatic diseases. In addition, the author reported that arabilin shows antagonist activities to not only of the wild type AR but also of mutant ARs which link to the development of resistance [37]. However, arabilin also shows cytotoxic effect by inhibiting the mitochondrial function. In fact, spectinabilin, that is structural isomer of arabilin, was reported to inhibit *Ascaris* NADH-fumarate reductase (Figure 3b) [38][39].

Though these compounds obtained by *in silico* screening and natural products screening showed cytotoxic effect, natural product-derived compound has the potential to show a high AR antagonist activity and to have unique structure. Therefore, the author further screened from secondary metabolites from microbial origin to obtain a new type-AR antagonist.

a)

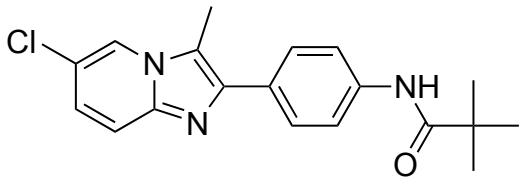

b)

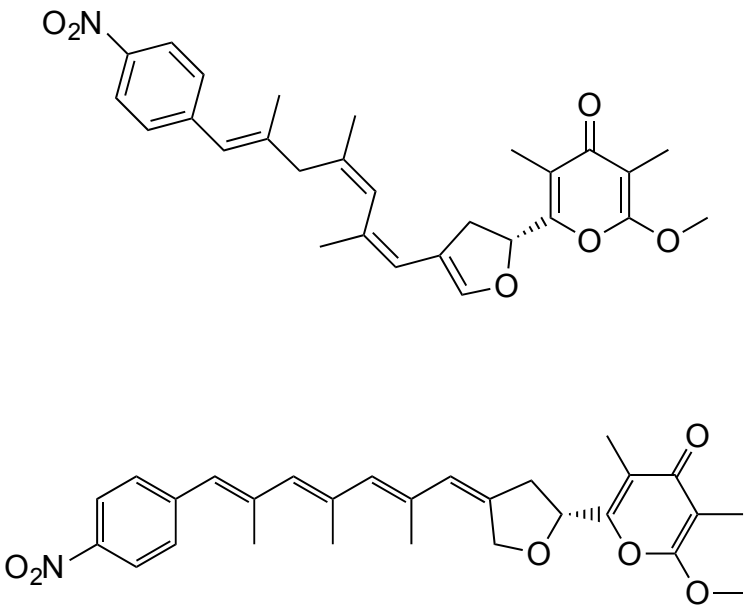

Figure 3. The structure of AR antagonists we discovered. (a) The structure of T5853872 obtained by *in silico* screening. (b) The structure of arabilin (top) and spectinabilin (bottom) obtained by natural products screening.

2.2 Results

2.2.1 Screening for AR-DHT binding inhibitors

The author screened secondary metabolites from more than 1,000 microbial origins to find a new type-AR antagonist that could inhibit the binding of [^{3}H]-labeled DHT to the AR in an *in vitro* binding assay [34]. From this screen, the author found that the microbial extract of strain BB47 inhibited the binding of [^{3}H]-DHT to the AR.

2.2.2 Taxonomy of the producing strain

The producing strain BB47 was isolated from a soil sample collected in Bangkok, Thailand (Figure 4). This strain was identified as a member of the genus *Streptomyces* on the basis of 98.7% similarity in the 16S rRNA gene sequence (1425 nucleotides; GenBank accession number HM051280) to *Streptomyces catenulae* ISP 5258 (accession number AY999778) [40].

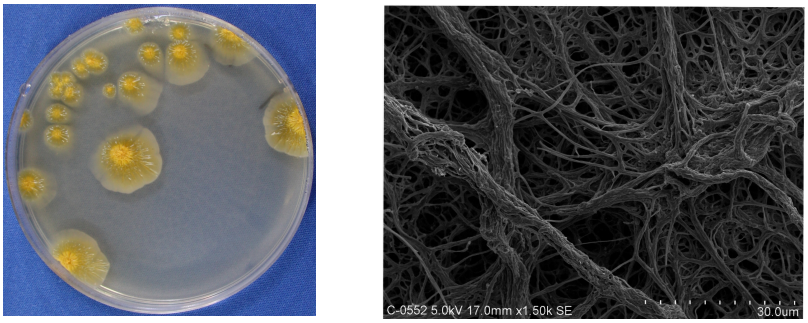

Figure 4. The agar plate picture (left) and scanning electron micrograph (right) of *Streptomyces* sp. BB47

2.2.3 Isolation of antarlides

2.2.3.1 Isolation of antarlides A-E

Streptomyces sp. BB47 was cultured in producing medium (10 L) at 30 °C for 6 days, and the whole culture broth was extracted with EtOAc. This extract (1.9 g) was partitioned between 10% aqueous MeOH and *n*-hexane, the former of which was further separated between EtOAc and H_2O (pH 10). In this purification, silicagel was not suitable because active components are unstable under acidic condition. Therefore, the EtOAc soluble fraction was fractionated by centrifugal liquid-liquid partition chromatography. The active stationary phase was repeatedly purified by reversed-phase column chromatography, followed by HPLC purification on a C30 column, to yield antarlide A (**1**) (55.2 mg), B (**2**) (13.8 mg), C (**3**) (17.7 mg), D (**4**) (13.8 mg), and E (**5**) (4.6 mg). Note that all isolation steps were carried out in dark, because **1**-**5** are unstable under room light. This isolation procedure of **1**-**5** was shown in Figure 5.

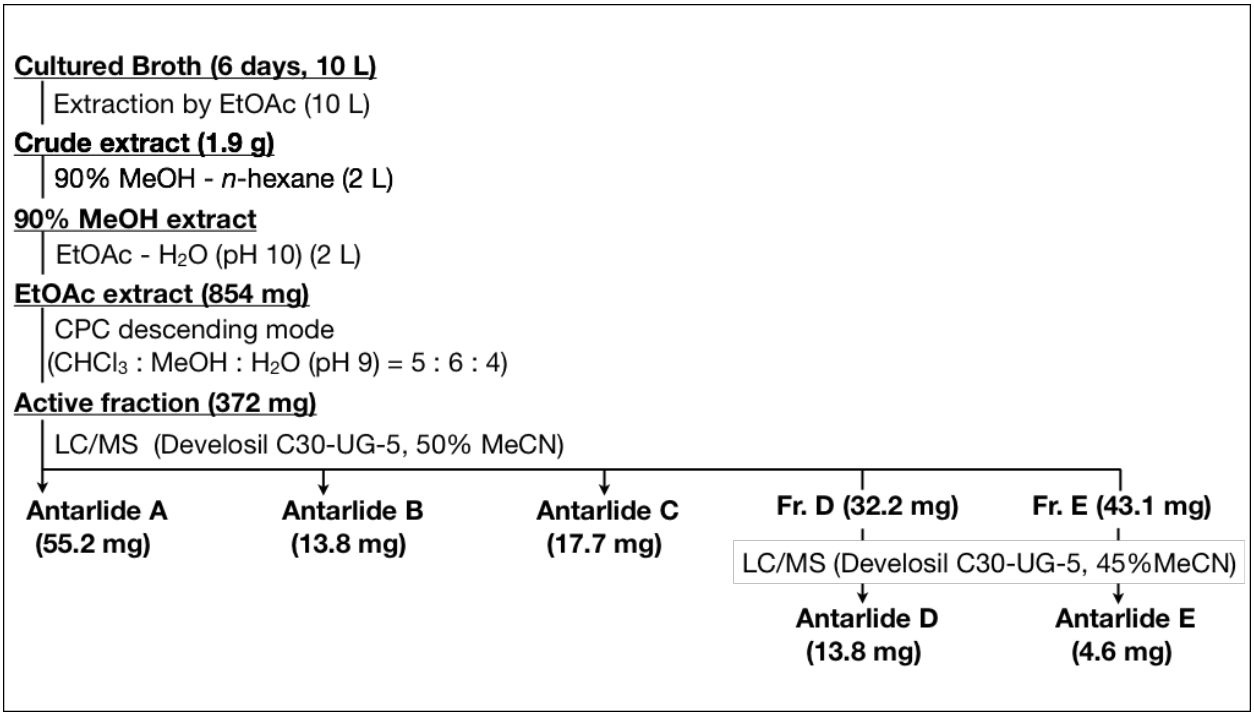

Figure 5. Isolation procedure of antarlides A-E (**1**-**5**) from *Streptomyces* sp. BB47

2.2.3.2 Isolation of antarlides F-H

Streptomyces sp. BB47 was cultured in producing medium (12 L) at 30 °C for 6 days, and the whole culture broth was extracted with EtOAc. LC-MS analysis of the crude extract indicated the presence of three minor peaks displaying UV and MS spectra similar to those of antarlides A-E (**1**-**5**) (Figure 6). This extract (3.9 g) was partitioned between 10% aqueous MeOH and *n*-hexane, the former of which was further separated between EtOAc and H_2O (pH 10). In this purification, silicagel was not suitable because active components are unstable under acidic condition. Therefore, the EtOAc soluble fraction was fractionated by centrifugal liquid-liquid partition chromatography. The active stationary phase was repeatedly purified by reversed-phase column chromatography, followed by HPLC purification on a C30 column, to yield antarlides F (**6**) (2.2 mg), G (**7**) (1.6 mg), and H (**8**) (1.0 mg). Note that all isolation steps were carried out in dark, because **6**-**8** are unstable under room light. This isolation procedure of **6**-**8** was shown in Figure 7.

a)

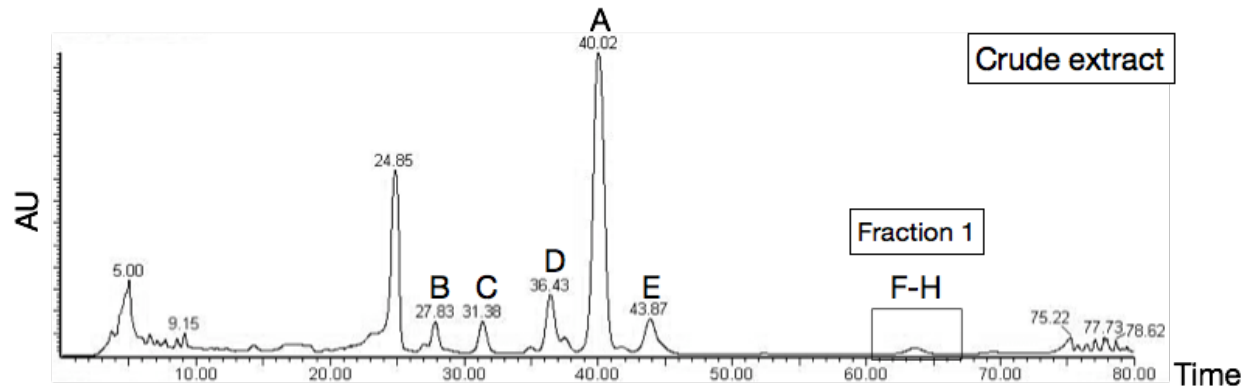

b)

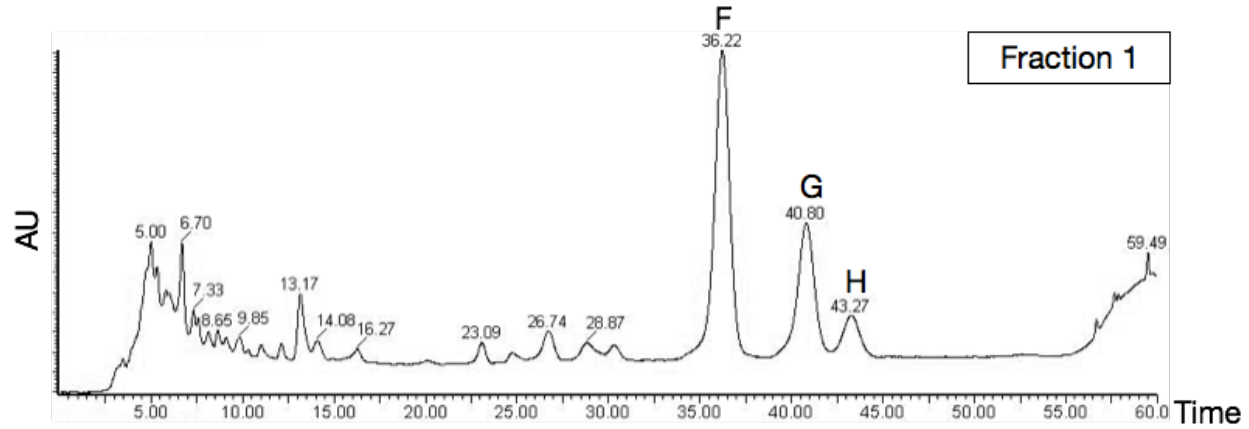

Figure 6. (a) PDA chromatogram of crude extract containing antarlides A-H (**1**-**8**) (solvent: MeCN:H_2O=1:1). (b) PDA chromatogram of fraction 1 containing antarlides F-H (**6**-**8**) (solvent: MeOH:H_2O=3:1).

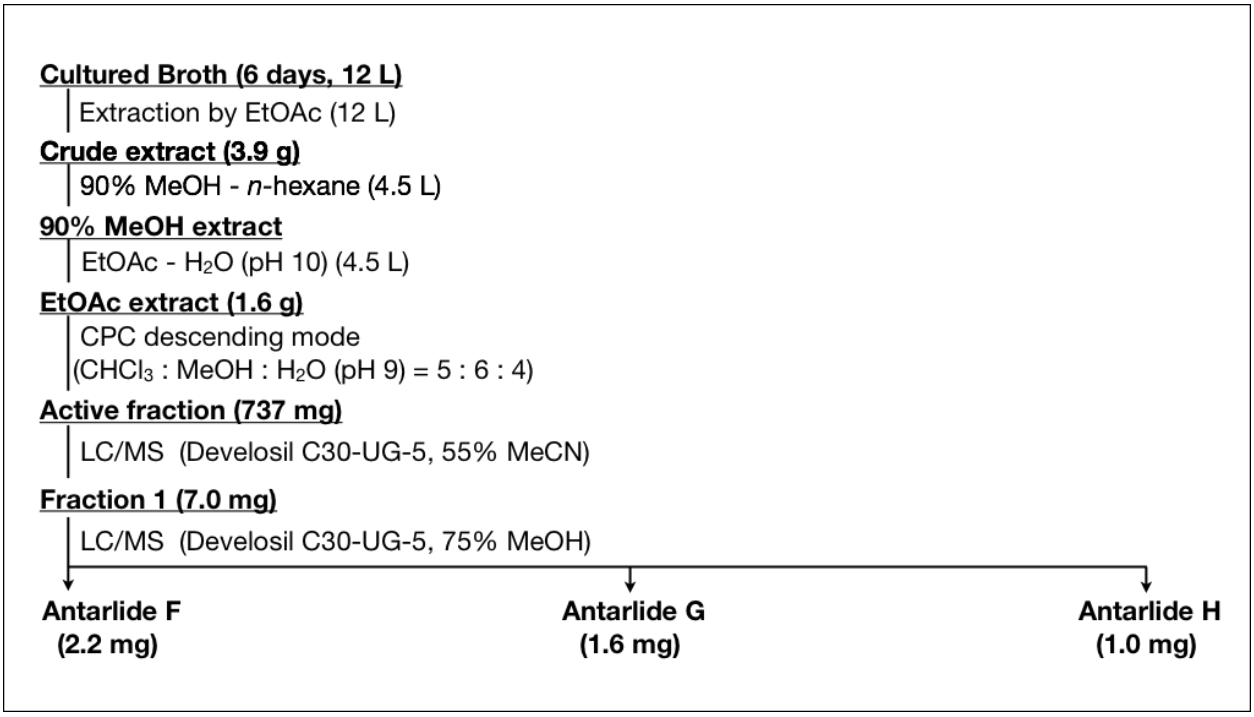

Figure 7. Isolation procedure of antarlides F-H (**6**-**8**) from *Streptomyces* sp. BB47

2.2.4 Planar structure elucidation of antarlides

2.2.4.1 Antarlide A

Antarlide A (**1**) was obtained as a pale yellow powder and the molecular formula was found to be $C_{33}H_{44}O_6$ by high-resolution ESITOFMS ($[M-H]^-$ *m/z* 535.3055). The IR spectrum of **1** displayed absorption bands at 3313 and 1670 cm^{-1}, indicating the presence of hydroxy and carbonyl groups (Figure 8a). The UV absorption bands at 337 nm suggested the presence of a conjugated polyene moiety (Figure 8b).

^1H and ^{13}C NMR data (Figure 9,10) in combination with the HSQC analysis (Figure 11) revealed the presence of 33 carbons attributable to one carbonyl, eighteen sp^2 carbons (fourteen are proton-bearing, one is oxygenated), four sp^3 methylenes, six sp^3 methines (four is oxygenated), and four methyl groups. One carbonyl and eighteen sp^2 carbons require the presence of two rings from the unsaturation degrees of the formula of **1**. The full planar structure of **1** was assigned through interpretation of 1D and 2D NMR spectroscopic data recorded in acetone-d_6 (Table 1). A detailed analysis of the ^1H-^1H COSY spectrum (Figure 12) revealed five partial proton-proton connectivities: (a) from H-3 to H-11, (b) from H-13 to H-15, (c) from H-16 to H-21 and the methyl group H-16a, (d) from H-22 to H-23 and the methyl group H-22a, and (e) from H-27 to H-29 (Figure 15).

Interpretation of the HMBC NMR data (Figure 13) allowed the ^1H-^1H COSY-defined fragments of **1** to be connected as shown in Figure 15. The linkage of the partial structures between (a) and (c) was established by HMBC correlations from H-2a to C-1, C-2, and C-3 and from H-21 to C-1. Furthermore, the partial structure (c) and the correlations from the H-12a to C-11, C-12, and C-13 and from H-16a to C-15, C-16, and C-17 constructed a macrocyclic structure of a

22-membered ring. This macrocyclic ring was connected to the partial structure (d) on the basis of HMBC correlations from H-22a to C-21. The remaining partial structure (e) was connected to a three-carbon unit (C-24, C-25, C-26) on the basis of HMBC correlations from H-28 to C-24 and C-26, from H-27 to C-25 and from H-29 to C-25. These data established a benzene ring possessing oxygen-bearing C-26 (δ 157.2). This benzene ring was expanded to the partial structure (d) based on HMBC correlations from H-25 to C-23 and H-29 to C-23. The molecular formula of **1** indicated four protons left to be assigned but these protons could be assigned to the hydroxy protons at C-11 (δ 77.2), C-19 (δ 68.8), C-23 (δ 75.5), and C-26 (δ 157.2).

The double bond geometries of **1** were assigned by analysis of the proton coupling constants and NOESY (Figure 14) correlations as shown in Figure 15. C-2-C-3, C-4-C-5, C-6-C-7, C-8-C-9, C-12-C-13 and C-14-C-15 double bonds were assigned as *E, E, E, E, E* and *E* on the coupling constants of $J_{4,5}$ = 14.4 Hz, $J_{6,7}$ = 14.7 Hz, $J_{8,9}$ = 14.3 Hz, and the basis of NOESY correlations for H-2a-H-4, H-3-H-5, H-5-H-7, H-7-H-9, H-8-H-10, H-12a-H-14 and H-14-H-16a.

a)

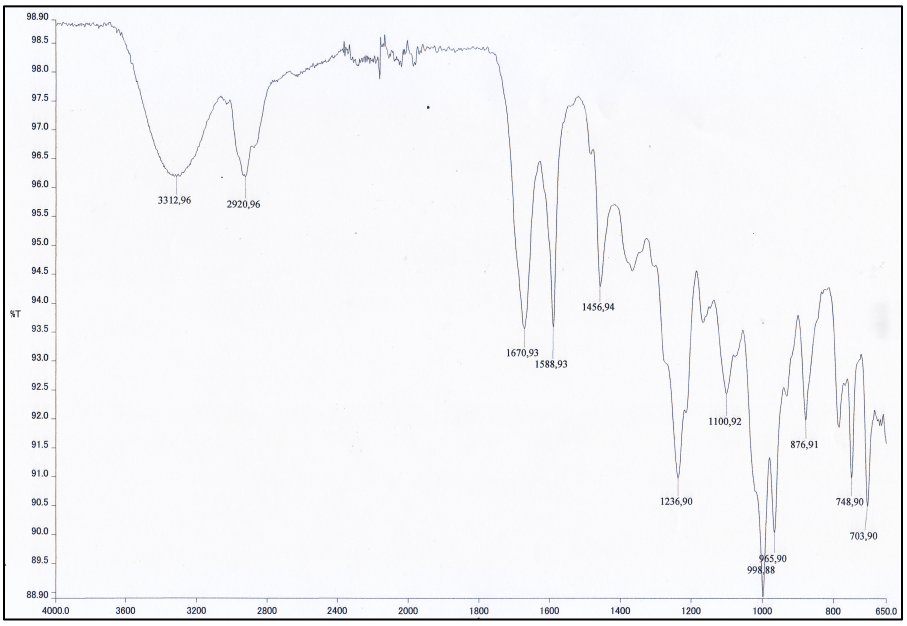

b)

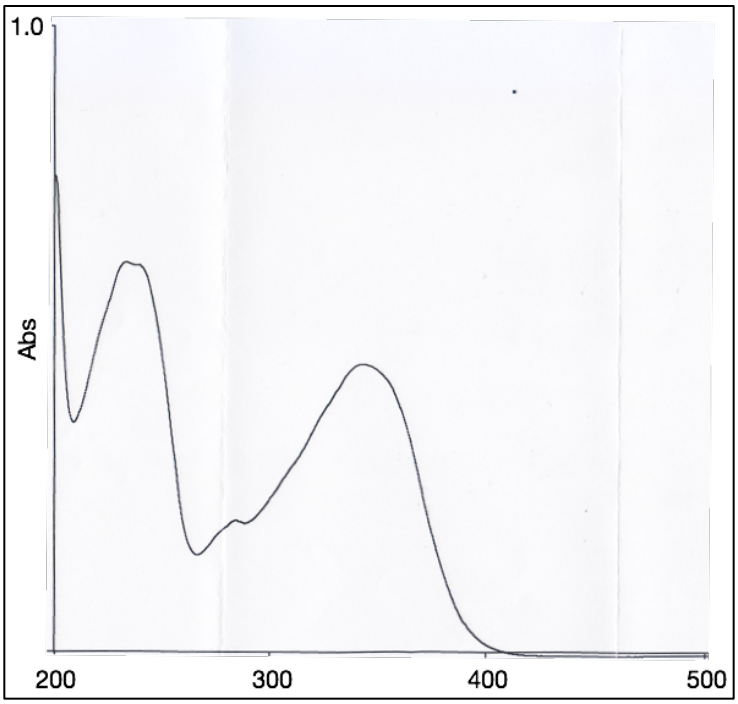

Figure 8. IR spectrum (a) and UV spectrum (b) of antarlide A (**1**)

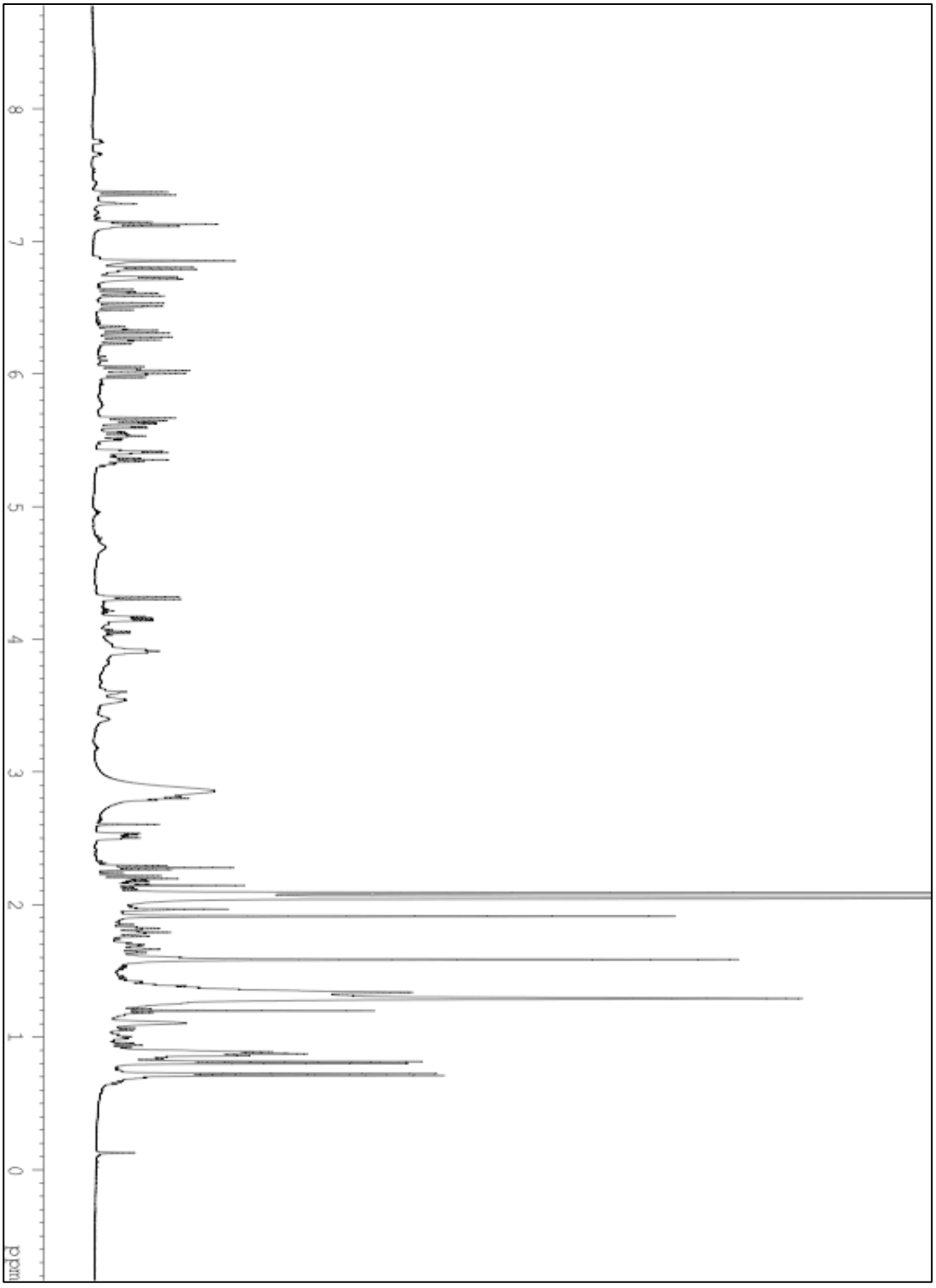

Figure 9. ^{1}H NMR spectrum of antarlide A (**1**)

(500 MHz, Acetone-d_6, Acetone-d_6 = 2.05 ppm)

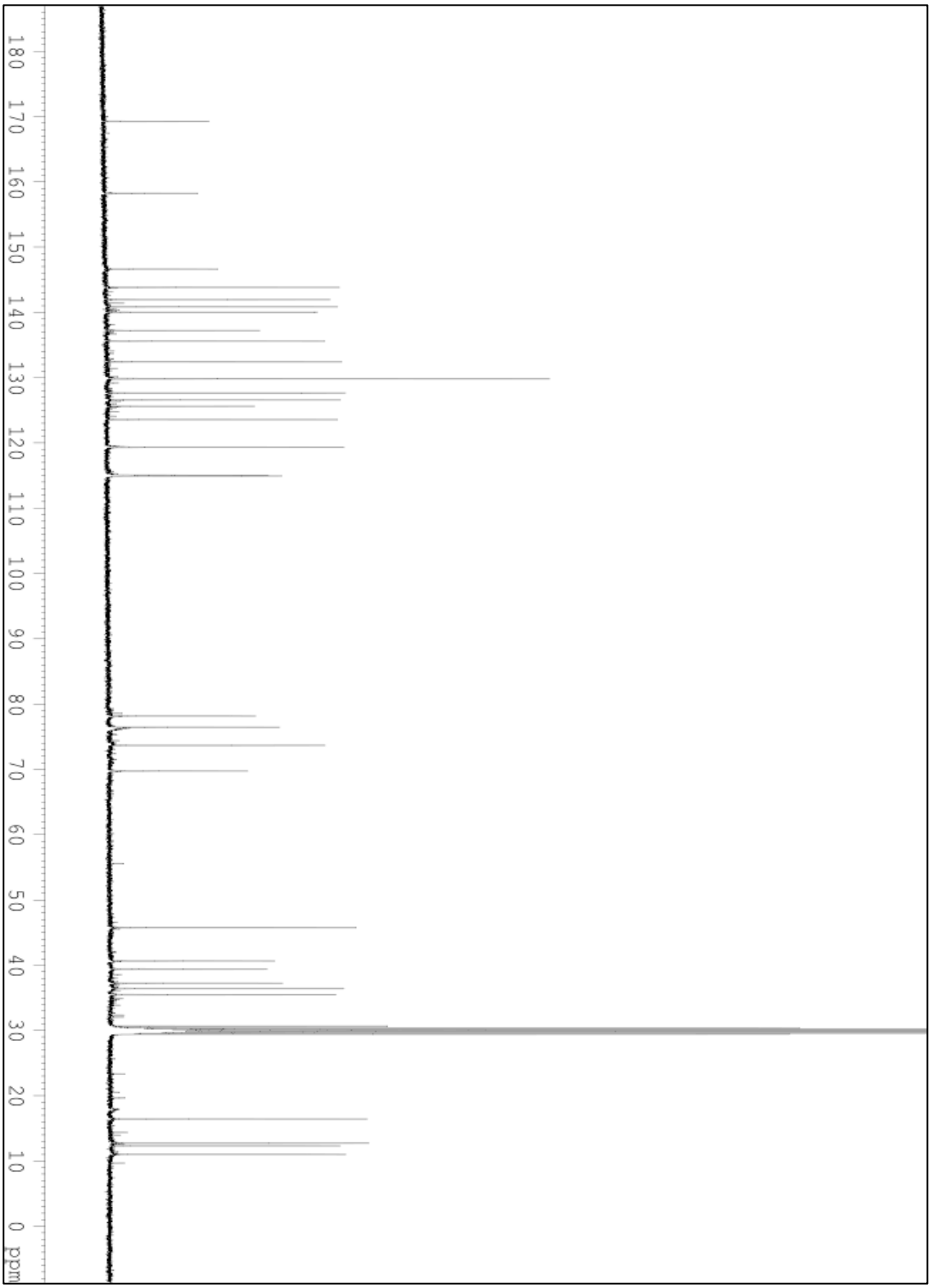

Figure 10. ^{13}C NMR spectrum of antarlide A (**1**)

(125 MHz, Acetone-d_6, Acetone-d_6 = 29.8 ppm)

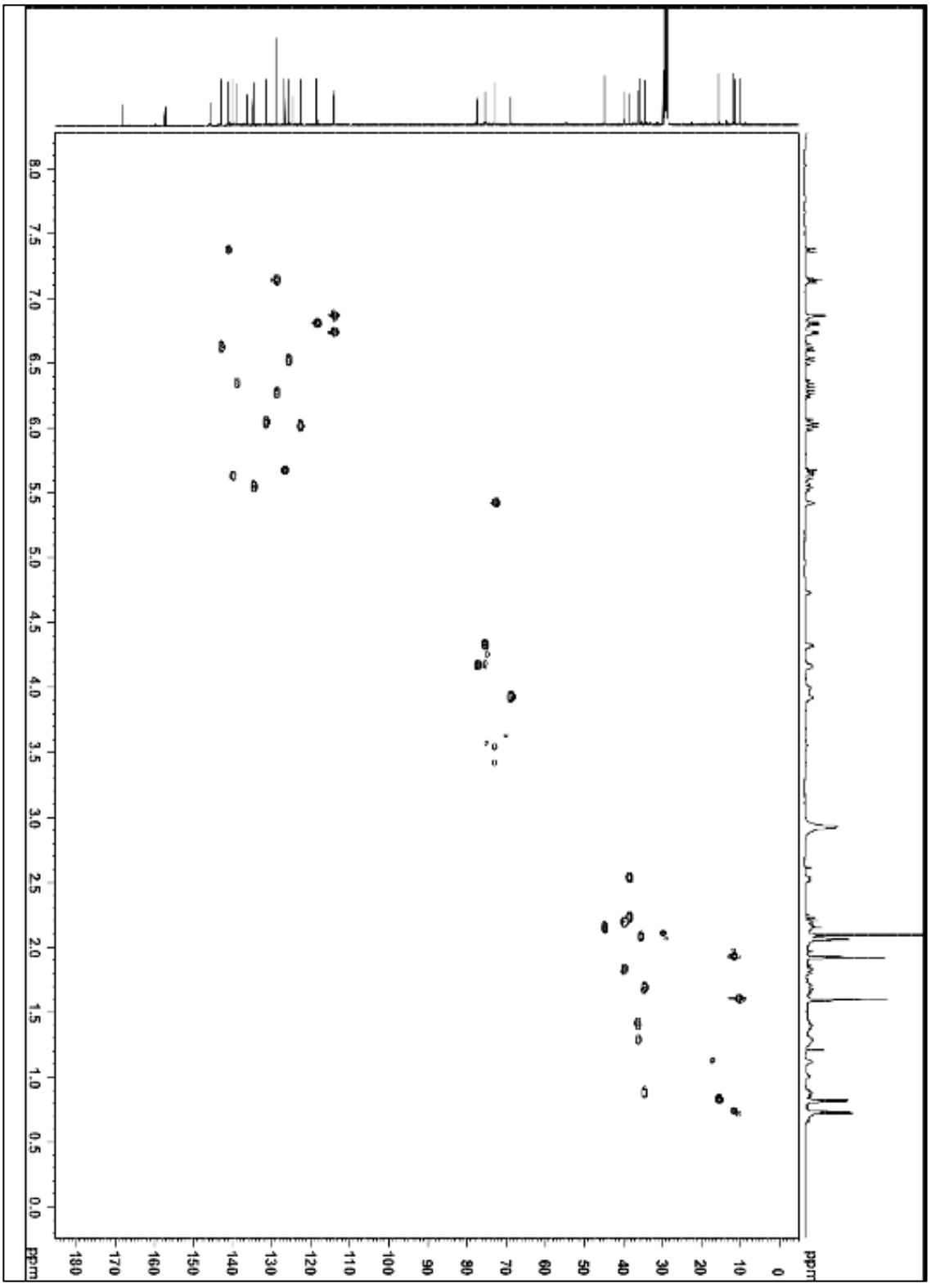

Figure 11. HSQC spectrum of antarlide A (**1**) (500 MHz, Acetone-d_6)

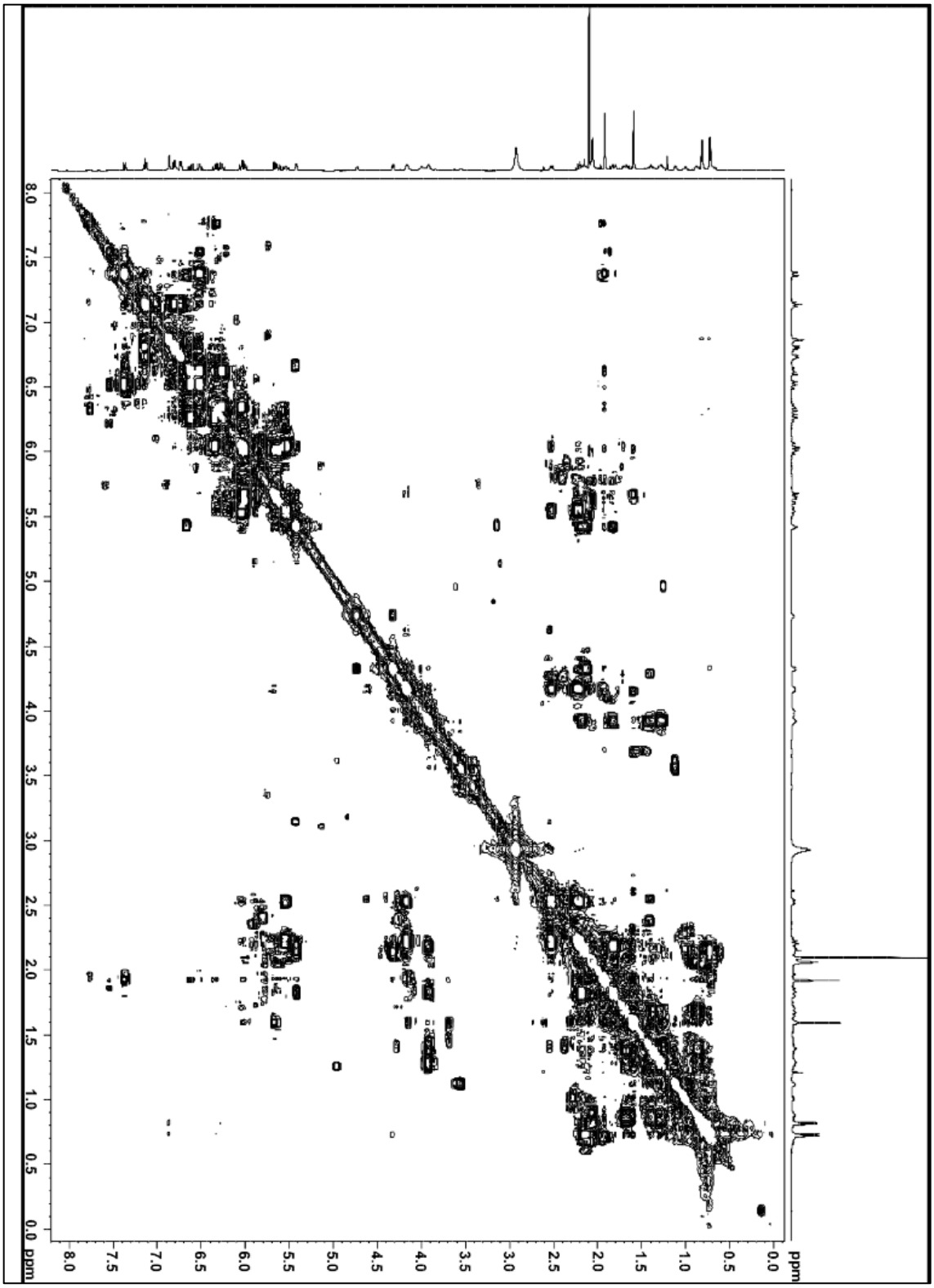

Figure 12. ^{1}H-^{1}H COSY spectrum of antarlide A (**1**) (500 MHz, Acetone-d_6)

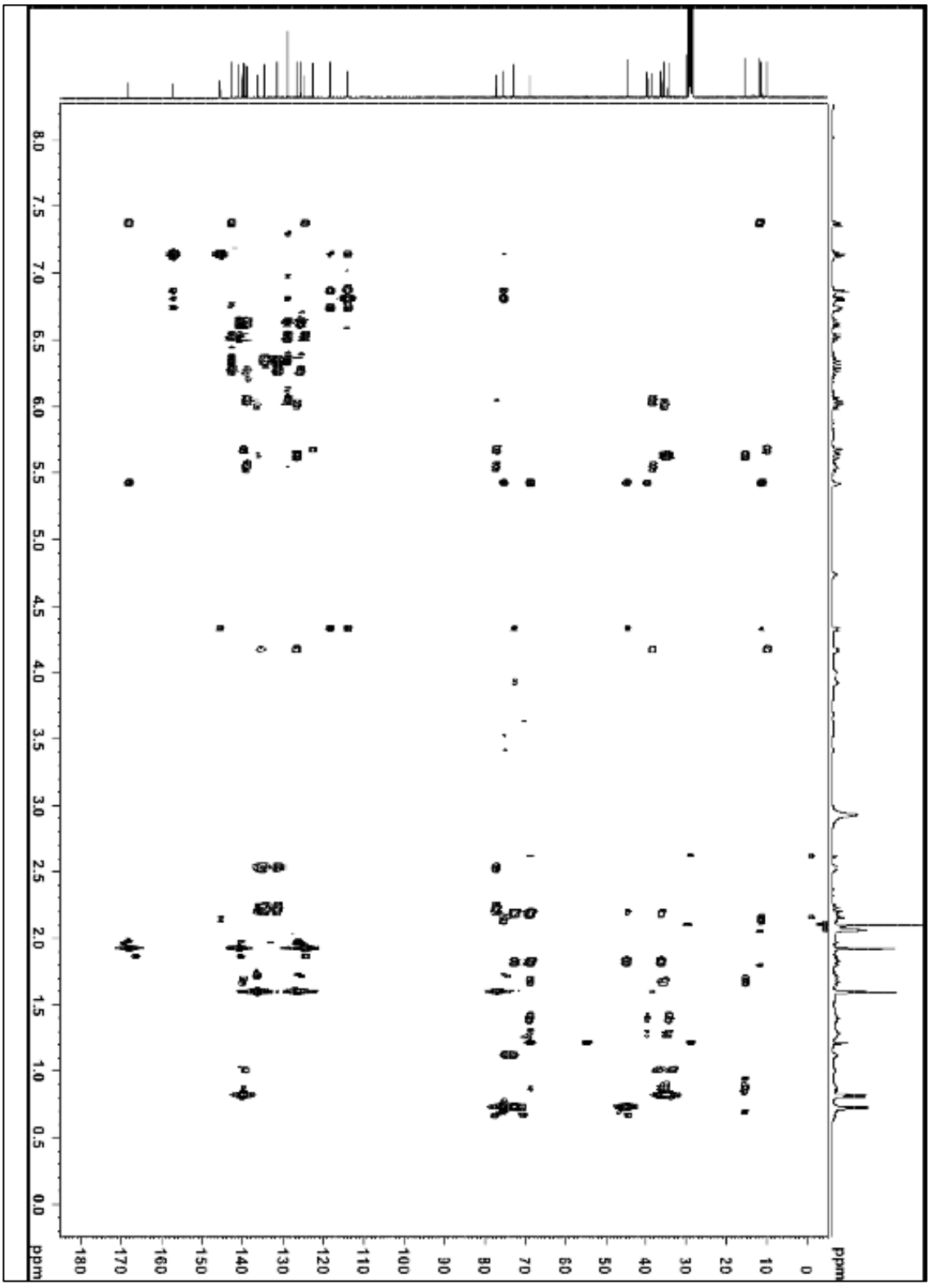

Figure 13. HMBC spectrum of antarlide A (**1**) (500 MHz, Acetone-d_6)

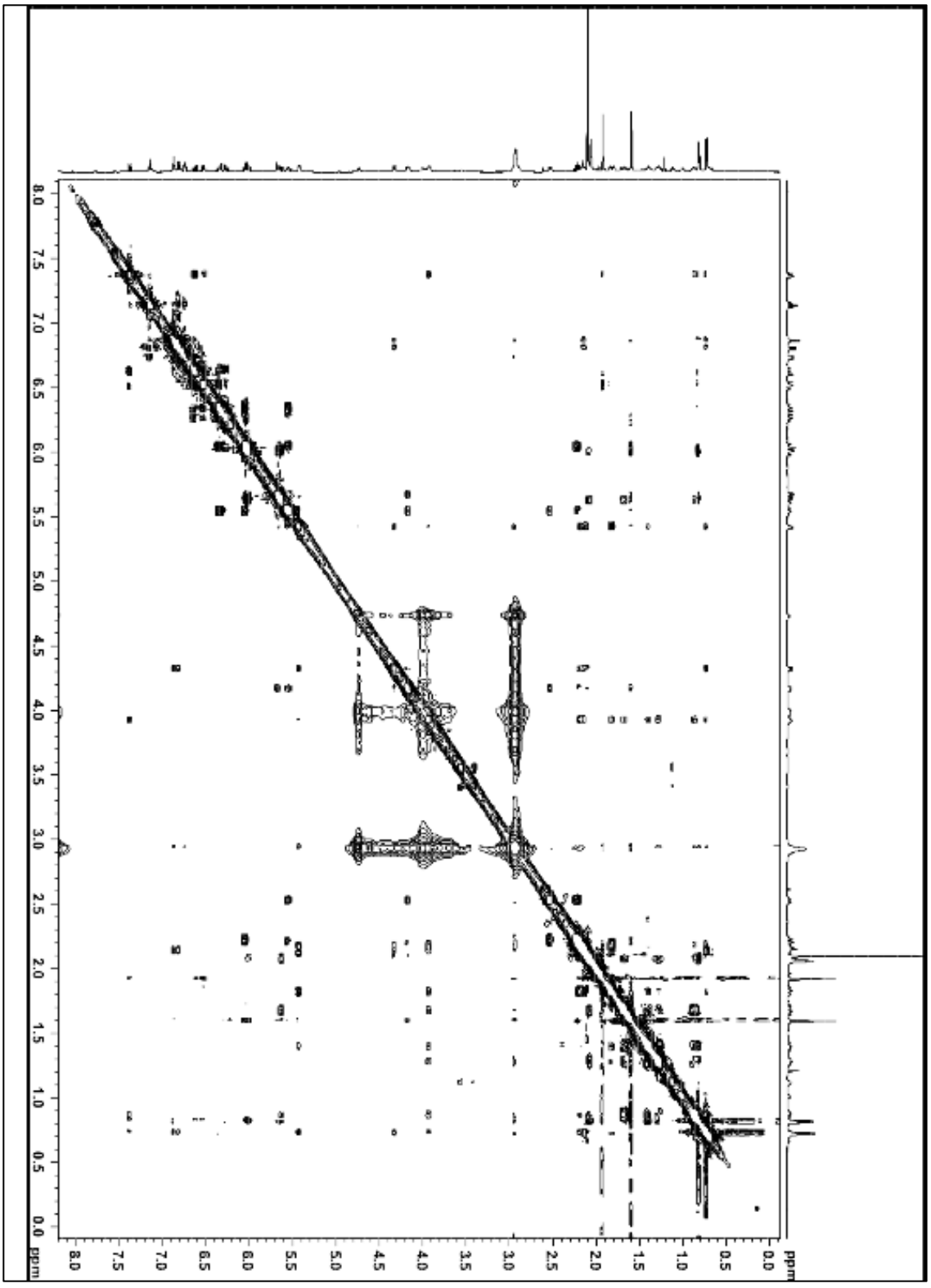

Figure 14. NOESY spectrum of antarlide A (**1**) (500 MHz, Acetone-d_6)

Table 1. ^{1}H and ^{13}C NMR data for antarlide A (**1**) in Acetone-d_6

position	δ_C	δ_H mult (*J* in Hz)
1	168.3	-
2	124.6	-
2a	11.8	1.93 (3H, s)
3	141.0	7.38 (1H, d, 11.7)
4	125.6	6.53 (1H, dd, 11.7, 14.4)
5	142.3	6.63 (1H, dd, 10.8, 14.4)
6	129.6	6.28 (1H, dd, 10.8, 14.7)
7	139.0	6.35 (1H, dd, 10.8, 14.7)
8	131.5	6.04 (1H, dd, 10.8, 14.3)
9	134.6	5.55 (1H, dt, 4.0, 14.3)
10	38.9	2.23, 2.53 (2H, m)
11	77.2	4.17 (1H, dd, 4.9, 9.6)
12	136.3	-
12a	10.1	1.60 (3H, s)
13	126.7	5.68 (1H, d, 10.6)
14	122.6	6.02 (1H, dd, 10.5, 15.5)
15	139.9	5.63 (1H, dd, 3.7, 15.3)
16	36.3	2.07 (1H, m)
16a	13.5	0.83 (3H, d, 6.5)
17	35.5	0.89, 1.68 (2H, m)
18	38.5	1.21, 1.40 (2H, m)
19	68.8	3.93 (1H, m)
20	39.7	1.82, 2.15 (2H, m)
21	72.7	5.43 (1H, m)
22	44.8	2.15 (1H, m)
22a	11.4	0.74 (3H, d, 7.0)
23	75.5	4.33 (1H, d, 9.0)
24	145.7	-
25	113.9	6.87 (1H, s)
26	157.2	-
27	114.0	6.74 (1H, d, 7.7)
28	129.7	7.15 (1H, t, 7.7)
29	118.4	6.81 (1H, d, 7.7)

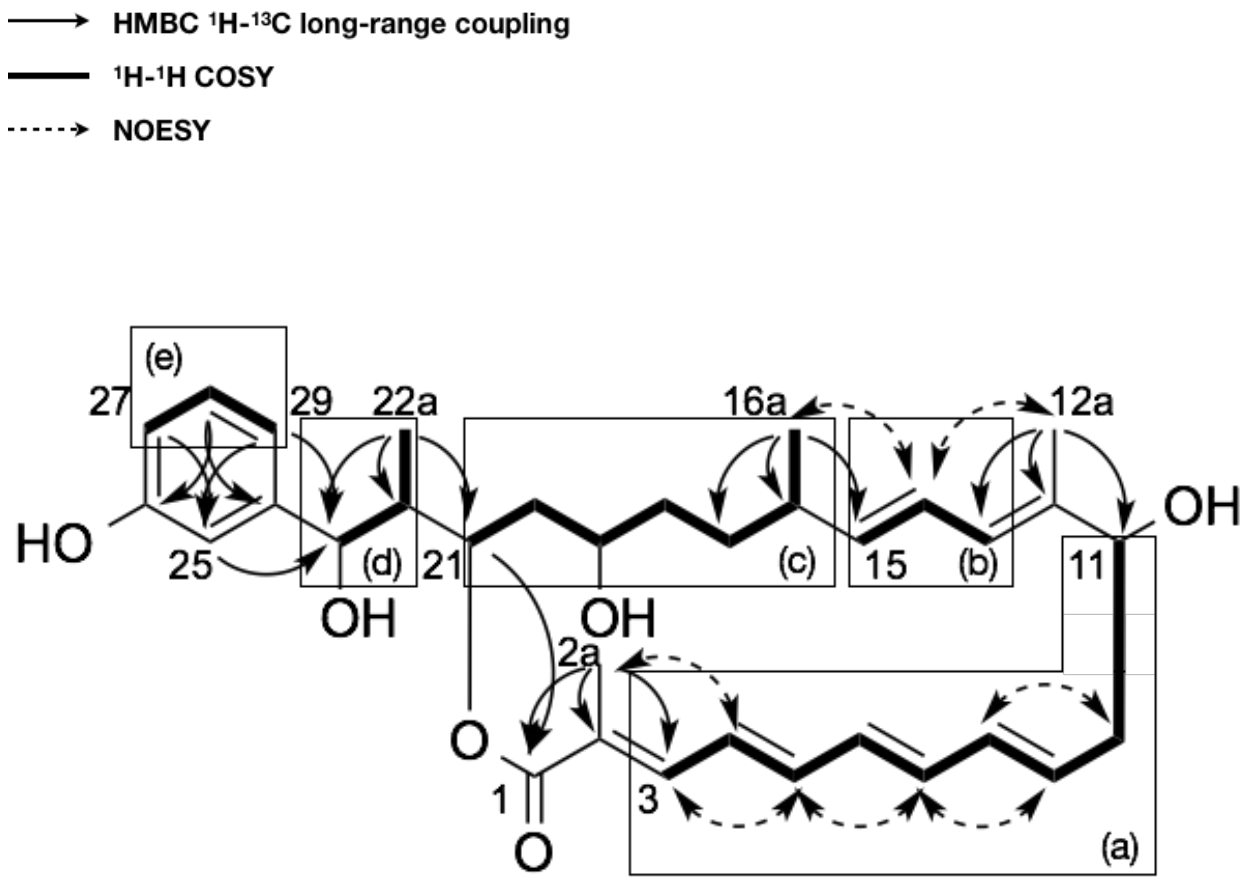

Figure 15. Structure elucidation of antarlide A (**1**) determined by 2D-NMR analysis

2.2.4.2 Antarlides B-F

Antarlides B-F (**2**-**6**) were obtained as a pale yellow powder and these molecular formula were found to be $C_{33}H_{44}O_6$ by high-resolution ESITOFMS. The IR and UV spectrum of **2**-**6** were also similar to those of antarlide A (**1**). Furthermore, the ^{1}H and ^{13}C NMR data of **2**-**6** were also similar to those of **1**. Analysis of the ^{1}H-^{1}H COSY, HMQC, and HMBC data for **2**-**6** led to a planar structure identical to that of **1**. Among the four oxygenated sp^3 methines in **2**-**6**, H-21 showed the low-field shift in **2**-**6** due to the lactone formation, though HMBC correlation from H-21 to C-1 of only antarlide E (**5**) was not observed. These results suggested that **2**-**6** have a 22-membered macrocyclic structure. The double-bond geometries of **2**-**6** were assigned by analysis of NOESY correlations. These results suggested that antarlides A-F (**1**-**6**) are mutually isomeric with respect to the double bond.

The planar structures of antarlides A-F (**1**-**6**) and physico-chemical properties are shown in Figure 16 and Table 2, respectively. In addition, all NMR data of **2**-**6** are shown in Table S1-S5 and Figure S1-S30.

2.2.4.3 Antarlides G, H

Antarlides G,H (**7**,**8**) were obtained as a pale yellow powder. High-resolution ESITOFMS suggested a molecular formula of $C_{33}H_{44}O_6$, which is the same as the molecular formulae of antarlides A-F (**1**-**6**). The IR and UV spectrum of **7** and **8** were also similar to those of **1**-**6**. Furthermore, the ^{1}H and ^{13}C NMR data were also similar to those of **1**-**6**. Analysis of the ^{1}H-^{1}H COSY, HSQC, and HMBC data for **7** and **8** led to a planar structure identical to that of **1**-**6** except for the position of the macrocyclic ring formation. Among the four oxygenated sp^3 methines in the **1**-**6**, H-21 shows the low-field shift in **1**-**6** due to the lactone formation (Table 1, S1-5). However, H-19 shows the low-field shift among the oxymethine protons in **7** and **8** (Table S6, S7). Moreover, HMBC correlation from H-19 to C-1 was observed by using selective HMBC; increased HMBC sensitivity for correlating poorly resolved proton (Figure S36, S43) [41]. Therefore, these results suggested that **7** and **8** have a 20-membered-ring macrocyclic structure, though HMBC correlation from H-19 to C-1 was not observed. The double-bond geometries of **7** and **8** were assigned by analysis of NOESY correlations. These results suggested that **7** and **8** are mutually isomeric with respect to the double bond. These double-bond geometries of **7** and **8** were the same as antarlide E (**5**) and antarlide D (**4**), respectively.

The planar structures of **7** and **8** and physico-chemical properties are shown in Figure 16 and Table 2, respectively. In addition, all NMR data of **7** and **8** are shown in Table S6-S7 and Figure S31-S44.

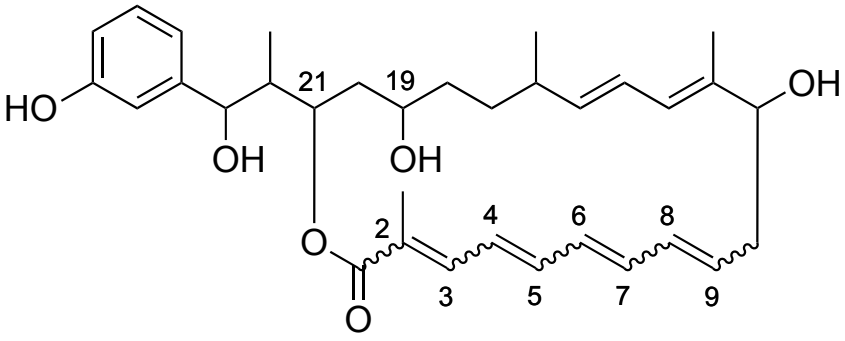

Antarlide

A (**1**) : $\Delta^{2,3} = E, \Delta^{4,5} = E, \Delta^{6,7} = E, \Delta^{8,9} = E$

B (**2**) : $\Delta^{2,3} = E, \Delta^{4,5} = Z, \Delta^{6,7} = E, \Delta^{8,9} = Z$

C (**3**) : $\Delta^{2,3} = E, \Delta^{4,5} = E, \Delta^{6,7} = Z, \Delta^{8,9} = Z$

D (**4**) : $\Delta^{2,3} = E, \Delta^{4,5} = E, \Delta^{6,7} = Z, \Delta^{8,9} = E$

E (**5**) : $\Delta^{2,3} = E, \Delta^{4,5} = Z, \Delta^{6,7} = E, \Delta^{8,9} = E$

F (**6**) : $\Delta^{2,3} = Z, \Delta^{4,5} = E, \Delta^{6,7} = E, \Delta^{8,9} = E$

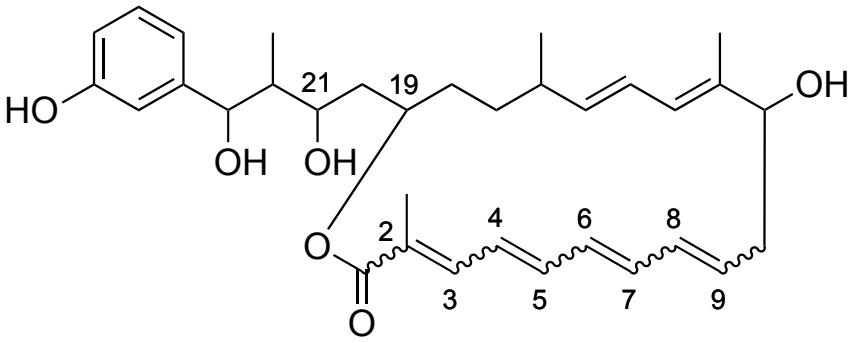

Antarlide

G (**7**) : $\Delta^{2,3} = E, \Delta^{4,5} = Z, \Delta^{6,7} = E, \Delta^{8,9} = E$

H (**8**) : $\Delta^{2,3} = E, \Delta^{4,5} = E, \Delta^{6,7} = Z, \Delta^{8,9} = E$

Figure 16. The structure of antarlides A-H (**1**-**8**)

Table 2. Physico-chemical properties of antarlides A-H (**1**-**8**)

	Antarlide A	Antarlide B	Antarlide C	Antarlide D
Appearance	Pale yellow powder	Pale yellow powder	Pale yellow powder	Pale yellow powder
Molecular formula	$C_{33}H_{44}O_6$	$C_{33}H_{44}O_6$	$C_{33}H_{44}O_6$	$C_{33}H_{44}O_6$
Molecular weight	536	536	536	536
HR-ESITOFMS (*m*/*z*, nega)				
Calcd.	535.3060	535.3060	535.3060	535.3060
Found.	535.3055	535.3068	535.3064	535.3064
Optical rotation $[\alpha]^{22}_D$	+34	+22	+22	+22
	(*c* 1.0, MeOH)	(*c* 1.0, MeOH)	(*c* 1.0, MeOH)	(*c* 1.0, MeOH)
IR ν_{max} (cm^{-1})	3313, 1670	3381, 1676	3379, 1675	3367, 1675
UV λ_{max} (nm) (log ε)	236 (4.59)	240 (4.29)	239 (4.59)	220 (4.15)
in MeOH	337 (4.38)	328 (4.10)	333 (4.39)	320 (3.88)

	Antarlide E	Antarlide F	Antarlide G	Antarlide H
Appearance	Pale yellow powder	Pale yellow powder	Pale yellow powder	Pale yellow powder
Molecular formula	$C_{33}H_{44}O_6$	$C_{33}H_{44}O_6$	$C_{33}H_{44}O_6$	$C_{33}H_{44}O_6$
Molecular weight	536	536	536	536
HR-ESITOFMS (*m*/*z*, nega)				
Calcd.	535.3060	535.3060	535.3060	535.3060
Found.	535.3059	535.3062	535.3061	535.3061
Optical rotation $[\alpha]^{22}_D$	+22	+129	+209	+51
	(*c* 1.0, MeOH)	(*c* 0.1, MeOH)	(*c* 0.1, MeOH)	(*c* 0.1, MeOH)
IR ν_{max} (cm^{-1})	3397, 1675	3393, 1685	3363, 1684	3370, 1685
UV λ_{max} (nm) (log ε)	220 (4.07)	237 (4.56)	235 (4.48)	237 (4.76)
in MeOH	326 (3.83)	332 (4.28)	335 (4.14)	335 (4.35)

2.2.5 Absolute structure elucidation of antarlides

All NMR data in this section are shown in Table S8-S13 and Figure S45-S82.

2.2.5.1 Antarlide A

Instability of antarlides is likely due to the ring strain of the polyolefinic macrocyclic structure. To release the strain to avoid the double bond isomerization, the lactone linkage of antarlide A (**1**) was cleaved by methanolysis with NaOMe in MeOH to yield the methyl ester **9** (Figure 17) [42].

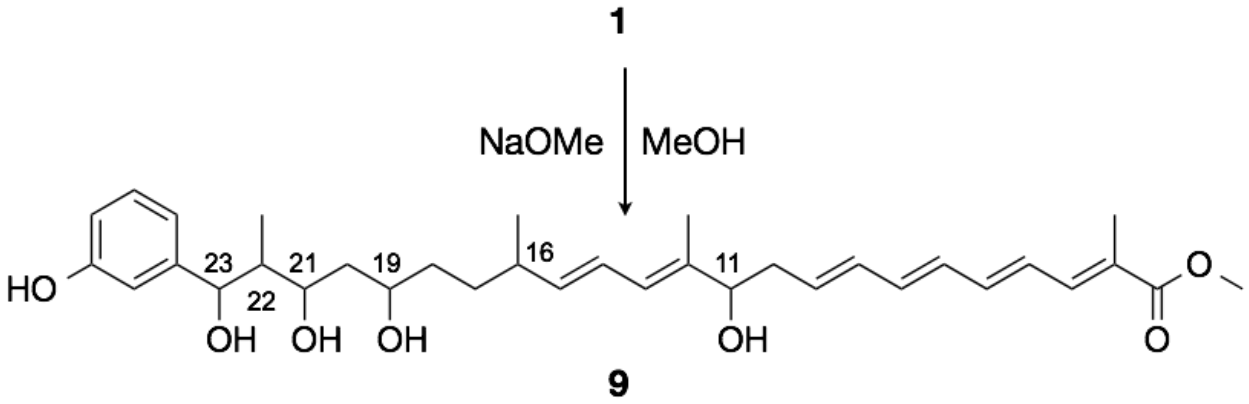

Figure 17. Methanolysis of antarlide A (**1**) to yield ester **9**

The stereochemistry at C-11 and C-19 of **9** were determined by application of the Trost ester NMR method [43]. Condensation of **9** with (*R*)-methoxyphenylacetic acid (*R*-MPA) and (*S*)-methoxyphenylacetic acid (*S*-MPA), yielded the *R*-Trost ester **10a** and *S*-Trost ester **10b**, respectively. Analysis of chemical shift difference ($\Delta\delta_{R\text{-}S}$) between **10a** and **10b** revealed that the absolute configurations of C-11 and C-19 are *R* and *S* (Figure 18). The absolute configurations of C-21 and C-23 in **9** could not be assigned.

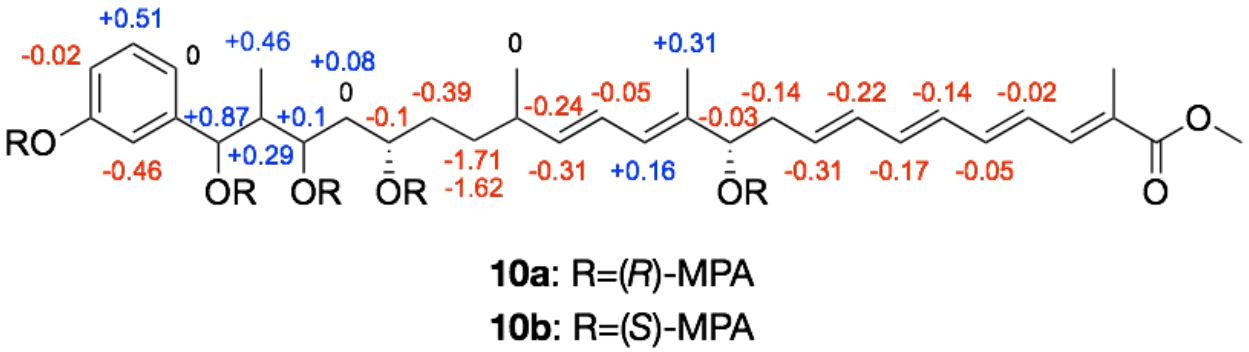

10a: R=(*R*)-MPA
10b: R=(*S*)-MPA

Figure 18. $\Delta\delta_{R\text{-}S}$ values for the Trost esters **10a**/**10b** of **9**

Treatment of **9** with 2,2-dimethoxypropane and pyridinium *p*-toluenesulfonate (PPTS) in acetone yielded the mono-acetone ketal **11**, resulting from ketal formation at the C-19 and C-21 hydroxy groups (Figure 19). ^{13}C chemical shifts of the acetonide methyl groups were observed at δ 19.2 and δ 29.8 (HSQC spectral data), indicating that the six-membered 1,3-dioxane ring was in a chair conformation [44]. The hydroxy groups at C-19 and C-21 were therefore assigned as *syn* and thus the absolute configuration of C-21 is *S*.

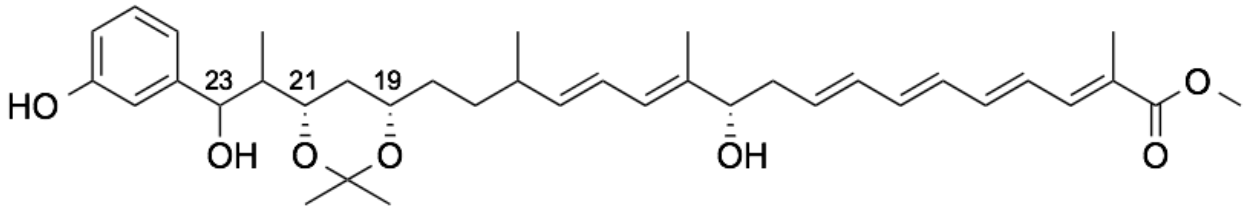

19.2 and 29.8 ppm

11

Figure 19. Acetonide **11** illustrating the ^{13}C NMR chemical shifts of acetonide methyl carbons

Although the absolute configurations at C-22 and C-23 of **1** were not assignable, the relative configuration from C-21 to C-23 of **1** could be determined by NOESY and *J*-based configuration analysis [45]. To elucidate the relative configuration of **1** by the *J*-based method, $^{3}J_{H,H}$ and $^{2}J_{C,H}$ values were obtained from ^{1}H NMR and *J*-resolved HMBC spectra (Figure 20). As for the C-21-C-22 axis, the small coupling constants $^{3}J_{H21,H22}$ = 4.5 Hz and $^{2}J_{C21,H22}$ = 2.2 Hz inferred the *gauche* relationship for oxygen substituent at C-21 and C-22a methyl (Figure 21). Therefore, the absolute configuration of C-22 was established as *R*. Also, the large coupling constants $^{3}J_{H22,H23}$ = 9.0 Hz and $^{2}J_{C23,H22}$ = 6.4 Hz inferred the *anti* relationship for the C-22a methyl and 23-OH groups with regard to the C-22-C-23 axis. The absolute configuration of C-23 was thus determined to be *R*.

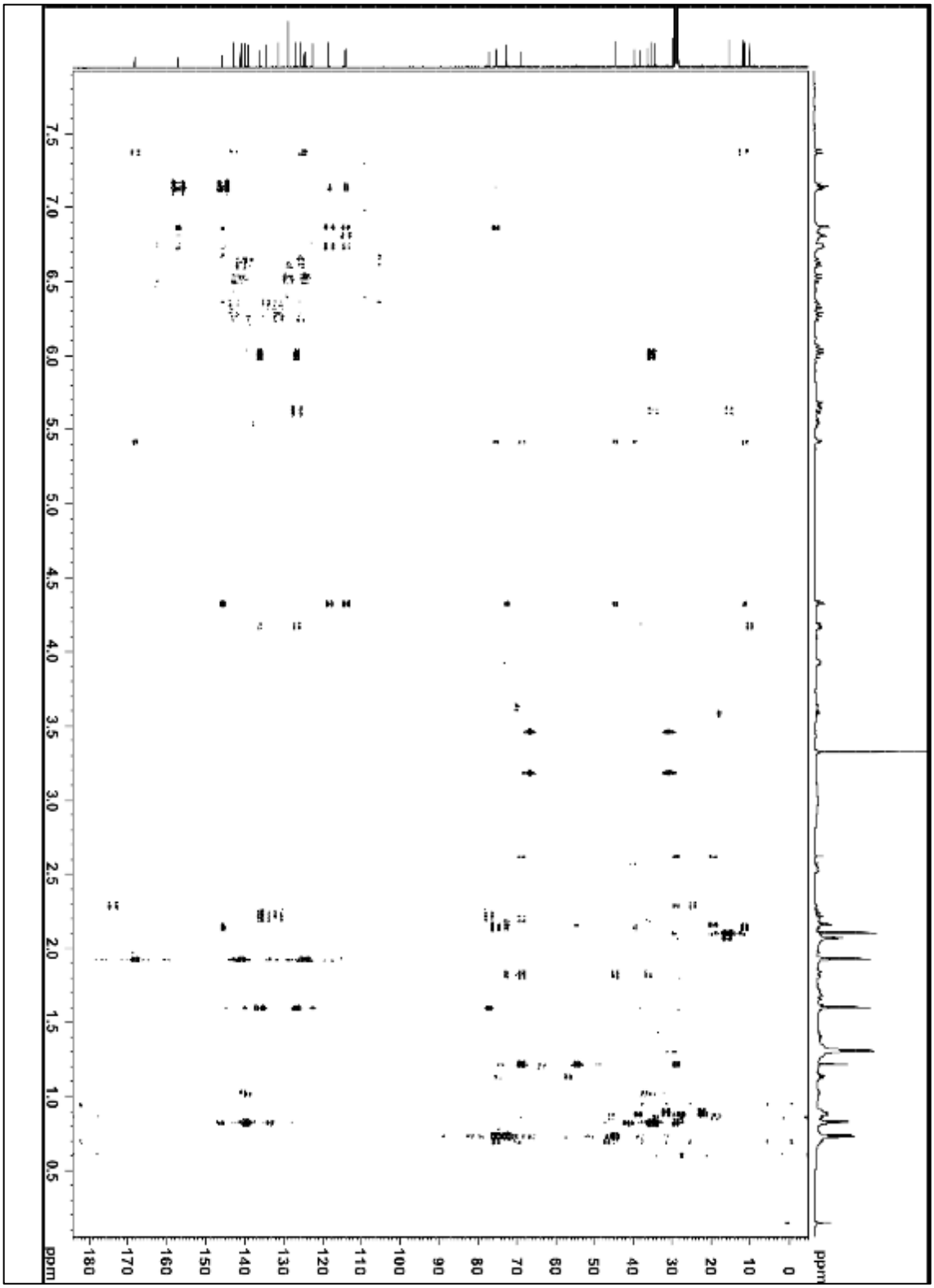

Figure 20. 2D *J*-resolved HMBC spectrum of **1** (500 MHz, Acetone-d_6)

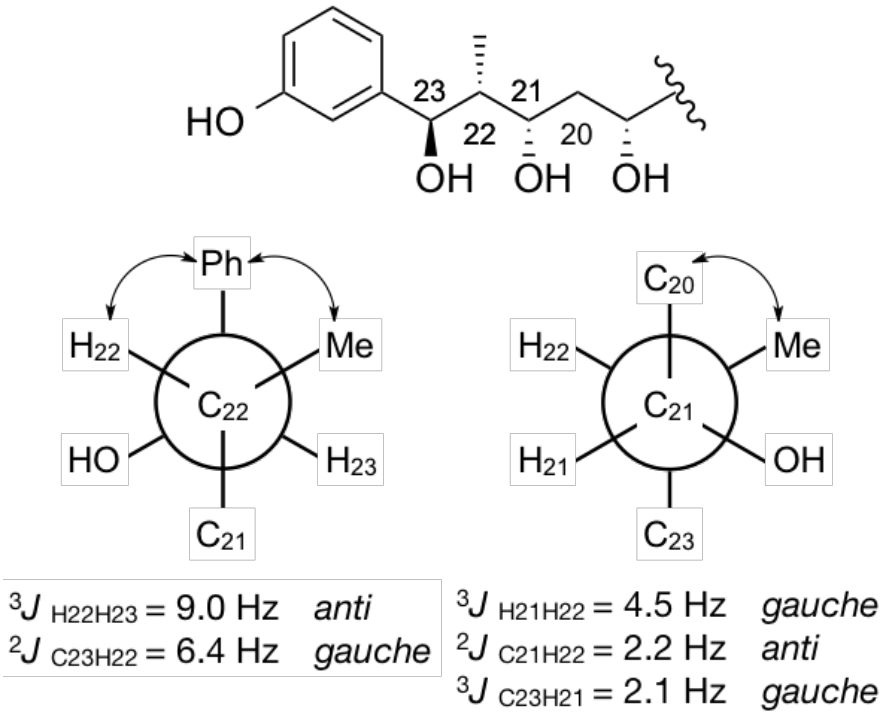

Figure 21. H-H, C-H coupling values and relative configuration determined for C-21-C-23. Arrows showing NOESY correlations

In order to determine the absolute configuration of the remaining C-16 methyl, peracetylated derivative of **9** (**12**) was subjected to oxidative cleavage employing $RuCl_3$ as a catalyst to provide a carboxylic acid **13** [46]. This was then converted to mono-(*R*)- and (*S*)-PGME amides (**14a** and **14b**, respectively) [47]. Analysis of chemical shift differences ($\Delta\delta_{S-R}$) between **14a** and **14b** revealed that the absolute configuration of C-16 is *R* (Figure 22).

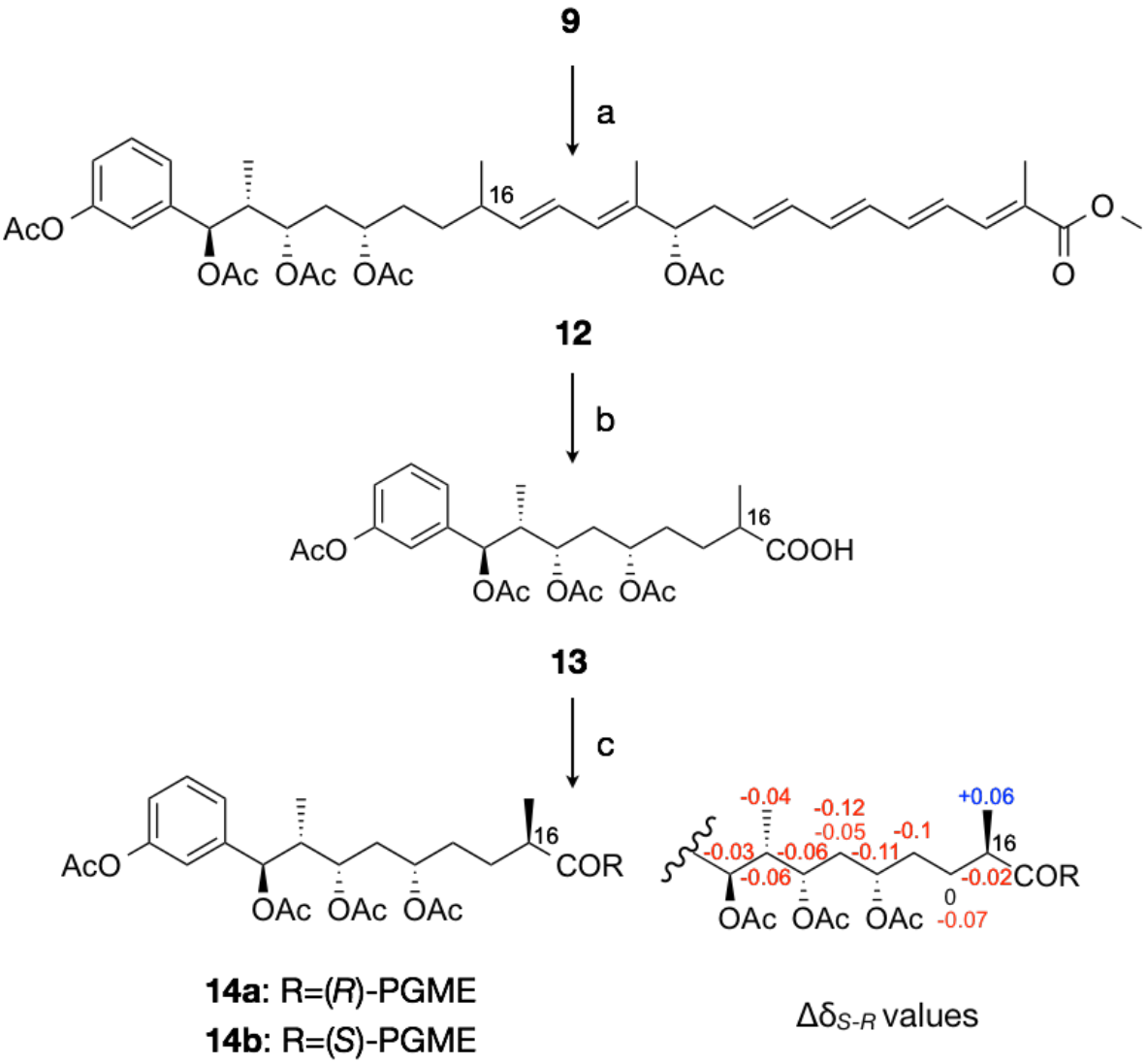

Figure 22. Preparation of compounds **14a/14b** (Reagents and conditions: (a) acetic anhydride, pyridine, room temperature; (b) $NaIO_4$, $RuCl_3$, $MeCN/CCl_4/H_2O$, 0 °C; (c) (*R*,*S*)-PGME, PyBOP, HOBt, triethylamine, dry DMF, room temperature)

2.2.5.2 Antarlides B-F

It is known that the geometric isomerism of *cis-trans* in a polyene system is affected by light [48]. When methanol solutions of antarlides B-F (**2**-**6**) were exposed to room light in a capped clear eppendorf, these compounds isomerized to antarlide A (**1**) within 2 hour (Figure 23). Based on this observation, as well as on the fact that **1** is the main product in the culture, it is conceivable that the strain produces **1** as a 'natural product', which then isomerizes to other congeners during bacterial cultivation and/or compound isolation. The asymmetric centers in **2**-**6** are most likely to have the same absolute configurations as that of **1** (Figure 24).

a) b)

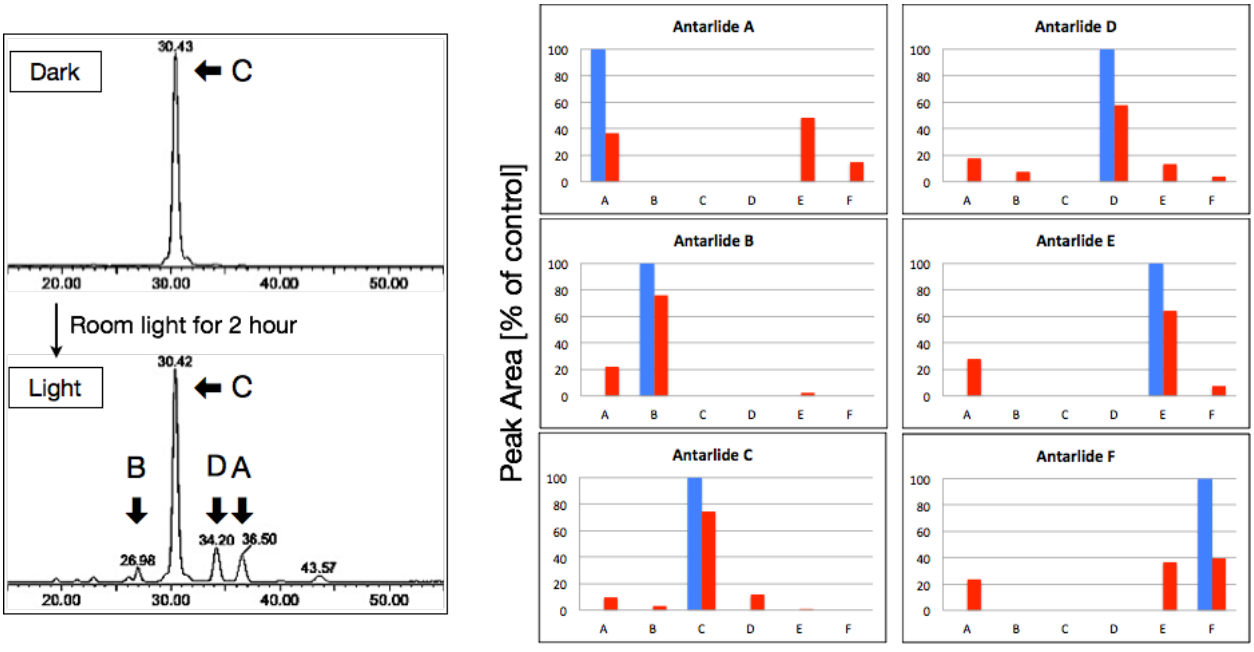

Figure 23. Photoisomerization of antarlides A-F (**1**-**6**)

(a) PDA chromatogram of antarlide C (**3**) which is not exposed to the room light (top). PDA chromatogram of **3** which is exposed to the room light for 2 hour (bottom). (b) Peak area of **1**-**6** (blue front : light shielding, red front : light irradiation).

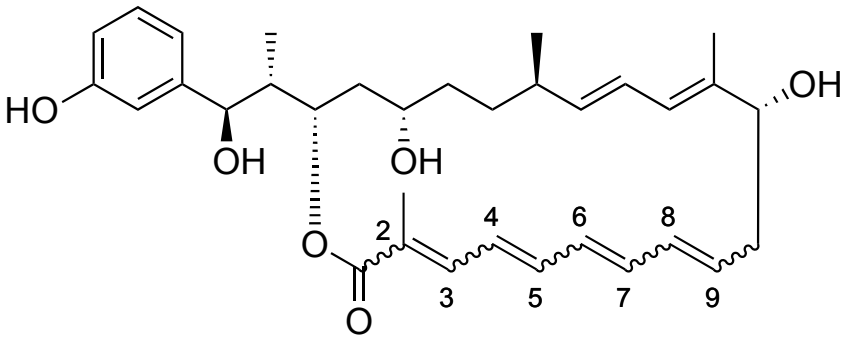

Antarlide

A (**1**) : $\Delta^{2,3} = E, \Delta^{4,5} = E, \Delta^{6,7} = E, \Delta^{8,9} = E$

B (**2**) : $\Delta^{2,3} = E, \Delta^{4,5} = Z, \Delta^{6,7} = E, \Delta^{8,9} = Z$

C (**3**) : $\Delta^{2,3} = E, \Delta^{4,5} = E, \Delta^{6,7} = Z, \Delta^{8,9} = Z$

D (**4**) : $\Delta^{2,3} = E, \Delta^{4,5} = E, \Delta^{6,7} = Z, \Delta^{8,9} = E$

E (**5**) : $\Delta^{2,3} = E, \Delta^{4,5} = Z, \Delta^{6,7} = E, \Delta^{8,9} = E$

F (**6**) : $\Delta^{2,3} = Z, \Delta^{4,5} = E, \Delta^{6,7} = E, \Delta^{8,9} = E$

Figure 24. The gross structure of antarlides A-F (**1**-**6**)

2.2.6 Biological activities of antarlides

2.2.6.1 AR-[^{3}H] DHT *in vitro* binding assay, ER-[^{3}H] Estradiol *in vitro* binding assay

Antarlides A-H (**1**-**8**) were tested for their AR-DHT binding inhibition activities *in vitro*. They inhibited the binding of AR-DHT in a dose-dependent manner. Their IC_{50} values were *ca*. 16 μM (Table 3). Furthermore, these inhibitory activities were equal to that of hydroxyflutamide (IC_{50} 18 μM), which is the major active metabolite of flutamide (Figure 25). On the other hand, **1**-**8** did not show inhibitory activity against estrogen receptor (ER)-estradiol binding at up to 100 μM (Table 3). These data suggested that **1**-**8** specifically block the binding of androgen to the ligand-binding domain of AR *in vitro*. Moreover, these data suggested that the double-bond geometries and the ring size of the **1**-**8** have no effect on the binding to AR and ER. Interestingly, the methyl ester **9** from antarlide A (**1**) did not show inhibitory activity against AR-DHT binding at up to 20 μM. These data suggested that the macrocyclic structure of the **1**-**8** is necessary to bind to AR.

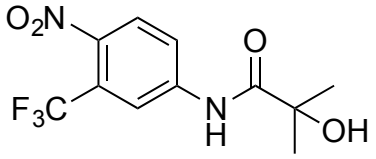

Figure 25. The structure of hydroxylflutamide

Table 3. IC_{50} values (μM) for **1**-**9** inhibition of binding of DHT to the AR or estradiol to the ER

Compound	**1**	**2**	**3**	**4**	**5**	**6**	**7**	**8**	**9**	Hydroxy flutamide
AR	20	15	14	14	18	15	15	14	> 20	18
ER	>100	>100	>100	>100	>100	> 100	>100	>100	> 100	>100

2.2.6.2 Effect of antarlides B and G on DHT-induced PSA mRNA and cell growth

Among the 22-membered-ring or 20-membered-ring antarlides, antarlide B (**2**) or antarlide G (**7**) is more stable (Figure 23b), therefore, AR antagonist activities against prostate cancer cells were evaluated by using **2** and **7**.

Prostate-specific antigen (PSA) is a 33-kDa serine protease, whose expression is triggered by androgen-mediated action of the AR [49]. As shown in Figure 26a, **2** and **7** inhibited DHT-induced expression of endogenous PSA mRNA in LNCaP cells with an IC_{50} value of 0.18 μM and 0.24 μM, respectively. Furthermore, **2** and **7** were found to inhibit DHT-induced cell growth in LNCaP cells with an IC_{50} value of 0.31 μM and 0.53 μM, respectively (Figure 26b). These AR antagonist activities of **2** and **7** were superior to the respective activities of hydroxyflutamide (IC_{50} 1.3, 1.2 μM).

On the other hand, **2** and **7** did not show the cytotoxic effects in PC3 cells, androgen-independent prostate cancer cells, at the concentration which **2** and **7** show AR antagonist activity against LNCaP cells (Figure 26c). These data indicated that antarlides shows antagonist activity by inhibiting the function of AR.

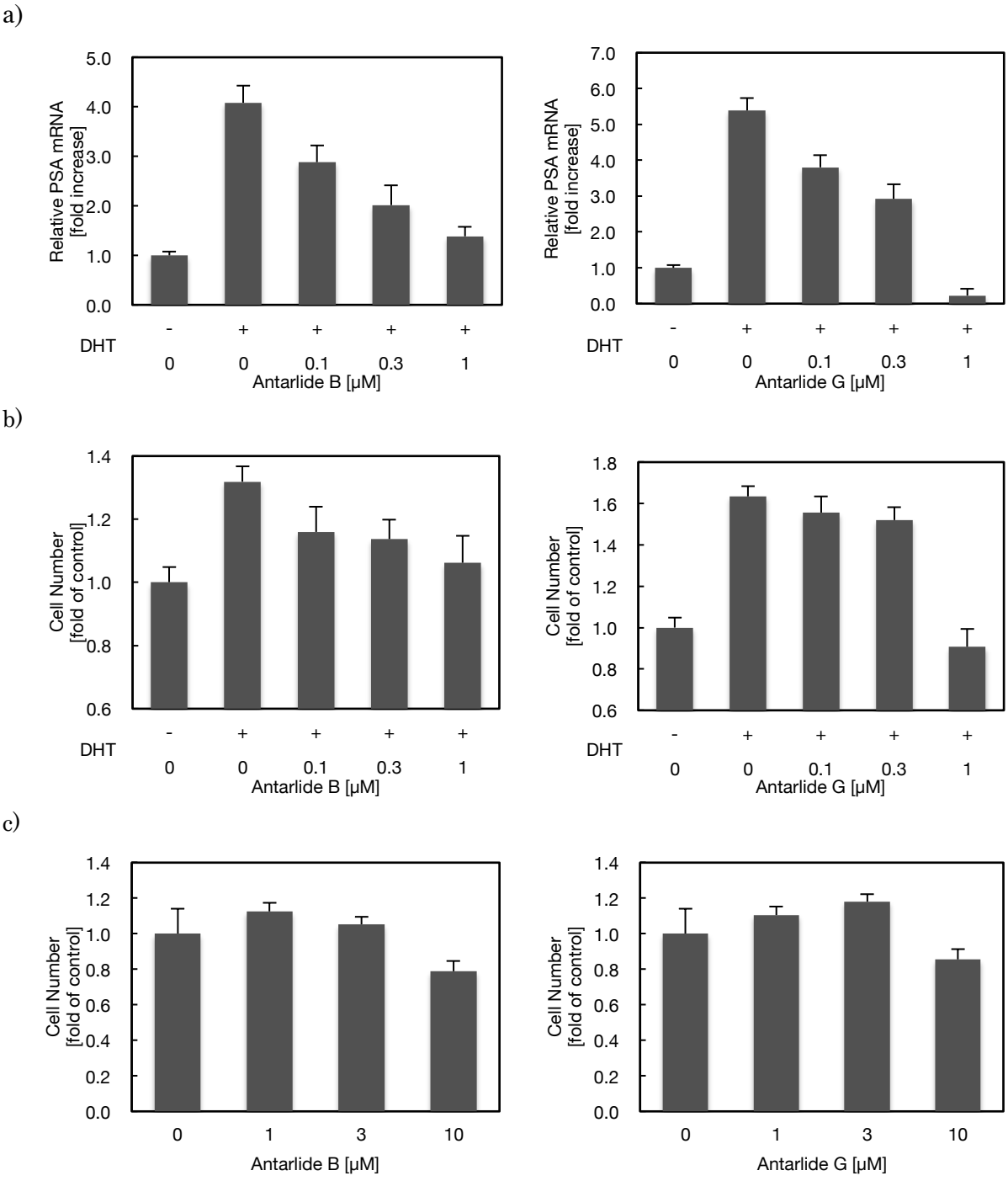

Figure 26. Effect of antarlide B (**2**) and G (**7**) on DHT-induced PSA mRNA (a), DHT-dependent cell growth in LNCaP cells (b) and DHT-independent cell growth in PC3 cells (c)

2.2.6.3 Effect of antarlides B and G on transcriptional activity of wild type or mutant AR

The emergence of a mutant AR has been shown to link to resistance to first- and second-generation AR antagonists (T877A for flutamide resistance, W741C for bicalutamide resistance and F876L for enzalutamide resistance). Therefore, we next evaluated whether antarlides are capable of inhibiting the activity of these mutant ARs. The effects of anti-androgens on mutants AR (F876L), AR (W741C), and AR (T877A) were studied in transactivation assays in HEK293T cells transiently transfected with expression vectors encoding the corresponding mutant ARs and an androgen-responsive luciferase reporter gene construct. As shown in Figure 27a, hydroxyflutamide inhibited DHT-induced transcriptional activity of wild type AR, AR (F876L) and AR (W741C), but not that of hydroxyflutamide-resistant AR (T877A). Similarly, bicalutamide or enzalutamide inhibited DHT-induced transcriptional activity of all AR except its corresponding mutant AR. On the other hand, antarlide B (**2**) inhibited this transcriptional activity not only of the wild type AR but also of all mutant ARs that we tested at 1 μM. In addition, antarlide G (**7**) also inhibited this transcriptional activity not only of the wild type AR but also of mutant AR (F876L) (Figure 27b). These data suggested that antarlides could overcome resistance to first- and second- generation AR antagonists.

a)

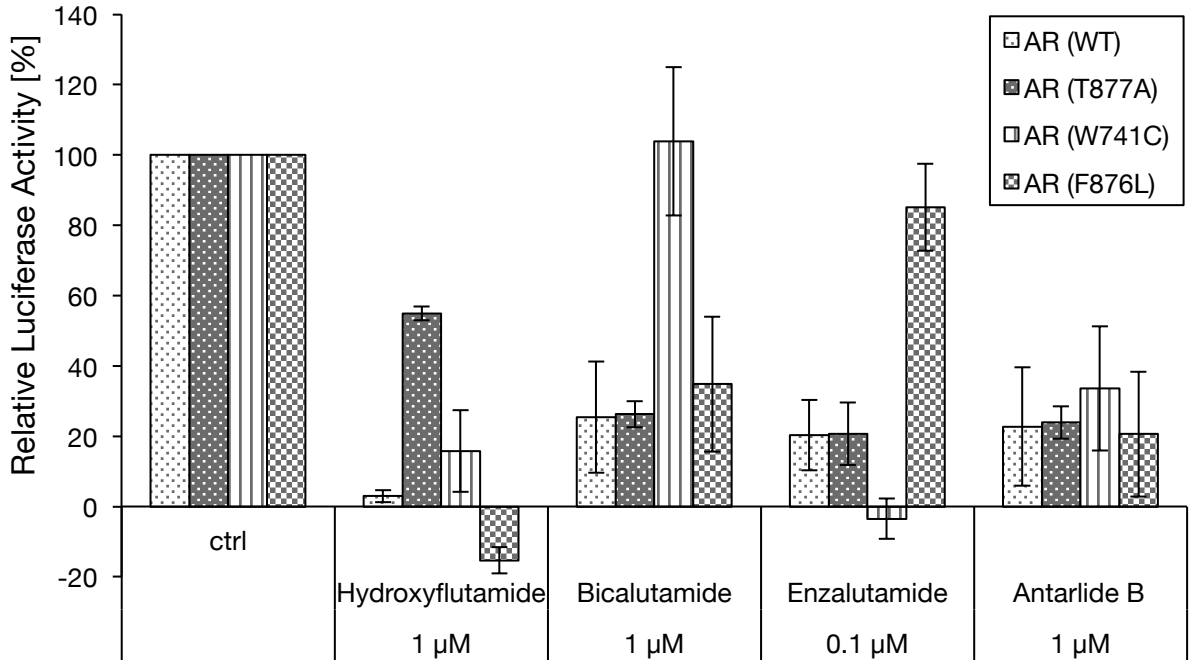

b)

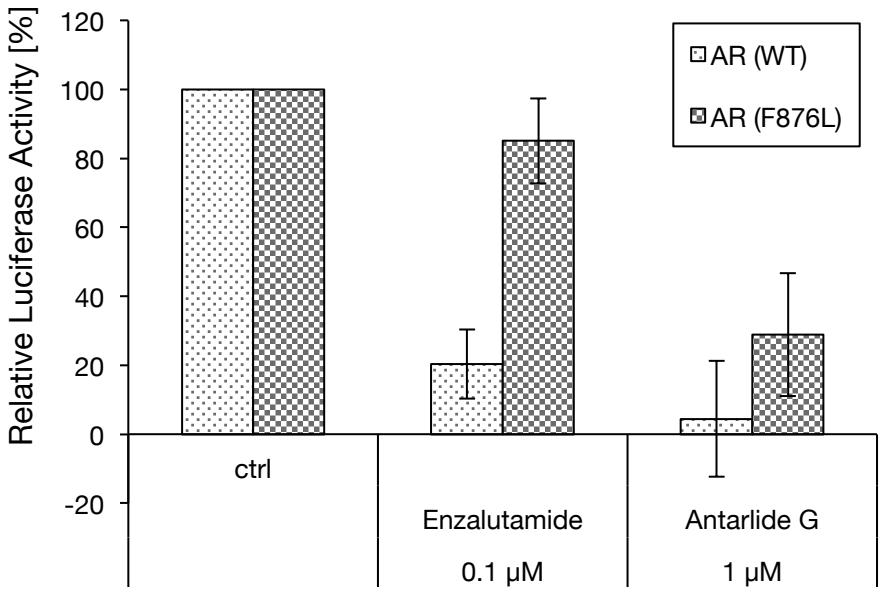

Figure 27. Effect of antarlide B (**2**) (a) and antarlide G (**7**) (b) on transcriptional activity of wild type or mutant AR

2.2.6.4 Effect of antarlides B and G on nuclear translocation of wild type and mutant AR

Next, we examined the effect of antarlides B (**2**) and G (**7**) on the nuclear translocation of wild type and mutant AR. For this, wild type GFP-AR or mutant GFP-AR (F876L) was overexpressed in HEK293T cells, and their subcellular localizations were observed with confocal microscopy. As shown in Figure 28, wild type AR and mutant AR (F876L) were predominantly cytoplasmic in the absence of DHT, while treatment of cells with 100 nM DHT for 1 hour induced nuclear translocation of AR. As it has been reported that the F876L substitution in AR switches enzalutamide from an antagonist to an agonist, treatment of cells with enzalutamide alone for 1 hour induced nuclear translocation of mutant AR (F876L). In this condition, **2** and **7** failed to induce nuclear translocation not only of the wild type AR but also of mutant AR (F876L). These results indicated that **2** and **7** do not act as an agonist in enzalutamide-resistant cells.

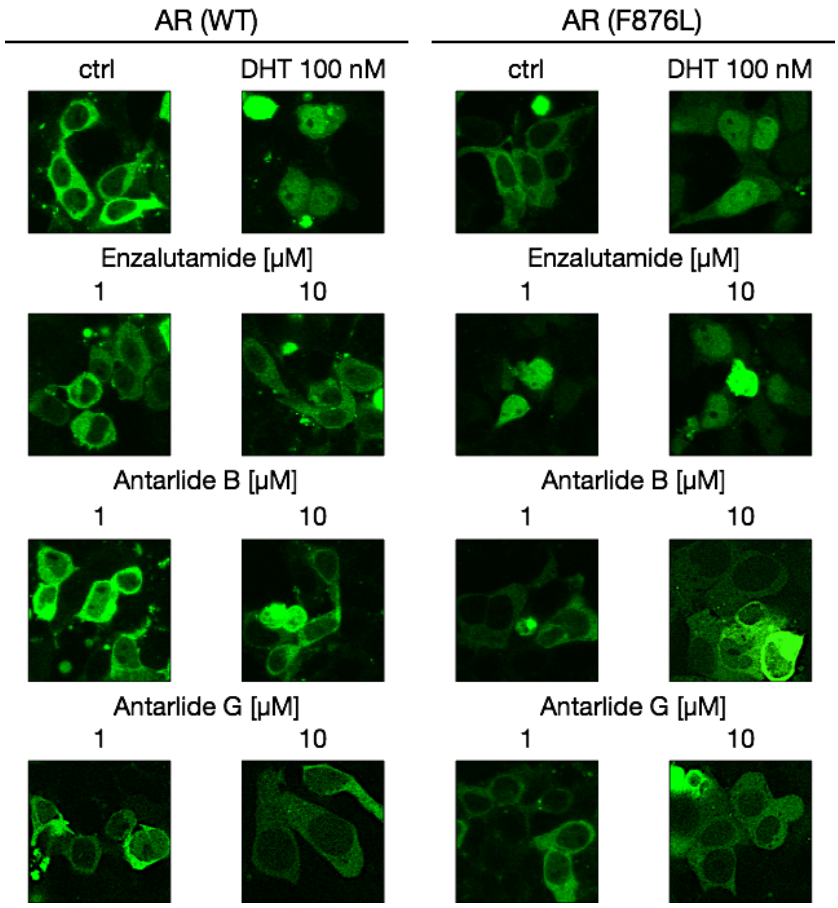

Figure 28. Effect of antarlides B (**2**) and G (**7**) on nuclear translocation of wild type and mutant AR (F876L)

2.3 Experimental procedures

General Experimental Procedures

Antarlide A (1) Optical rotation was measured using a JASCO DIP-3000 polarimeter. UV spectrum was recorded on a Hitachi U-3210 spectrophotometer. IR spectrum was measured on a Perkin-Elmer Spectrum 100. NMR spectra were obtained on a Bruker AVANCE 500 spectrometer. HR-ESITOFMS was recorded on a Bruker microTOF focus.

Antarlides B-E (2-5) Optical rotation was measured using a JASCO DIP-3000 polarimeter. UV spectrum was recorded on a Hitachi U-3210 spectrophotometer. IR spectrum was measured on a JASCO RT/IR-4200. NMR spectra were obtained on a JEOL JNM-ECA500 spectrometer. HR-ESITOFMS was recorded on a Bruker microTOF focus.

Antarlides F-H (6-8) Optical rotation was measured using a JASCO P-1020 polarimeter. UV spectrum was recorded on a Beckman DU530 UV/VIS spectrophotometer. IR spectrum was measured on a JASCO RT/IR-4200. NMR spectra were obtained on a Bruker AVANCE 500 spectrometer (antarlide G (**7**)) or JEOL JNM-ECA500 spectrometer (antarlides F and H (**6** and **8**)). Selective HMBC spectra were obtained on a JEOL JNM-ECZ600R spectrometer with Ultra COOL probe (antarlide G and H (**7** and **8**)). HR-ESITOFMS was recorded on a LCT premier EX spectrometer (Waters Corporation, Milford, MA, USA).

9-14a/14b NMR spectra were obtained on a Bruker AVANCE 500 spectrometer. HR-ESITOFMS was recorded on a Bruker microTOF focus.

Producing microorganism

The taxonomic characterization of strain BB47 was described previously [40].

Fermetation

Strain BB47 cultured on a Bn-2 agar medium [soluble starch 0.5%, glucose 0.5%, meat extract (Kyokuto Pharmaceutical Industrial Co., Ltd., Tokyo, Japan) 0.1%, yeast extract (Difco Laboratories, Sparks, MD, USA) 0.1%, NZ-case (Wako Pure Chemical Industries, Ltd., Osaka, Japan) 0.2%, NaCl 0.2%, $CaCO_3$ 0.1% and agar 1.5%] was inoculated into 500 mL Erlenmeyer flasks each containing 100 mL of the V-22 seed medium [soluble starch 1%, glucose 0.5%, NZ-case 0.3%, yeast extract 0.2%, tryptone (Difco Laboratories, Sparks, MD, USA) 0.5%, K_2HPO_4 0.1%, $MgSO_4 \cdot 7H_2O$ 0.05%, and $CaCO_3$ 0.3% (pH 7.0)]. The flasks were shaken on a rotary shaker (170 rpm) at 30°C for 4 days. The seed culture (3 mL) was transferred into 500 mL Erlenmeyer flasks each containing 100 mL of the A3MP production medium [A3M production medium (glucose 0.5%, glycerol 2%, soluble starch 2%, pharmamedia (Archer Daniels Midland Company, Lubbock, IL, USA) 1.5%, yeast extract 0.3%, HP-20 (Mitsubishi Chemical Co., Kanagawa, Japan) 1%) mixed with Na_2HPO_4 1%]. The pH of the medium was adjusted to 8.0 before sterilization. The flasks were shaken on a rotary shaker (170 rpm) at 30°C for 6 days.

Extraction and Isolation

Antarlides A-E (1-5) At the end of the fermentation period, 100 mL of EtOAc was added to each flask, and the mixtures were shaken for 1 hour. The mixture was centrifuged at 5000 rpm for 10 min, and the organic layer was separated from the aqueous layer containing the mycelium. Evaporation of the solvent gave 1.9 g of extract from 10 L of culture. The crude extract (1.9 g) was partitioned between 10% aqueous MeOH (1 L) and *n*-hexane (1 L×2), the former of which was further separated between EtOAc (1 L) and H_2O (pH 10) (1 L×2). The EtOAc-soluble fraction (854 mg) was fractionated by centrifugal liquid-liquid partition chromatography (CPC; Senshu Scientific Co., Ltd., Tokyo, Japan, CPC240 apparatus) with $CHCl_3$-MeOH-H_2O (pH 9)

(5:6:4, lower phase stationary). The active stationary phase (372 mg) was repeatedly purified by reversed-phase C30 column (Develosil C30-UG-5; Nomura Chemical Co., Ltd., Aichi, Japan) chromatography with MeCN/H_2O (1:1). The fraction containing antarlides A-E (**1**-**5**) was evaporated, and the remaining aqueous solution was extracted with EtOAc. The organic layer was then concentrated to give a **1** (55.2 mg), **2** (13.8 mg), and **3** (17.7 mg). Final purification was achieved by preparative C30 column chromatography with MeCN/H_2O (9:11). The fraction containing **4** or **5** was evaporated, and the remaining aqueous solution was extracted with EtOAc. The organic layer was then concentrated to give a **4** (13.8 mg), **5** (4.6 mg). Note that all isolation steps were carried out in dark, because **1**-**5** are unstable under room light.

Antarlides F-H (6-8) At the end of the fermentation period, 100 mL of EtOAc was added to each flask, and the mixtures were shaken for 1 hour. The mixture was centrifuged at 5000 rpm for 10 min, and the organic layer was separated from the aqueous layer containing the mycelium. Evaporation of the solvent gave 3.9 g of extract from 12 L of culture. The crude extract (3.9 g) was partitioned between 10% aqueous MeOH (1.5 L) and *n*-hexane (1.5 L×3), the former of which was further separated between EtOAc (1.5 L) and H_2O (pH 10) (1.5 L×3). The EtOAc-soluble fraction (1.6 g) was fractionated by centrifugal liquid-liquid partition chromatography (CPC; Senshu Scientific Co., Ltd., Tokyo, Japan, CPC240 apparatus) with $CHCl_3$-MeOH-H_2O (pH 9) (5:6:4, lower phase stationary). The active stationary phase (737 mg) was repeatedly purified by reverse-phase C30 column (Develosil C30-UG-5; Nomura Chemical Co., Ltd., Aichi, Japan) chromatography with MeCN/H_2O (11:9). The fraction containing antarlides F-H (**6**-**8**) was evaporated, and the remaining aqueous solution was extracted with EtOAc. The organic layer was then concentrated. Final purification was achieved by preparative C30 column chromatography with MeOH/H_2O (3:1). The fraction containing **6**-**8** was evaporated, and the remaining aqueous solution was extracted with EtOAc. The organic layer was then

concentrated to give a **6** (2.2 mg), **7** (1.6 mg), and **8** (1.0 mg). Note that all isolation steps were carried out in the dark, because **6**-**8** are unstable under room light.

Methanolysis of 1 to yield ester 9

Antarlide A (**1**, 5.0 mg, 9.3 μmol) was dissolved in 5% NaOMe in MeOH 5 mL and stirred for 30 min with ice cooling. The reaction mixture was neutralized with 1 M aqueous HCl, and the aqueous phase was extracted with EtOAc to yield compound **9** (3.0 mg) : for ^{1}H and ^{13}C NMR data, see Table S8; HR-ESITOFMS (*m/z*) $[M-H]^-$ calcd for $C_{34}H_{47}O_7$, 567.3327; found, 567.3335.

Trost MPA esters of 9 (10a and 10b)

To a solution of **9** (2.0 mg, 3.7 μmol) in dichloromethane (240 μL) and *N*,*N*'-diisopropylcarbodiimide (DIC) (7 μL, 5.6 mg, 44 μmol) was added *N*,*N*-dimethyl-4-aminopyridine (DMAP) (1.4 mg, 12 μmol) and (*R*)-methoxyphenylacetic acid (*R*-MPA) (5.8 mg, 35 μmol) at room temperature. After 1 hour, the reaction mixture was extracted with EtOAc, and the residue after solvent removal was purified by reversed-phase C18 column (XTerra $RP_{18,}$; Waters Corporation, Milford, MA, USA) chromatography with MeCN-H_2O (10 mM NH_4CO_3) (7:3) to yield (*R*)-Trost ester (**10a**): for ^{1}H and ^{13}C NMR data, see Table S9; HR-ESITOFMS (*m/z*) $[M+Na]^+$ calcd for $C_{79}H_{88}NaO_{17}$, 1331.5913; found, 1331.5910. In the same manner as described for **10a**, **10b** was prepared from **6** and (*S*)-methoxyphenylacetic acid (*S*-MPA). : for ^{1}H and ^{13}C NMR data, see Table S9; HR-ESITOFMS (*m/z*) $[M+Na]^+$ calcd for $C_{79}H_{88}NaO_{17}$, 1331.5913; found, 1331.5909.

Mono-acetonide 11.

To a solution of **9** (6.0 mg, 11 μmol) in 2,2-dimethoxypropane (3 mL) and acetone (3 mL) was

added pyridinium-*p*-toluenesulfonate (PPTS) (3.0 mg, 12 μmol) at 4 °C. After standing overnight, a saturated solution $NaHCO_3$ was added to quench the reaction, and extracted with EtOAc. The residue after solvent removal was fractionated by silica gel column chromatography (*n*-hexane-EtOAc) to provide compound **11** (1.6 mg). : for ^1H and ^{13}C NMR data, see Table S10; HR-ESITOFMS (*m/z*) $[M-H]^-$ calcd for $C_{37}H_{51}O_7$, 607.3640; found, 607.3630.

Acetylation of 12

To a solution of **9** (2.5 mg, 4.4 μmol) in pyridine (0.25 mL) was added Ac_2O (0.25 mL) at room temperature. After standing overnight, 0.5 M HCl was added to quench the reaction, and extracted with EtOAc to yield compound **12**. : for ^1H and ^{13}C NMR data, see Table S11; HR-ESITOFMS (*m/z*) $[M+Na]^+$ calcd for $C_{44}H_{58}Na_1O_{12}$, 801.3820; found, 801.3812.

Oxidative degradation of 12 to yield 13

To a solution of **12** (2.5 mg, 3.2 μmol) in MeCN/CCl_4/H_2O (0.75 mL, each 0.25 mL) was added $NaIO_4$ (25 mg, 0.12 mmol) and a solution of $RuCl_3$ in 0.1 M Na_2HPO_4 solution (1.0 mg/mL, 0.25 mL, 1.2 μmol) at 0-5°C. After stirring overnight, a saturated solution $Na_2S_2O_3$ (1 mL) was added to quench the reaction, and 1 M HCl (75 μL) was then added and extracted with EtOAc. The organic layer was concentrated, and crude compound **13** (2.0 mg) was obtained. : for ^1H and ^{13}C NMR data, see Table S12; HR-ESITOFMS (*m/z*) $[M-H]^-$ calcd for $C_{25}H_{34}O_{10}$, 493.2079; found, 493.2074.

(*R*)- and (*S*)-PGME amides of 13 (14a and 14b).

To a solution of **13** (1.0 mg, 2.0 μmol) in dry *N*,*N*-dimethylformamide (DMF) (80 μL) and triethylamine (80 μL) was added (*R*)-phenylglycine methyl ester (*R*-PGME) (1.6 mg, 7.9 μmol),

benzotriazolyloxy-tris[pyrrolidino]-phosphonium hexafluorophosphate (PyBOP) (3.8 mg, 7.3 μmol) and 1-hydroxybenzotriazole (HOBt) (1.0 mg, 7.4 μmol) at room temperature. After standing for 3 hour, the reaction mixture was extracted with EtOAc, and the residue after solvent removal was purified by reversed-phase C18 column (COSMOSIL $5C_{18}$-AR-II ; Waters Corporation, Milford, MA, USA) chromatography with MeCN-H_2O (15:85 to 85:15 over 35 min). Evaporation of the collected fraction and extraction with EtOAc gave (*R*)-PGME amide (**14a**). : for ^{1}H and ^{13}C NMR data, see Table S13; HR-ESITOFMS (*m/z*) $[M-H]^-$ calcd for $C_{34}H_{42}NO_{11}$, 640.2763; found, 640.2761. In the same manner as described for **14a**, **14b** was prepared from **13** and (*S*)-phenylglycine methyl ester (*S*-PGME). : for ^{1}H and ^{13}C NMR data, see Table S13; HR-ESITOFMS (*m/z*) $[M-H]^-$ calcd for $C_{34}H_{42}NO_{11}$, 640.2763; found, 640.2770.

Photoisomerization of antarlides A-H (1-8)

A solution of antarlides A-H (**1**-**8**) (0.5 mg/mL) in MeOH was exposed to room light (32 W) in a capped clear eppendorf. After 2 hour irradiation, each solution was analyzed by a liquid chromatography (LC)-photodiode array (PDA)-MS system (Waters Corporation, Milford, MA, USA) with a photodiode array detector (2996) and mass analyzer (Micromass ZQ; Waters Corporation, Milford, MA, USA). From retention time of **1**-**8**, peak area of these compounds within 2 hour were quantified.

Materials

Dihydrotestosterone (DHT), flutamide and hydroxyflutamide were purchased from Sigma Chemical Co. (St. Louis, MO, USA). Bicalutamide was obtained from LKT Laboratosries, Inc. (St. Paul, MN, USA). Enzalutamide was obtained from AdooQ Bio Science (Irvine, CA, USA). The human AR cDNA plasmid, pTri-AR was provided by Kazuhisa Minamiguchi (Hannno

Research Center, Taiho Pharmaceutical Co., Ltd, Saitama, Japan). All mutant AR constructs were generated from pTri-AR by the inverse PCR method. The luciferase reporter constructs, PSA enhancer/promoter-Luc, was provided by Hiroyuki Seimiya (Division of Molecular Biotherapy Center, Japanese Foundation for Cancer Research, Tokyo, Japan).

Cell culture

A human prostate cancer cell line LNCaP, PC3 and a human embryonic kidney cell line HEK293T cells were cultured in RPMI media (Nissui, Ohita, Japan) supplemented with 10% fetal bovine serum, 100 U/ml penicillin G, and 0.1 mg/mL kanamycin at 37°C in a humidified 5% CO_2 atmosphere.

AR-[^{3}H] DHT *in vitro* binding assay

The gene sequence corresponding to the ligand-binding domain (LBD, 609-919 amino acids) in the C-terminus of AR was expressed in *Escherichia coli* strain DH5α as a maltose-binding protein-fused protein (MBP-LBD), followed by purification using amylose resin (Bio-Rad Laboratories, Hercules, CA, USA). Thus, the obtained recombinant MBP-LBD (50 μg/mL), [^{3}H] DHT (2 nM) and test samples were incubated at 4°C for 3 hour. Then, [^{3}H] DHT-bound MBP-LBD was precipitated with hydroxyapatite and radioactivity was measured with a liquid scintillation counter.

ER-[^{3}H] Estradiol *in vitro* binding assay

The gene sequence corresponding to the ligand-binding domain (LBD, 301-551 amino acids) in the C-terminus of ER was expressed in *Escherichia coli* strain DH5α as a maltose-binding protein-fused protein (MBP-LBD), followed by purification using amylose resin (Bio-Rad

Laboratories, Hercules, CA, USA). Thus, the obtained recombinant MBP-LBD (50 μg/mL), [^{3}H] Estradiol (1 nM) and test samples were incubated at 4°C for 15 min. Then, [^{3}H] Estradiol-bound MBP-LBD was precipitated with hydroxyapatite and radioactivity was measured with a liquid scintillation counter.

Real-time RT-PCR

LNCaP cells were plated at 5×10^4 cells/well onto 24-well plate and incubated in RPMI 1640 medium supplemented with 2% charcoal-stripped serum for 24 hour. The cells were then treated with DHT (1 nM) and test samples. After 12 hour, RNA from the cells was isolated, and the expression of PSA genes was determined by real-time quantitative reverse transcription PCR, and normalized to GAPDH mRNA.

DHT-dependent cell growth

LNCaP cells were plated at 1×10^4 cells/well onto 48-well plate and incubated in RPMI 1640 medium supplemented with 2% charcoal-stripped serum for 24 hour. The cells were then treated with DHT (1 nM) and test samples. After 72 hour, cell proliferation was evaluated by crystal violet staining method.

DHT-independent cell growth

PC3 cells were plated at 0.5×10^4 cells/well onto 48-well plate and incubated in RPMI 1640 medium supplemented with 10% fetal bovine serum for 24 hour. The cells were then treated with test samples. After 72hour, cell proliferation was evaluated by crystal violet staining method.

Luciferase reporter assay

HEK293T cells were plated at 35×10^4 cells/well onto 6-well plate and incubated in RPMI media supplemented with 10% fetal bovine serum for 24 hour. The cells were transfected with 0.1 μg of pTri-AR expression construct, 1 μg of PSA enhancer/promoter-Luc, and 10 ng of control plasmid pCAGGS-lacZ for normalization of transfection efficiency using Lipofectamine (Invitrogen, Carlsbad, CA, USA). Transfection media was removed 24 hour later and replaced with RPMI 1640 medium containing 2% charcoal-stripped serum. Furthermore, the cells were then treated with DHT (100 nM) and test samples. After 24 hour, cells were harvested and assayed for luciferase activity and β-galactosidase activity with the β-gal reporter gene assay system (Roche, Mannheim, Germany).

Nuclear translocation of AR

HEK293T cells were plated at 100×10^4 cells/dish in 10-cm dishes and incubated in RPMI media supplemented with 10% fetal bovine serum for 24 hour. The cells were transfected with 7.5 μg of EGFP-AR expression construct using Lipofectamine (Invitrogen, Carlsbad, CA, USA). Transfection media was removed 24 hour later and the cells were reseeded at 1.0×10^5 cells/well in 12-well plate and incubated in RPMI media supplemented with 10% fetal bovine serum for 24 hour. The cells were treated with DHT (100 nM) or test samples. After 1 hour, cells were fixed with 3% paraformaldehyde in phosphate-buffered saline at room (ambient) temperature and observed under a confocal laser scanning microscope system FV1000 (Olympus Corp. Tokyo, Japan).

Chapter 3

Conclusion and Discussion

In recent years, the number of prostate cancer patients has been increasing rapidly in Japan. In fact, the morbidity of prostate cancer is increasing, and predicted to become the first in 2020. Androgen receptor (AR) signaling plays a central role in the malignancy of prostate cancers. Therefore, AR antagonists that compete with androgens for binding to the AR are clinically used for the treatment of prostatic diseases. However, all existing AR antagonists, that are clinically used, are reported to emerge the resistance possibly due to structural similarity. Thus, the development of a new type-AR antagonist is an attractive strategy to overcome prostate cancers that are resistant to existing antagonists.

In this study, the author has discovered novel compounds, antarlides A-H (**1**-**8**) from *Streptomyces* sp. BB47, as new type-AR antagonists (Figure 16). Antarlides A-F (**1**-**6**) are mutually isomeric with regard to the double bond, having a novel macrocyclic structure of a 22-membered ring. On the other hand, though antarlides G,H (**7**, **8**) are also mutually isomeric with regard to the double bond, **7** and **8** have a novel macrocyclic structure of a 20-membered ring. Therefore, it found that antarlides are structurally distinct from all existing AR antagonists.

The full stereostructure of antarlide A (**1**) was established by chemical modifications, including methanolysis, the Trost method, acetonide formation, and the PGME method. On the other hand, when antarlides B-F (**2**-**6**) were exposed to room light, these compounds were isomerized to **1**. These data suggested that asymmetric centers in **2**-**6** are most likely to have the same absolute configurations as that of **1** (Figure 24). Unfortunately, the full stereostructure of **7** and **8** are not determined because the obtained **7** and **8** are small in amount.

These data suggested that the strain produces antarlide A (**1**) as a ‘natural product’, which then isomerizes to antarlides B-F (**2**-**6**) during bacterial cultivation and/or compound isolation. However, **1** was not isomerized to antarlides B-D (**2**-**4**) though **1** was isomerized to antarlides E and F (**5** and **6**) by 2 hour irradiation of room light (Figure 23). Therefore, it is also possible that

2-**4** are produced by *Streptomyces* sp. BB47 as a 'natural product'. In future, it is necessary that **1** is exposed room light for a long time to analyze isomerization of antarlides. On the other hand, antarlides G and H (**7** and **8**) are not generated from **1** by 2 hour irradiation of room light. It is also possible that **7** and **8** are converted from antarlides A-F (**1**-**6**) during bacterial cultivation and/or compound isolation. In addition, it is likely that when the polyketide chain is cleaved and the lactone linkage is formed, fluctuation of substrate recognition by a thioesterase leads to the production of 20-membered- and 22-membered macrocycles in *Streptomyces* sp. BB47. Therefore, the biosynthetic genes of antarlides are needed to analyze to elucidate whether **7** and **8** are produced by *Streptomyces* sp. BB47 as a 'natural product'.

Antarlides A-H (**1**-**8**) bound AR specifically in a dose-dependent manner (Table 3). These data suggested that the double-bond geometries and the ring size of the antarlides have no effect on the binding to AR. On the other hand, the methyl ester **9** from antarlide A (**1**) did not show inhibitory activity against AR-DHT binding. These data also suggested that the macrocyclic structure of the **1**-**8** is necessary to bind to AR.

Among the 22-membered-ring or 20-membered-ring antarlides, antarlide B (**2**) or antarlide G (**7**) is more stable. Therefore, AR antagonist activities against prostate cancer cells were evaluated by using **2** and **7**. **2** and **7** showed AR antagonistic activity towards prostate cancer cells and this activity is equal to hydroxyflutamide (Figure 26a, 26b). To check this AR antagonist activity is not occurred by cytotoxic effect, the author evaluated proliferation inhibitory activity in PC3 cells, androgen-independent prostate cancer cell. **2** and **7** did not show the cytotoxic effect against PC3 cells at the concentration which **2** and **7** show antagonist activity against LNCaP cells (Figure 26c). These data indicated that antarlides show antagonist activity by inhibiting the function of AR.

Emergence of a mutant AR has been shown to link to resistance to first- and second-generation

AR antagonists (T877A for Flutamide resistance, W741C for Bicalutamide resistance and F876L for Enzalutamide resistance). Therefore, we next evaluated whether antarlides are capable of inhibiting the activity of these mutant ARs. Antarlides B and G (**2** and **7**) inhibited the transcriptional activity of wild type and mutant AR, which are seen in patients with acquired resistance to current clinically used AR antagonists (Figure 27a, 27b). Moreover, **2** and **7** did not induce nuclear translocation of wild type and mutant AR (F876L) (Figure 28). These data indicated that **2** and **7** do not act as an agonist in enzalutamide-resistant cells. In addition, these data also indicated that anatarlides bind to AR, and inhibit the translocation of AR to the nucleus same as enzalutamide.

In recent years, the number of new-generation AR antagonists is in clinical development. Apalutamide (ARN-509) is currently in phase III clinical trials for CRPC, however, it does not show the antagonist activity to mutant AR (F876L), possibly due to the structural similarity with enzalutamide (Figure 2c). On the other hand, darolutamide (ODM-201) is a synthetic AR antagonist presently in a phase III study, and it is novel and structurally distinct from any known AR antagonists including enzalutamide (Figure 2c). Darolutamide has been shown a full antagonist for the mutant AR same as antarlides. Previously, the author also reported that arabilin, isolated from *Streptomyces* sp. MK756-CF1, shows antagonist activity to not only of the wild type AR but also of mutant AR (Figure 3b). Arabilin is also structurally distinct from any known AR antagonist. Moreover, antarlides are also structurally distinct from these AR antagonists including arabilin. These data suggested that the unique structure may be important for developing AR antagonists that can overcome resistance to AR-targeted therapy. In addition, natural products are potent screening sources for development of AR antagonist.

Therefore, antarlides may have the potential to become a drug seed as third generation AR antagonists that overcome resistance to existing AR-targeted therapies.

Supplementary Figures

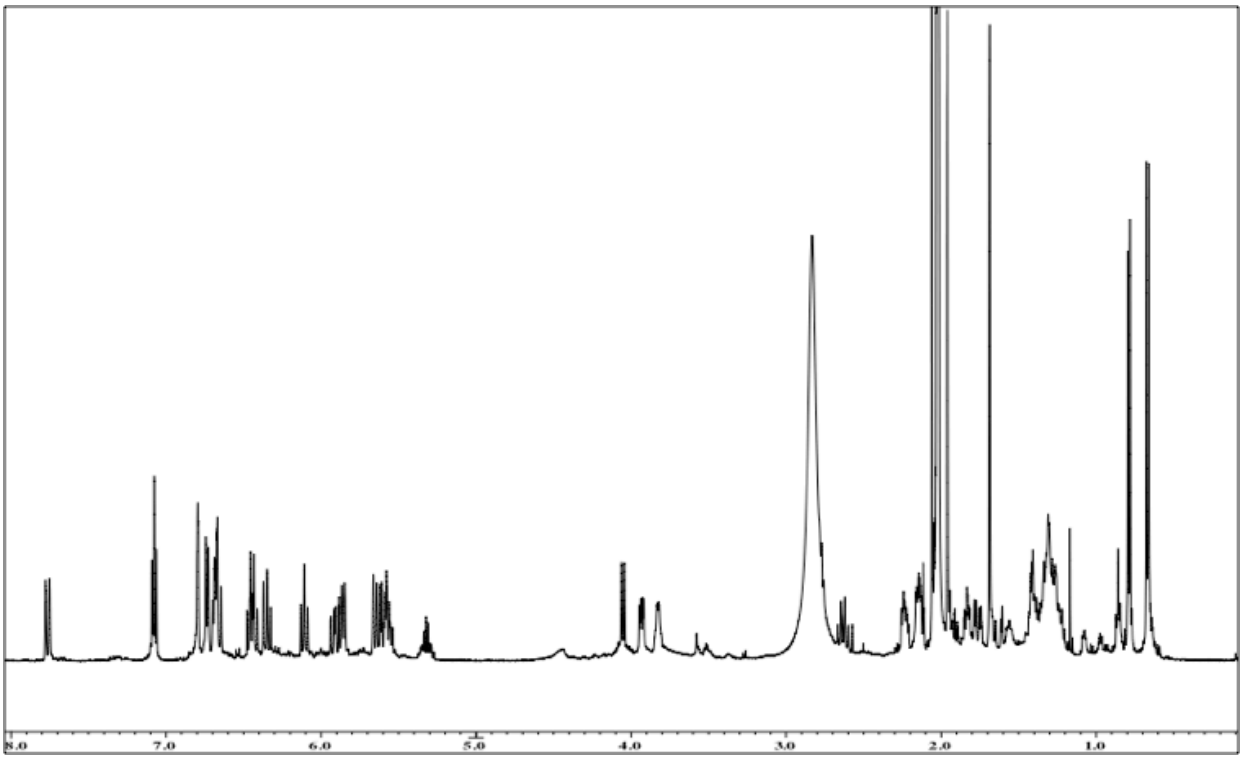

Figure S1. ^{1}H NMR spectrum of antarlide B (**2**)
(500 MHz, Acetone-d_6, TMS = 0.00 ppm)

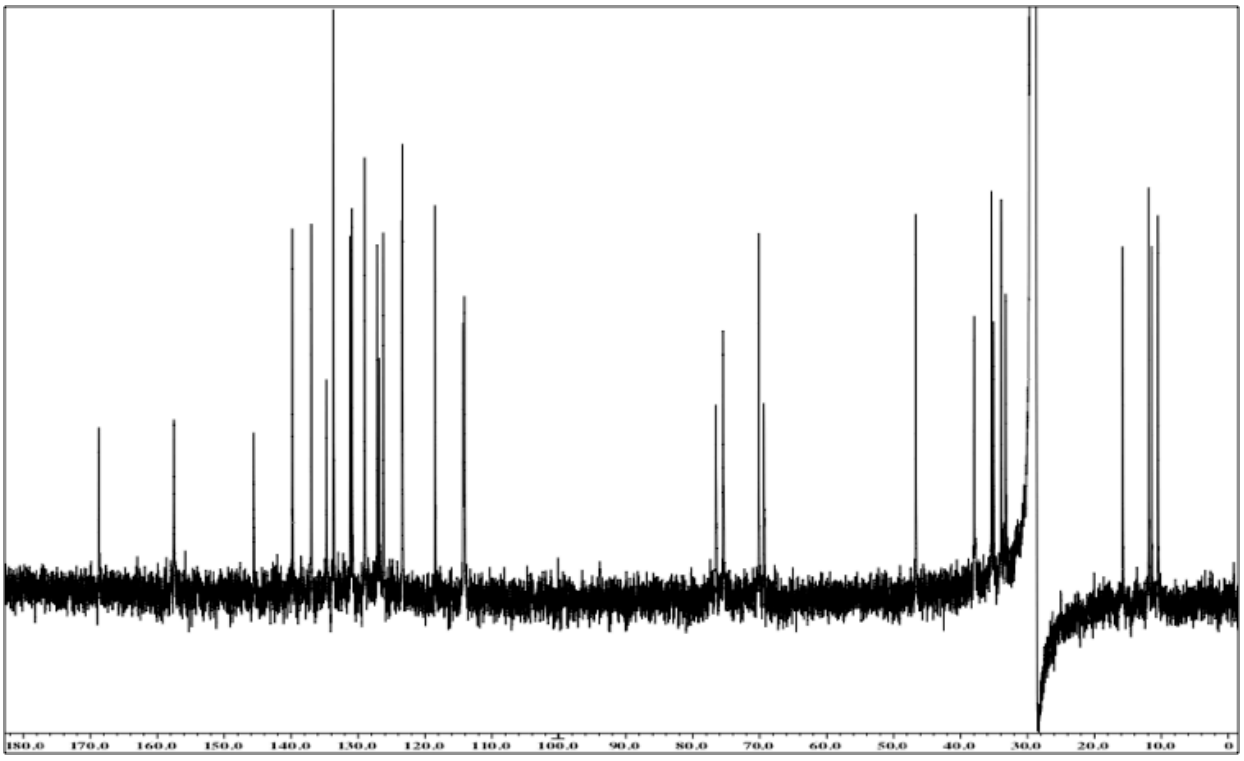

Figure S2. ^{13}C NMR spectrum of antarlide B (**2**)
(125 MHz, Acetone-d_6, Acetone-d_6 = 29.8 ppm)

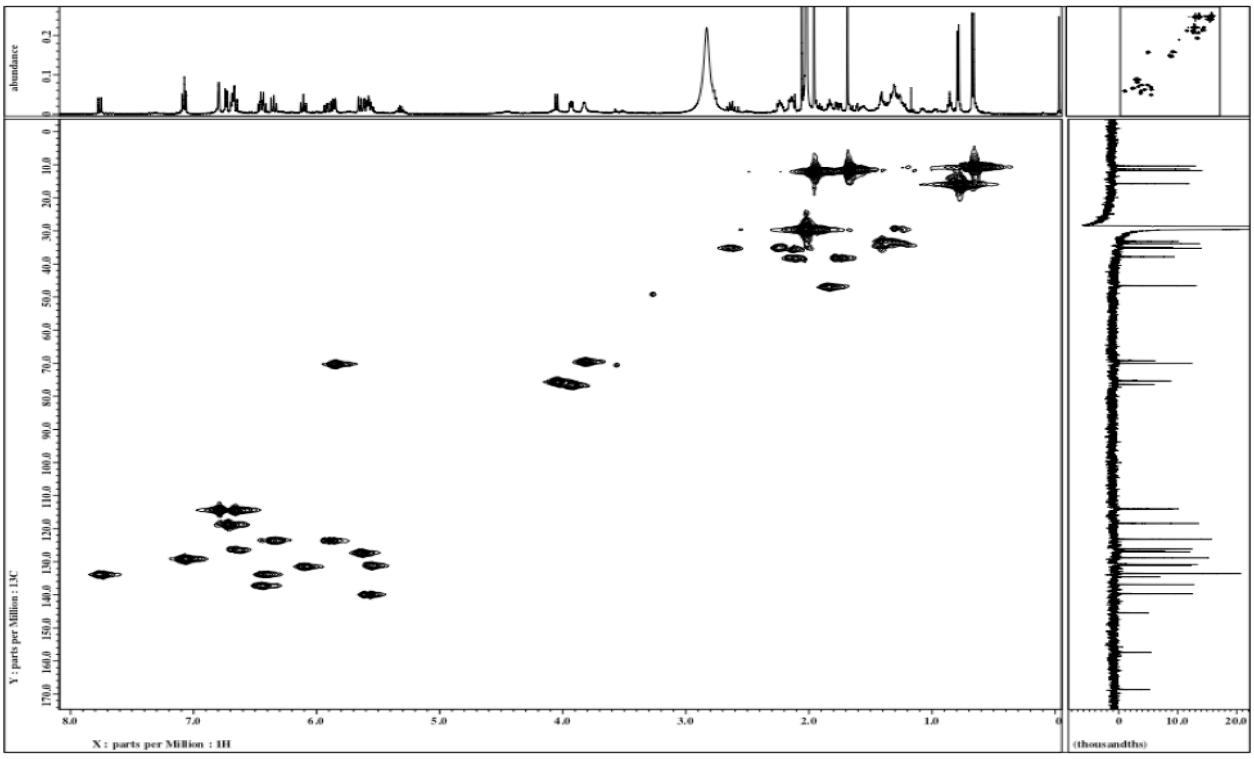

Figure S3. HMQC spectrum of antarlide B (**2**) (500 MHz, Acetone-d_6)

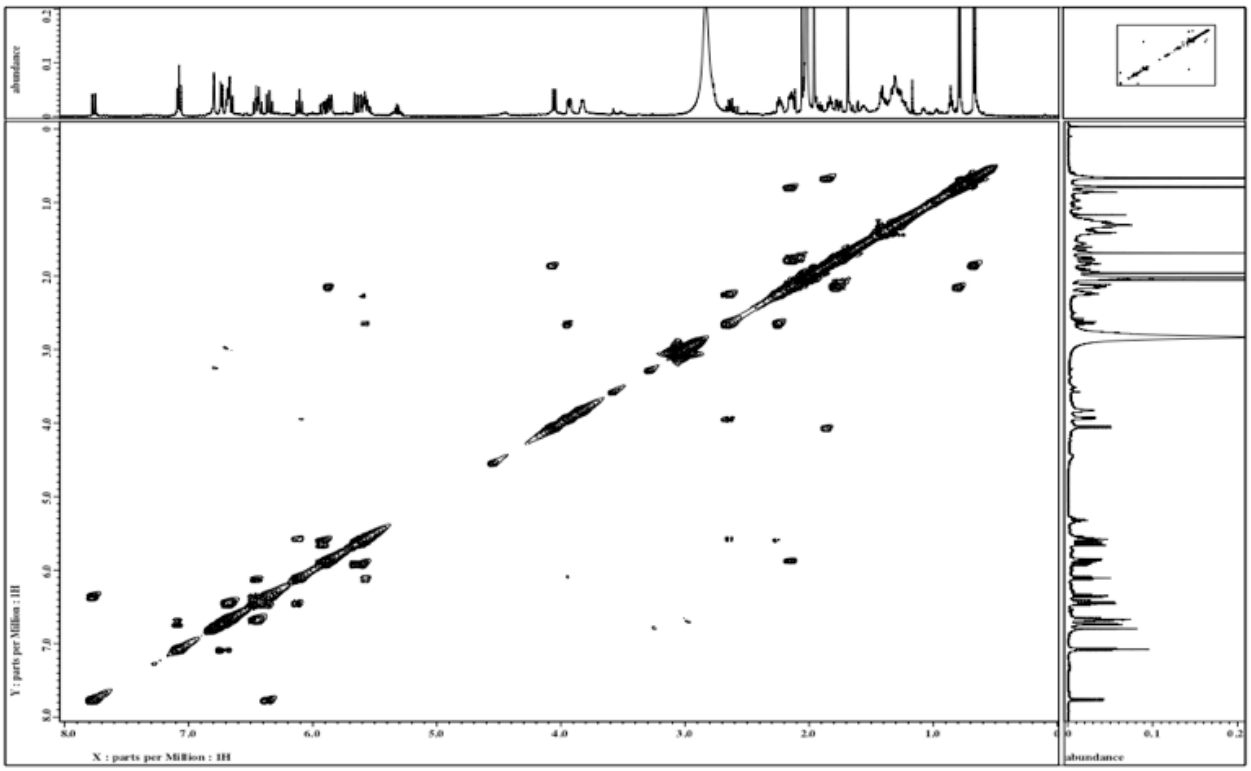

Figure S4. ^{1}H-^{1}H COSY spectrum of antarlide B (**2**) (500 MHz, Acetone-d_6)

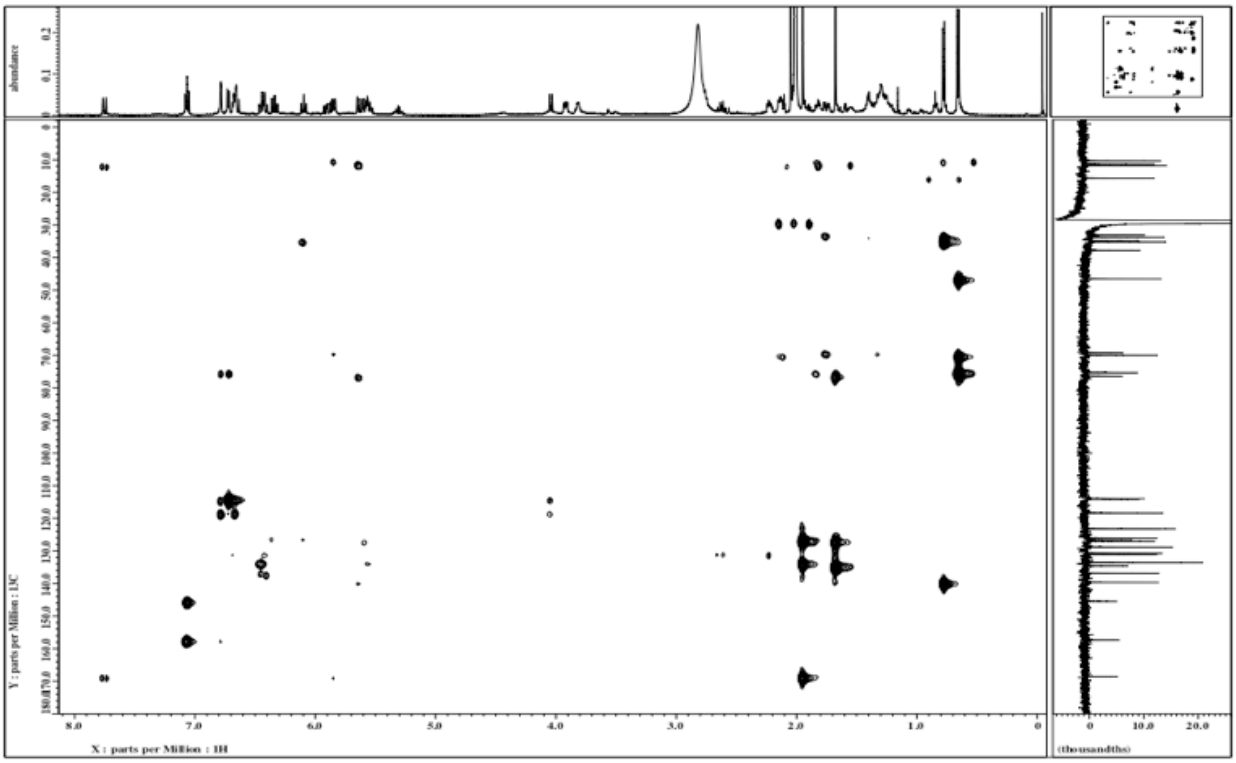

Figure S5. HMBC spectrum of antarlide B (**2**) (500 MHz, Acetone-d_6)

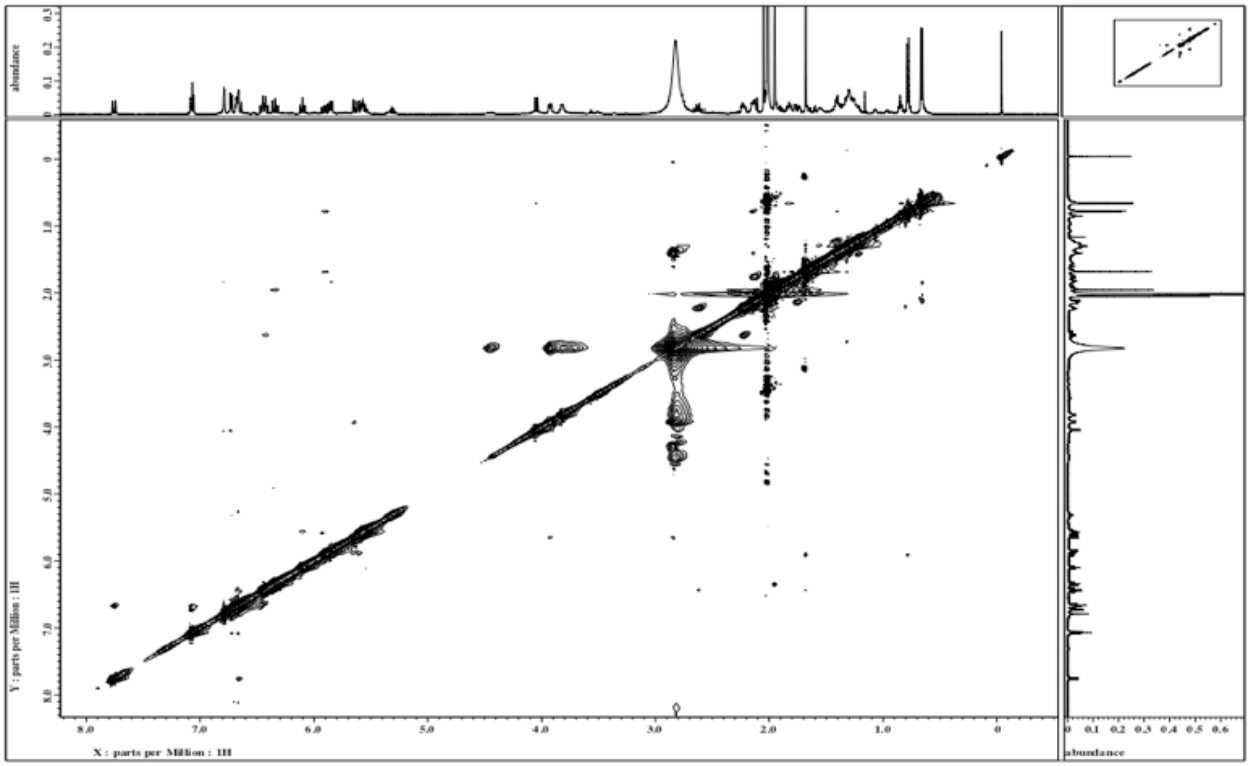

Figure S6. NOESY spectrum of antarlide B (**2**) (500 MHz, Acetone-d_6)

Table S1. ^{1}H and ^{13}C NMR Data for antarlide B (**2**) in Acetone-d_6

position	δ_c	δ_H mult (*J* in Hz)
1	168.7	-
2	126.9	-
2a	11.9	1.99 (3H, s)
3	133.7	7.79 (1H, d, 12.0)
4	123.4	6.38 (1H, t, 12.0)
5	133.7	6.46 (1H, m)
6	126.3	6.70 (1H, dd, 12.0, 15.1)
7	137.0	6.49 (1H , m)
8	131.2	6.14 (1H, t, 10.5)
9	130.9	5.60 (1H, m)
10	35.1	2.28, 2.69 (2H, m)
11	76.6	3.96 (1H, dd, 4.2, 9.9)
12	134.8	-
12a	11.5	1.72 (3H, s)
13	127.2	5.68 (1H, d, 10.7)
14	123.5	5.94 (1H, m)
15	139.8	5.63 (1H, dd, 4.6, 14.8)
16	35.4	2.16 (1H, m)
16a	15.8	0.82 (3H, d, 6.6)
17	34.0	1.25-1.50 (2H, m)
18	33.3	1.25-1.50 (2H, m)
19	69.4	3.86 (1H, m)
20	38.0	1.79, 2.15 (2H, m)
21	70.1	5.89 (1H, m)
22	46.7	1.88 (1H, m)
22a	10.5	0.70 (3H, d, 7.0)
23	75.5	4.08 (1H, d, 9.7)
24	145.6	-
25	114.1	6.83 (1H, s)
26	157.5	-
27	114.3	6.71 (1H, d, 7.8)
28	129.0	7.11 (1H, t, 7.8)
29	118.5	6.76 (1H, d, 7.8)

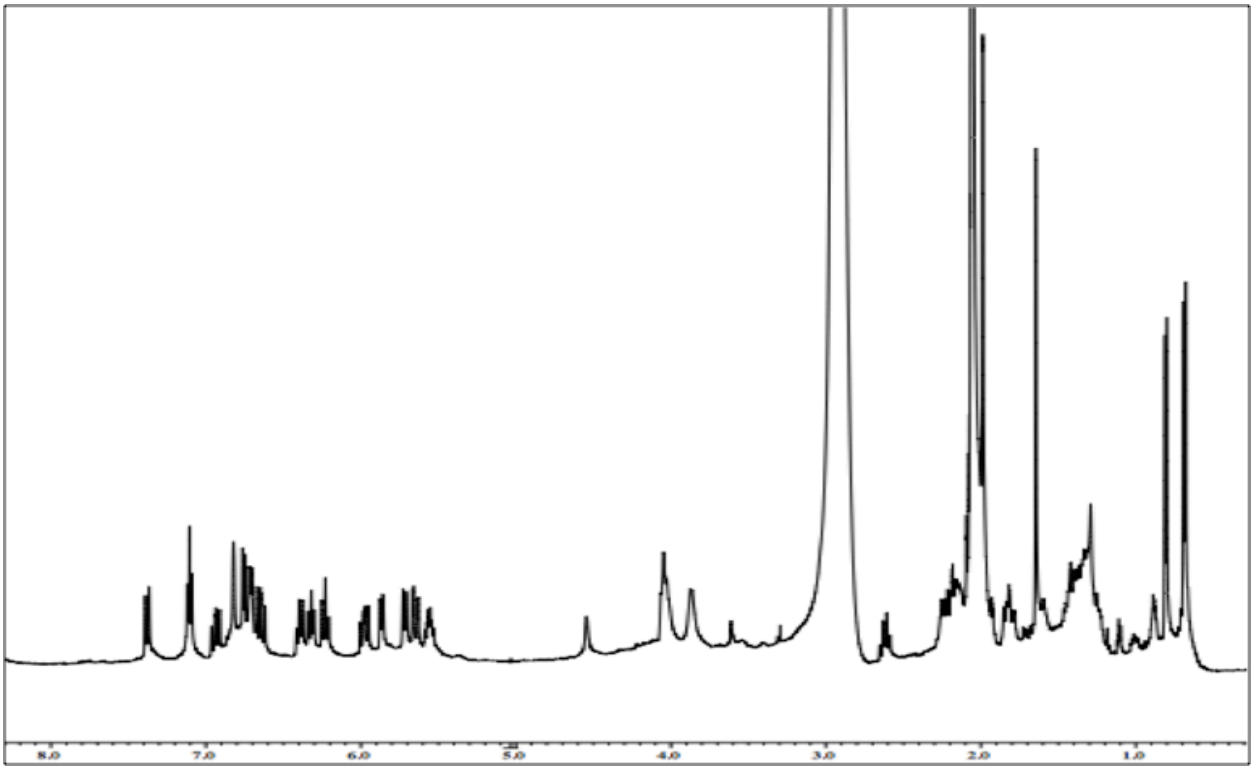

Figure S7. ^{1}H NMR spectrum of antarlide C (**3**)
(500 MHz, Acetone-d_6, TMS = 0.00 ppm)

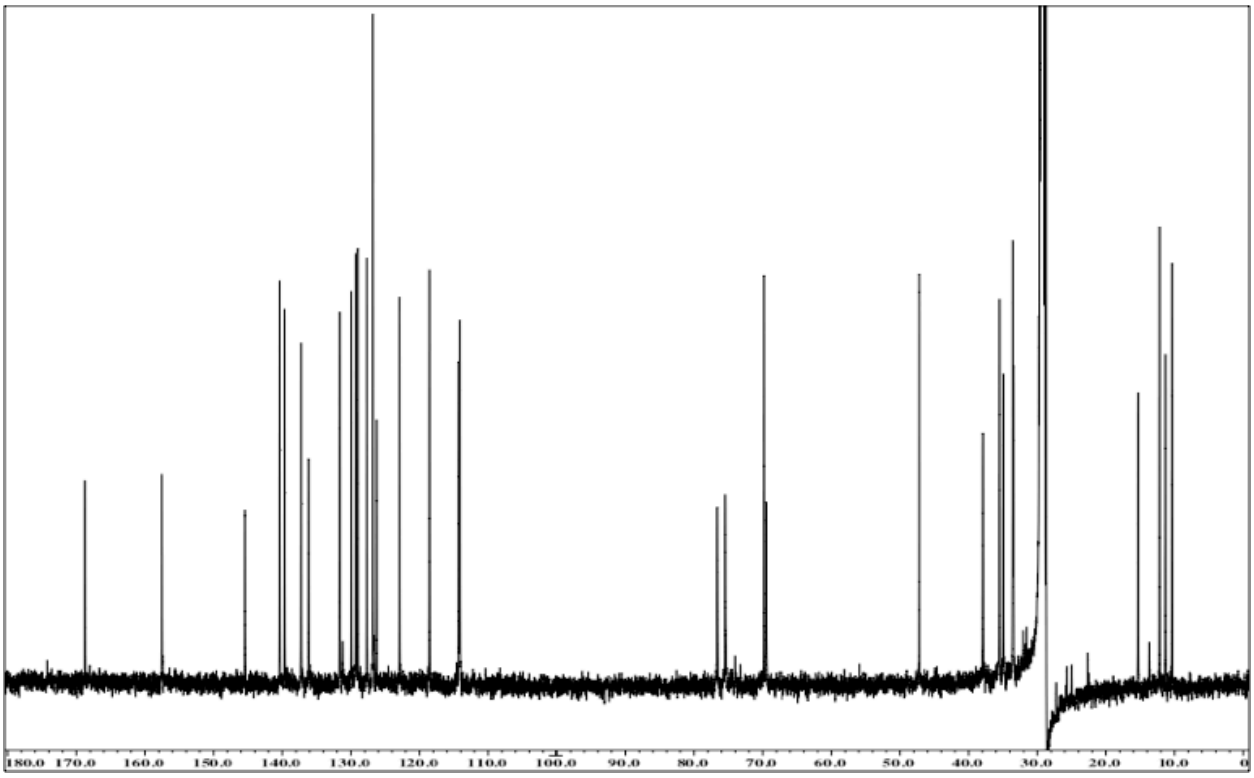

Figure S8. ^{13}C NMR spectrum of antarlide C (**3**)
(125 MHz, Acetone-d_6, Acetone-d_6 = 29.8 ppm)

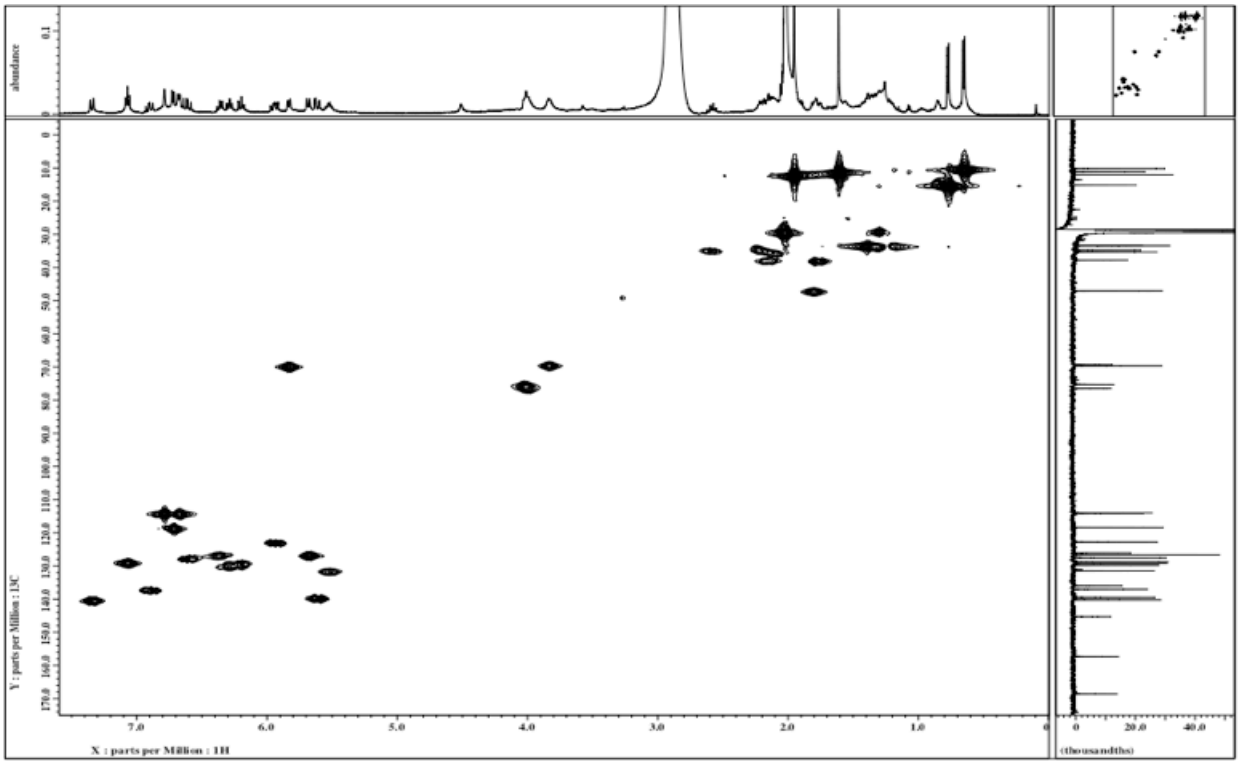

Figure S9. HMQC spectrum of antarlide C (**3**) (500 MHz, Acetone-d_6)

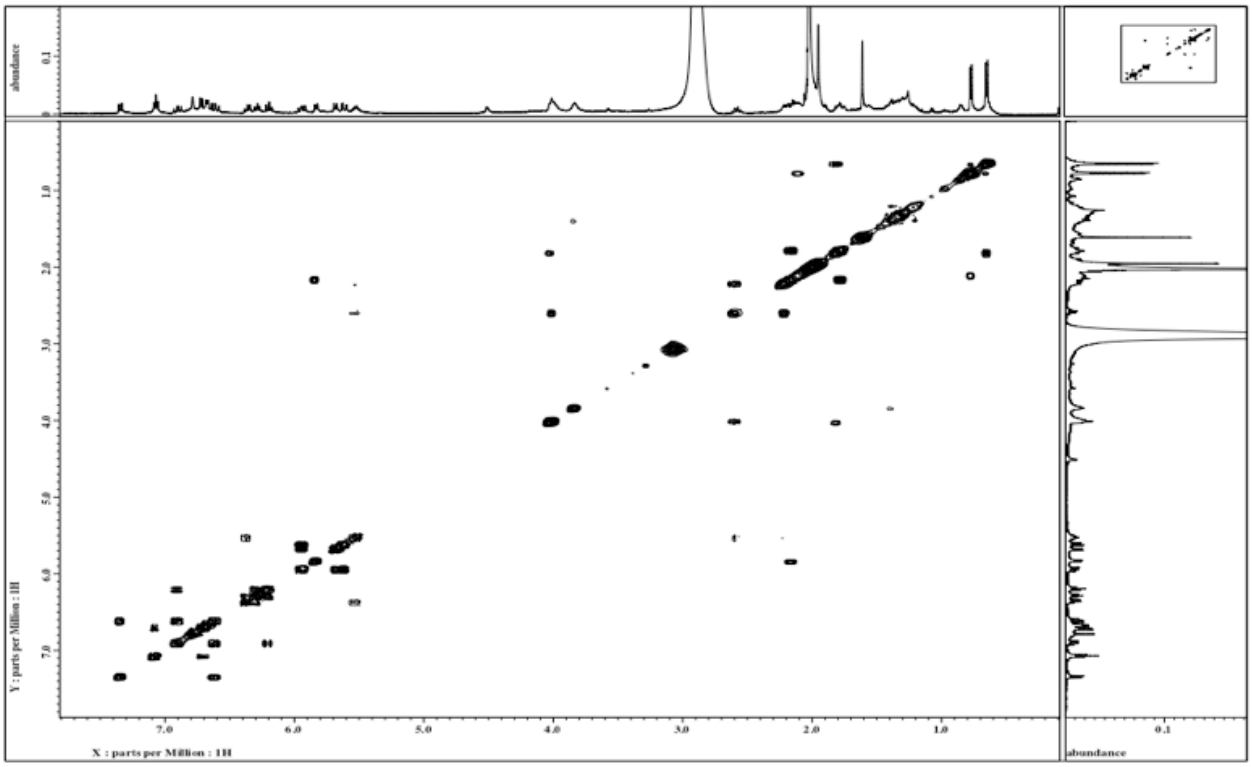

Figure S10. ^{1}H-^{1}H COSY spectrum of antarlide C (**3**) (500 MHz, Acetone-d_6)

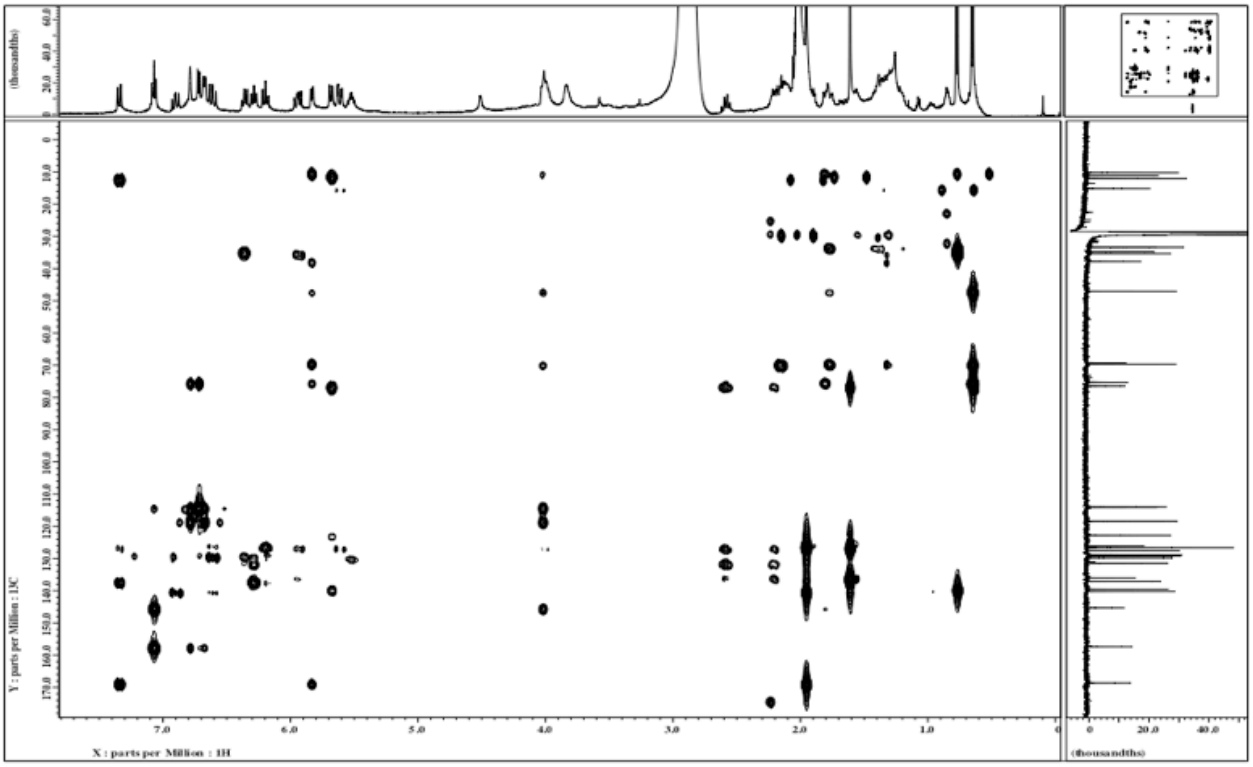

Figure S11. HMBC spectrum of antarlide C (**3**) (500 MHz, Acetone-d_6)

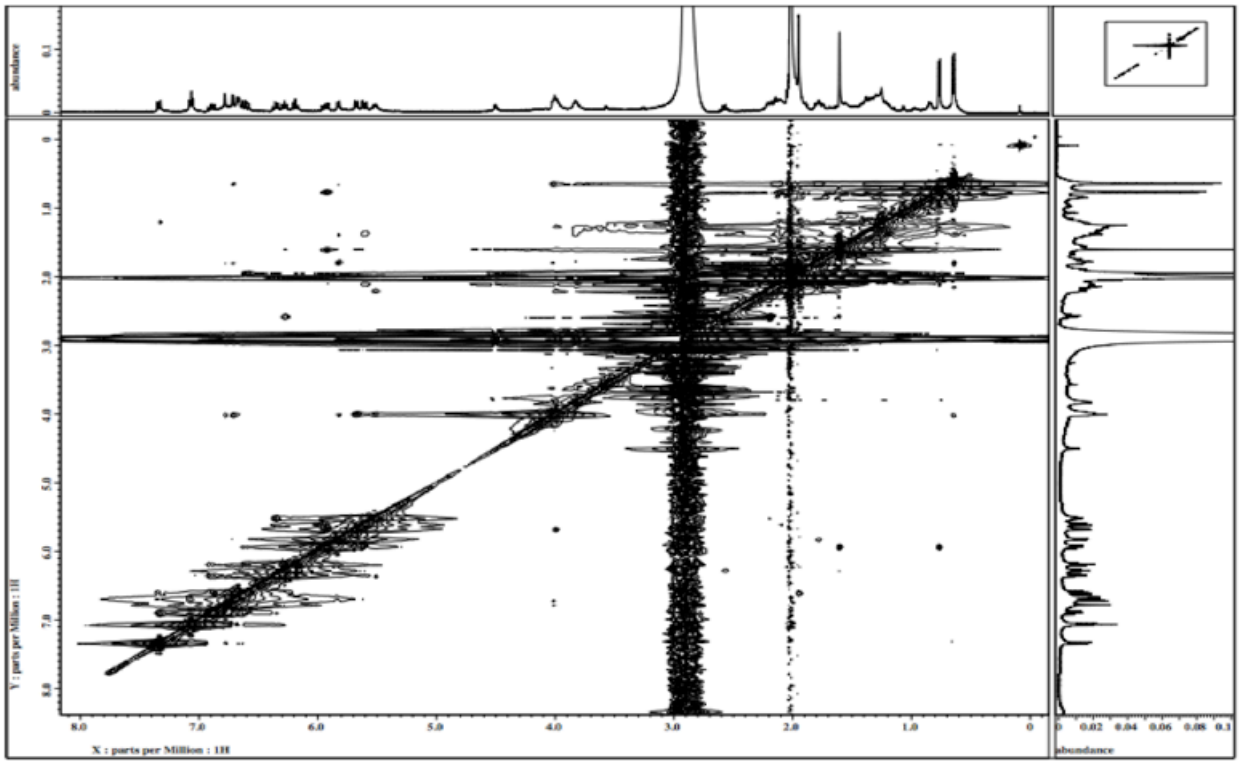

Figure S12. NOESY spectrum of antarlide C (**3**) (500 MHz, Acetone-d_6)

Table S2. ^{1}H and ^{13}C NMR Data for antarlide C (**3**) in Acetone-d_6

position	δ_c	δ_H mult (*J* in Hz)
1	168.7	-
2	126.2	-
2a	12.2	1.99 (3H, s)
3	140.4	7.38 (1H, d, 11.8)
4	127.7	6.65 (1H, dd, 11.8, 14.2)
5	137.2	6.94 (1H, dd, 11.4, 14.2)
6	129.3	6.23 (1H, t, 11.4)
7	129.9	6.32 (1H, t, 9.9)
8	126.8	6.40 (1H, t, 9.9)
9	131.6	5.56 (1H, m)
10	34.9	2.24, 2.63 (2H, m)
11	76.6	4.05 (1H, m)
12	136.1	-
12a	11.3	1.65 (3H, s)
13	126.8	5.72 (1H, d, 10.6)
14	122.9	5.98 (1H, ddd, 2.0, 10.6, 15.3)
15	139.7	5.65 (1H, dd, 4.0, 15.3)
16	35.5	2.15 (1H, m)
16a	15.3	0.81 (3H, d, 6.6)
17	33.6	1.20, 1.37 (2H, m)
18	33.5	1.20, 1.44 (2H, m)
19	69.5	3.87 (1H, m)
20	37.9	1.82, 2.20 (2H, m)
21	69.8	5.87 (1H, d)
22	47.2	1.85 (1H, m)
22a	10.3	0.69 (3H, d, 7.0)
23	75.5	4.07 (1H, m)
24	145.4	-
25	114.1	6.82 (1H, s)
26	157.5	-
27	114.3	6.71 (1H, d, 7.6)
28	129.0	7.10 (1H, t, 7.6)
29	118.5	6.75 (1H, d, 7.6)

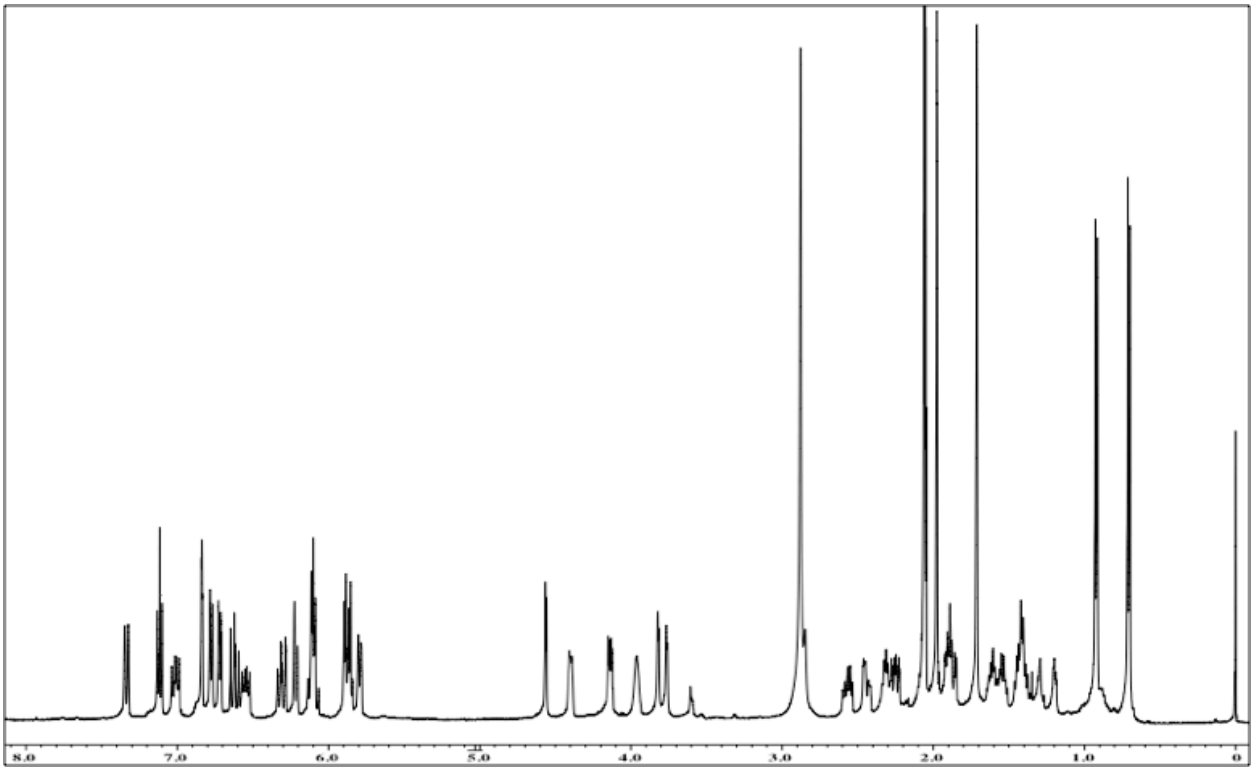

Figure S13. ^{1}H NMR spectrum of antarlide D (**4**)
(500 MHz, Acetone-d_6, TMS = 0.00 ppm)

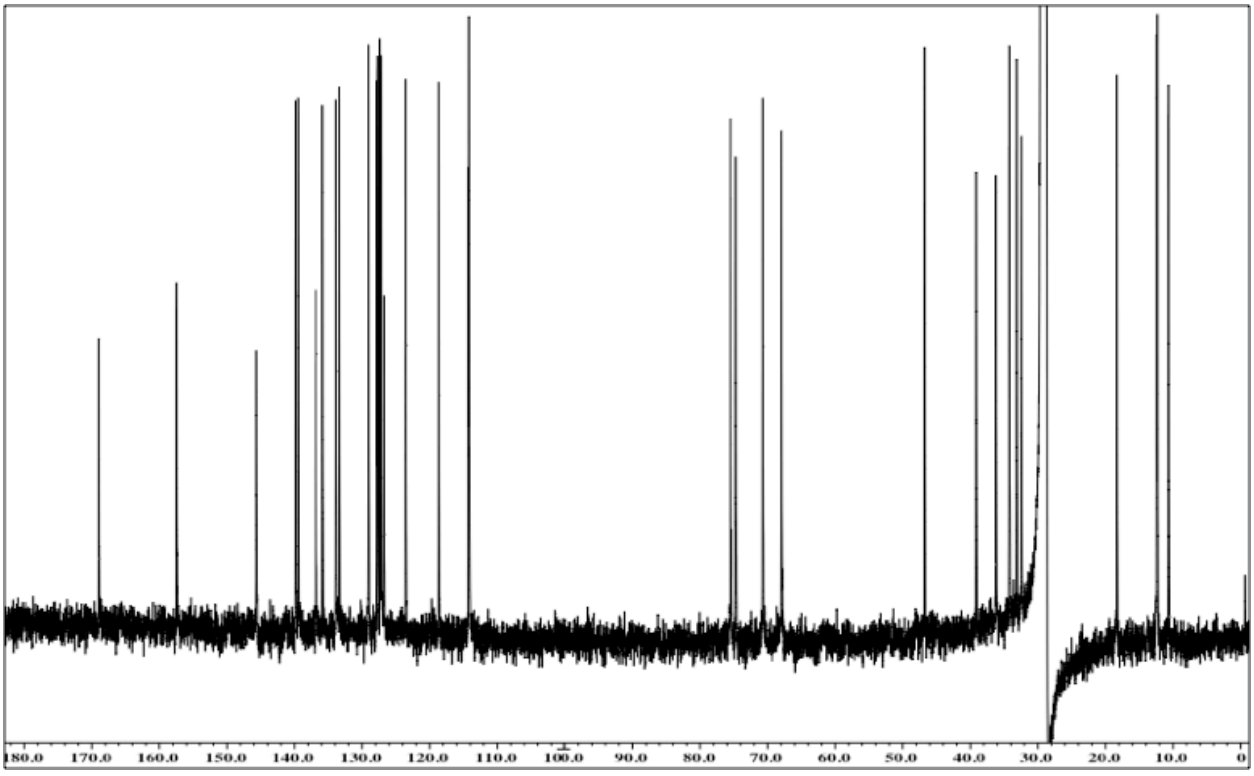

Figure S14. ^{13}C NMR spectrum of antarlide D (**4**)
(125 MHz, Acetone-d_6, Acetone-d_6 = 29.8 ppm)

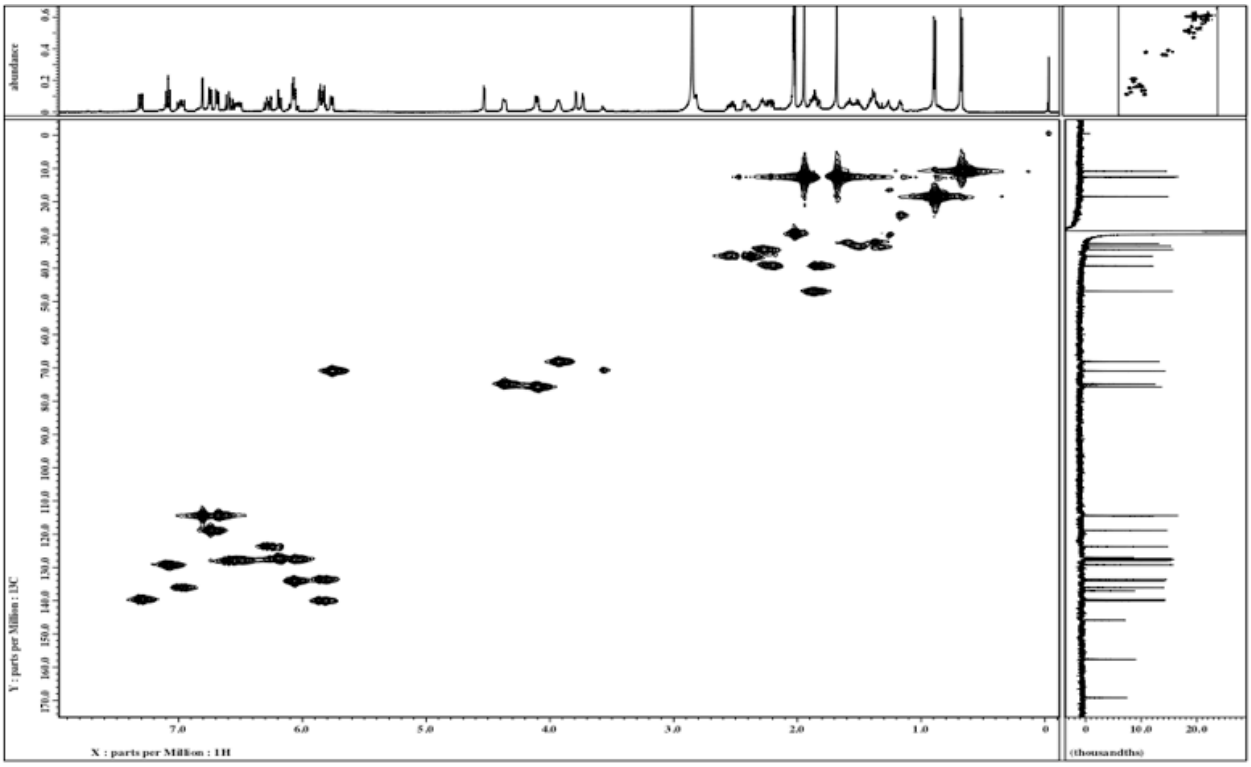

Figure S15. HMQC spectrum of antarlide D (**4**) (500 MHz, Acetone-d_6)

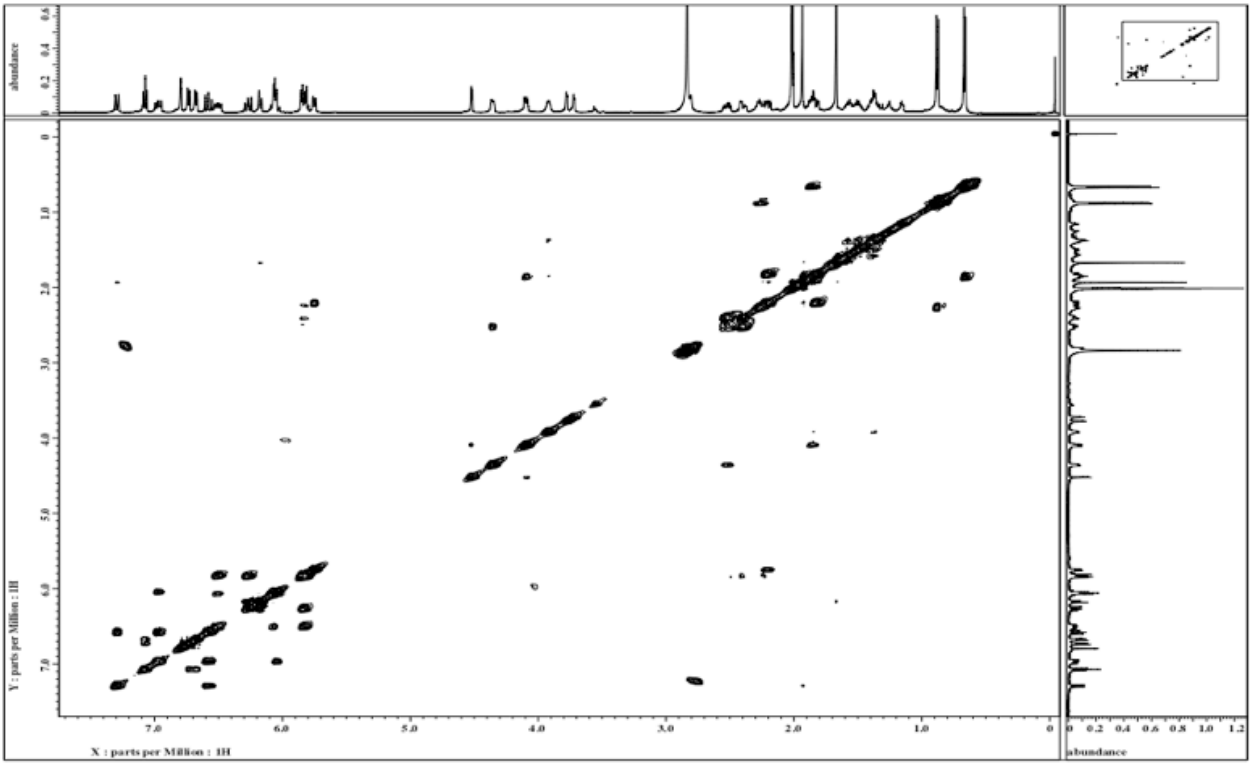

Figure S16. ^{1}H-^{1}H COSY spectrum of antarlide D (**4**) (500 MHz, Acetone-d_6)

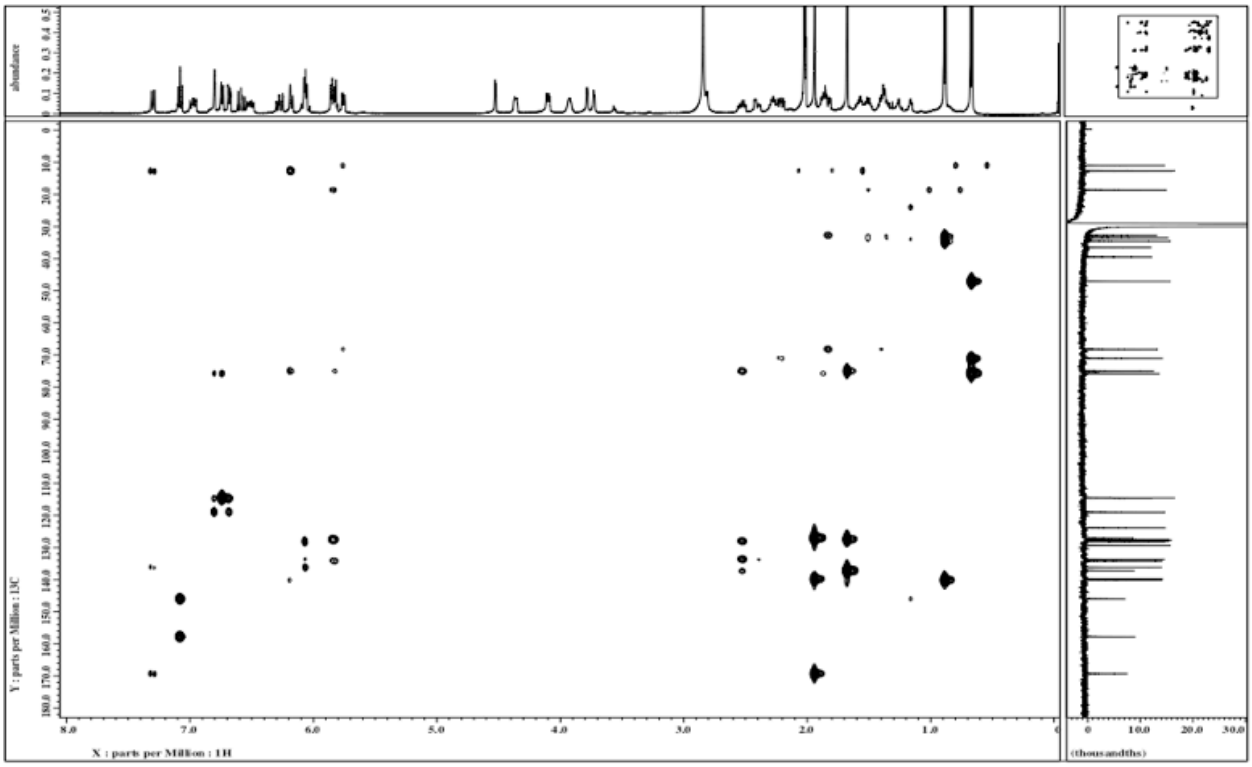

Figure S17. HMBC spectrum of antarlide D (**4**) (500 MHz, Acetone-d_6)

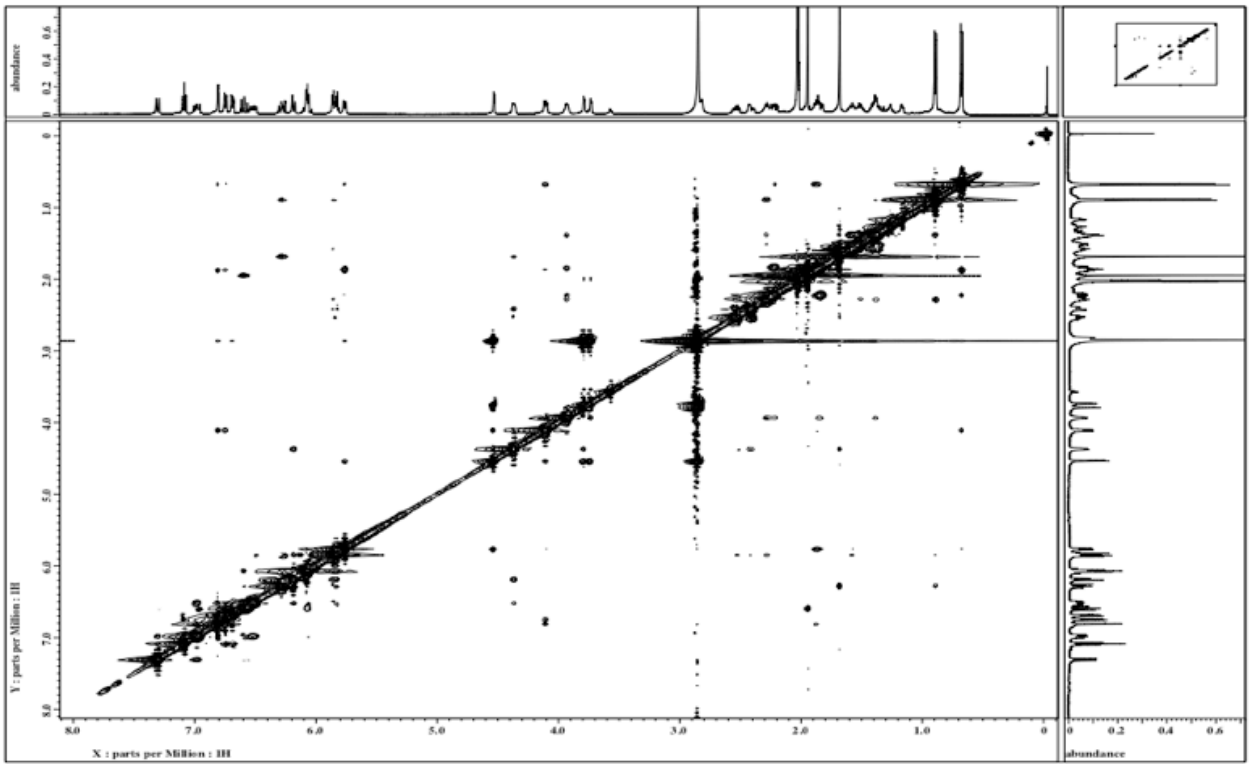

Figure S18. NOESY spectrum of antarlide D (**4**) (500 MHz, Acetone-d_6)

Table S3. ^{1}H and ^{13}C NMR Data for antarlide D (**4**) in Acetone-d_6

position	δ_c	δ_H mult (*J* in Hz)
1	169.0	-
2	126.8	-
2a	12.4	1.98 (3H, s)
3	139.5	7.34 (1H, d, 11.7)
4	127.8	6.62 (1H, dd, 11.7, 14.5)
5	135.9	7.00 (1H, dd, 10.4, 14.5)
6	127.4	6.10 (1H, m)
7	133.9	6.10 (1H, m)
8	127.7	6.55 (1H, dd, 9.8, 16.0)
9	133.4	5.87 (1H, m)
10	36.2	244, 2.57 (2H, m)
11	74.7	4.40 (1H, m)
12	136.9	-
12a	12.3	1.71 (3H, s)
13	127.2	6.22 (1H, d, 10.6)
14	123.6	6.31 (1H, ddd, 1.4, 10.6, 15.7)
15	139.8	5.89 (1H, m)
16	34.2	2.31 (1H, m)
16a	18.3	0.92 (3H, d, 7.4)
17	33.2	1.40, 1.55 (2H, m)
18	32.4	1.41 , 1.60 (2H, m)
19	67.9	3.96 (1H, m)
20	39.2	1.83, 2.21 (2H, m)
21	70.7	5.79 (1H, m)
22	46.8	1.91 (1H, m)
22a	10.7	0.71 (3H, d, 7.0)
23	75.5	4.14 (1H, dd, 3.8, 9.5)
24	145.6	-
25	114.2	6.84 (1H, s)
26	157.5	-
27	114.3	6.72 (1H, ddd, 1.0, 2.5, 7.8)
28	129.0	7.12 (1H, t, 7.8)
29	118.7	6.78 (1H, d, 7.8)

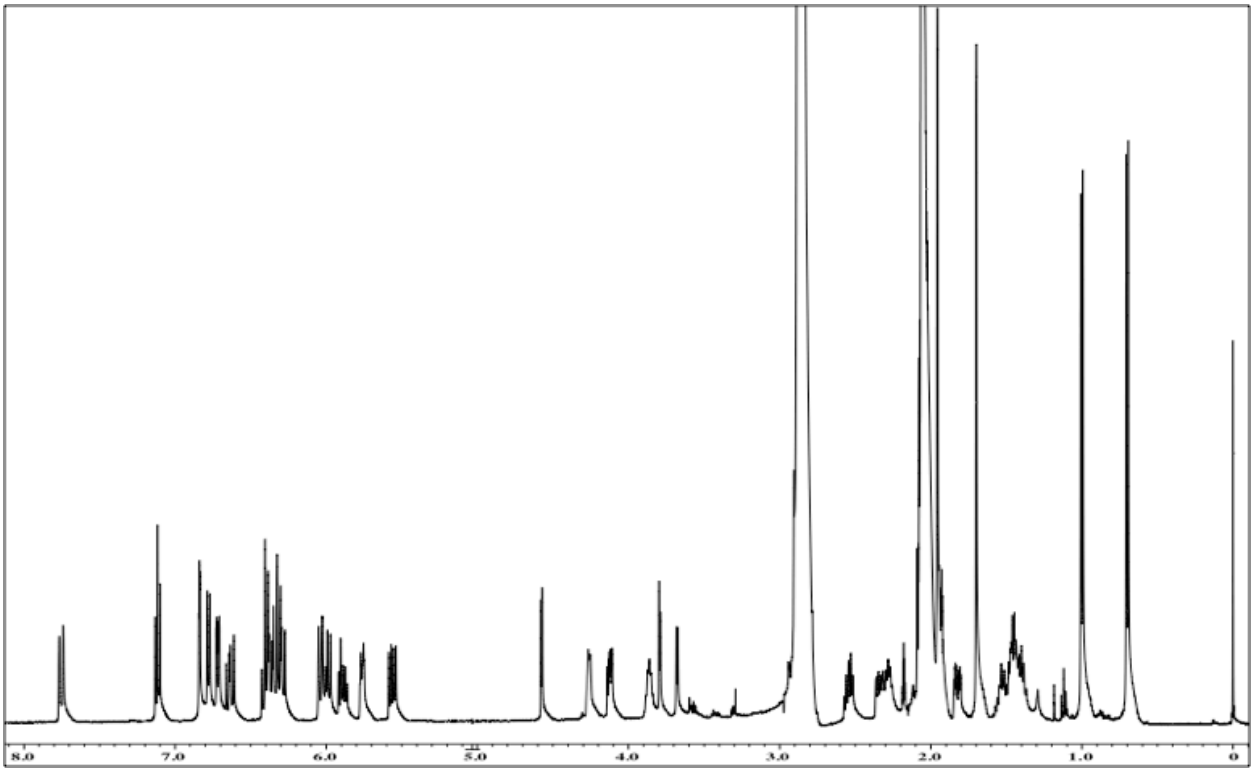

Figure S19. ^{1}H NMR spectrum of antarlide E (**5**)
(500 MHz, Acetone-d_6, TMS = 0.00 ppm)

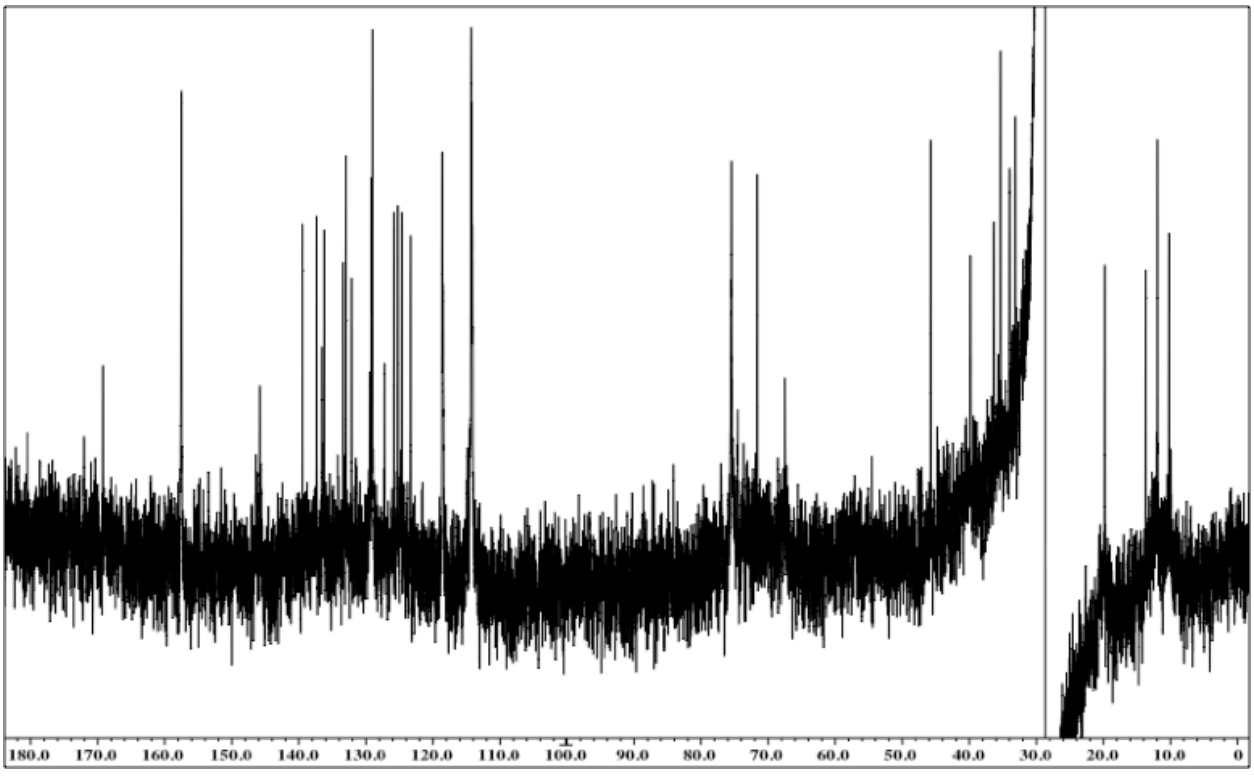

Figure S20. ^{13}C NMR spectrum of antarlide E (**5**)
(125 MHz, Acetone-d_6, Acetone-d_6 = 29.8 ppm)

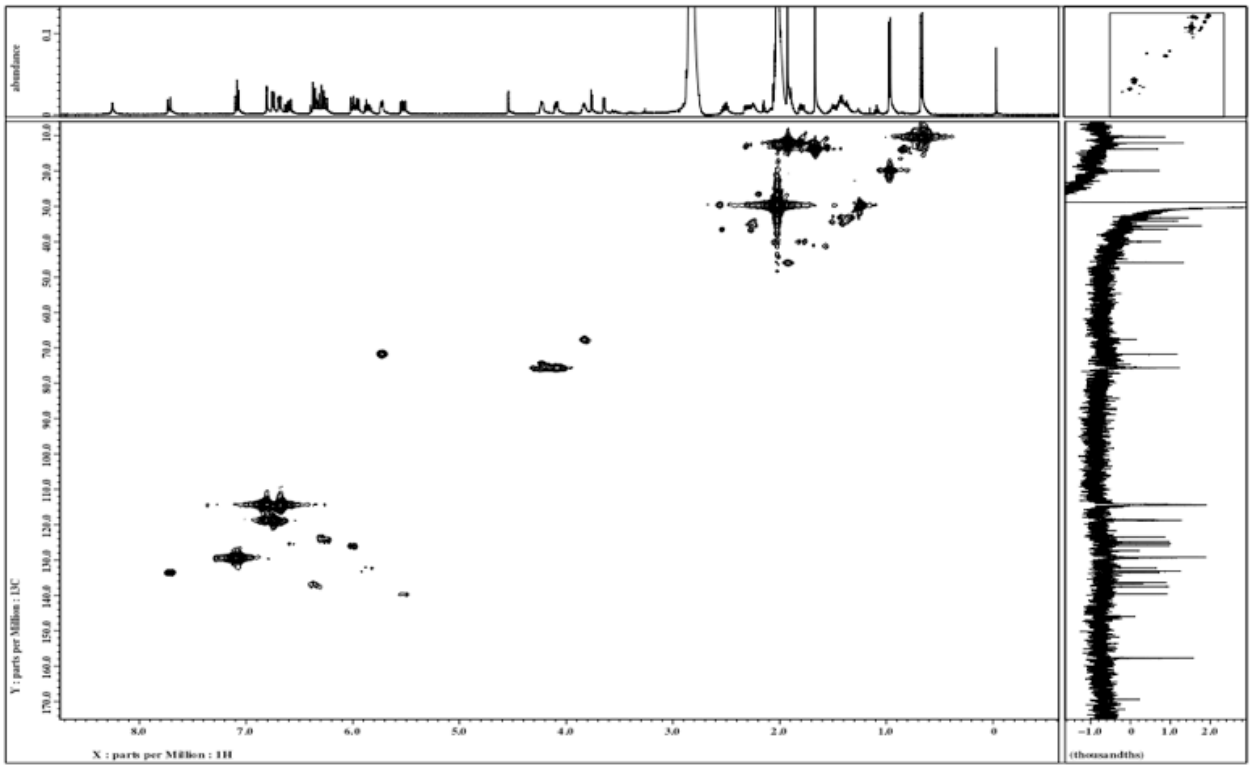

Figure S21. HMQC spectrum of antarlide E (**5**) (500 MHz, Acetone-d_6)

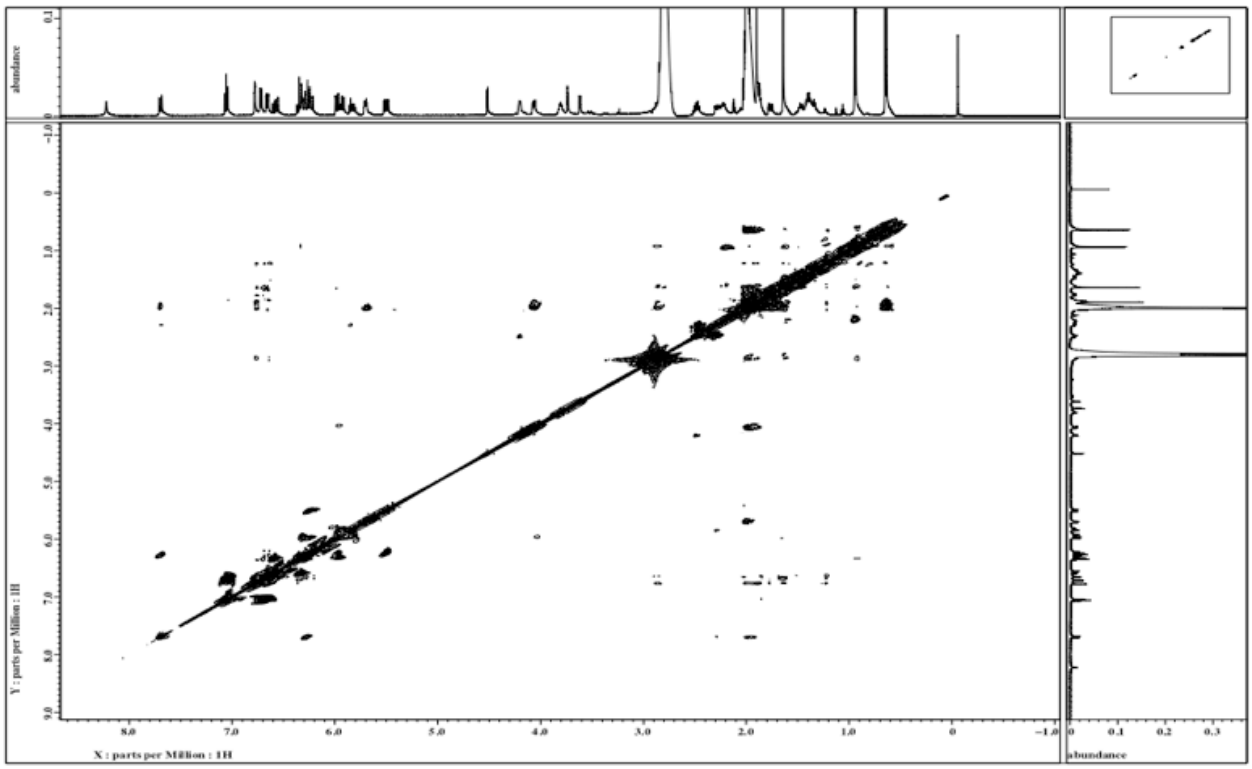

Figure S22. ^{1}H-^{1}H COSY spectrum of antarlide E (**5**) (500 MHz, Acetone-d_6)

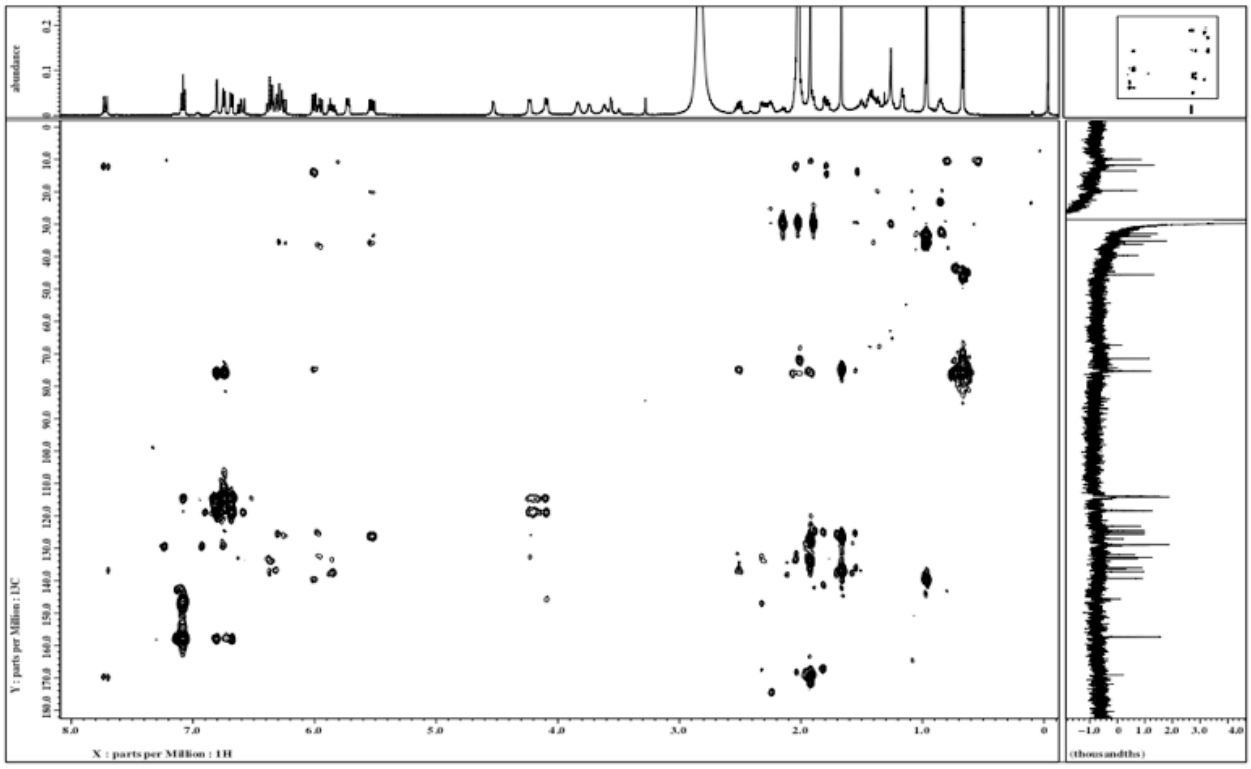

Figure S23. HMBC spectrum of antarlide E (**5**) (500 MHz, Acetone-d_6)

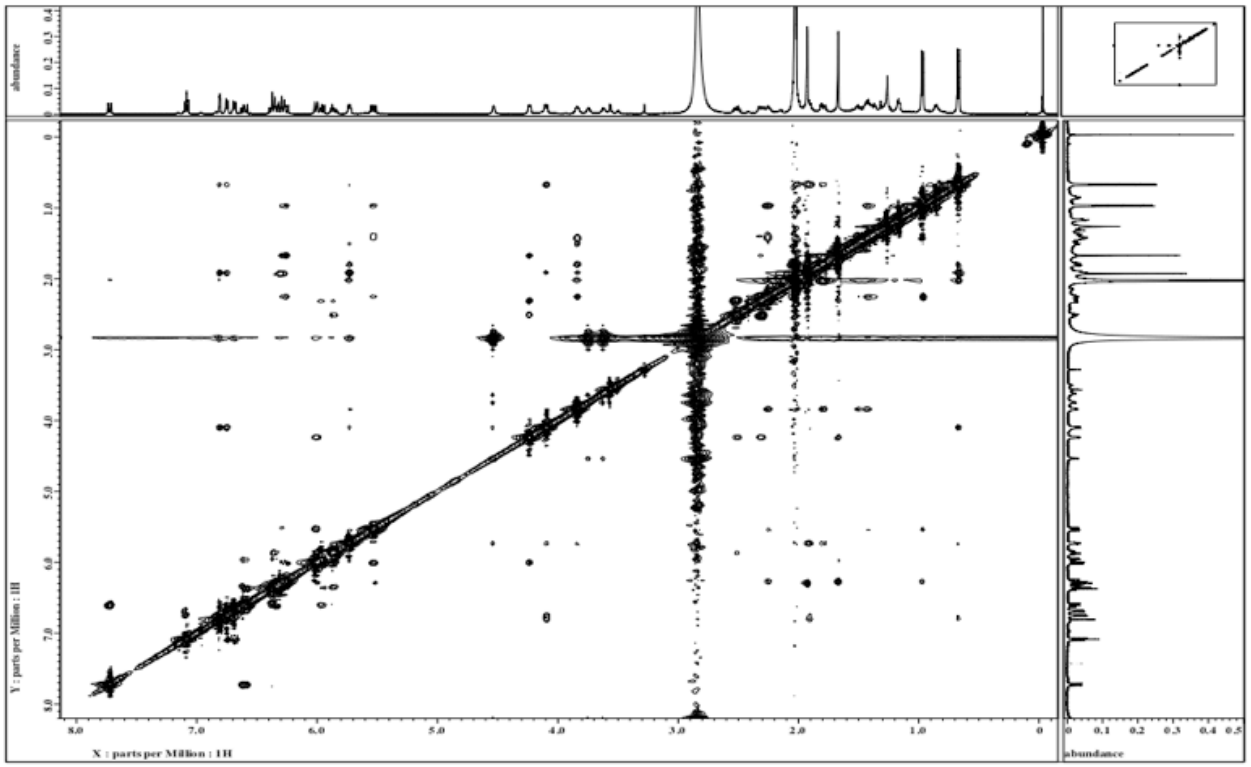

Figure S24. NOESY spectrum of antarlide E (**5**) (500 MHz, Acetone-d_6)

Table S4. ^{1}H and ^{13}C NMR Data for antarlide E (**5**) in Acetone-d_6

position	δ_c	δ_H mult (*J* in Hz)
1	169.2	-
2	127.2	-
2a	11.9	1.95 (3H, s)
3	133.3	7.75 (1H, d, 12.3)
4	123.3	6.32 (1H, m)
5	136.2	6.39 (1H, m)
6	125.2	6.64 (1H, dd, 11.2, 14.8)
7	137.4	6.35 (1H, m)
8	133.0	6.00 (1H, dd, 9.9, 15.6)
9	132.1	5.89 (1H, dt, 7.0, 15.6)
10	36.3	2.34, 2.56 (2H, m)
11	75.5	4.23 (1H, d)
12	136.5	-
12a	13.7	1.70 (3H, s,)
13	125.8	6.04 (1H, d, 11.6)
14	124.6	6.30 (1H, m)
15	139.4	5.56 (1H, dd, 7.9, 15.2)
16	36.3	2.29 (1H, m)
16a	19.8	1.00 (3H, d, 6.7)
17	35.4	1.38, 1.47 (2H, m)
18	34.0	1.43, 1.54 (2H, m)
19	67.5	3.86 (1H, m)
20	39.8	1.82 (2H, m)
21	71.6	5.76 (1H, m)
22	45.8	1.97 (2H, m)
22a	10.2	0.70 (3H, d, 7.1)
23	75.5	4.12 (1H, dd, 2.6, 6.8)
24	145.8	-
25	114.2	6.84 (1H, s)
26	157.5	-
27	114.3	6.72 (1H, ddd, 1.0, 2.7, 8.0)
28	129.2	7.12 (1H, t, 8.0)
29	118.6	6.78 (1H, d, 8.0)

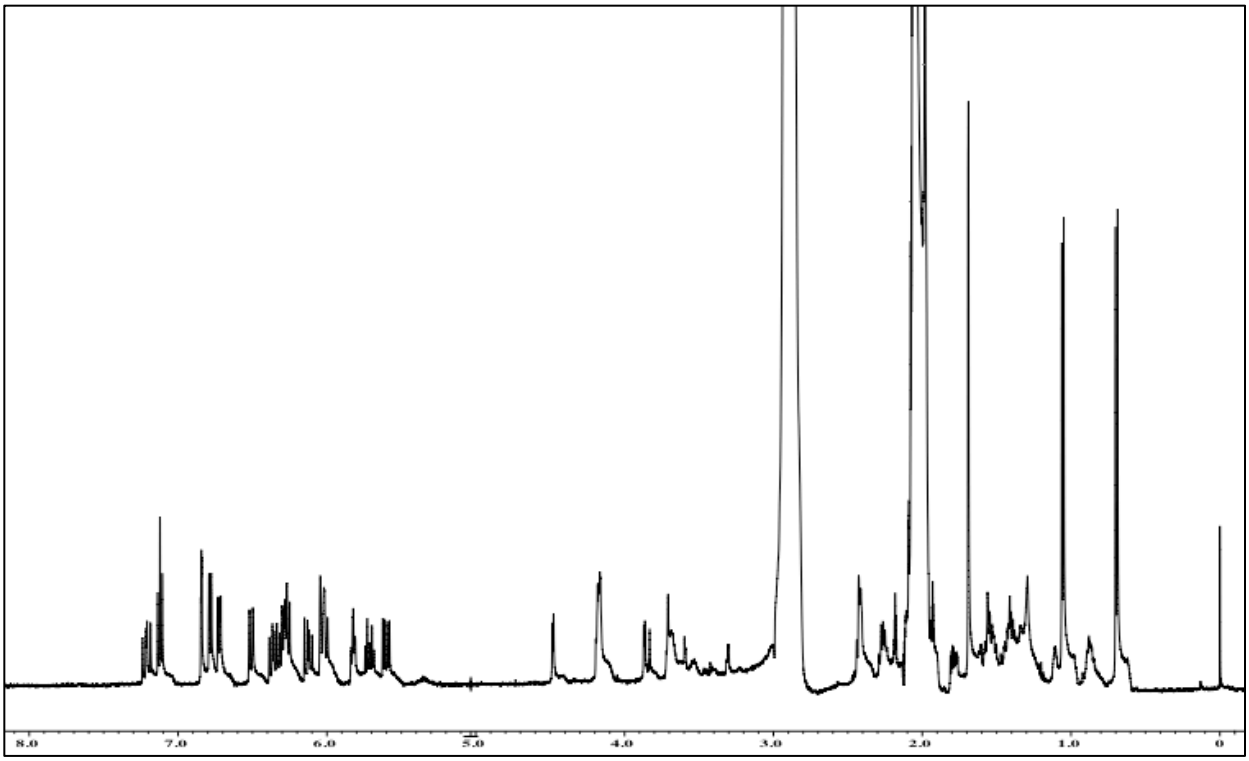

Figure S25. ^{1}H NMR spectrum of antarlide F (**6**)
(500 MHz, Acetone-d_6, TMS = 0.00 ppm)

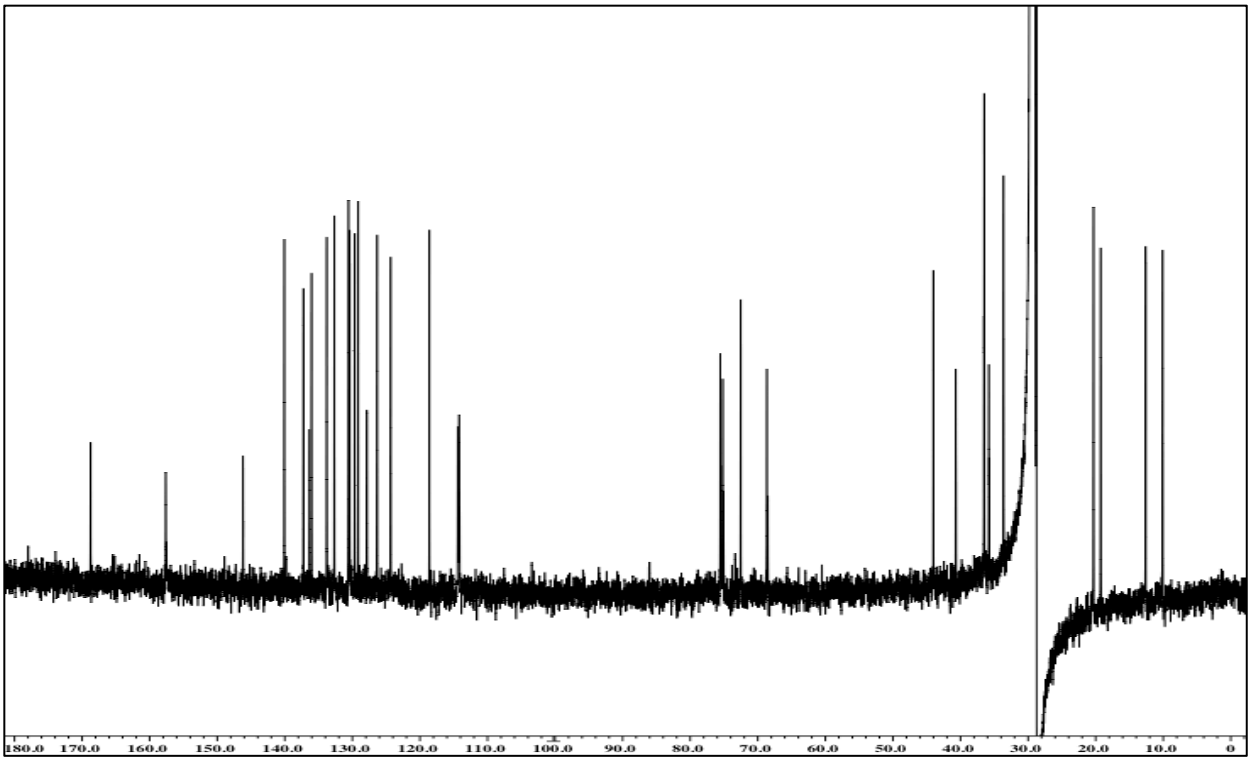

Figure S26. ^{13}C NMR spectrum of antarlide F (**6**)
(125 MHz, Acetone-d_6, Acetone-d_6 = 29.8 ppm)

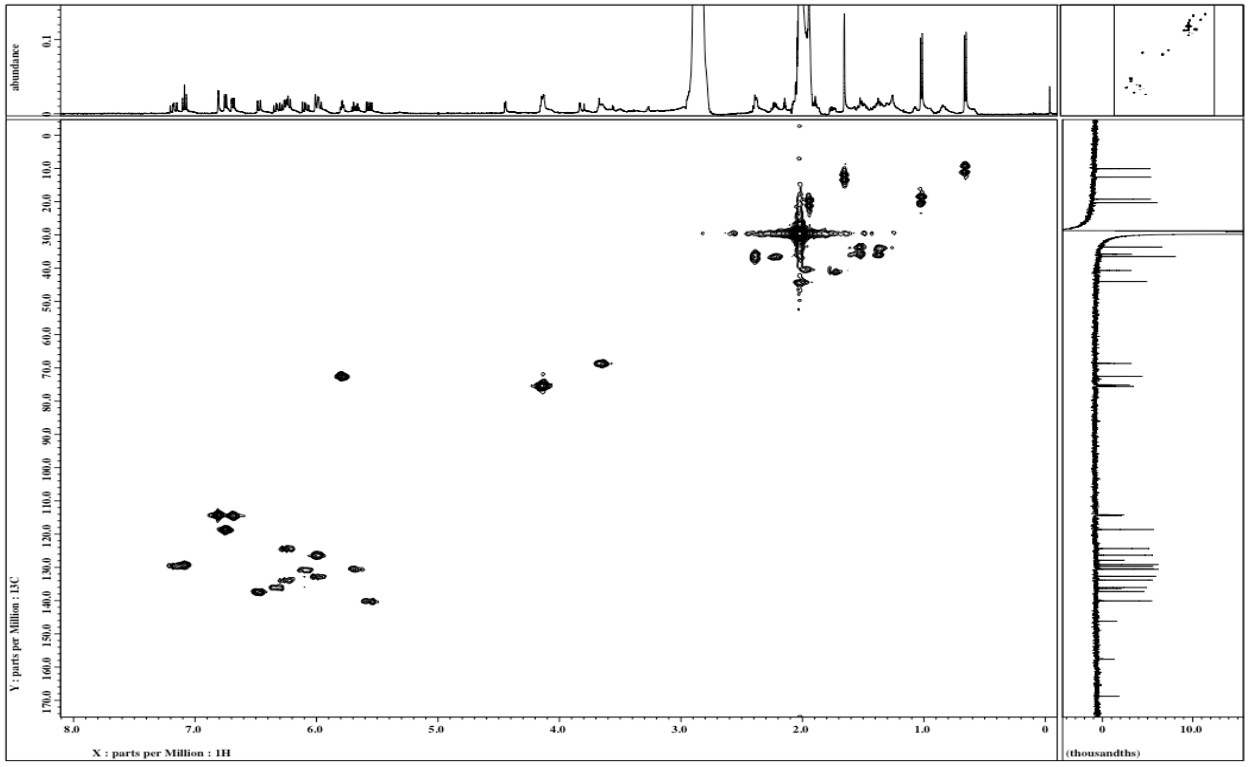

Figure S27. HMQC spectrum of antarlide F (**6**) (500 MHz, Acetone-d_6)

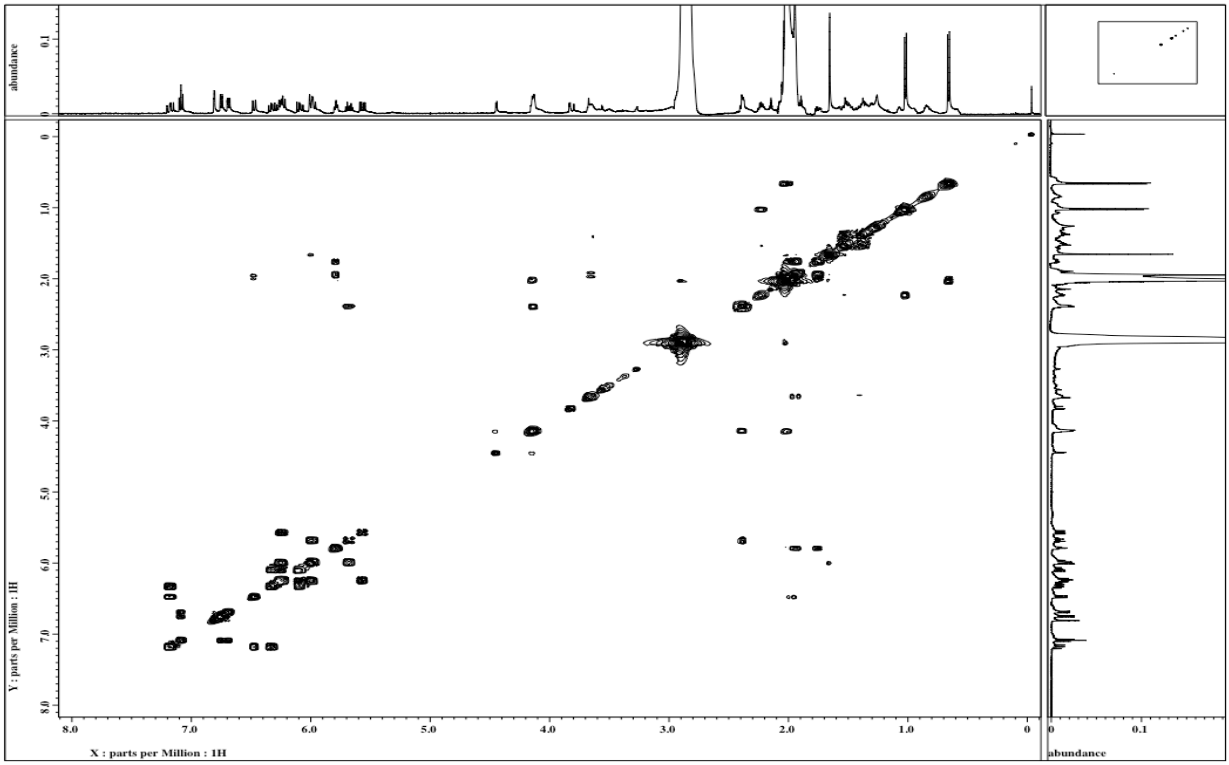

Figure S28. ^{1}H-^{1}H COSY spectrum of antarlide F (**6**) (500 MHz, Acetone-d_6)

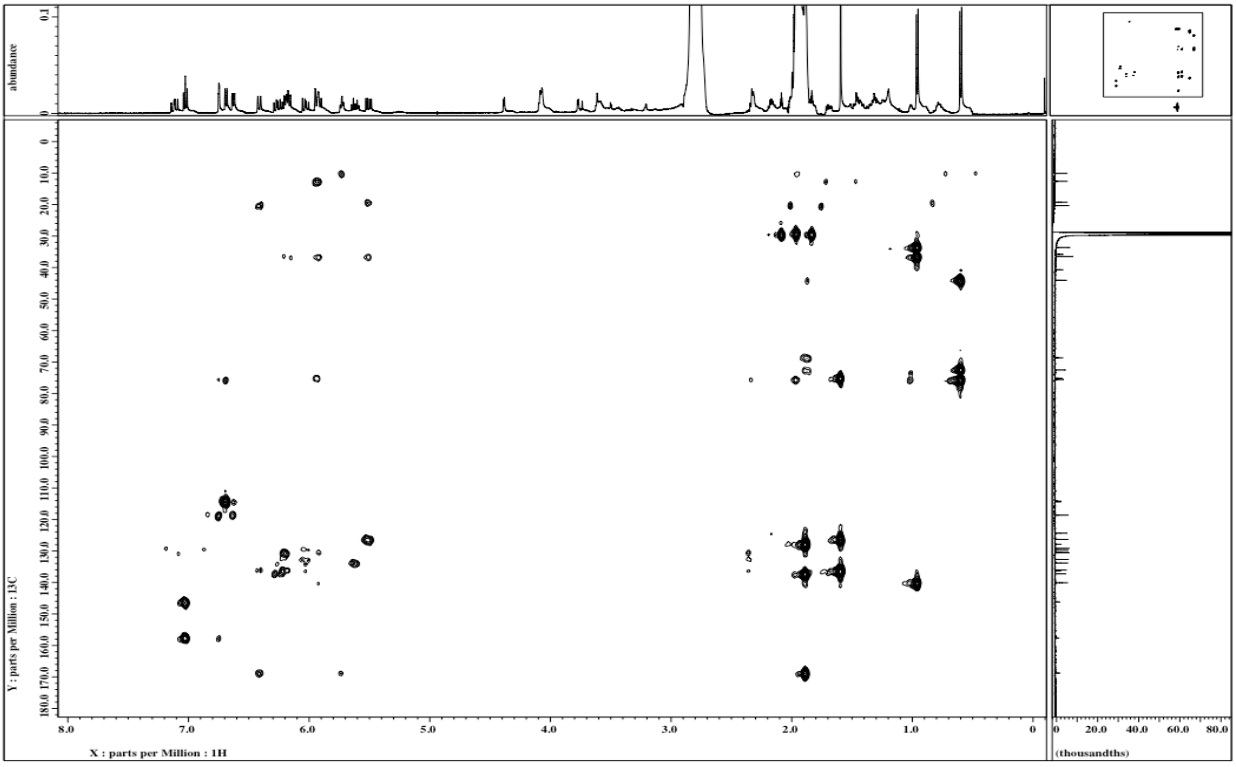

Figure S29. HMBC spectrum of antarlide F (**6**) (500 MHz, Acetone-d_6)

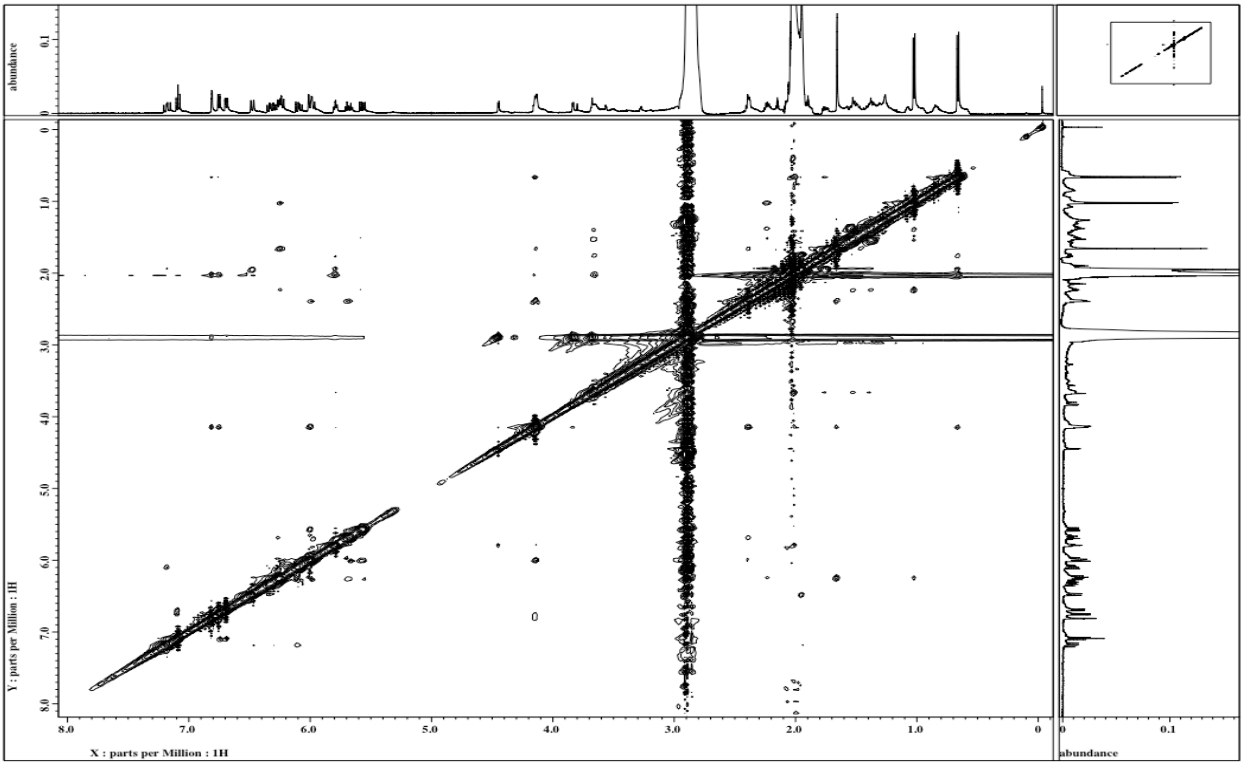

Figure S30. NOESY spectrum of antarlide F (**6**) (500 MHz, Acetone-d_6)

Table S5. ^{1}H and ^{13}C NMR Data for antarlide F (**6**) in Acetone-d_6

position	δ_c	δ_H mult (*J* in Hz)
1	168.7	-
2	127.8	-
2a	20.3	1.98 (3H, s)
3	137.2	6.51 (1H, d, 11.4)
4	129.6	7.21 (1H, dd, 11.4, 15.0)
5	136.0	6.36 (1H, dd, 10.1, 15.0)
6	130.5	6.12 (1H, dd, 10.1, 15.0)
7	124.3	6.27 (1H, m)
8	132.6	6.02 (1H, m)
9	130.4	5.71 (1H, ddd, 6.4, 7.9)
10	36.5	2.43 (2H, m)
11	75.1	4.17 (1H, m)
12	136.3	-
12a	12.6	1.69 (3H, s)
13	126.3	6.02 (1H, m)
14	133.6	6.27 (1H, m)
15	140.0	5.60 (1H, dd, 7.2, 15.2)
16	36.5	2.25 (1H, m)
16a	19.2	1.06 (3H, d, 6.8)
17	33.5	1.40, 1.56 (2H, m)
18	35.6	1.40, 1.55 (2H, m)
19	68.6	3.68 (1H, m)
20	40.7	1.78, 1.99 (2H, m)
21	72.5	5.82 (1H, m)
22	44.0	2.05 (1H, m)
22a	10.0	0.69 (3H, d, 6.9)
23	75.5	4.17 (1H, m)
24	146.1	-
25	114.2	6.84 (1H, t, 1.85)
26	157.6	-
27	114.4	6.72 (1H, dd, 2.7, 7.7)
28	129.1	7.12 (1H, t, 7.7)
29	118.6	6.78 (1H, d, 7.7)

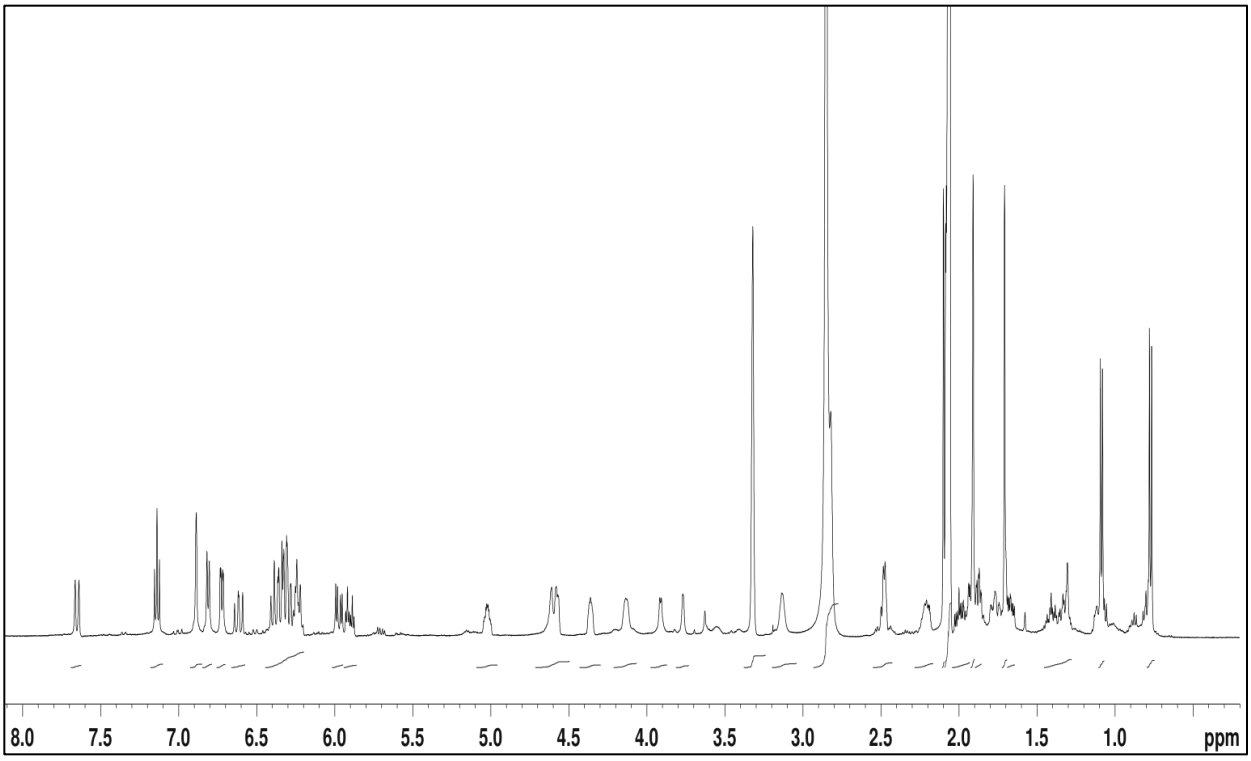

Figure S31. ^{1}H NMR spectrum of antarlide G (**7**)
(500 MHz, Acetone-d_6, Acetone-d_6 = 2.05 ppm)

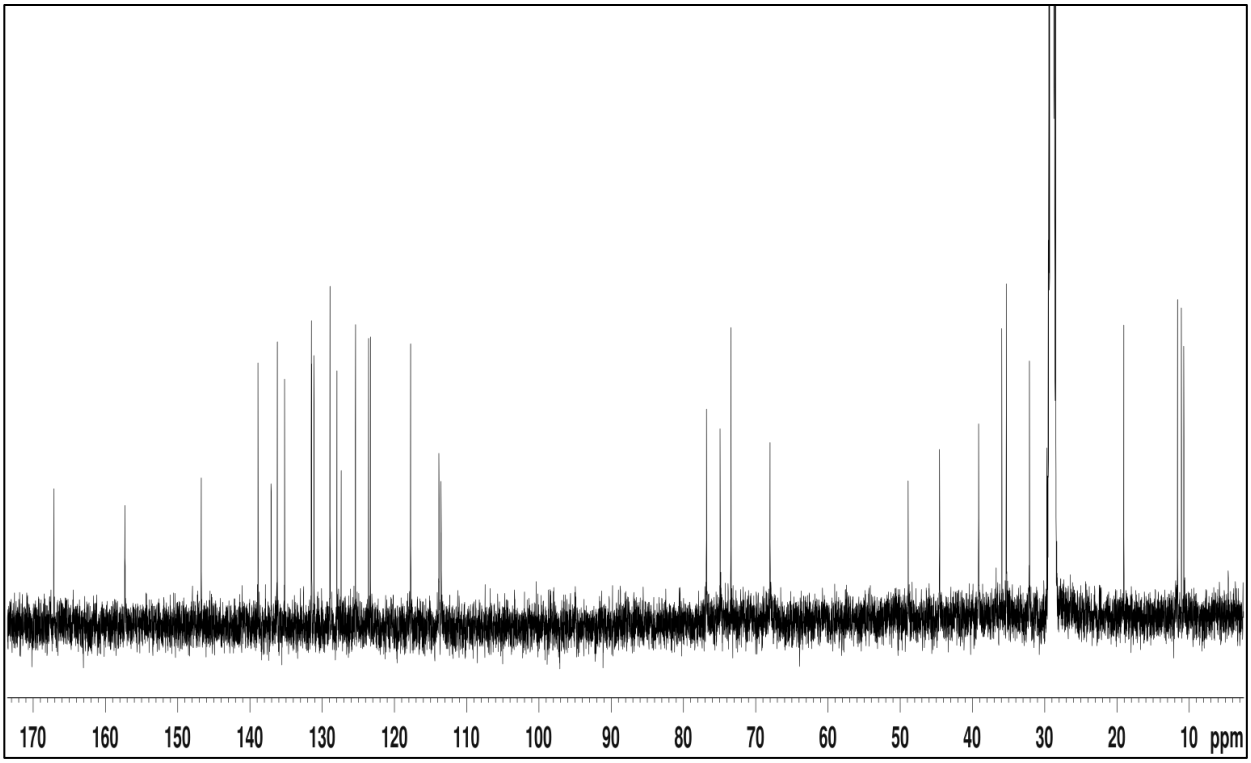

Figure S32. ^{13}C NMR spectrum of antarlide G (**7**)
(500 MHz, Acetone-d_6, Acetone-d_6 = 29.8 ppm)

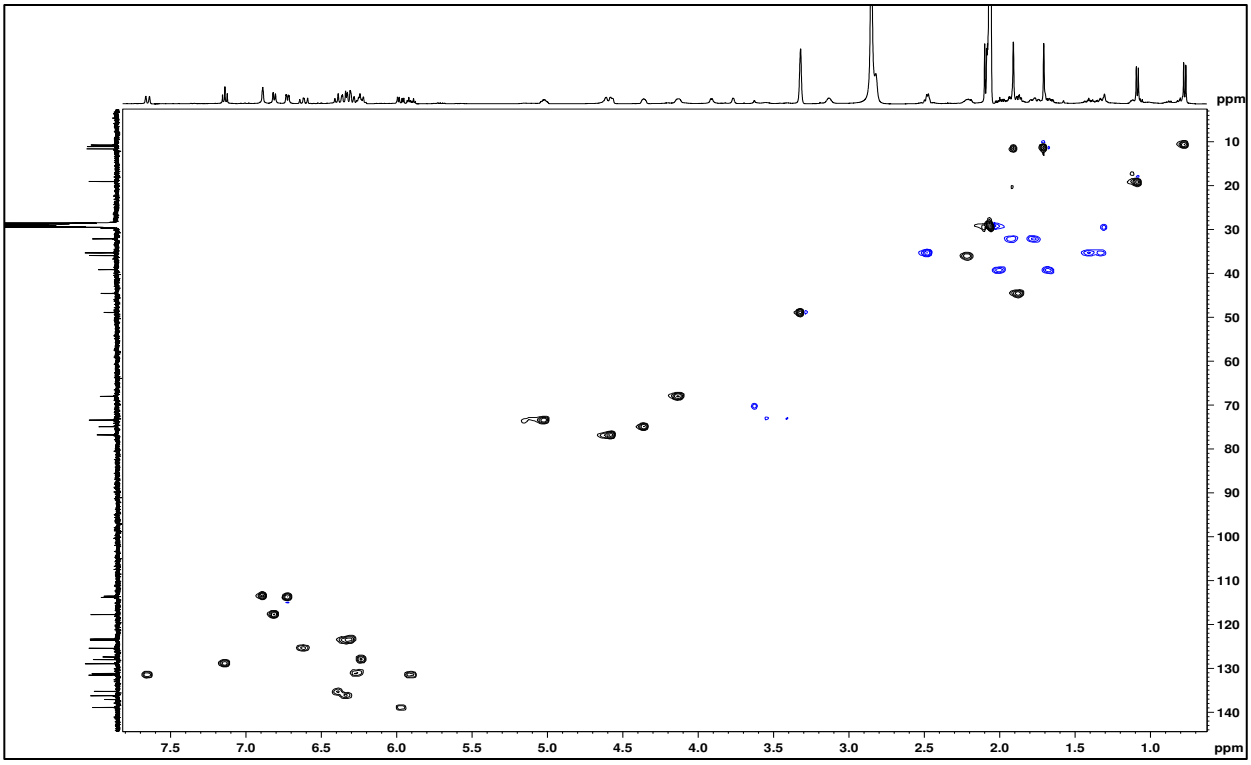

Figure S33. HSQC spectrum of antarlide G (**7**) (500 MHz, Acetone-d_6)

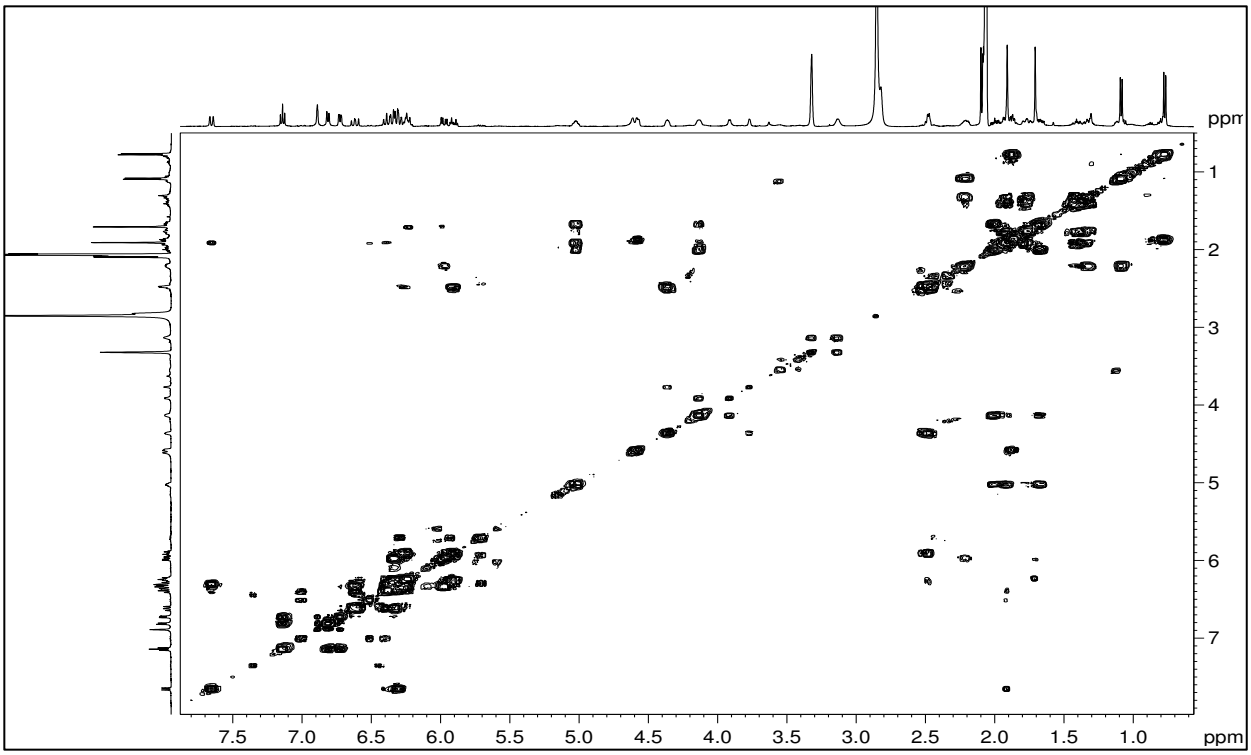

Figure S34. ^{1}H-^{1}H COSY spectrum of antarlide G (**7**) (500 MHz, Acetone-d_6)

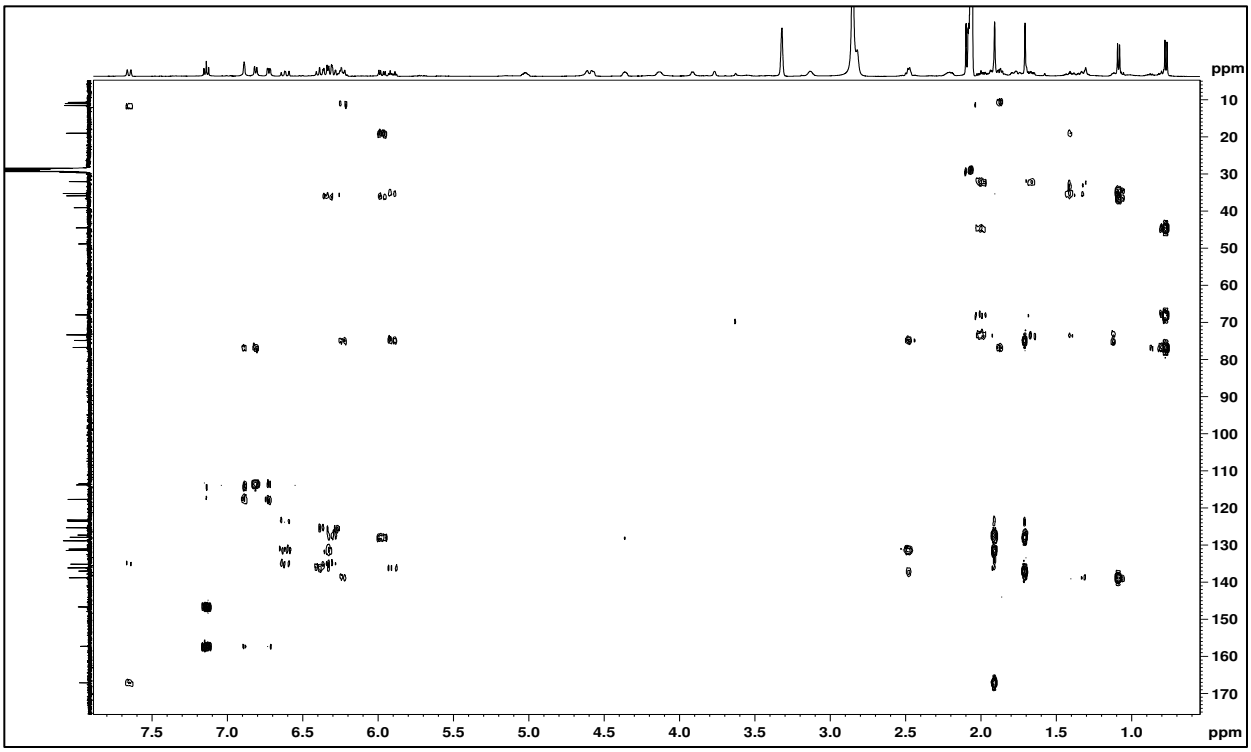

Figure S35. HMBC spectrum of antarlide G (**7**) (500 MHz, Acetone-d_6)

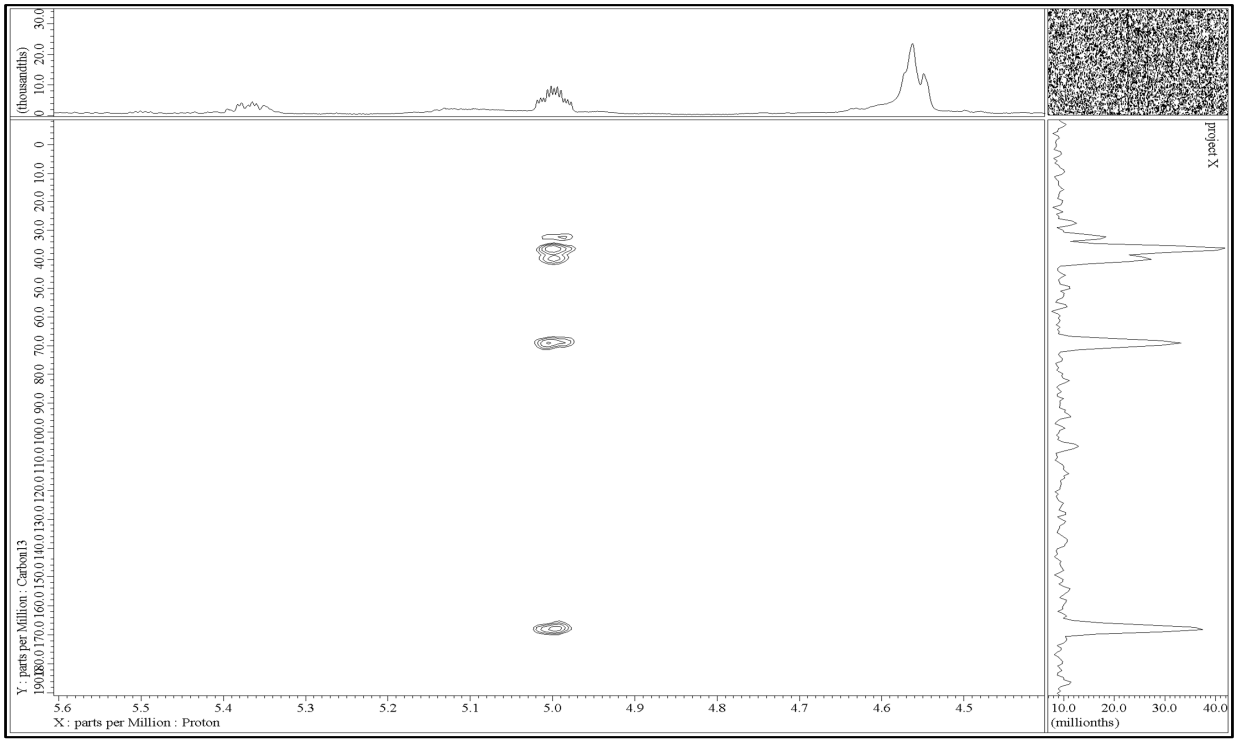

Figure S36. Selective HMBC spectrum of antarlide G (**7**) (600 MHz, Acetone-d_6)

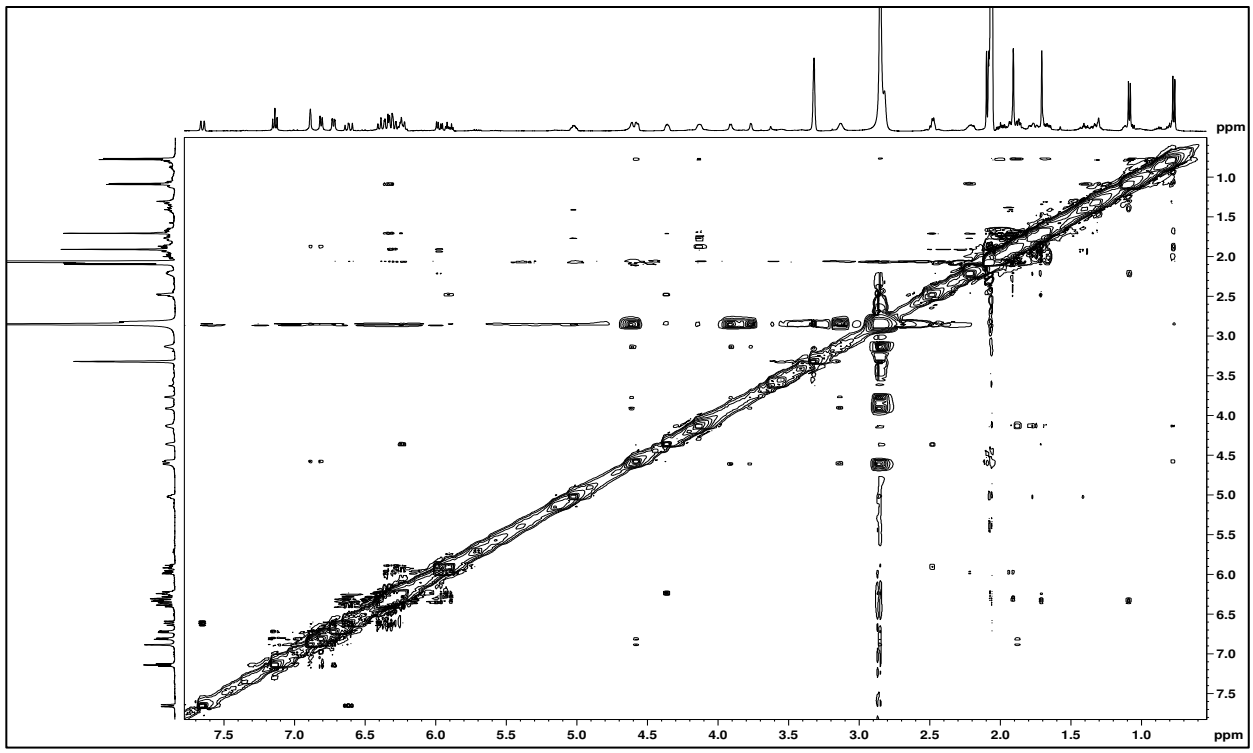

Figure S37. NOESY spectrum of antarlide G (**7**) (500 MHz, Acetone-d_6)

Table S6. ^{1}H and ^{13}C NMR data for antarlide G (**7**) in Acetone-d_6

position	δ_c	δ_H mult (*J* in Hz)
1	167.1	-
2	127.3	-
2a	11.8	1.91 (3H, s)
3	131.5	7.65 (1H, d, 12.2)
4	123.3	6.31 (1H, m)
5	135.2	6.39 (1H, m)
6	125.4	6.62 (1H, dd, 11.7, 15.2)
7	136.2	6.34 (1H, m)
8	131.1	6.26 (1H, m)
9	131.4	5.90 (1H, ddd, 5.0, 15.2)
10	35.3	2.48 (2H, m)
11	74.9	4.36 (1H, m)
12	137.0	-
12a	11.1	1.71 (3H, s)
13	127.9	6.24 (1H, m)
14	123.5	(1H, dd, 10.5, 15.3)
15	138.9	5.97 (1H, dd, 5.6, 15.3)
16	35.9	2.22 (1H, m)
16a	19.0	1.09 (3H, d, 6.7)
17	35.3	1.33, 1.41 (2H, m)
18	32.1	1.77, 1.92 (2H, m)
19	73.4	5.02 (1H, m)
20	39.1	1.68, 2.00 (2H, m)
21	68.0	4.13 (1H, m)
22	44.5	1.87 (1H, m)
22a	10.7	0.77 (3H, d, 7.2)
23	76.8	4.57 (1H, m)
24	146.7	-
25	113.5	6.89 (1H, s)
26	157.3	-
27	113.8	6.72 (1H, dd, 2.4, 8.0)
28	128.9	7.14 (1H, t, 8.0)
29	117.7	6.81 (1H, d, 8.0)

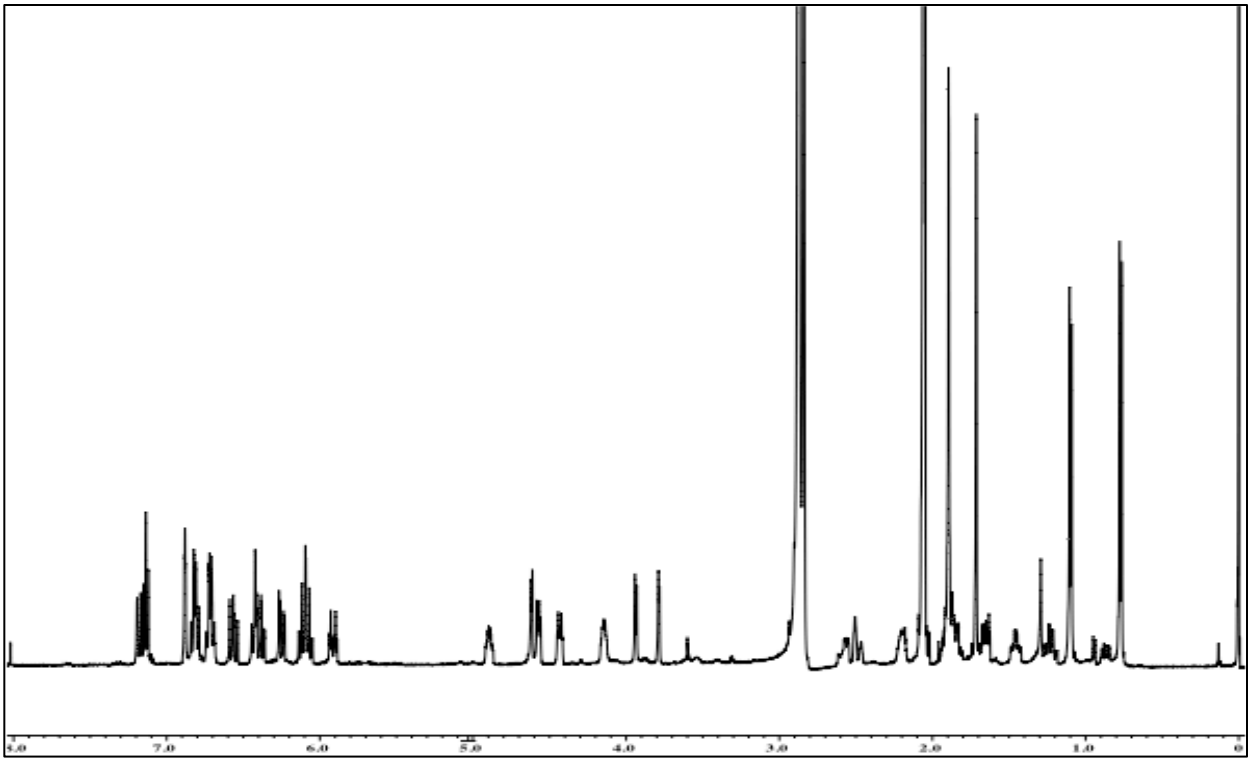

Figure S38. ^{1}H NMR spectrum of antarlide H (**8**)
(500 MHz, Acetone-d_6, TMS = 0.00 ppm)

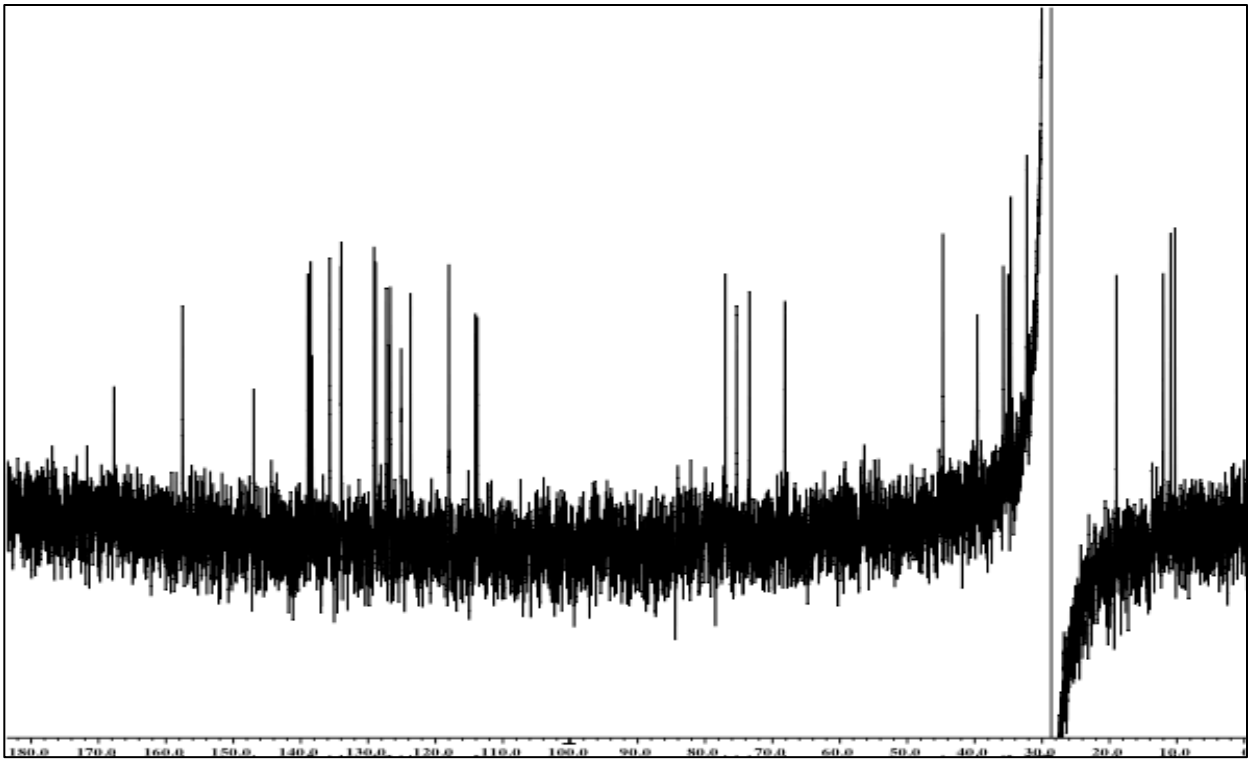

Figure S39. ^{13}C NMR spectrum of antarlide H (**8**)
(500 MHz, Acetone-d_6, Acetone-d_6 = 29.8 ppm)

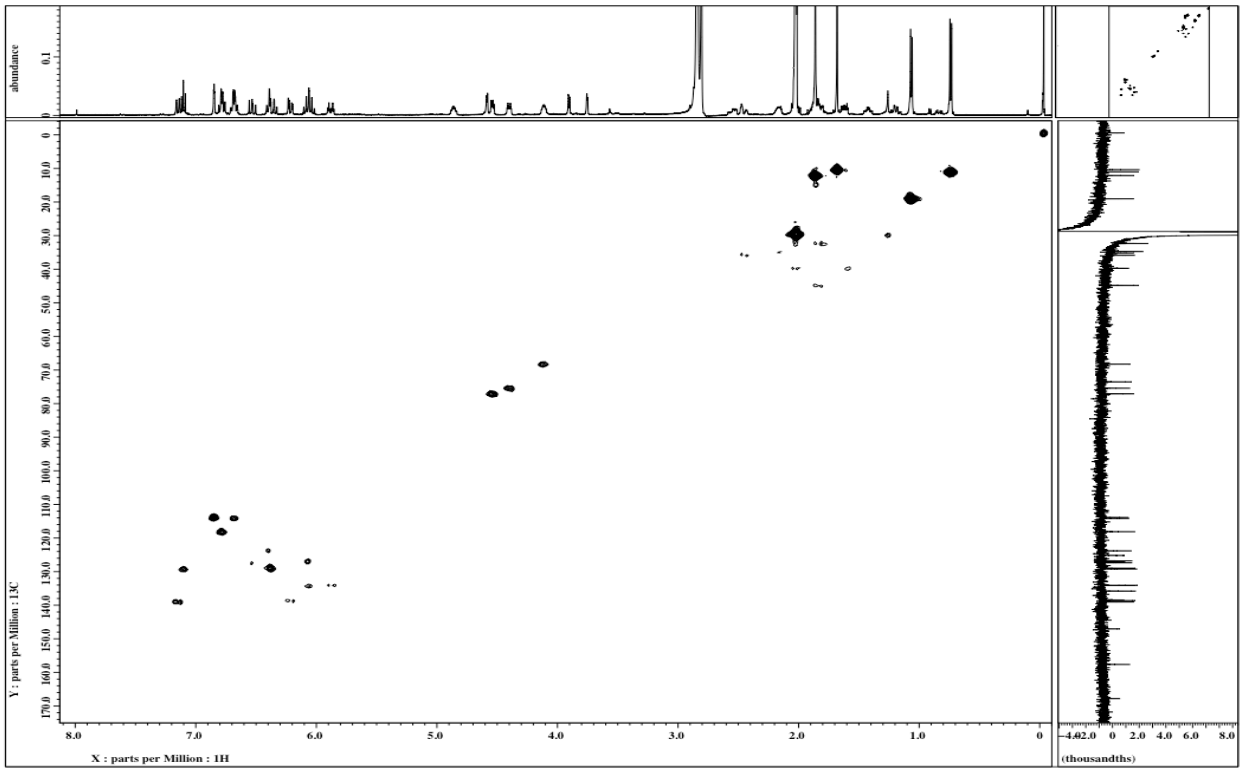

Figure S40. HMQC spectrum of antarlide H (**8**) (500 MHz, Acetone-d_6)

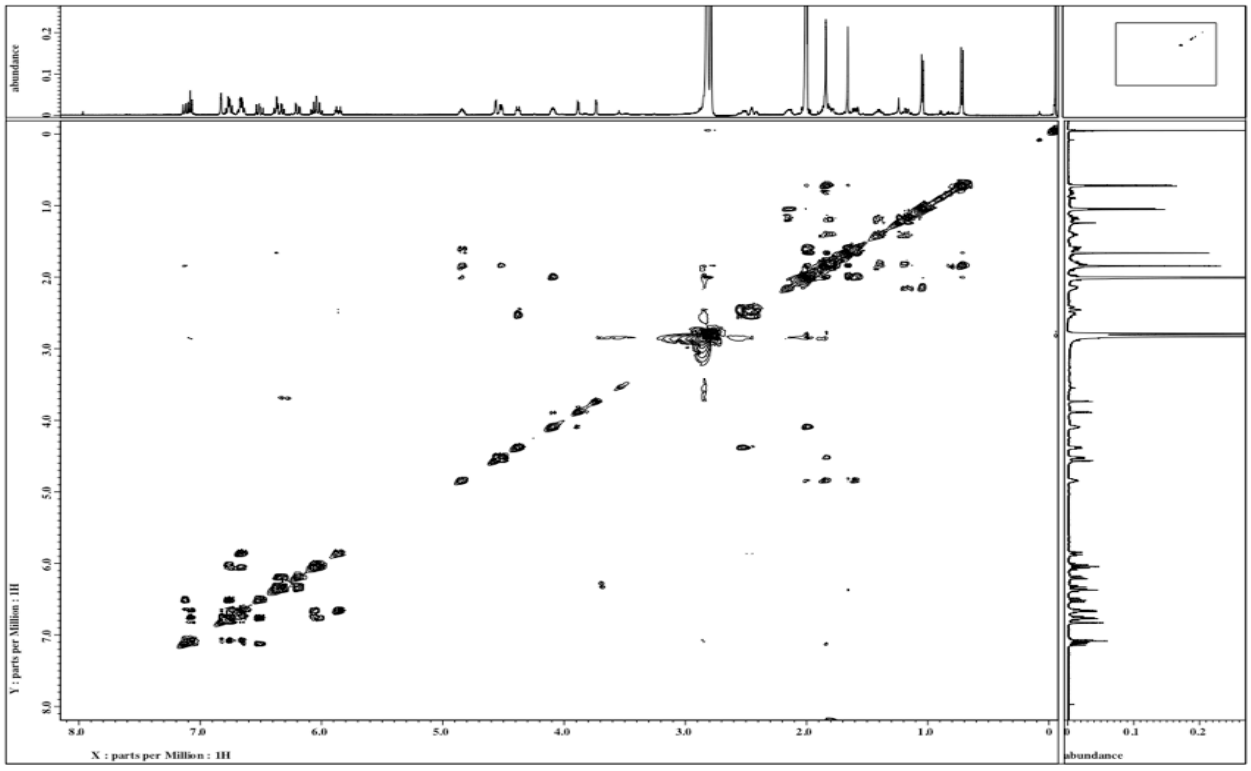

Figure S41. ^{1}H-^{1}H COSY spectrum of antarlide H (**8**) (500 MHz, Acetone-d_6)

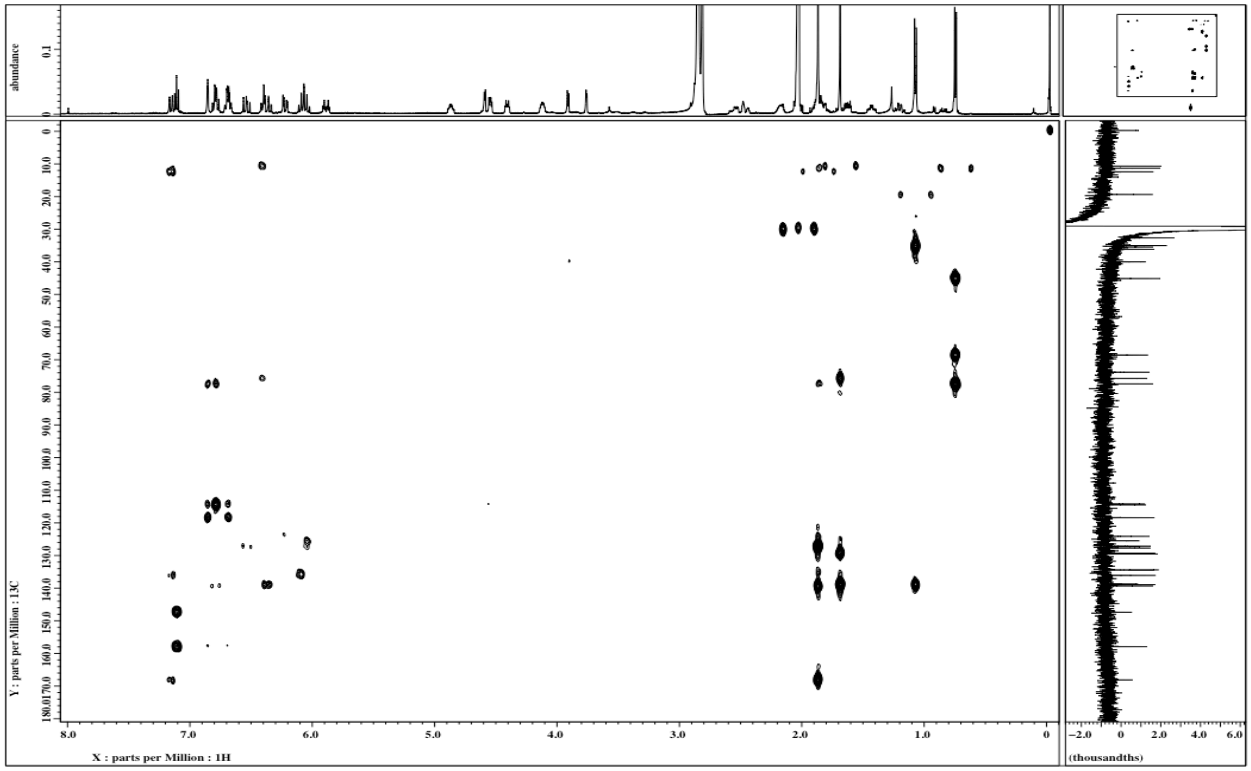

Figure S42. HMBC spectrum of antarlide H (**8**) (500 MHz, Acetone-d_6)

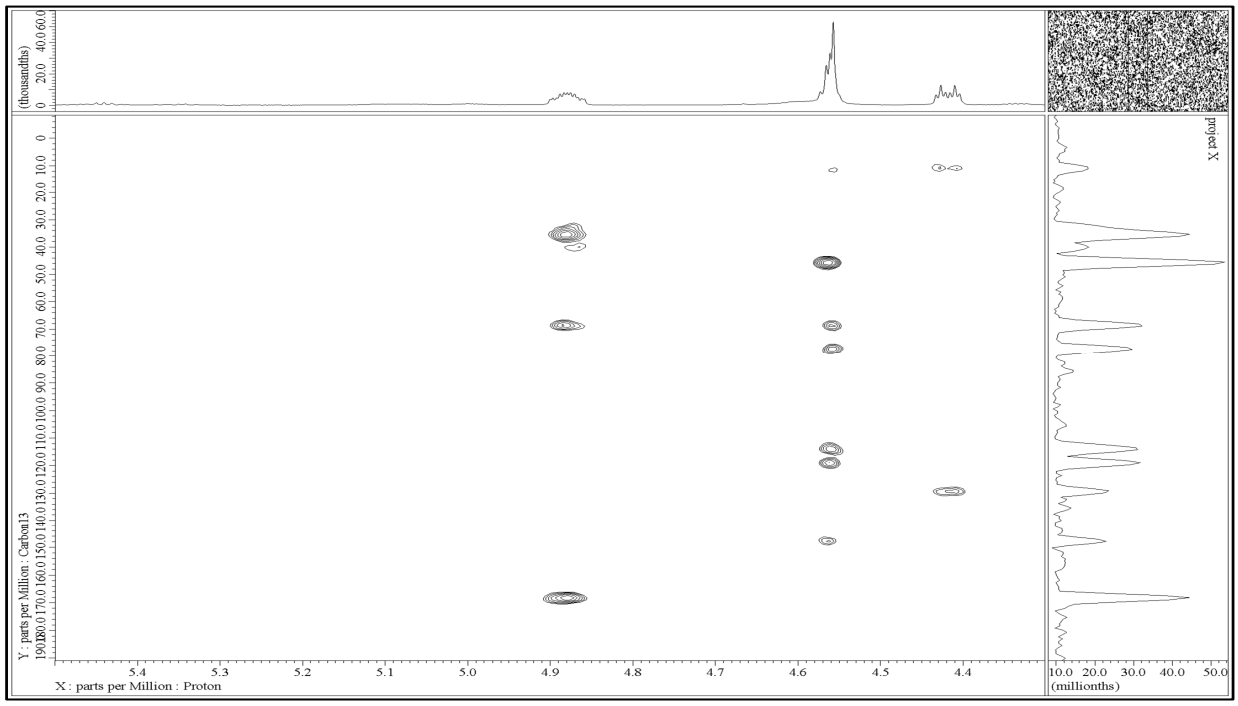

Figure S43. Selective HMBC spectrum of antarlide H (**8**) (600 MHz, Acetone-d_6)

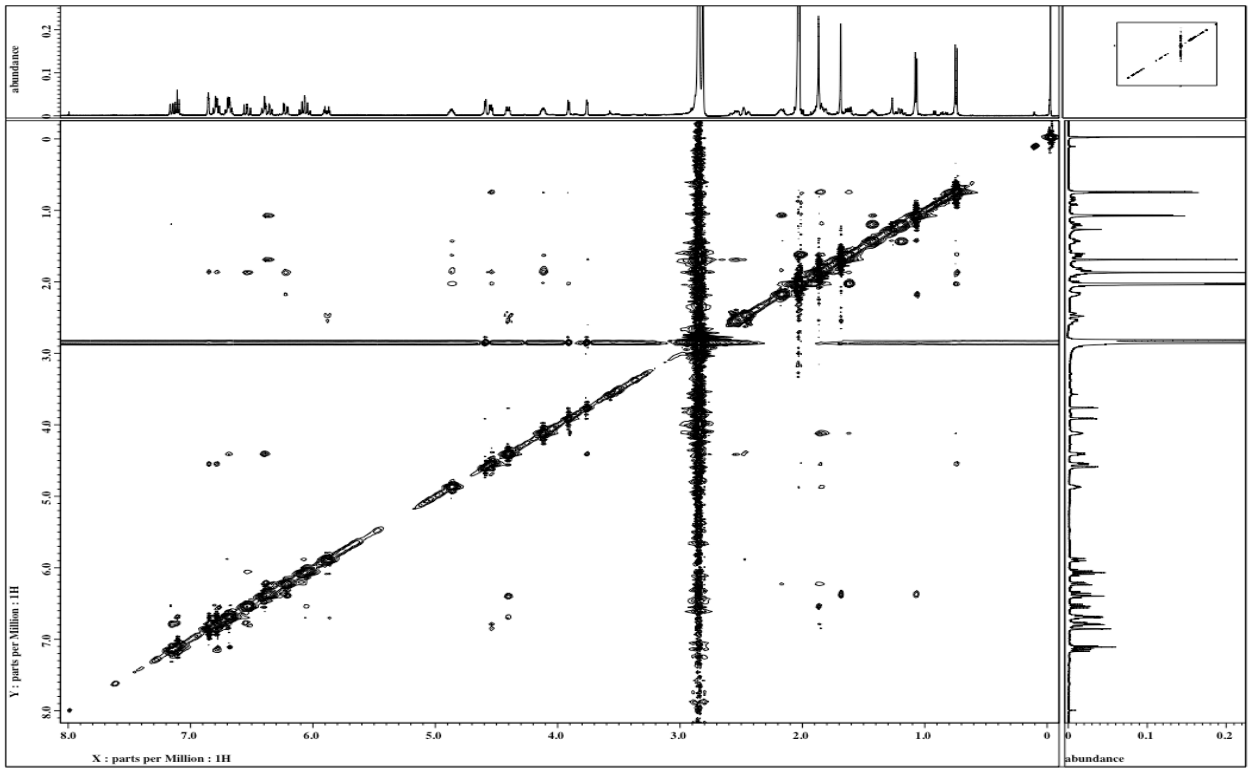

Figure S44. NOESY spectrum of antarlide H (**8**) (500 MHz, Acetone-d_6)

Table S7. ^{1}H and ^{13}C NMR data for antarlide H (**8**) in Acetone-d_6

position	δ_c	δ_H mult (*J* in Hz)
1	167.7	-
2	126.9	-
2a	12.0	1.89 (3H, s)
3	138.9	7.18 (1H, d, 11.6)
4	127.3	6.56 (1H, dd, 11.6, 14.4)
5	135.7	6.82 (1H, m)
6	134.0	6.08 (1H, m)
7	126.7	6.10 (1H, m)
8	125.1	6.71 (1H, m)
9	134.0	5.91 (1H, ddd, 4.8, 15.9)
10	35.8	2.57 (2H, m)
11	75.3	4.43 (1H, dt, 0.3, 7.0)
12	138.3	-
12a	10.3	1.71 (3H, s)
13	128.9	6.41 (1H, m)
14	123.7	6.42 (1H, m)
15	138.5	6.25 (1H, dd, 3.9, 14.2)
16	34.6	2.19 (1H, m)
16a	19.0	1.10 (3H, d, 6.7)
17	35.1	1.22, 1.45 (2H, m)
18	32.2	1.83 (2H, m)
19	73.4	4.89 (1H, m)
20	39.6	1.65, 2.05 (2H, m)
21	68.2	4.14 (1H, m)
22	44.7	1.85 (1H, m)
22a	10.9	0.77 (3H, d, 7.1)
23	77.0	4.57 (1H, m)
24	147.0	-
25	113.8	6.88 (1H, s)
26	157.5	-
27	114.1	6.71 (1H, m)
28	129.1	7.14 (1H, t, 7.8)
29	118.0	6.82 (1H, m)

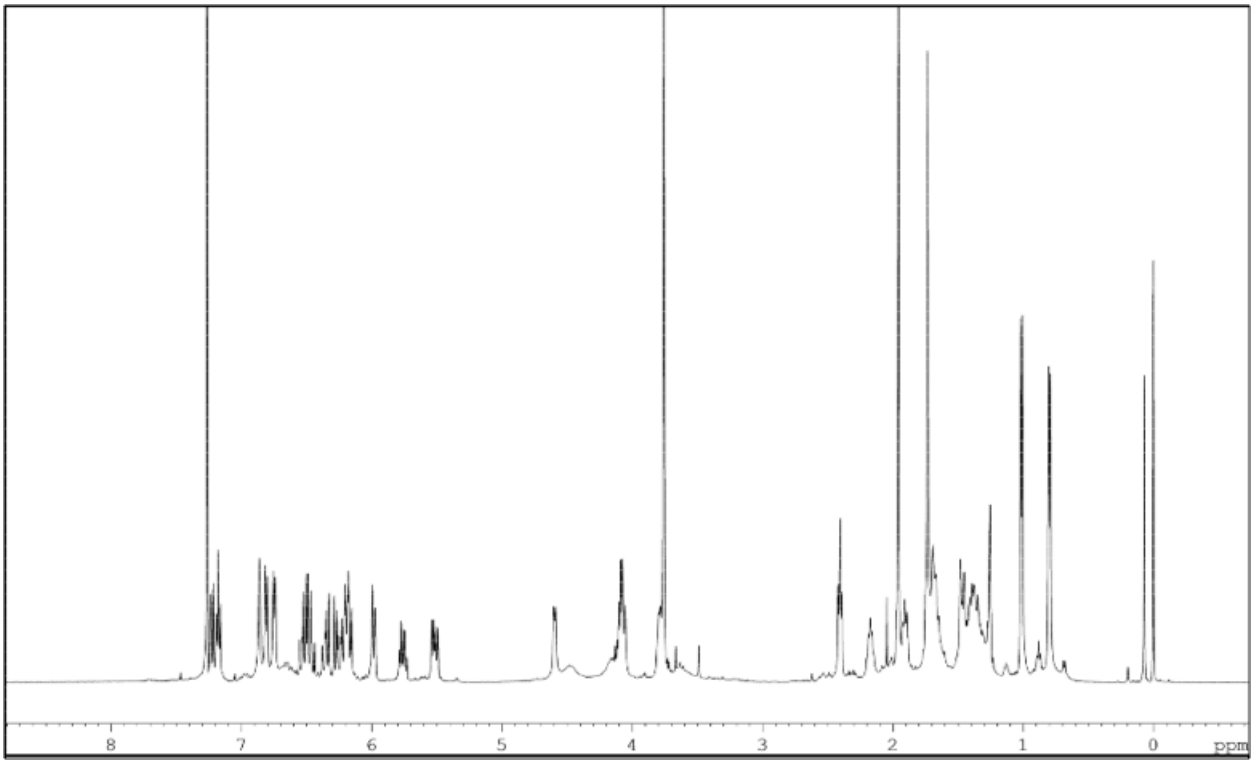

Figure S45. ^{1}H NMR spectrum of **9**
(500 MHz, $CDCl_3$, TMS = 0.00 ppm)

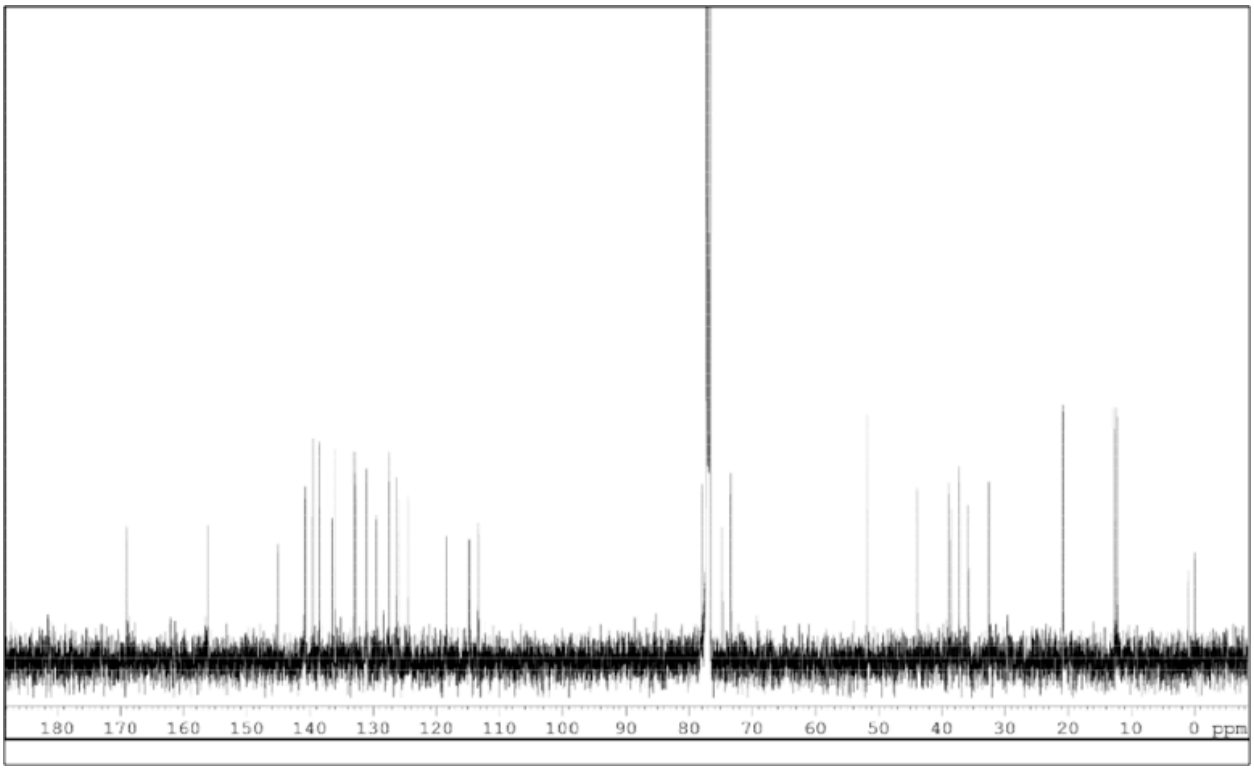

Figure S46. ^{13}C NMR spectrum of **9**
(500 MHz, $CDCl_3$, $CDCl_3$ = 77.2 ppm)

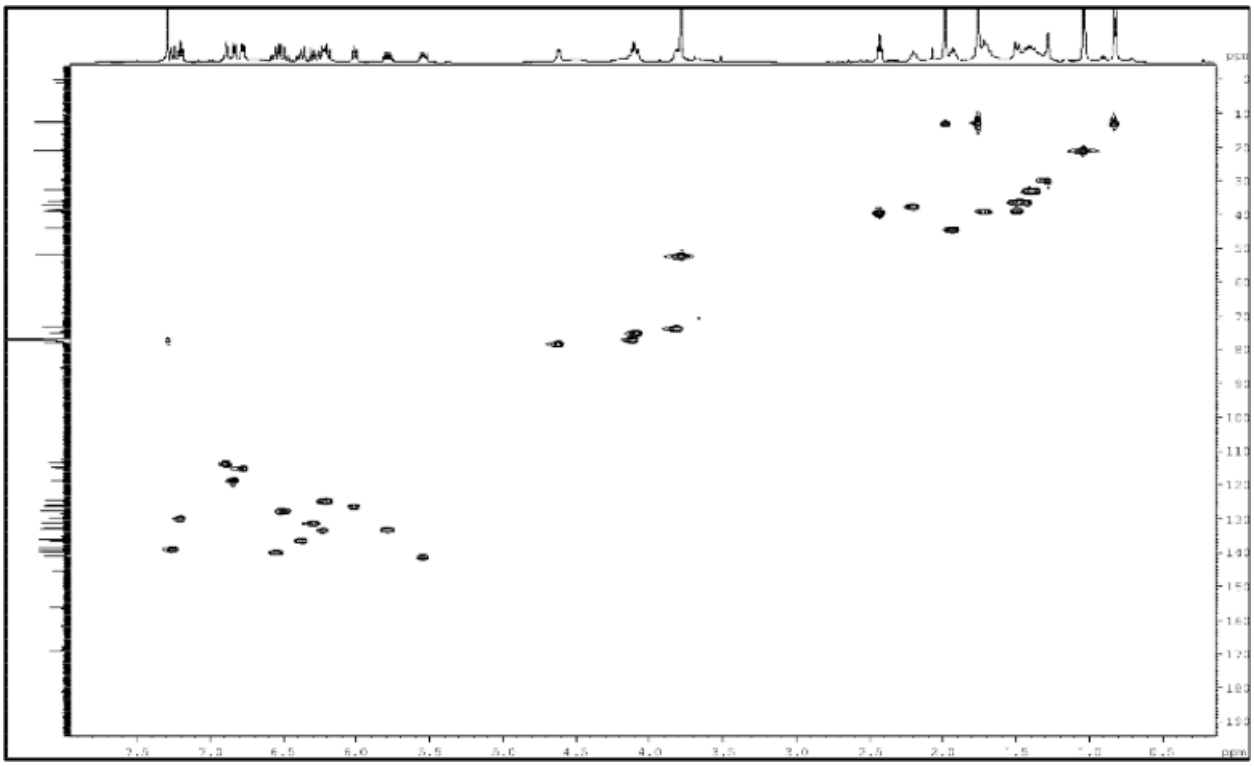

Figure S47. HSQC spectrum of **9** (500 MHz, $CDCl_3$)

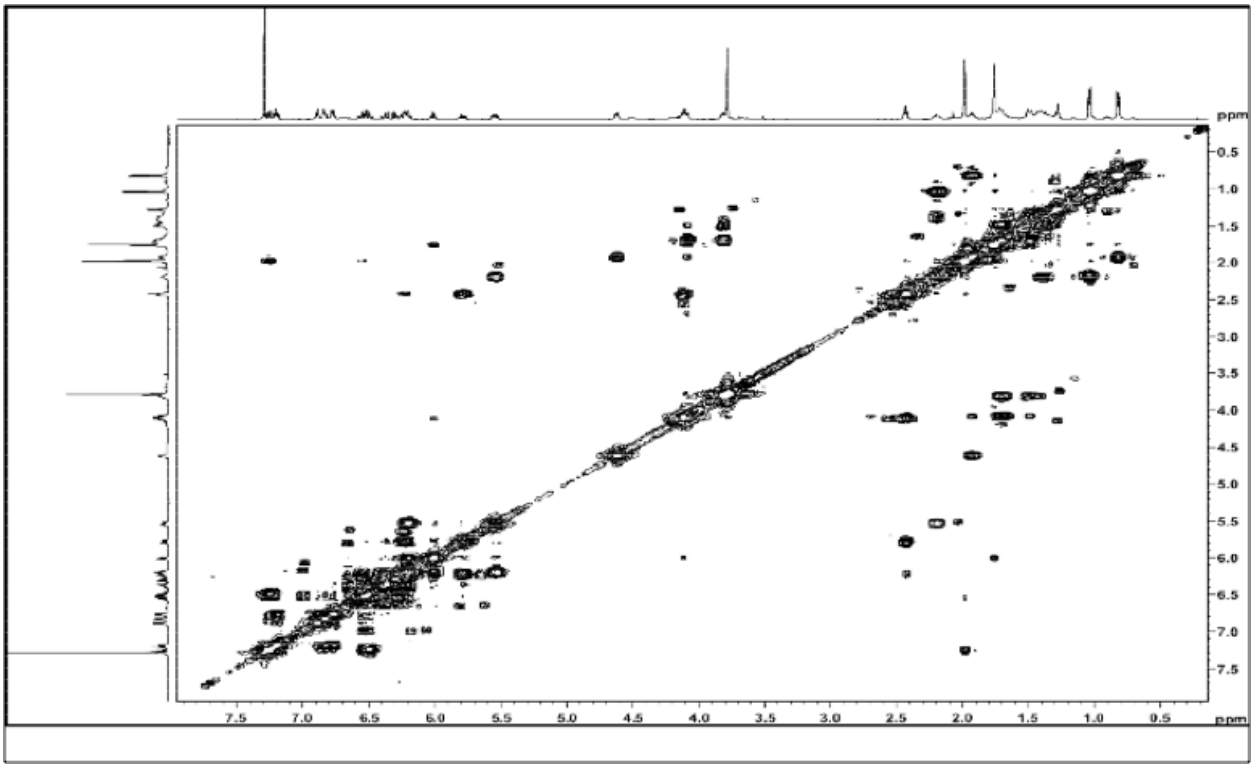

Figure S48. ^1H-^1H COSY spectrum of **9** (500 MHz, $CDCl_3$)

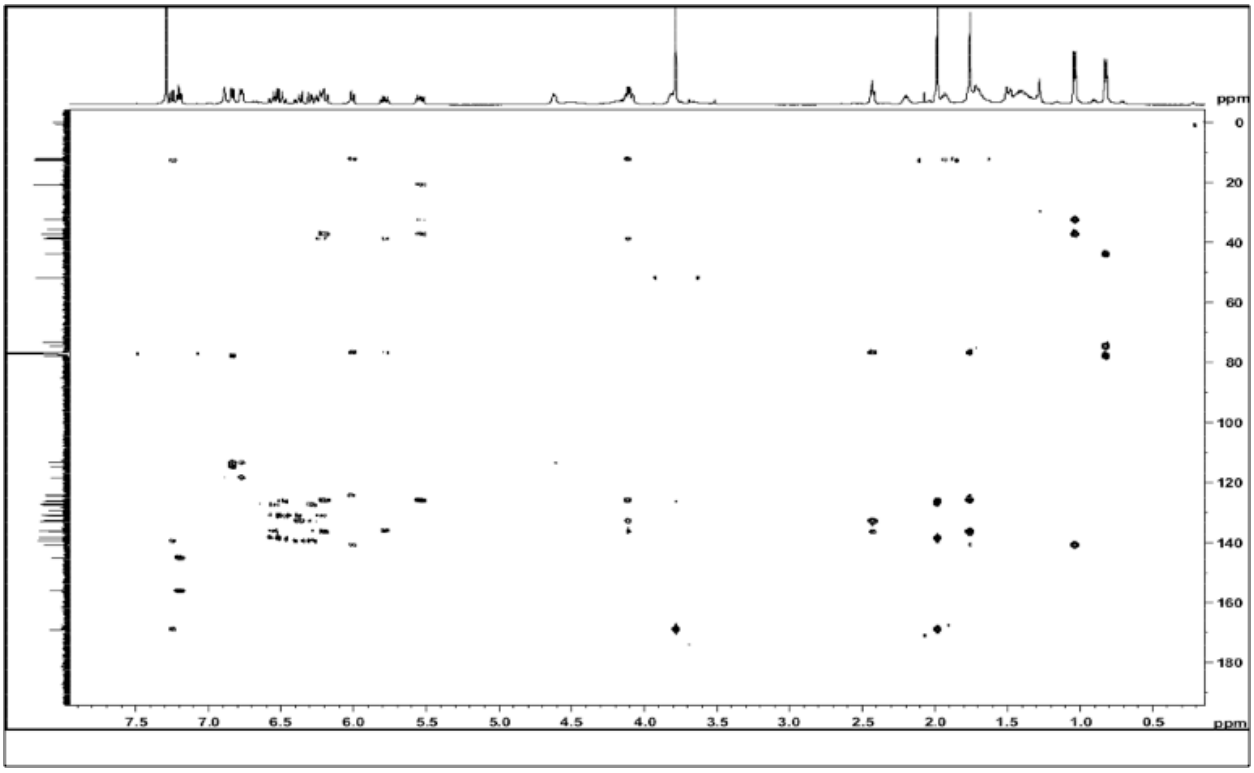

Figure S49. HMBC spectrum of **9** (500 MHz, $CDCl_3$)

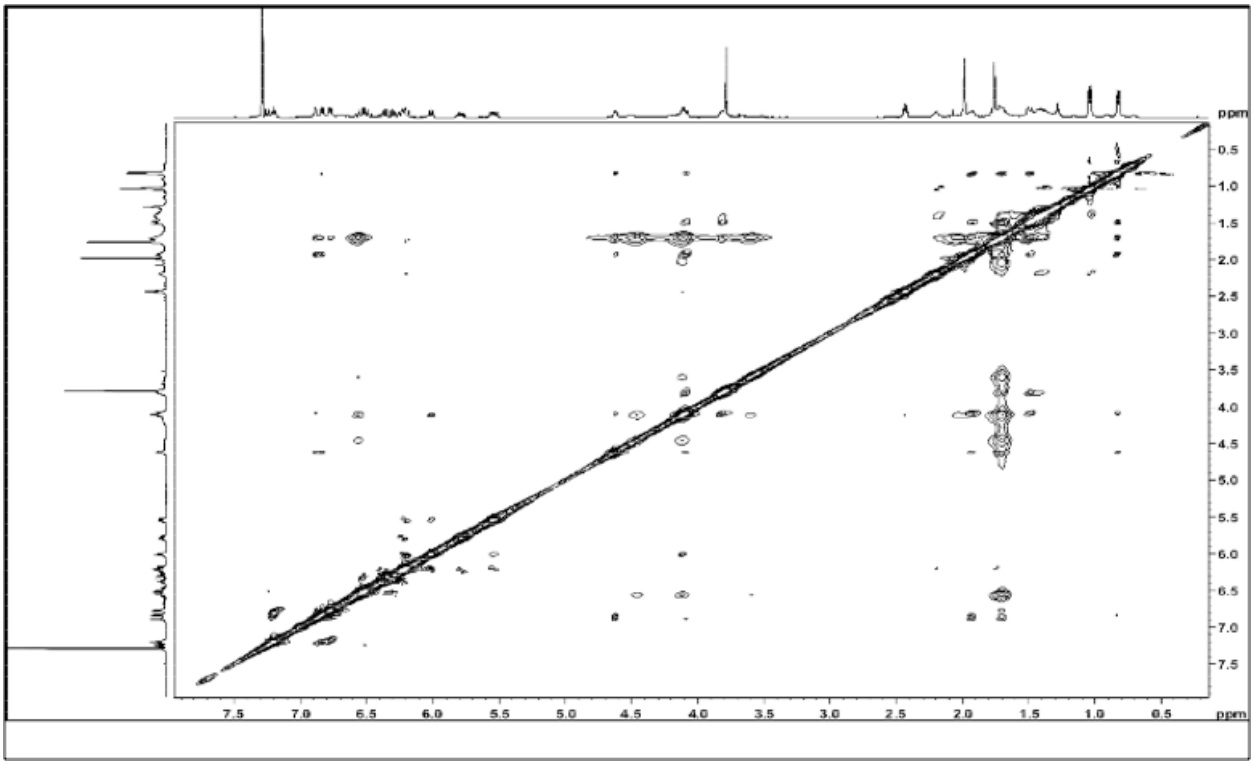

Figure S50. NOESY spectrum of **9** (500 MHz, $CDCl_3$)

Table S8. ^{1}H and ^{13}C NMR data for **9** in $CDCl_3$

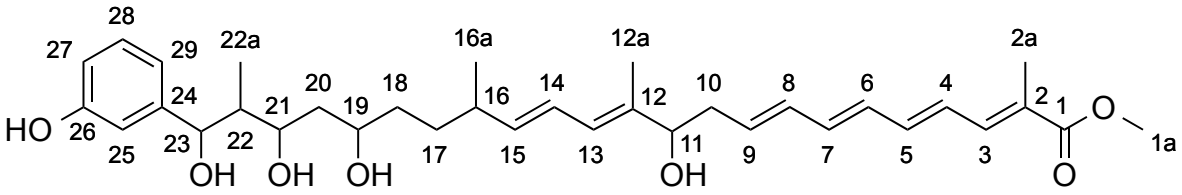

9

position	δ_c	δ_H mult (*J* in Hz)
1	169.0	
1a	51.9	3.78 (3H, s)
2	126.4	-
2a	12.8	1.98 (3H, s)
3	138.6	7.25 (1H, d, 11.0)
4	127.5	6.50 (1H, dd, 11.0, 14.6)
5	139.6	6.54 (1H, dd, 10.1, 14.6)
6	131.1	6.29 (1H, dd, 10.1, 14.8)
7	136.2	6.37 (1H, dd, 10.6, 14.8)
8	133.0	6.23 (1H, dd, 10.6, 15.0)
9	132.9	5.78 (1H, dt, 7.6, 15.0)
10	38.9	2.43 (2H, t, 7.6)
11	76.7	4.11 (1H, m)
12	136.6	-
12a	12.3	1.76 (3H, s)
13	126.0	6.01 (1H, d, 10.8)
14	124.5	6.21 (1H, dd, 10.8, 14.8)
15	140.9	5.54 (1H, dd, 8.2, 14.8)
16	37.3	2.20 (1H, m)
16a	20.8	1.04 (3H, d, 6.6)
17	32.6	1.39 (2H, m)
18	35.9	1.46, 1.50 (2H, m)
19	73.4	3.82 (1H, m)
20	38.6	1.50, 1.71 (2H, m)
21	74.7	4.09 (1H, m)
22	44.0	1.93 (1H, m)
22a	12.5	0.82 (3H, d, 6.9)
23	78.0	4.62 (1H, d, 6.9)
24	145.2	-
25	113.4	6.84 (1H, s)
26	156.3	-
27	114.8	6.77 (1H, d, 7.8)
28	129.6	7.20 (1H, dd, 7.5, 7.8)
29	118.5	6.84 (1H, d, 7.5)

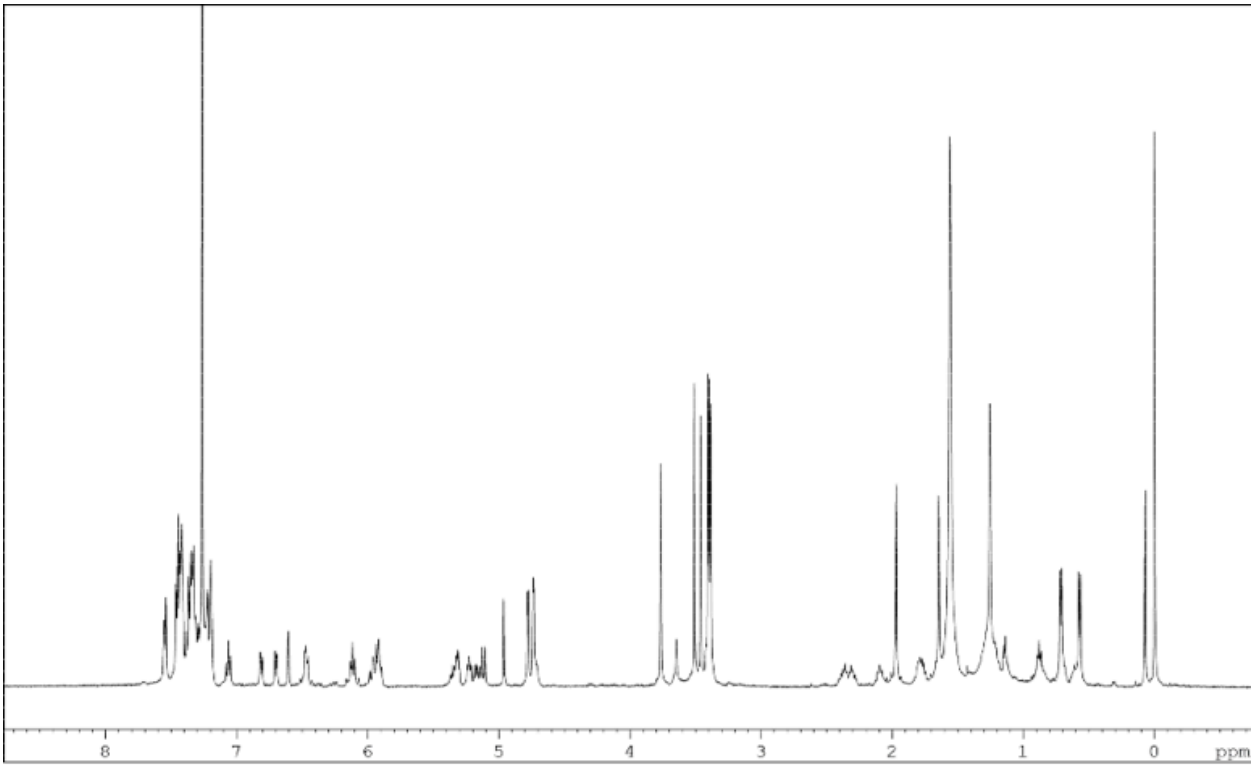

Figure S51. ^{1}H NMR spectrum of **10a**
(500 MHz, $CDCl_3$, TMS = 0.00 ppm)

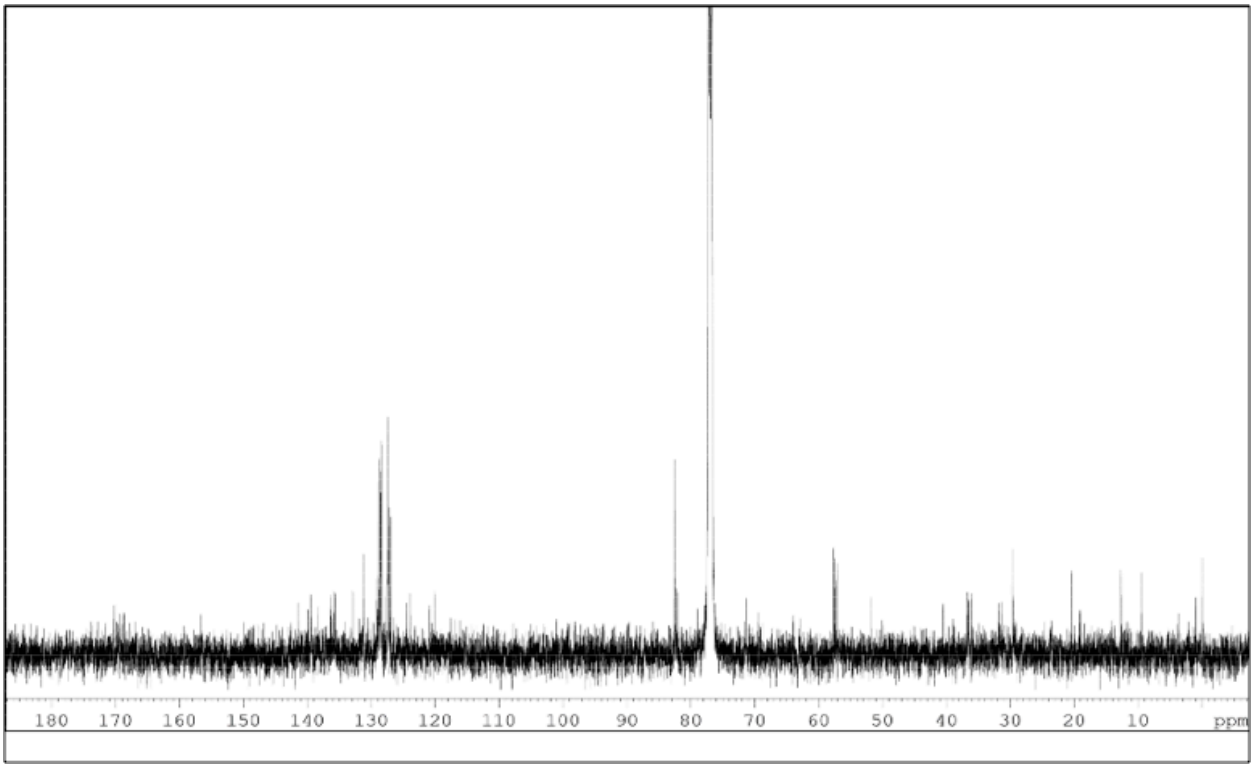

Figure S52. ^{13}C NMR spectrum of **10a**
(500 MHz, $CDCl_3$, $CDCl_3$ = 77.2 ppm)

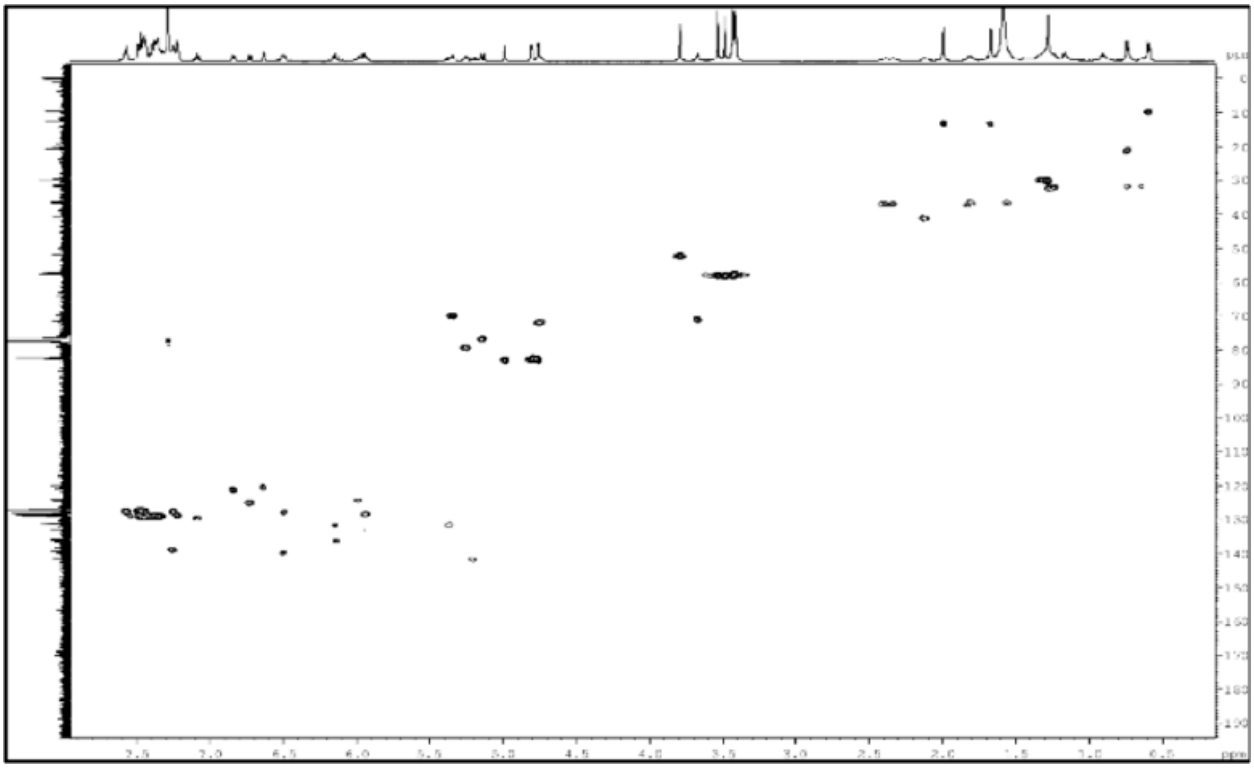

Figure S53. HSQC spectrum of **10a** (500 MHz, $CDCl_3$)

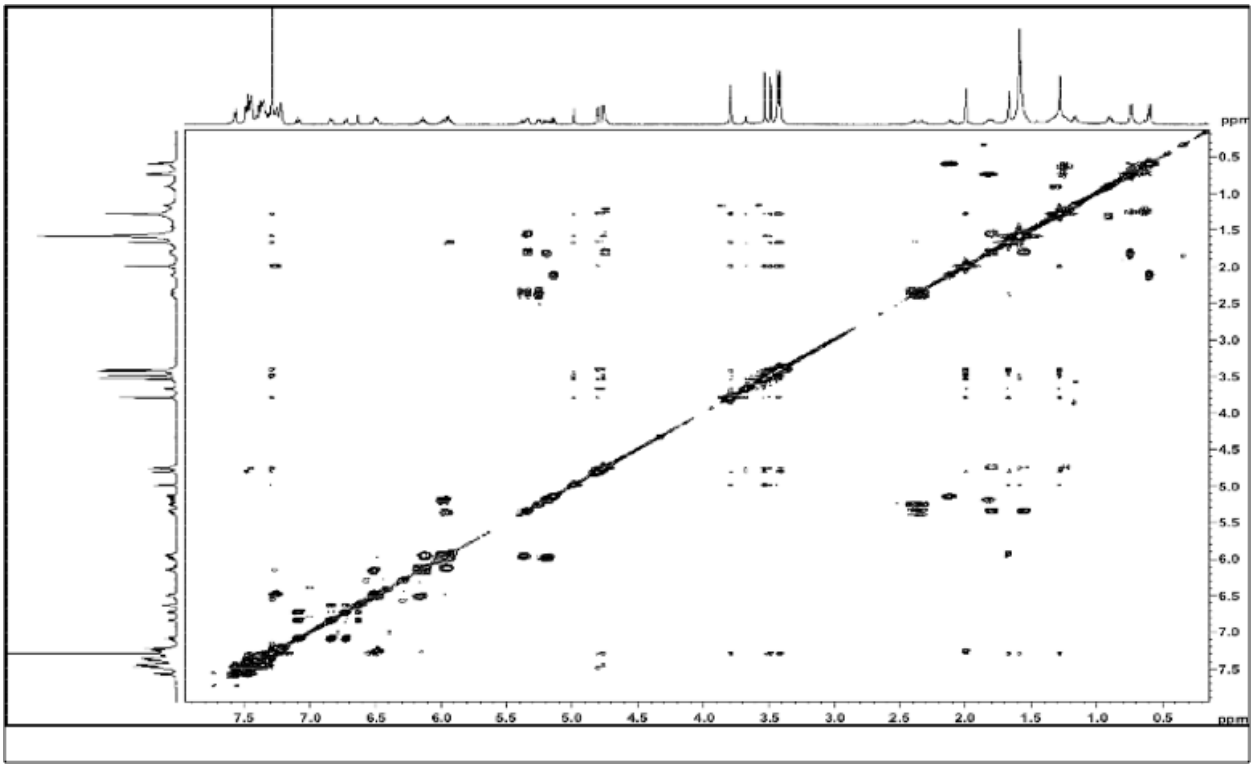

Figure S54. ^{1}H-^{1}H COSY spectrum of **10a** (500 MHz, $CDCl_3$)

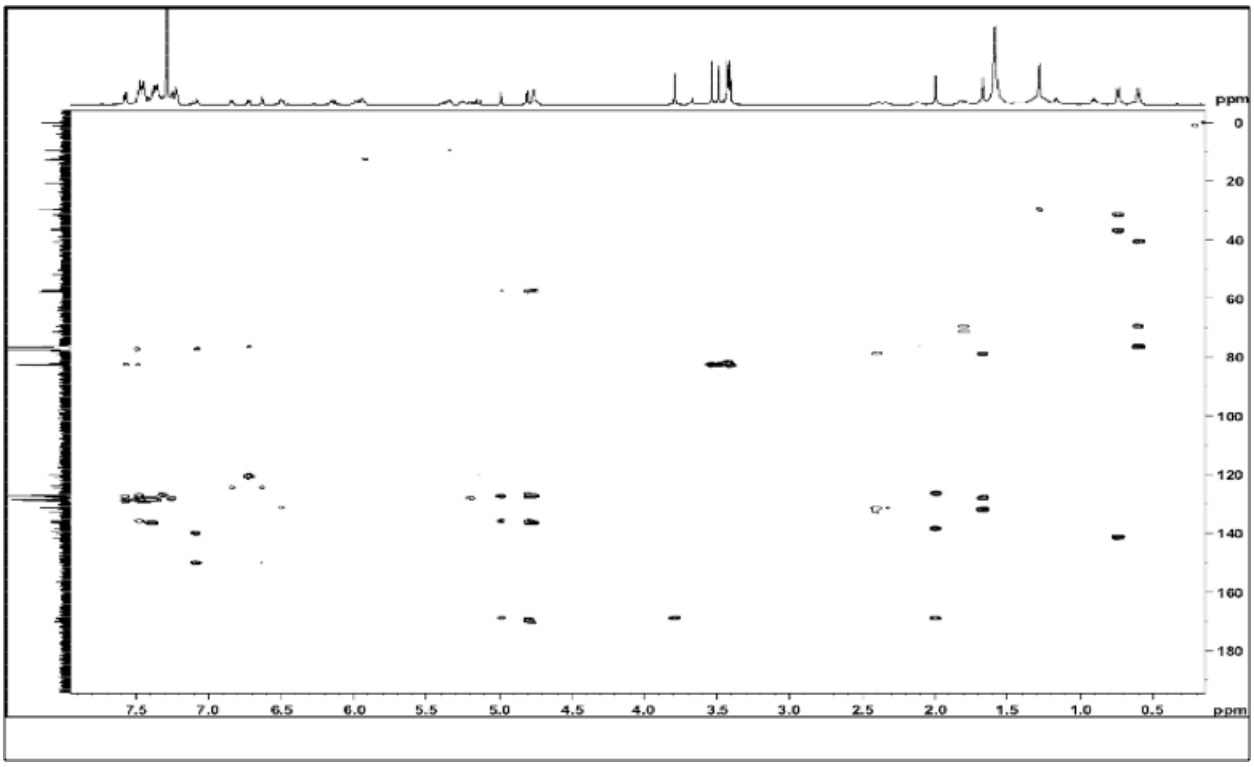

Figure S55. HMBC spectrum of **10a** (500 MHz, $CDCl_3$)

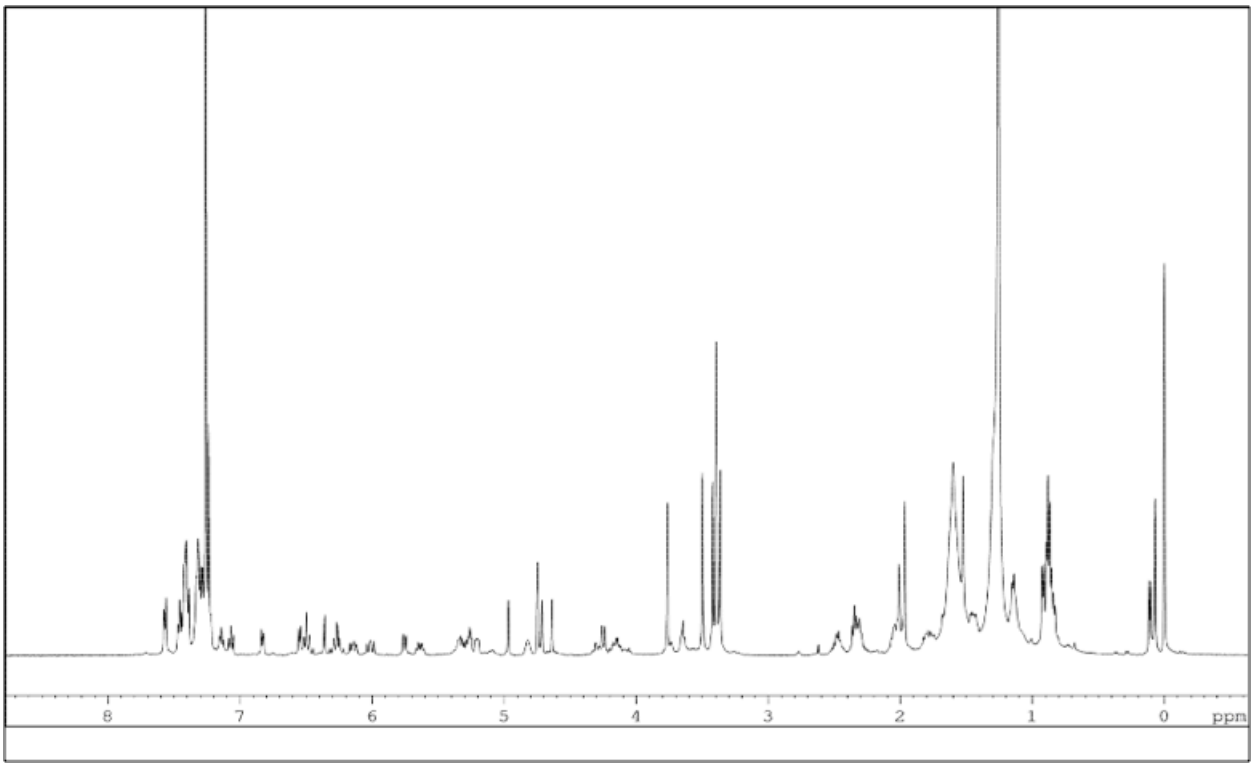

Figure S56. ^{1}H NMR spectrum of **10b**
(500 MHz, $CDCl_3$, TMS = 0.00 ppm)

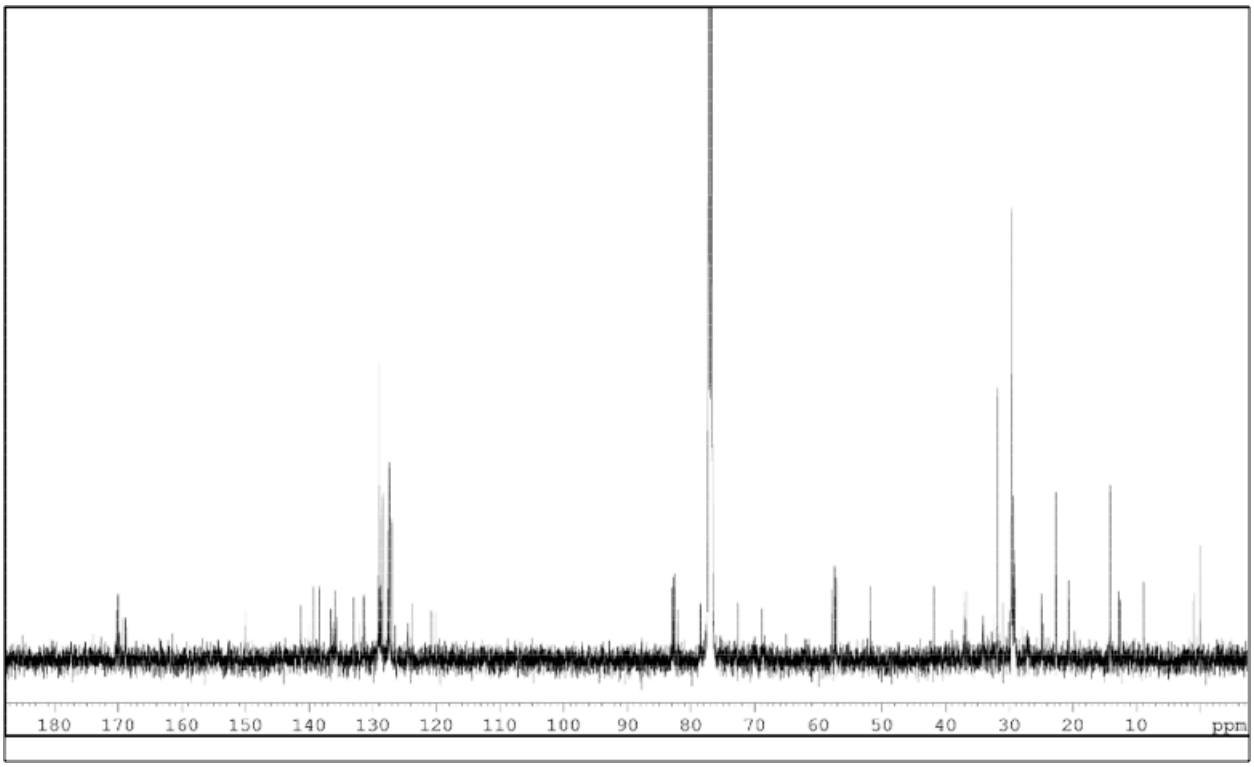

Figure S57. ^{13}C NMR spectrum of **10b**
(500 MHz, $CDCl_3$, $CDCl_3$ = 77.2 ppm)

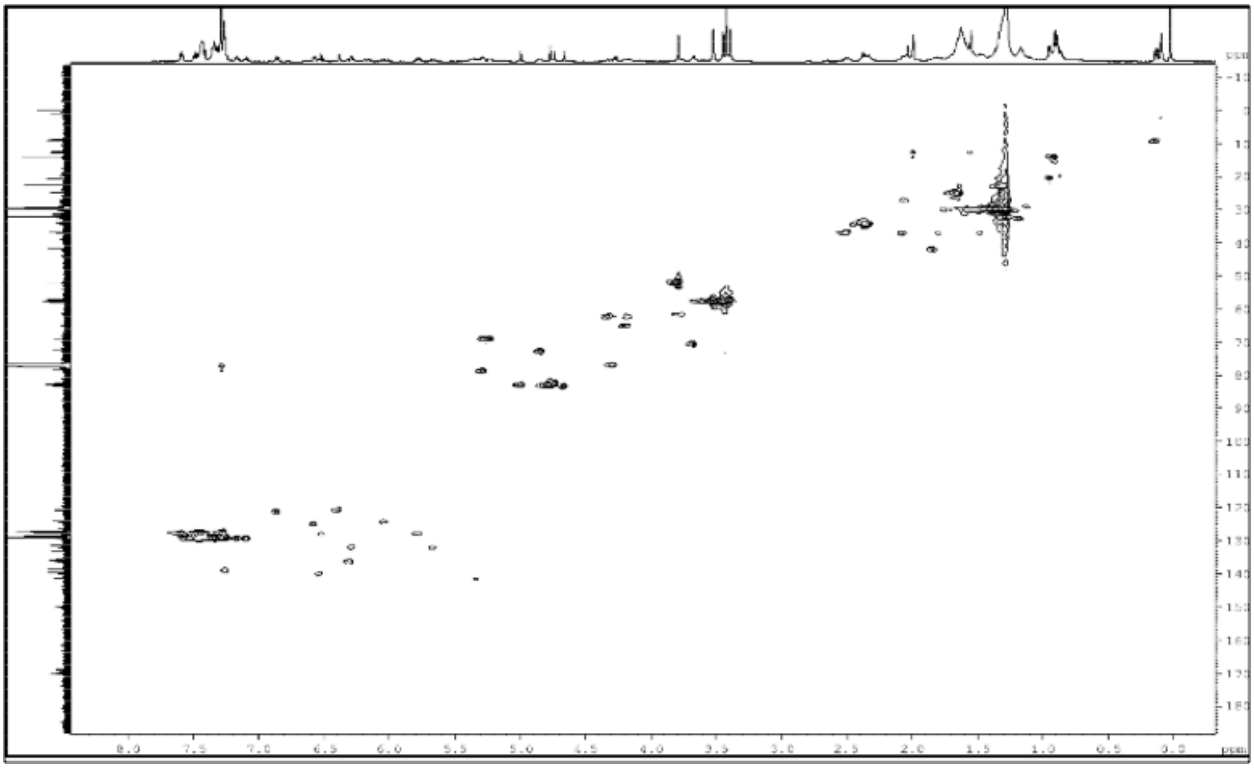

Figure S58. HSQC spectrum of **10b** (500 MHz, $CDCl_3$)

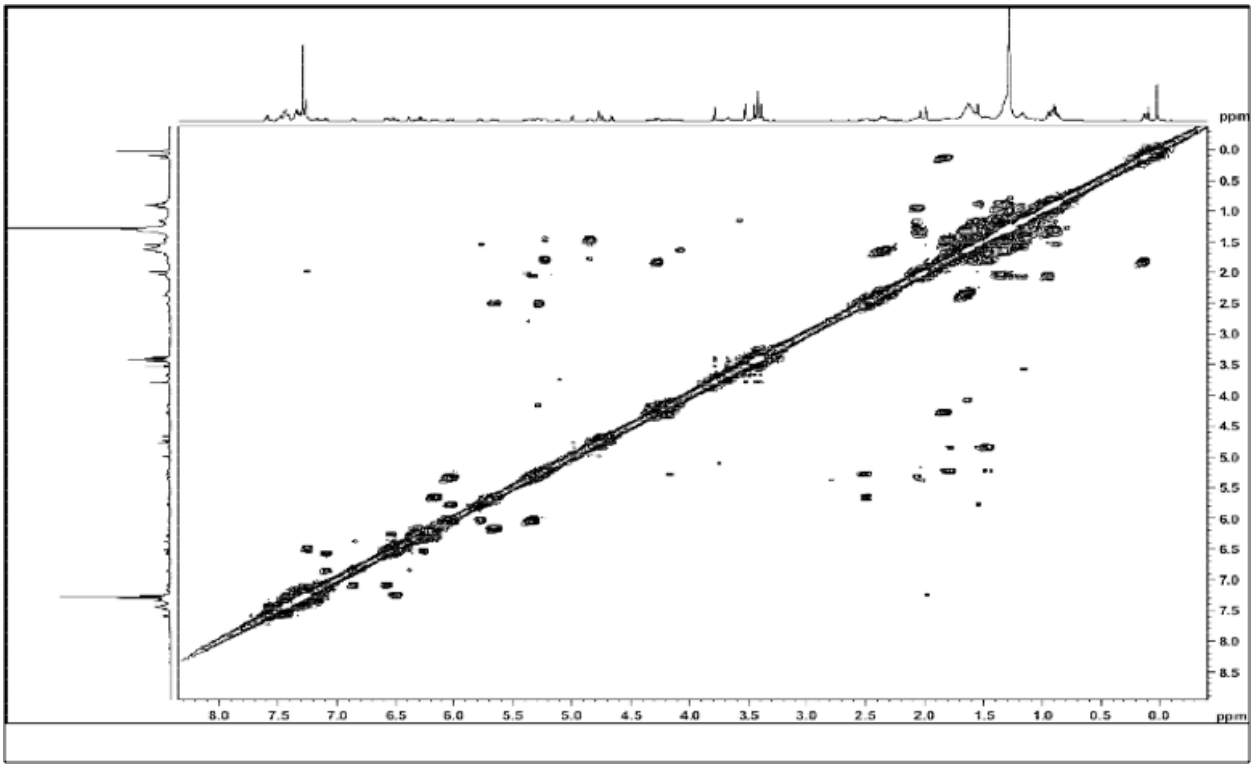

Figure S59. ^{1}H-^{1}H COSY spectrum of **10b** (500 MHz, $CDCl_3$)

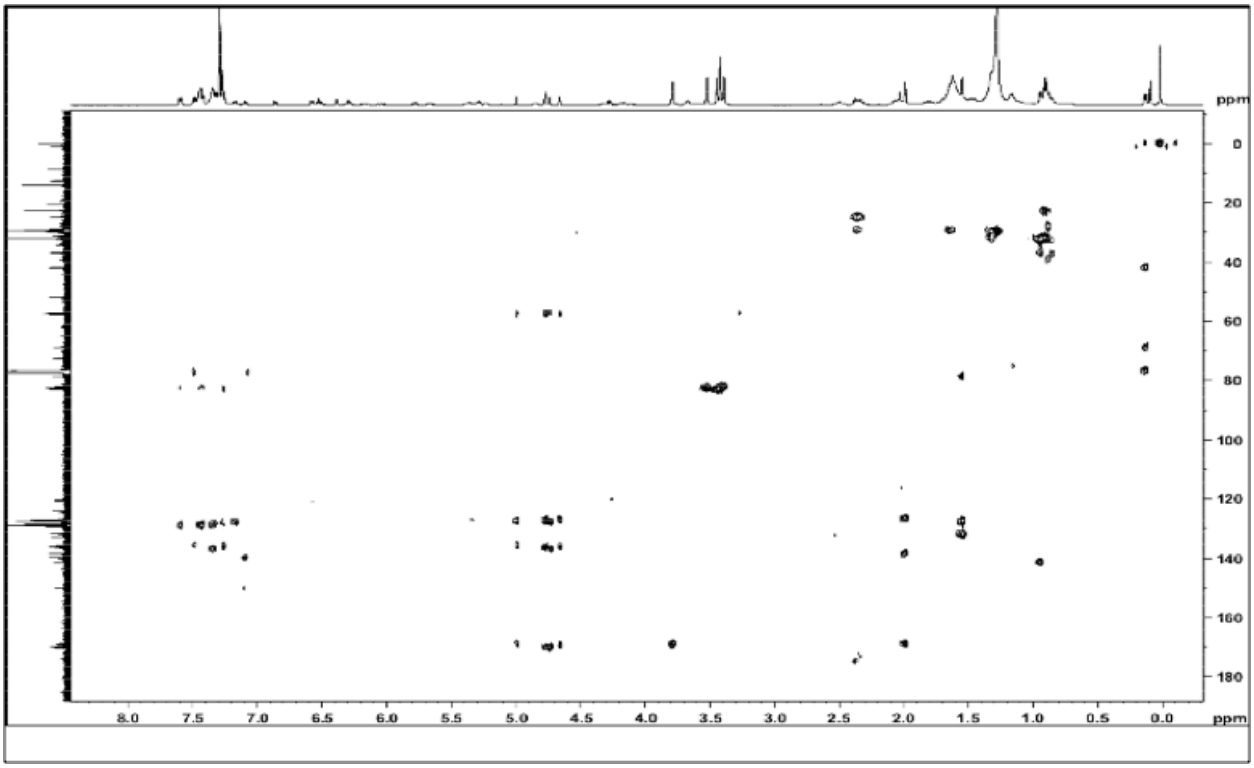

Figure S60. HMBC spectrum of **10b** (500 MHz, $CDCl_3$)

Table S9. ^{1}H and ^{13}C NMR data for **10a** and **10b** in $CDCl_3$

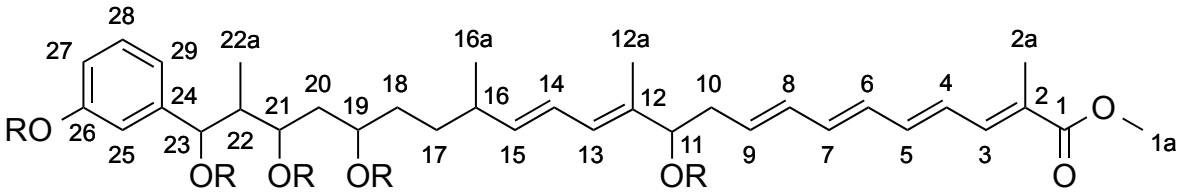

10a : R = (*R*)-MPA , **10b** : R = (*S*)-MPA

	10a		**10b**	
position	δ_c	δ_H mult (*J* in Hz)	δ_c	δ_H mult (*J* in Hz)
1	168.8	-	168.9	
1a	51.9	3.76 (3H, s)	51.9	3.76 (3H, s)
2	126.5	-	126.5	-
2a	12.6	1.97 (3H, s)	12.8	1.97 (3H, s)
3	138.4	7.23 (1H, d, 11.6)	138.4	7.23 (1H, m)
4	127.5	6.47 (1H, m)	127.8	6.49 (1H, m)
5	139.5	6.47 (1H, m)	139.4	6.52 (1H, m)
6	131.2	6.12 (1H, m)	131.3	6.26 (1H, m)
7	136.0	6.11 (1H, m)	136.0	6.28 (1H, m)
8	133.0	5.92 (1H, m)	133.1	6.14 (1H, dd, 9.6, 15.0)
9	131.2	5.34 (1H, m)	131.5	5.65 (1H, dt, 7.4, 15.0)
10	36.5	2.34 (2H, m)	36.7	2.48 (2H, m)
11	78.9	5.23 (1H, t, 7.6)	78.6	5.26 (1H, m)
12	132.0	-	132.0	-
12a	12.8	1.65 (3H, s)	12.6	1.52 (3H, s)
13	128.0	5.91 (1H, m)	127.5	5.75 (1H, d, 11.0)
14	124.0	5.96 (1H, dd, 11.3, 14.2)	123.9	6.01 (1H, dd, 11.0, 15.2)
15	141.4	5.18(1H, dd, 8.0, 11.4)	141.3	5.31(1H, dd, 8.5, 15.2)
16	36.7	1.81 (1H, m)	36.9	2.05 (1H, m)
16a	20.5	0.72 (3H, d, 6.5)	20.6	0.92 (3H, d, 6.3)
17	31.4	0.62, 0.71 (2H, m)	34.0	2.33 (2H, m)
18	31.8	1.23 (2H, m)	24.9	1.62 (2H, m)
19	71.4	4.72 (1H, m)	72.6	4.82 (1H, m)
20	36.1	1.53, 1.77 (2H, m)	37.1	1.45, 1.77 (2H, m)
21	69.5	5.31 (1H, m)	68.9	5.21 (1H, m)
22	40.6	2.10 (1H, m)	41.9	1.81 (1H, m)
22a	9.5	0.57 (3H, d, 7.0)	8.9	0.11 (3H, d, 7.1)
23	76.4	5.12 (1H, d, 9.6)	76.6	4.25 (1H, d, 10.5)
24	139.9	-	140.1	-
25	120.1	6.61 (1H, s)	129.0	7.07 (1H, s)
26	150.0	-	150.0	-
27	121.0	6.81 (1H, d, 8.1)	120.9	6.83 (1H, d, 8.0)
28	129.3	7.06 (1H, t, 8.1)	127.8	6.49 (1H, m)
29	124.6	6.70 (1H, d, 8.1)	124.5	6.55 (1H, d, 7.4)

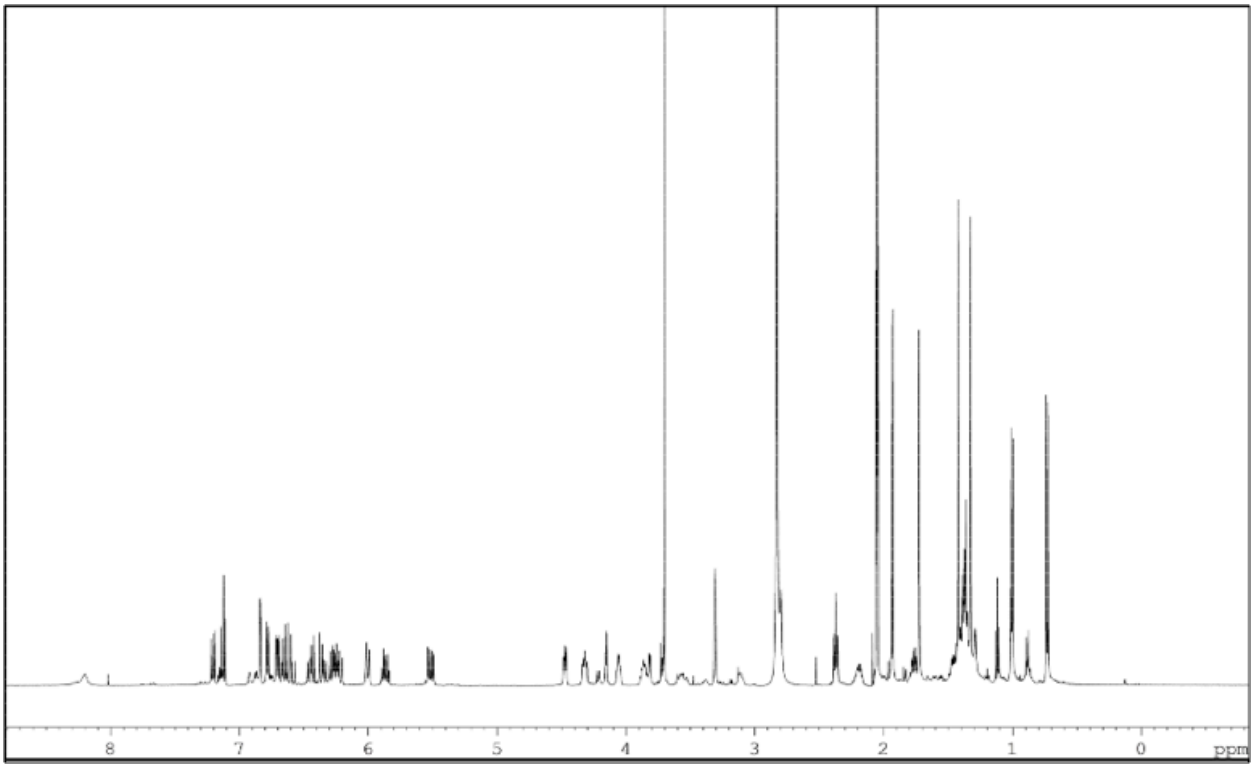

Figure S61. ^{1}H NMR spectrum of **11**
(500 MHz, Acetone-d_6, Acetone-d_6 = 2.05 ppm)

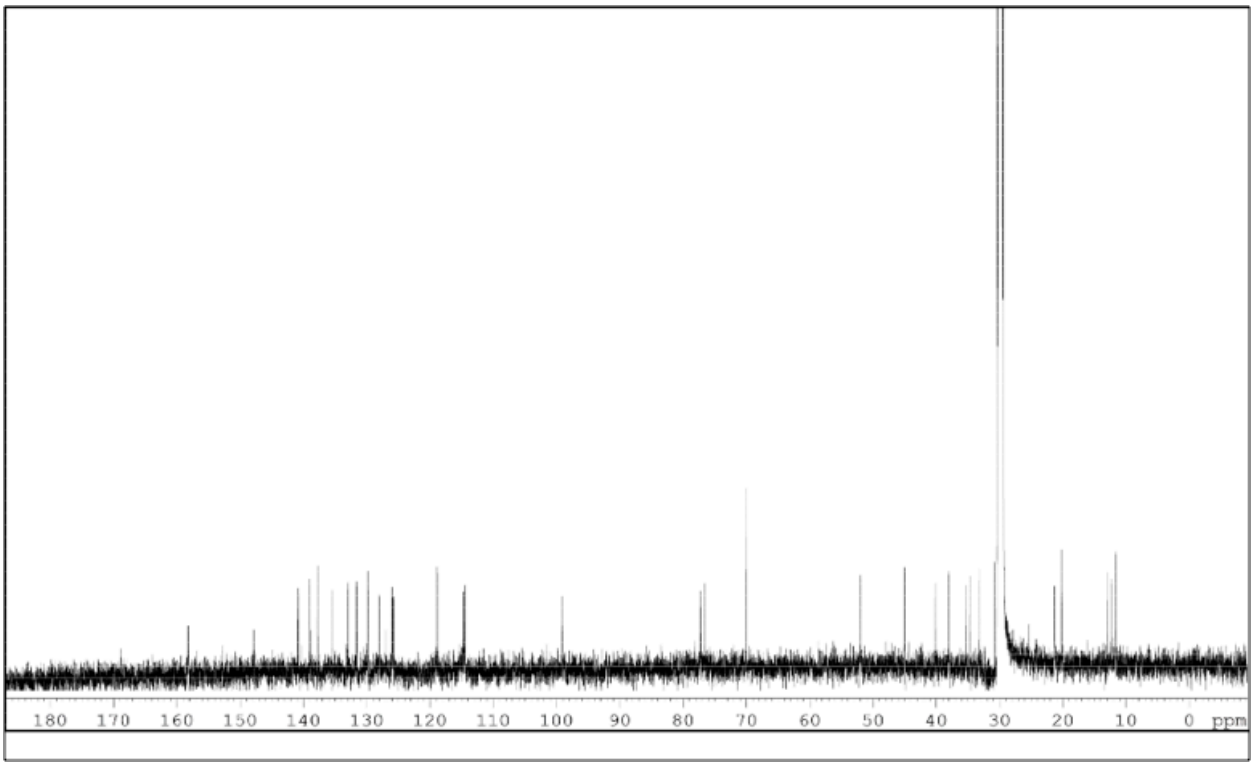

Figure S62. ^{13}C NMR spectrum of **11**
(500 MHz, Acetone-d_6, Acetone-d_6 = 29.8 ppm)

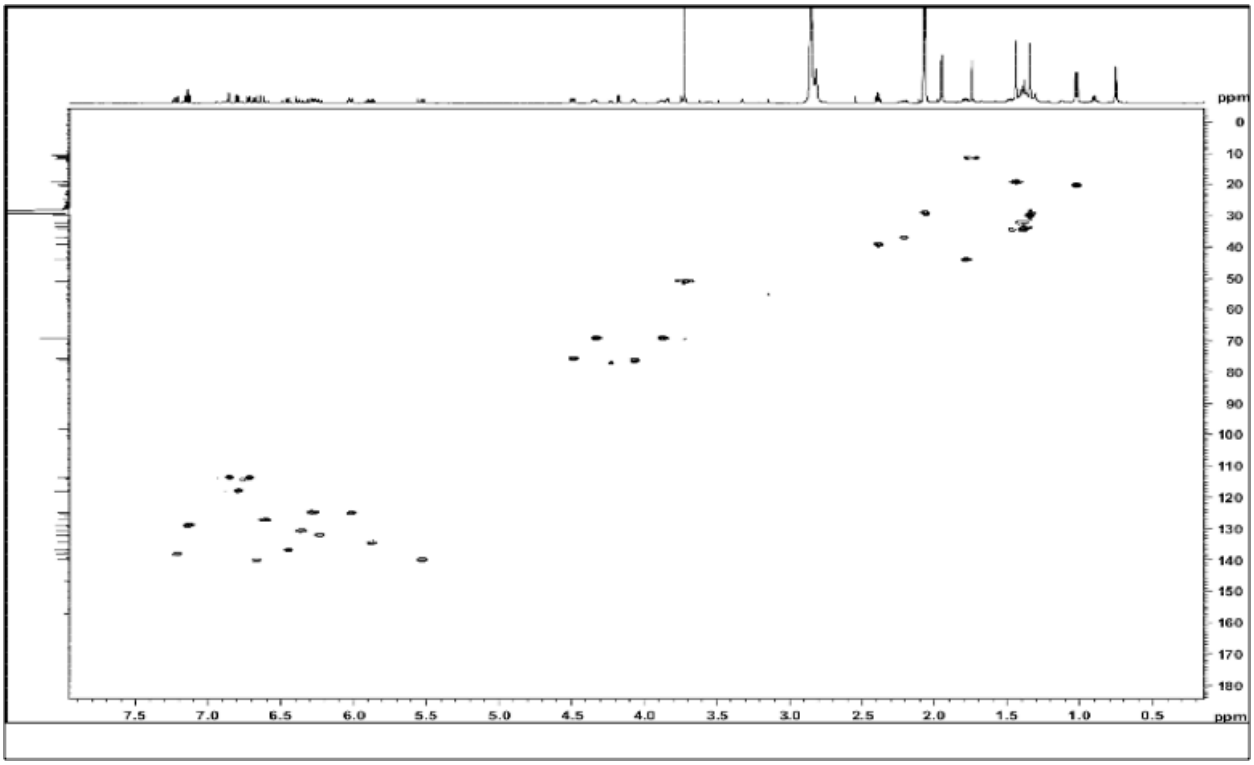

Figure S63. HSQC spectrum of **11** (500 MHz, Acetone-d_6)

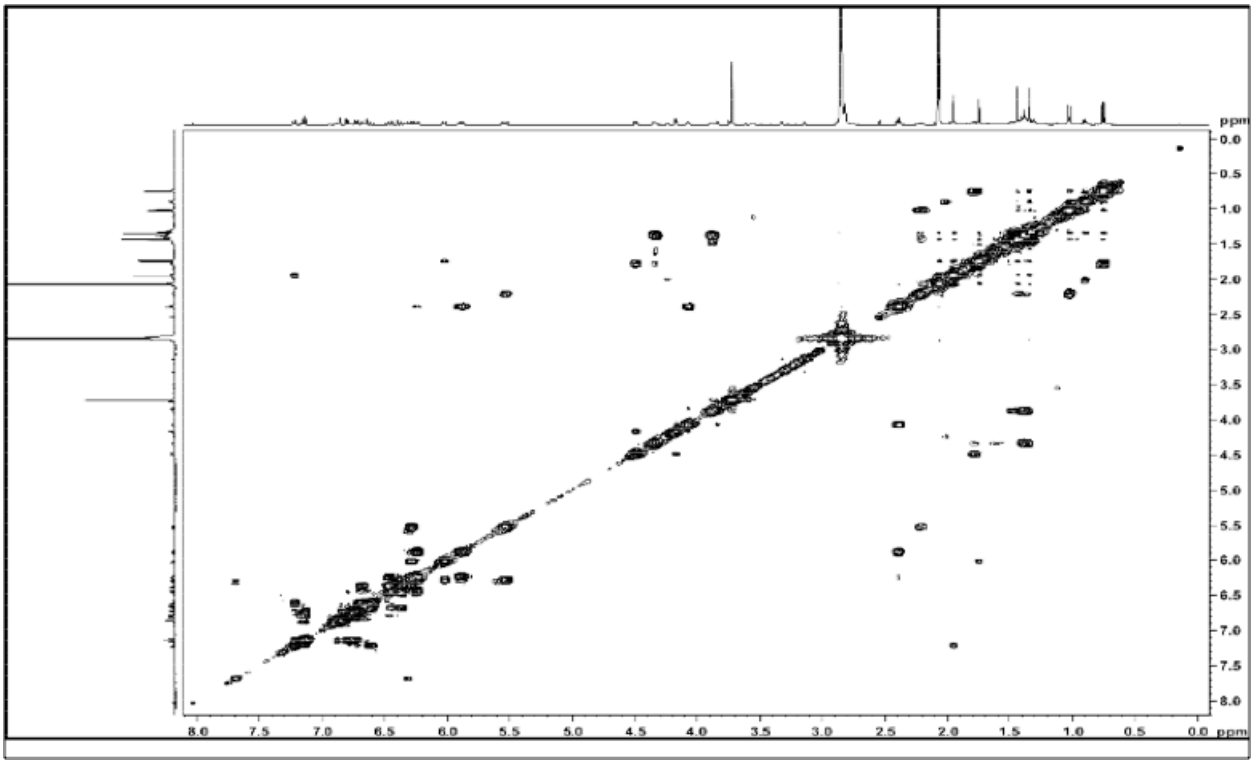

Figure S64. ^{1}H-^{1}H COSY spectrum of **11** (500 MHz, Acetone-d_6)

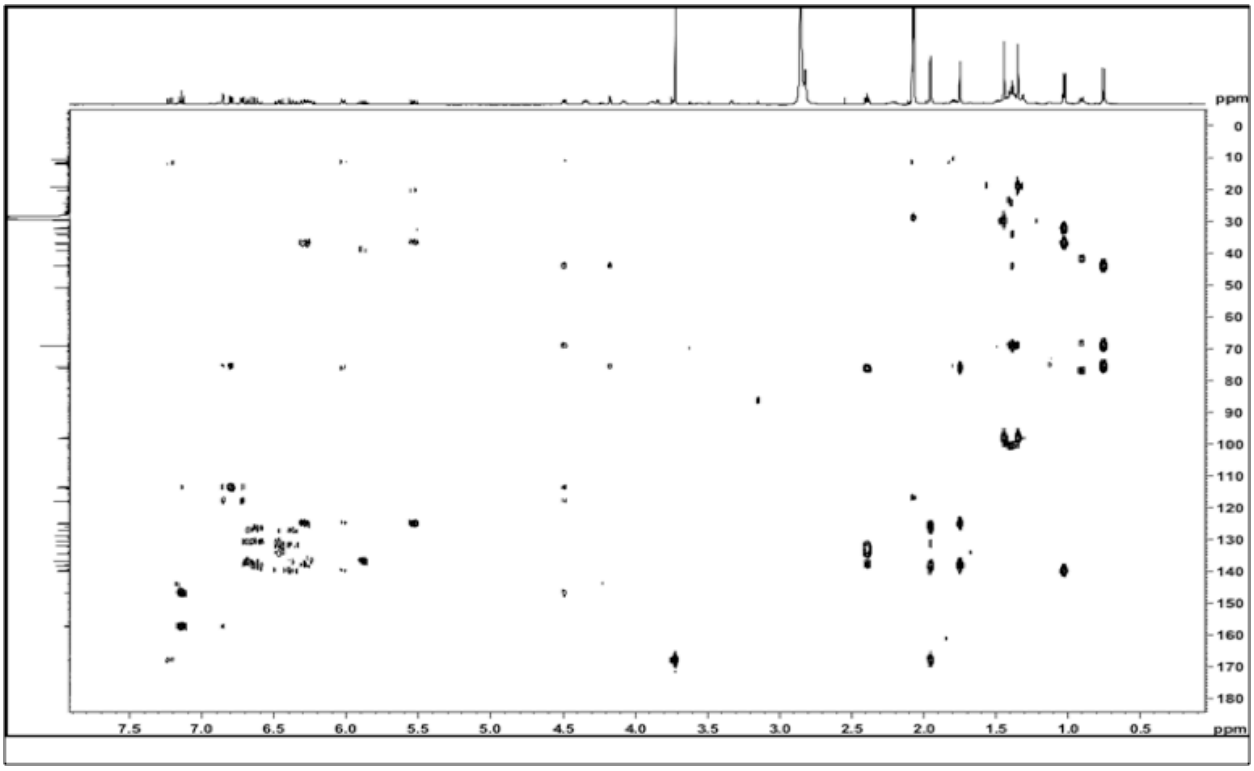

Figure S65. HMBC spectrum of **11** (500 MHz, Acetone-d_6)

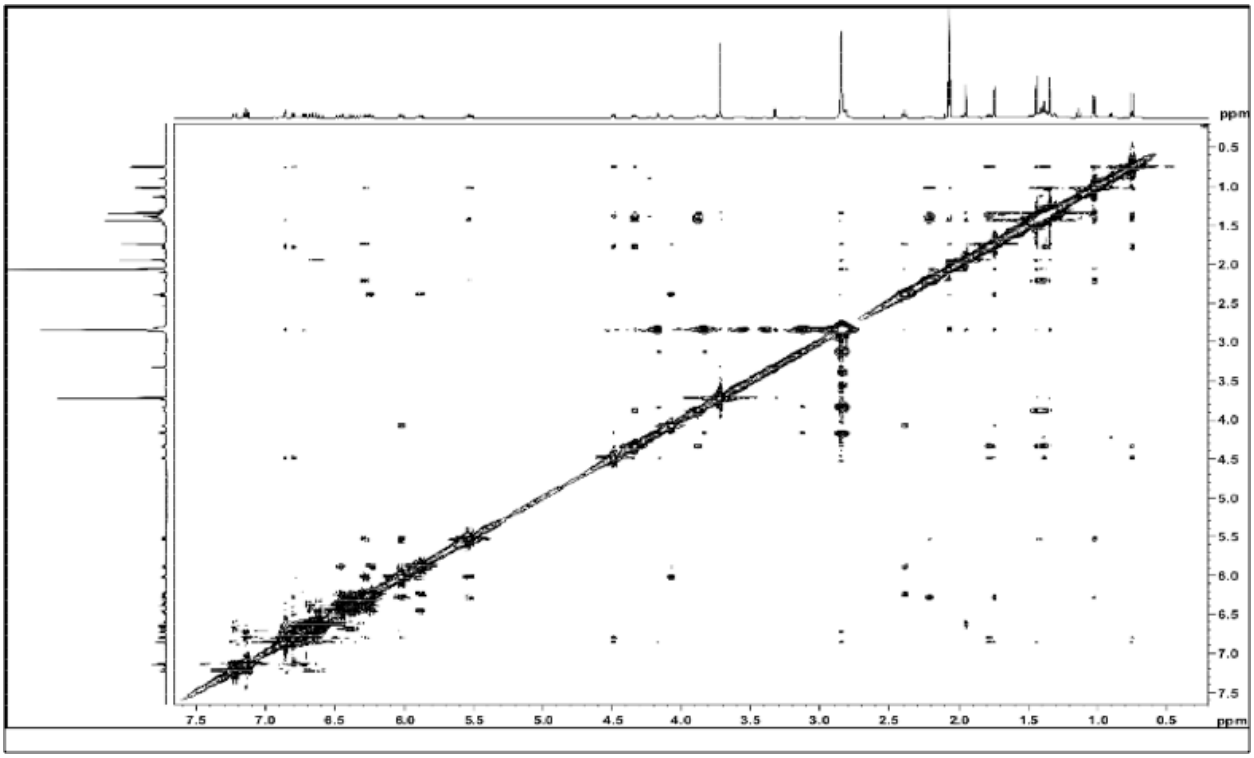

Figure S66. NOESY spectrum of **11** (500 MHz, Acetone-d_6)

Table S10. ^{1}H and ^{13}C NMR data for **11** in Acetone-d_6

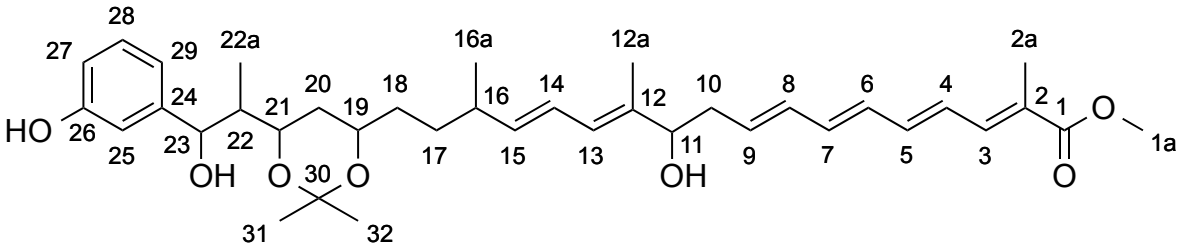

11

position	δ_c	δ_H mult (*J* in Hz)
1	167.9	-
1a	51.0	3.72 (3H, s)
2	126.1	-
2a	12.0	1.95 (3H, s)
3	138.2	7.22 (1H, dd, 1.6, 11.2)
4	127.1	6.61 (1H, dd, 11.2, 14.3)
5	140.0	6.68 (1H, dd, 10.2, 14.3)
6	130.6	6.39 (1H, dd, 10.2, 14.5)
7	136.9	6.46 (1H, dd, 10.6, 14.5)
8	132.0	6.24 (1H, dd, 10.6,15.3)
9	134.4	5.88 (1H, dt, 7.3, 15.3)
10	39.2	2.39 (2H, t, 7.3)
11	76.3	4.07 (1H, m)
12	137.9	-
12a	11.4	1.74 (3H, s)
13	125.0	6.02 (1H, d, 10.9)
14	124.8	6.28 (1H, dd, 10.9, 15.3)
15	139.8	5.53 (1H, dd, 9.0, 15.3)
16	37.1	2.21 (1H, m)
16a	20.3	1.02 (3H, d, 6.7)
17	32.2	1.37, 1.42 (2H, m)
18	34.4	1.38, 1.47 (2H, m)
19	73.4	3.84 (1H, m)
20	38.6	1.52, 1.73 (2H, m)
21	69.2	3.88 (1H, m)
22	44.1	1.78 (1H, m)
22a	10.7	0.75 (3H, d, 7.0)
23	75.7	4.49 (1H, dd, 4.7, 8.0)
24	146.9	-
25	113.6	6.86 (1H, s)
26	157.3	-
27	113.8	6.72 (1H, dd, 2.3, 8.0)
28	128.8	7.14 (1H, t, 8.0)
29	117.9	6.80 (1H, d, 8.0)
30	98.2	-
31	29.8	1.34 (3H, s)
32	19.2	1.44 (3H, s)

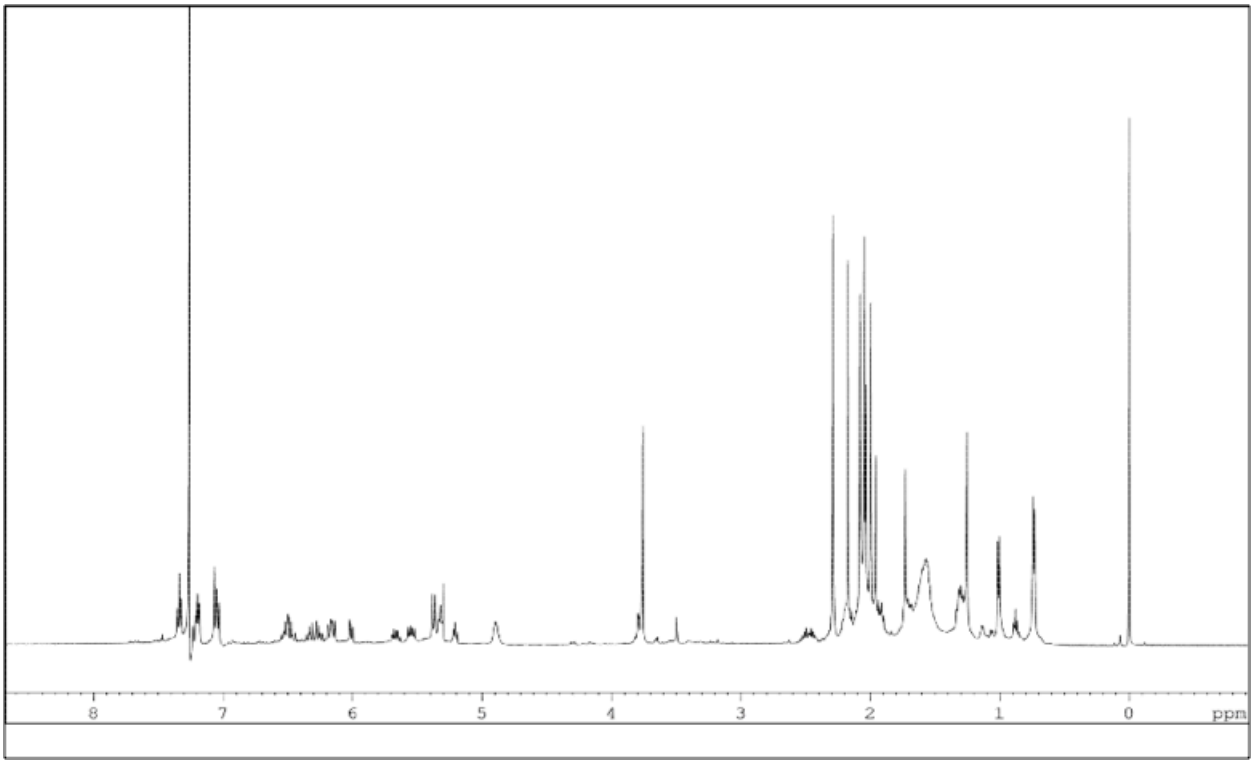

Figure S67. ^{1}H NMR spectrum of **12**
(500 MHz, $CDCl_3$, TMS = 0.00 ppm)

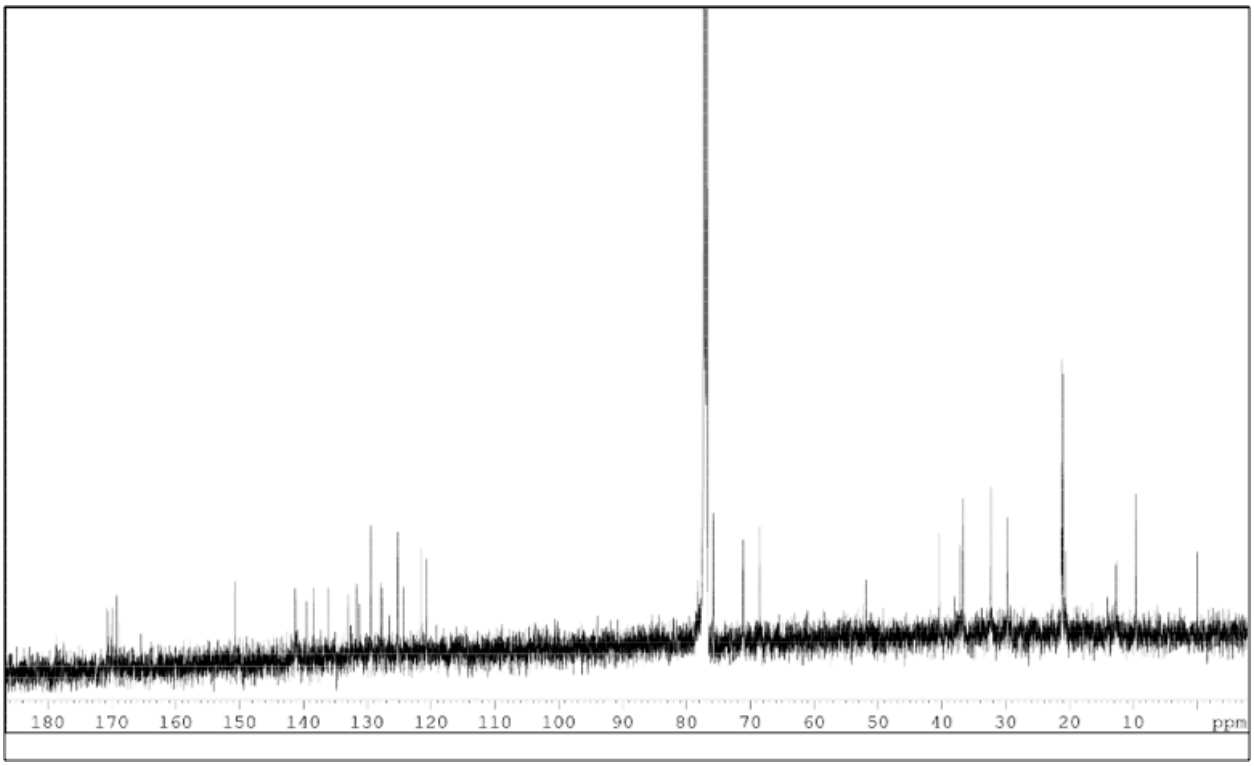

Figure S68. ^{13}C NMR spectrum of **12**
(500 MHz, $CDCl_3$, $CDCl_3$ = 77.2 ppm)

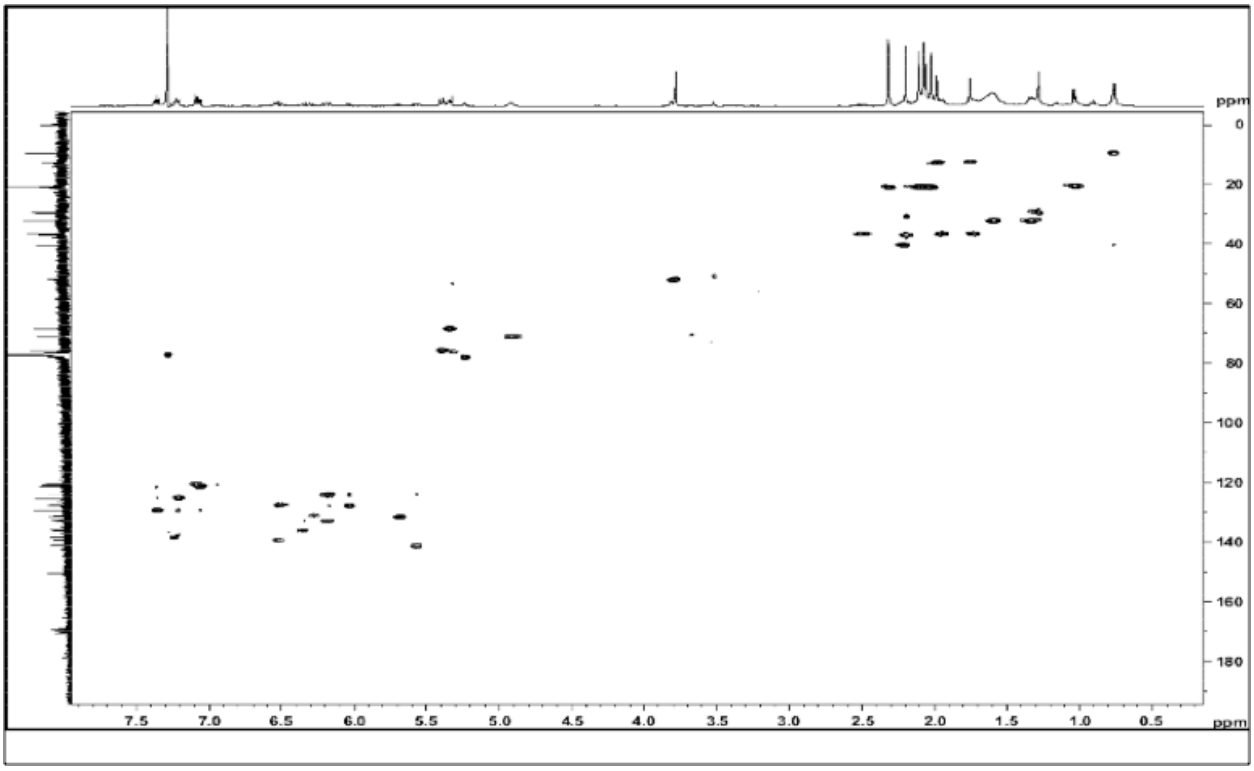

Figure S69. HSQC spectrum of **12** (500 MHz, $CDCl_3$)

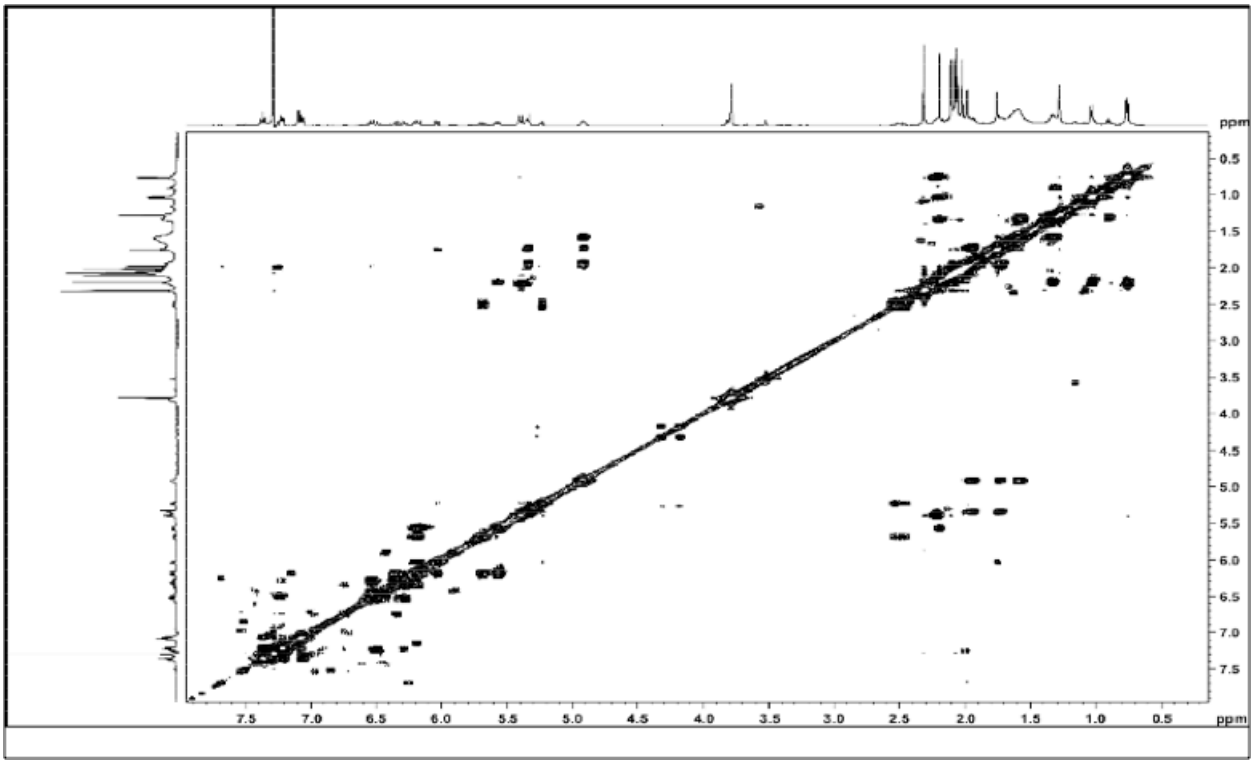

Figure S70. ^{1}H-^{1}H COSY spectrum of **12** (500 MHz, $CDCl_3$)

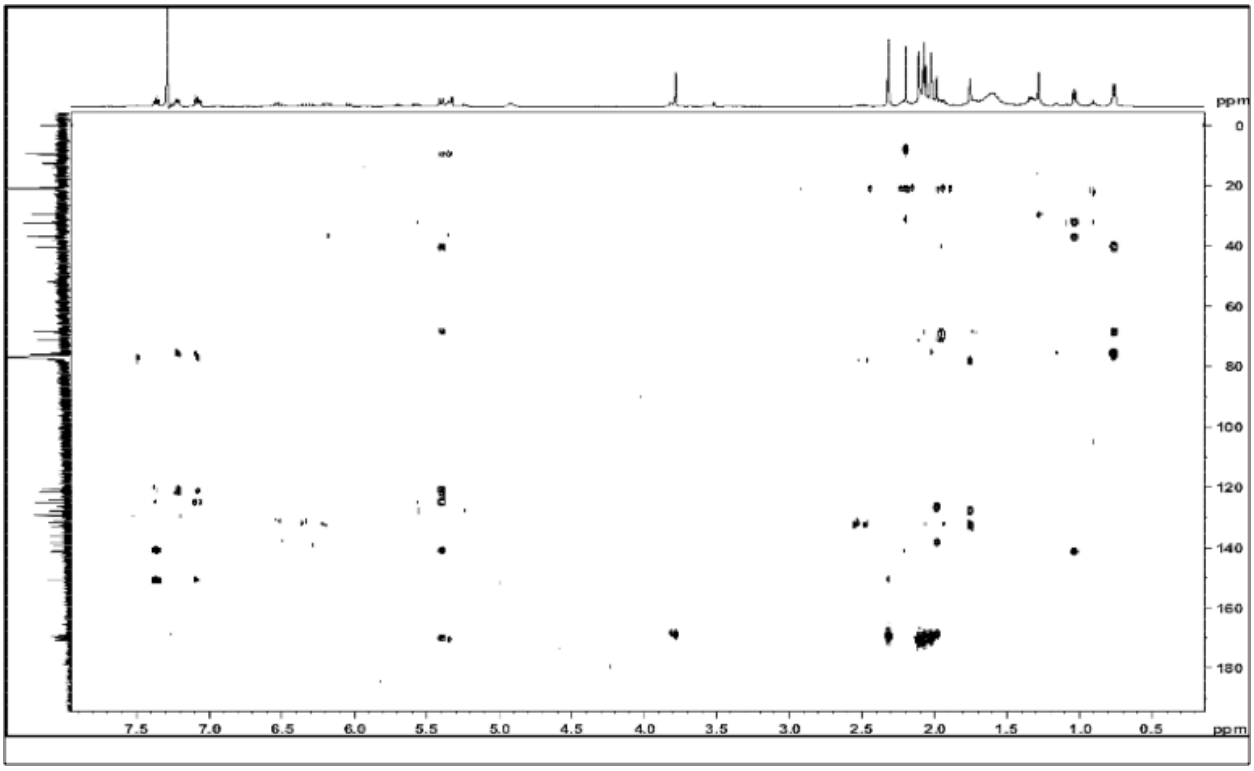

Figure S71. HMBC spectrum of **12** (500 MHz, $CDCl_3$)

Table S11. ^{1}H and ^{13}C NMR data for **12** in $CDCl_3$

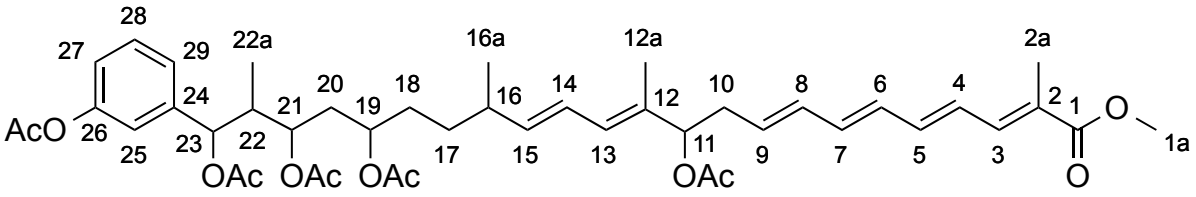

12

position	δ_c	δ_H mult (*J* in Hz)
1	168.9	-
1a	51.6	3.76 (3H, s)
2	126.4	-
2a	12.8	1.96 (3H, s)
3	138.4	7.22 (1H, d, 10.4)
4	127.6	6.47 (1H, dd, 10.4, 13.6)
5	139.4	6.49 (1H, dd, 9.7, 13.6)
6	131.2	6.25 (1H, dd, 9.7, 14.3)
7	136.0	6.33 (1H, dd, 11.0, 14.3)
8	132.9	6.16 (1H, dd, 11.0, 15.6)
9	131.6	5.66 (1H, dt, 7.1, 15.6)
10	36.7	2.47 (2H, m)
11	78.1	5.20 (1H, t, 7.5)
12	132.6	-
12a	12.6	1.73 (3H, s)
13	127.9	6.01 (1H, d, 11.0)
14	124.2	6.16 (1H, dd, 11.0, 15.8)
15	141.3	5.54 (1H, dd, 8.2, 15.8)
16	37.1	2.17 (1H, m)
16a	20.6	1.01 (3H, d, 6.8)
17	32.3	1.30 (2H, m)
18	32.3	1.56 (2H, m)
19	71.1	4.89 (1H, m)
20	36.7	1.70, 1.92 (2H, m)
21	68.5	5.32 (1H, m)
22	40.4	2.19 (1H, m)
22a	9.6	0.73 (3H, d, 6.9)
23	75.8	5.37 (1H, d, 10.2)
24	141.0	-
25	120.7	7.06 (1H, s)
26	150.8	-
27	121.5	6.77 (1H, d, 8.3)
28	129.4	7.20 (1H, t, 8.3)
29	125.2	7.19 (1H, d, 8.3)

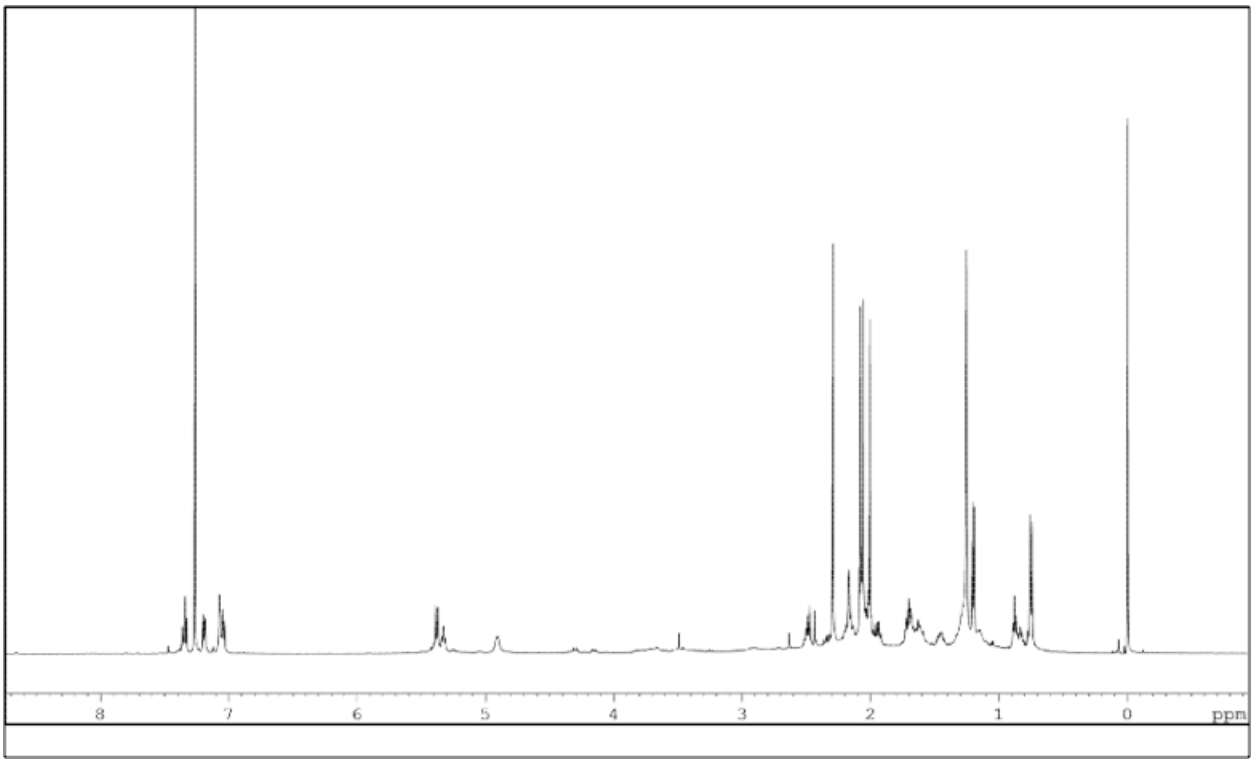

Figure S72. ^{1}H NMR spectrum of **13**
(500 MHz, $CDCl_3$, TMS = 0.00 ppm)

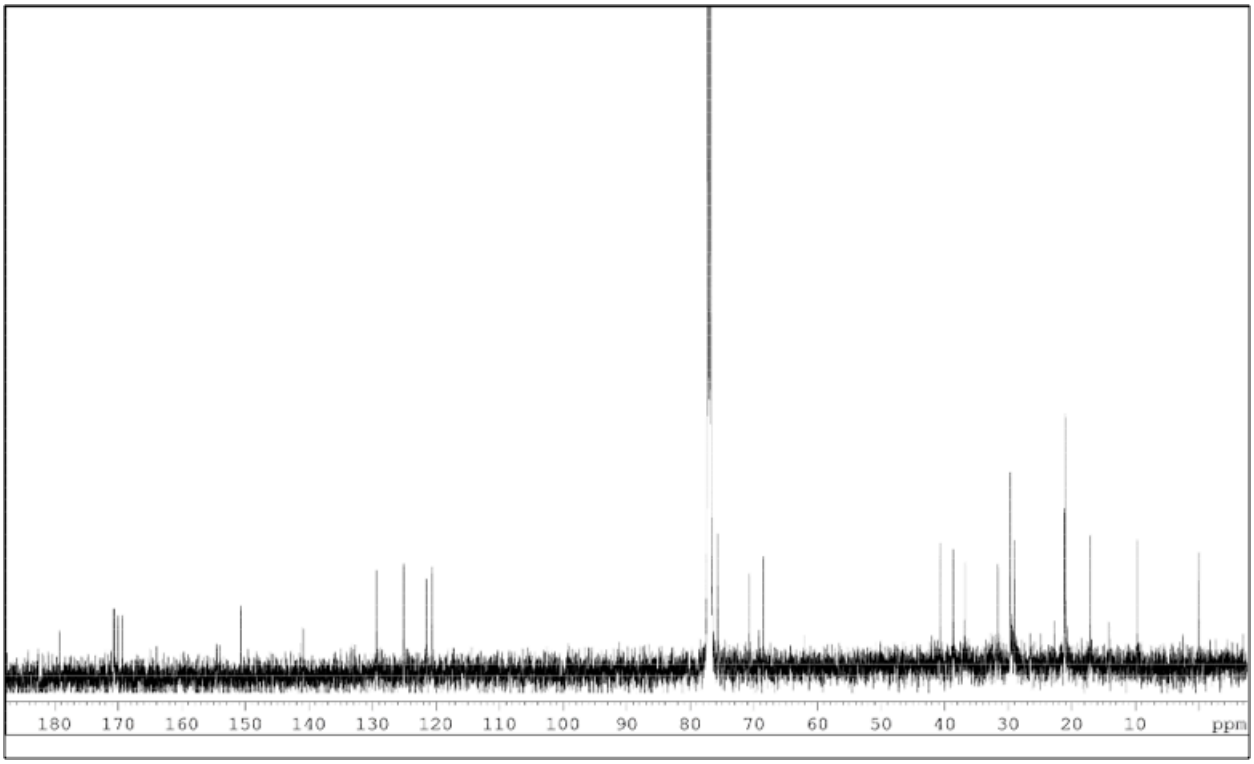

Figure S73. ^{13}C NMR spectrum of **13**
(500 MHz, $CDCl_3$, $CDCl_3$ = 77.2 ppm)

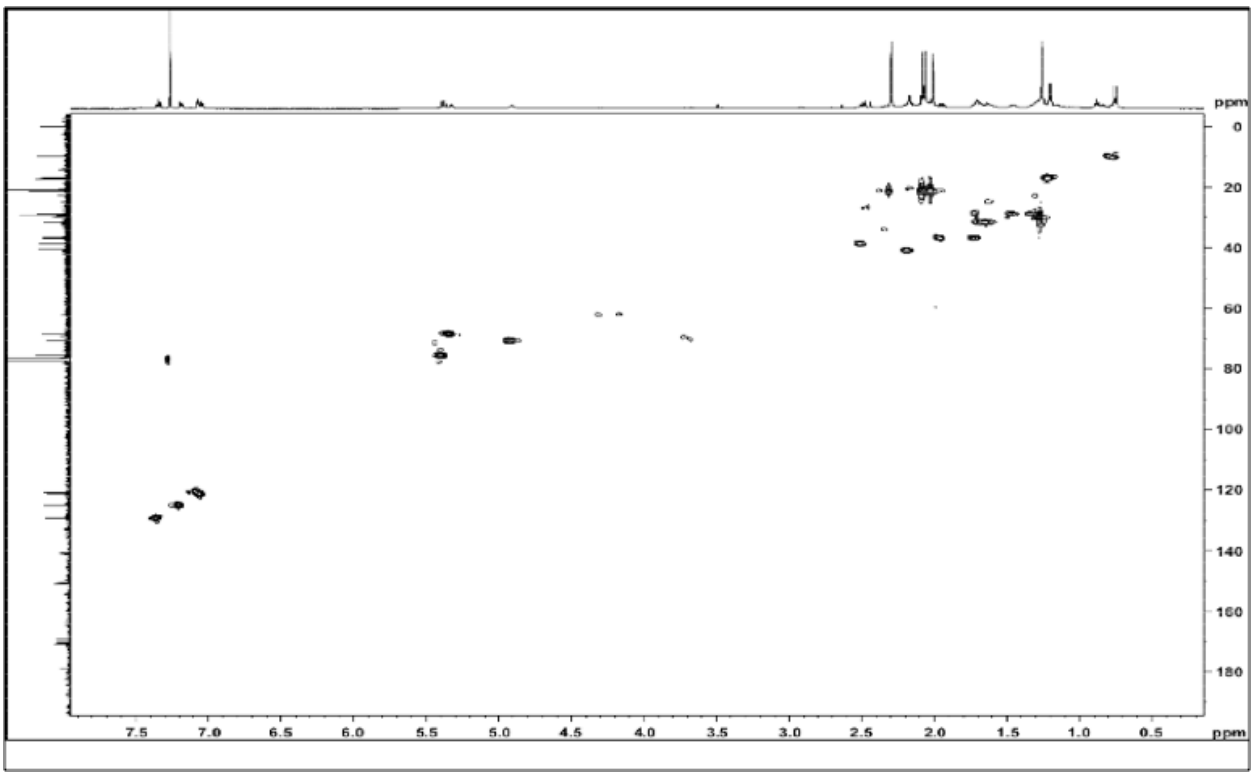

Figure S74. HSQC spectrum of **13** (500 MHz, $CDCl_3$)

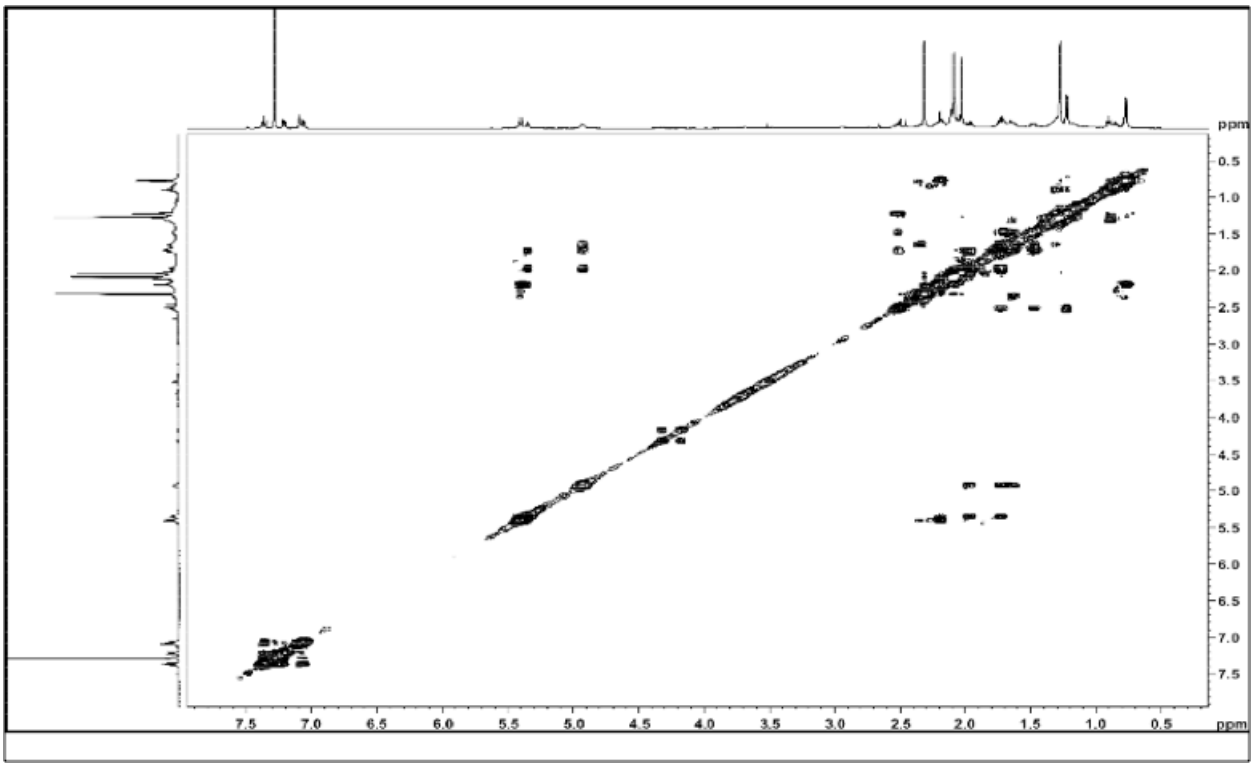

Figure S75. ^{1}H-^{1}H COSY spectrum of **13** (500 MHz, $CDCl_3$)

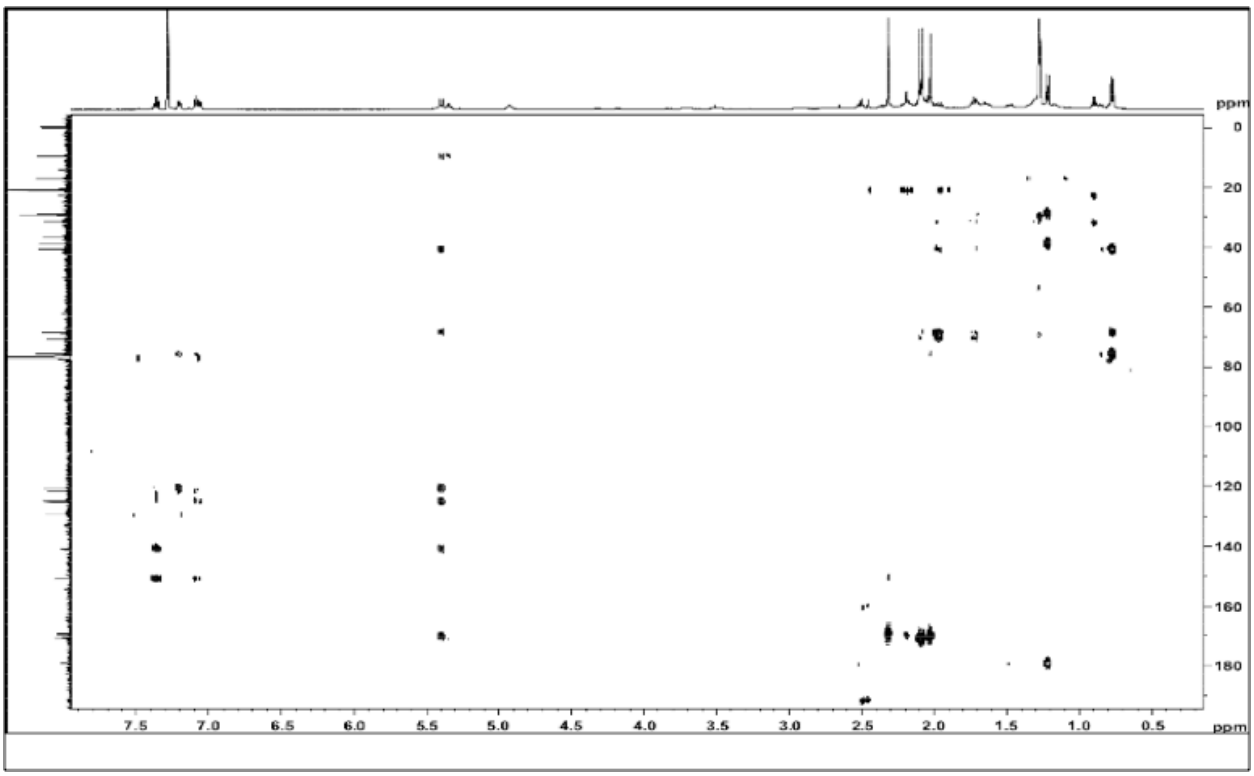

Figure S76. HMBC spectrum of **13** (500 MHz, $CDCl_3$)

Table S12. ^{1}H and ^{13}C NMR data for **13** in $CDCl_3$

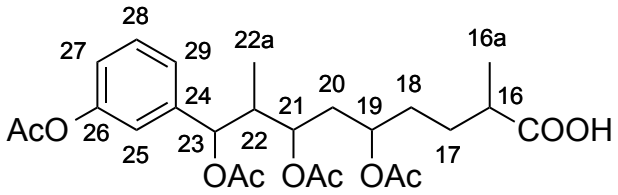

13

position	δ_c	δ_H mult (*J* in Hz)
1		
2		
2a		
3		
4		
5		
6		
7		
8		
9		
10		
11		
12		
12a		
13		
14		
15		
16	38.7	2.50 (1H, m)
16a	17.1	1.20 (3H, d, 7.1)
17	28.9	1.45, 1.70 (2H, m)
18	31.7	1.63, 1.67 (2H, m)
19	70.6	4.91 (1H, m)
20	36.8	1.71, 1.95 (2H, m)
21	69.5	5.33 (1H, m)
22	40.8	2.17 (1H, m)
22a	9.7	0.75 (3H, d, 7.0)
23	75.5	5.38 (1H, d, 10.3)
24	141.0	-
25	120.7	7.07 (1H, s)
26	150.8	-
27	121.5	7.04 (1H, d, 8.2)
28	129.4	7.34 (1H, t, 8.2)
29	125.2	7.19 (1H, d, 8.2)
COOH	179.2	

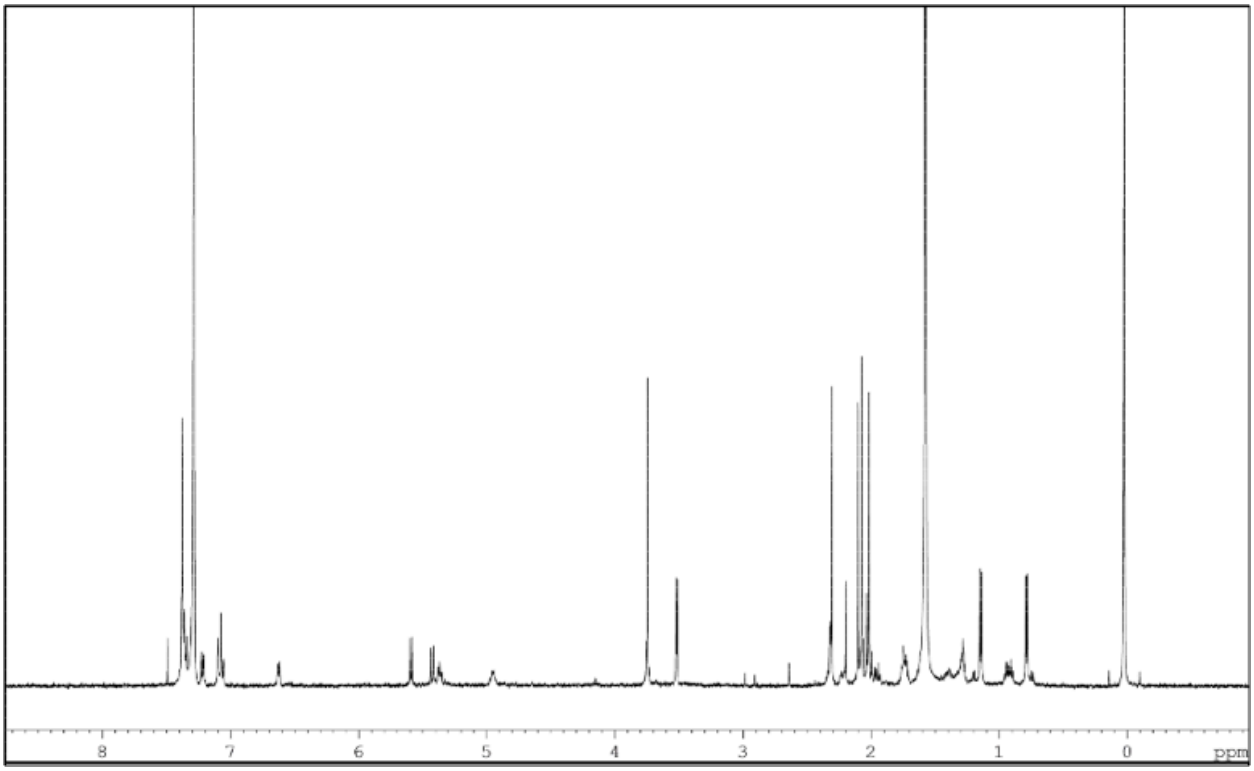

Figure S77. ^{1}H NMR spectrum of **14a**
(500 MHz, $CDCl_3$, TMS = 0.00 ppm)

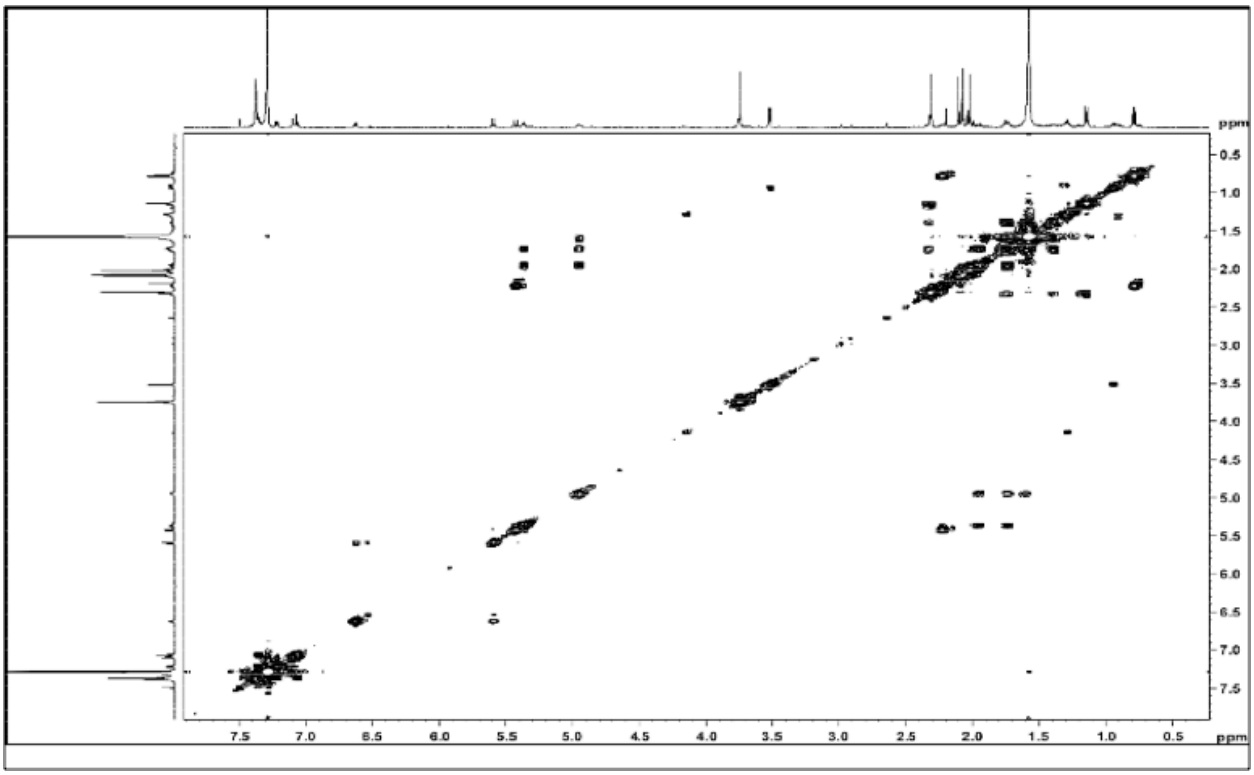

Figure S78. ^{1}H-^{1}H COSY spectrum of **14a** (500 MHz, $CDCl_3$)

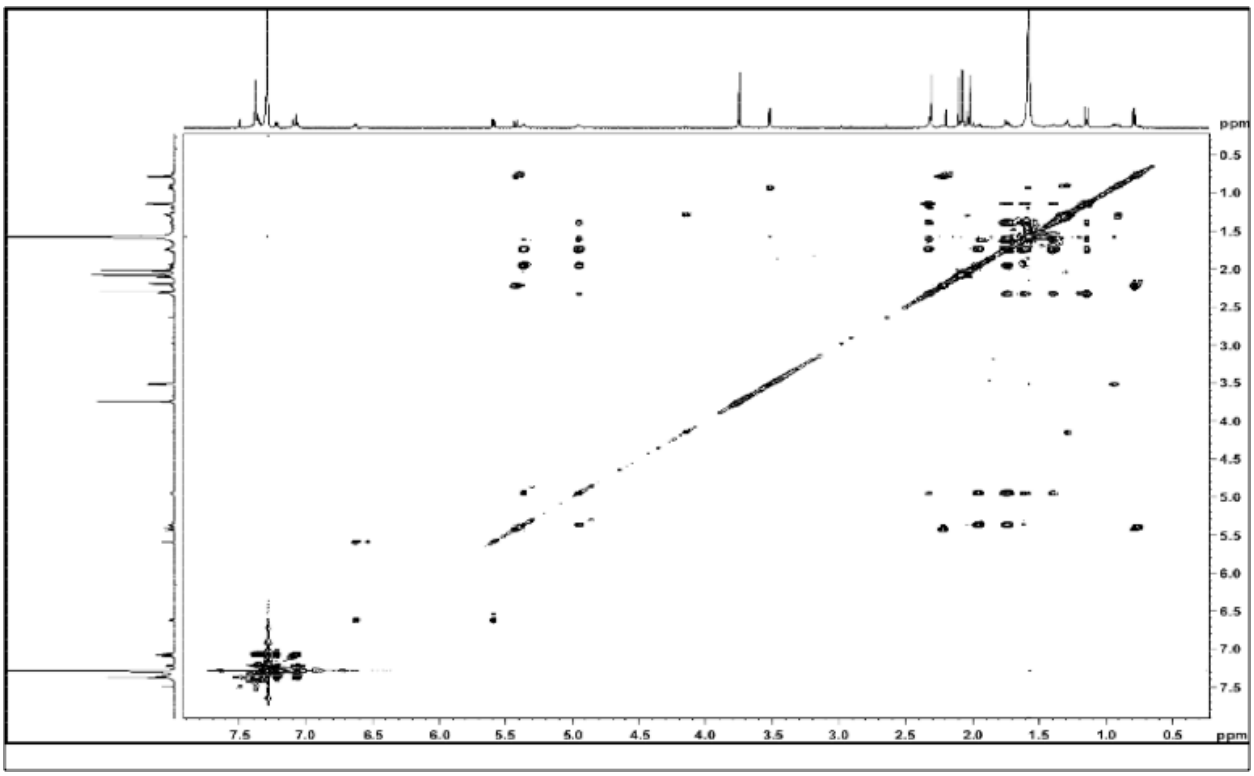

Figure S79. ^{1}H-^{1}H TOCSY spectrum of **14a** (500 MHz, $CDCl_3$)

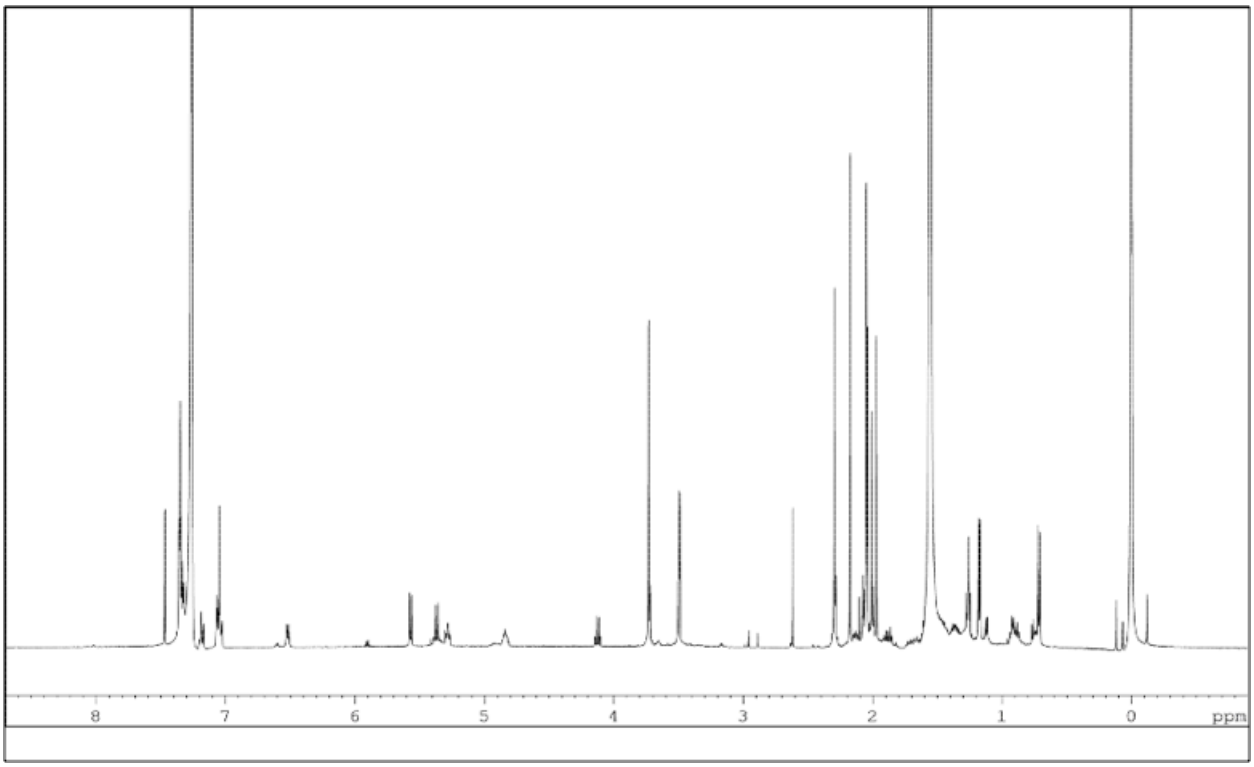

Figure S80. ^{1}H NMR spectrum of **14b**
(500 MHz, $CDCl_3$, TMS = 0.00 ppm)

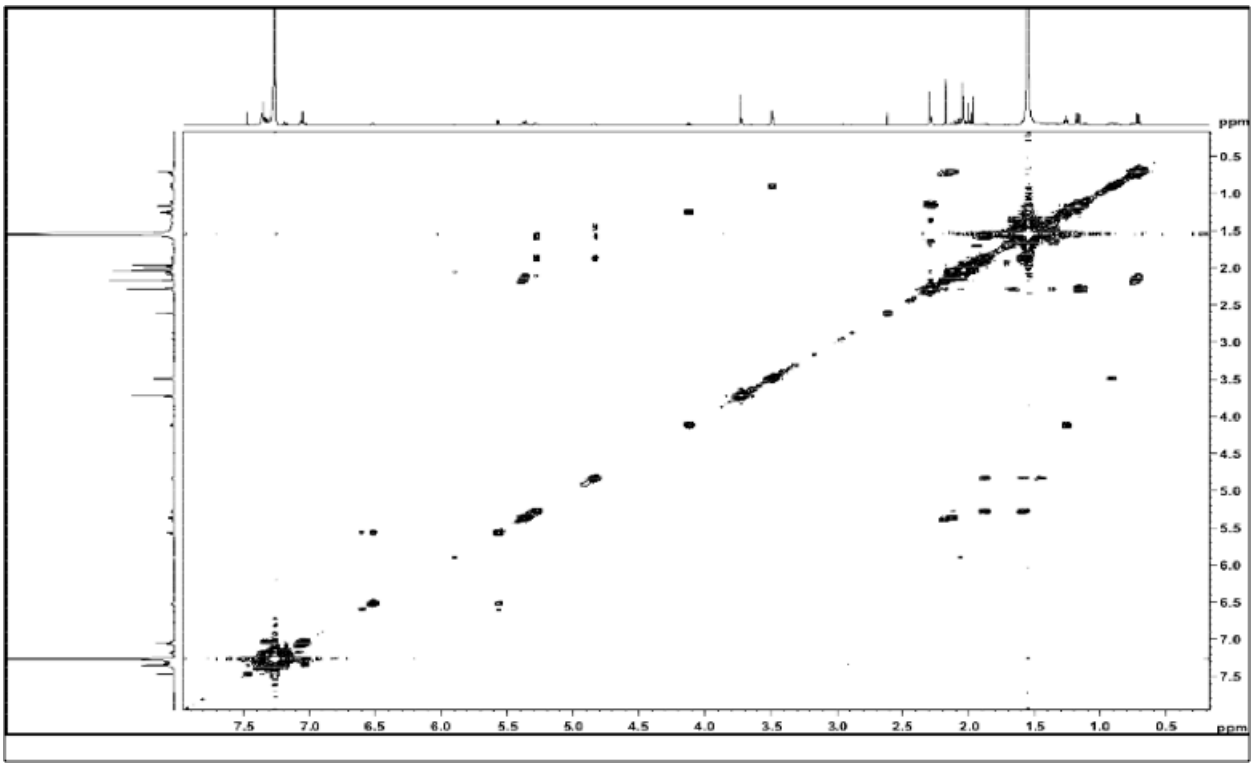

Figure S81. ^{1}H-^{1}H COSY spectrum of **14b** (500 MHz, $CDCl_3$)

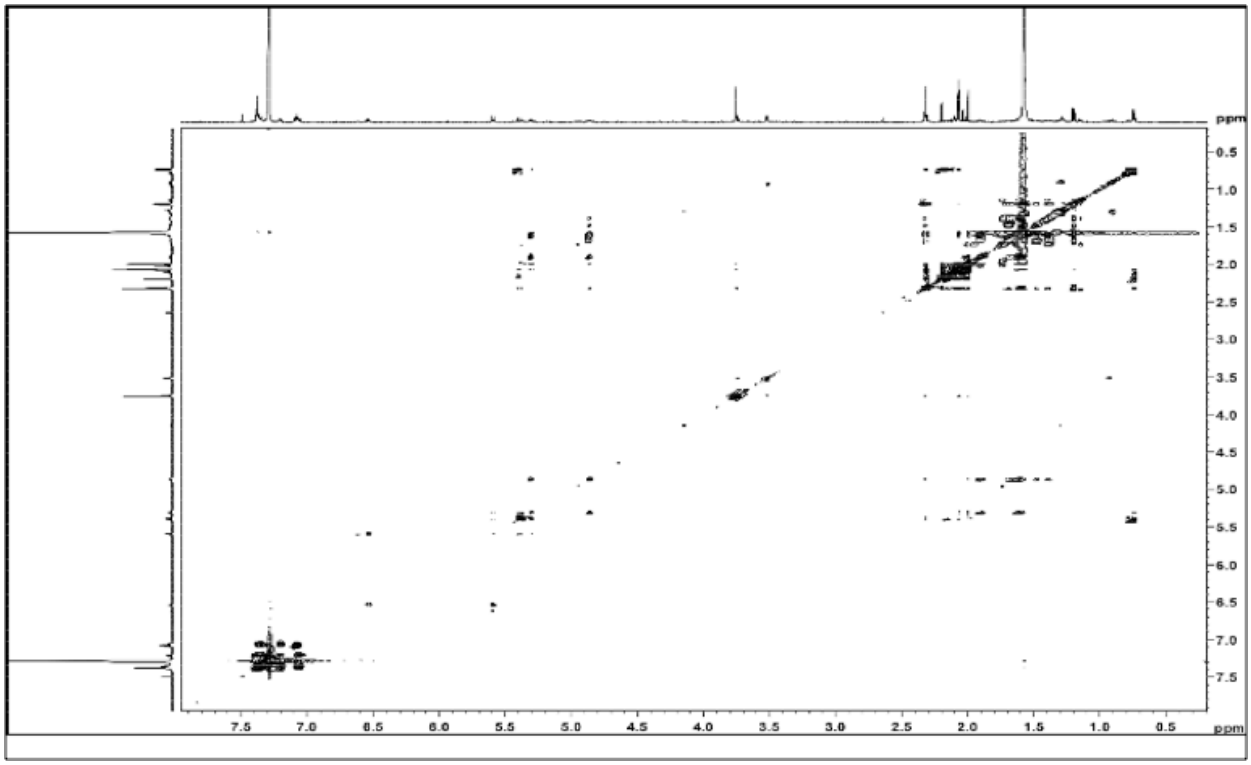

Figure S82. ^{1}H-^{1}H TOCSY spectrum of **14b** (500 MHz, $CDCl_3$)

Table S13. ^{1}H and ^{13}C NMR Data for **14a** and **14b** in $CDCl_3$

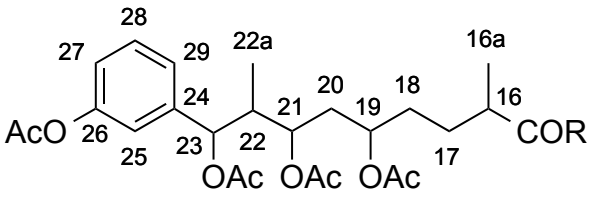

14a : R = (*R*)-PGME , **14b** : R = (*S*)-PGME

	14a		**14b**	
position	δ_c	δ_H mult (*J* in Hz)	δ_c	δ_H mult (*J* in Hz)
1				
2				
2a				
3				
4				
5				
6				
7				
8				
9				
10				
11				
12				
12a				
13				
14				
15				
16	-	2.30 (1H, m)	-	2.28 (1H, m)
16a	-	1.12 (3H, d, 6.8)	-	1.18 (3H, d, 7.0)
17	-	1.37, 1.72 (2H, m)	-	1.37, 1.65 (2H, m)
18	-	1.57 (2H, m)	-	1.47 (2H, m)
19	-	4.95 (1H, m)	-	4.84 (1H, m)
20	-	1.71, 1.93 (2H, m)	-	1.59, 1.88 (2H, m)
21	-	5.34 (1H, m)	-	5.28 (1H, m)
22	-	2.20 (1H, m)	-	2.14 (1H, m)
22a	-	0.76 (3H, d, 7.1)	-	0.72 (3H, d, 7.0)
23	-	5.40 (1H, d, 10.3)	-	5.37 (1H, d, 10.5)
24	-	-	-	-
25	-	-	-	-
26	-	-	-	-
27	-	-	-	-
28	-	-	-	-
29	-	-	-	-

References

1. Feher, M., Schmidt, J.M. Property distributions: differences between drugs, natural products, and molecules from combinatorial chemistry. *J. Chem. Inf. Comput. Sci.* **43**, 218-227 (2003).
2. Hart, C.P. Finding the target after screening the phenotype. *Drug Discov. Today* **10**, 513-519 (2005).
3. Kitagawa, M., Ikeda, S., Tashiro, E., Soga, T., Imoto, M. Metabolomic identification of the target of the filopodia protrusion inhibitor glucopiericidin A. *Chem. Biol.* **17**, 989-998 (2010).
4. Kobayashi, H., Harada, H., Nakamura, M., Futamura, Y., Ito, A., Yoshida, M., Iemura, S., Shin-Ya, K., Doi, T., Takahashi, T., Natsume, T., Imoto, M., Sakakibara, Y. Comprehensive predictions of target proteins based on protein-chemical interaction using virtual screening and experimental verifications. *BMC Chem. Biol.* **12**, 2 (2012).
5. Fleming, A. On the antibacterial action of cultures of a penicillium, with special reference to their use in the isolation of B. influenzae. 1929. *Bull. World Health Organ.* **79**, 780-790 (2001).
6. Waksman, S.A., Reilly, H.C., Johnstone, D.B. Isolation of Streptomycin-producing Strains of Streptomyces griseus. *J. Bacteriol.* **52**, 393-397 (1946).
7. HATA, T., HOSHI, T., KANAMORI, K., MATSUMAE, A., SANO, Y., SHIMA, T., SUGAWARA, R. Mitomycin, a new antibiotic from Streptomyces. I. *J. Antibiot.* **9**, 141-146 (1956).
8. Kino, T., Hatanaka, H., Hashimoto, M., Nishiyama, M., Goto, T., Okuhara, M., Kohsaka, M., Aoki, H., Imanaka, H. FK-506, a novel immunosuppressant isolated from a Streptomyces. I.

Fermentation, isolation, and physico-chemical and biological characteristics. *J. Antibiot*. **40**, 1249-1255 (1987).

9. Koehn, F.E., Carter, G.T. The evolving role of natural products in drug discovery. *Nat. Rev. Drug Discov*. **4**, 206-220 (2005).
10. Newman, D.J., Cragg, G.M. Natural products as sources of new drugs over the 30 years from 1981 to 2010. *J. Nat. Prod*. **75**, 311-335 (2012).
11. Smith, J.A., Wilson, L., Azarenko, O., Zhu, X., Lewis, B.M., Littlefield, B.A., Jordan, M.A. Eribulin binds at microtubule ends to a single site on tubulin to suppress dynamic instability. *Biochemistry* **49**, 1331-1337 (2010).
12. Burg, R.W., Miller, B.M., Baker, E.E., Birnbaum, J., Currie, S.A., Hartman, R., Kong, Y.L., Monaghan, R.L., Olson, G., Putter, I., Tunac, J.B., Wallick, H., Stapley, E.O., Oiwa, R., Omura, S. Avermectins, new family of potent anthelmintic agents: producing organism and fermentation. *Antimicrob Agents Chemother*. **15**, 361-367 (1979).
13. McDaniel, R., Ebert-Khosla, S., Hopwood, D.A., Khosla, C. Engineered biosynthesis of novel polyketides. *Science* **262**, 1546-1550 (1993).
14. Asai, T., Morita, S., Taniguchi, T., Monde, K., Oshima, Y. Epigenetic stimulation of polyketide production in Chaetomium cancroideum by an NAD(+)-dependent HDAC inhibitor. *Org Biomol Chem*. **14**, 646-651 (2016).
15. Amann, R.I., Ludwig, W., Schleifer, K.H. Phylogenetic identification and in situ detection of individual microbial cells without cultivation. *Microbiol. Rev*. **59**, 143-169 (1995).
16. Jemal, A., Siegel, R., Ward, E., Hao, Y., Xu, J., Murray, T., Thun, M.J. Cancer statistics, 2008. *CA Cancer J. Clin*. **58**, 71-96 (2008).
17. 大島 明 他（編）, がん・統計白書 2012, 篠原出版新社 (2012)

18. Heinlein, C.A., Chang, C. Androgen receptor in prostate cancer. *Endocr. Rev.* **25**, 276-308 (2004).

19. Mangelsdorf, D.J., Thummel, C., Beato, M., Herrlich, P., Schütz, G., Umesono, K., Blumberg, B., Kastner, P., Mark, M., Chambon, P., Evans, R.M. The nuclear receptor superfamily: the second decade. *Cell* **83**, 835-839 (1995).

20. Chen, C.D., Welsbie, D.S., Tran, C., Baek, S.H., Chen, R., Vessella, R., Rosenfeld, M.G., Sawyers, C.L. Molecular determinants of resistance to antiandrogen therapy. *Nat. Med.* **10**, 33-39 (2004).

21. Scher, H.I., Sawyers, C.L. Biology of progressive, castration-resistant prostate cancer: directed therapies targeting the androgen-receptor signaling axis. *J. Clin. Oncol.* **23**, 8253-8261 (2005).

22. Murakoshi, M., Ikeda, R., Fukui, N. The effects of chlormadinone acetate (CMA), antiandrogen, on the pituitary, testis, prostate and adrenal gland of the dog with spontaneous benign prostatic hyperplasia. *J. Toxicol. Sci.* **26**, 119-127 (2001).

23. Liao, S., Howell, D.K., Chang, T.M. Action of a nonsteroidal antiandrogen, flutamide, on the receptor binding and nuclear retention of 5 alpha-dihydrotestosterone in rat ventral prostate. *Endocrinology* **94**, 1205-1209 (1974).

24. Goa, K.L., Spencer, C.M. Bicalutamide in advanced prostate cancer. A review. *Drugs Aging*. **12**, 401-422 (1998).

25. Taplin, M.E., Bubley, G.J., Ko, Y.J., Small, E.J., Upton, M., Rajeshkumar, B., Balk, S.P. Selection for androgen receptor mutations in prostate cancers treated with androgen antagonist. *Cancer Res.* **59**, 2511-2515 (1999).

26. Ozers, M.S., Marks, B.D., Gowda, K., Kupcho, K.R., Ervin, K.M., De Rosier, T., Qadir, N., Eliason, H.C., Riddle, S.M., Shekhani, M.S. The androgen receptor T877A mutant recruits

LXXLL and FXXLF peptides differently than wild-type androgen receptor in a time-resolved fluorescence resonance energy transfer assay. *Biochemistry* **46**, 683-695 (2007).

27. Yoshida, T., Kinoshita, H., Segawa, T., Nakamura, E., Inoue, T., Shimizu, Y., Kamoto T., Ogawa, O. Antiandrogen bicalutamide promotes tumor growth in a novel androgen-dependent prostate cancer xenograft model derived from a bicalutamide-treated patient. *Cancer Res*. **65**, 9611-9616 (2005).
28. Tran, C., Ouk, S., Clegg, N.J., Watson, P.A., Arora, V., Wongvipat, J., Smith-Jones, P.M., Yoo, D., Kwon, A., Wasielewska, T., Welsbie, D., Chen, C.D., Higano, C.S., Beer, T.M., Hung, D.T., Scher, H.I., Jung, M.E., Sawyers, C.L. Development of a second-generation antiandrogen for treatment of advanced prostate cancer. *Science* **324**, 787-790 (2009).
29. Korpal, M., Korn, J. M., Gao, X., Rakiec, D. P., Ruddy, D. A., Doshi, S., Yuan, J., Kovats, S. G., Kim, S., Cooke, V. G., Monahan, J. E., Stegmeier, F., Roberts, T. M., Sellers, W. R., Zhou, W., Zhu, P. An F876L mutation in androgen receptor confers genetic and phenotypic resistance to MDV3100 (enzalutamide). *Cancer Discovery* **3**, 1030-1043 (2013).
30. Balbas, M.D., Evans, M.J., Hosfield, D.J., Wongvipat, J., Arora, V.K., Watson, P.A., Chen, Y,, Greene, G.L., Shen, Y., Sawyers, C.L. Overcoming mutation-based resistance to antiandrogens with rational drug design. *Elife* **2**, e00499 (2013).
31. Moilanen, A.M., Riikonen, R., Oksala, R., Ravanti, L., Aho, E., Wohlfahrt, G., Nykänen, P.S., Törmäkangas, O.P., Palvimo, J.J., Kallio, P.J. Discovery of ODM-201, a new-generation androgen receptor inhibitor targeting resistance mechanisms to androgen signaling-directed prostate cancer therapies. *Sci. Rep*. **5**, 12007 (2015).
32. Poutiainen, P.K., Huhtala, T., Jääskeläinen, T., Petsalo, A., Küblbeck, J., Kaikkonen, S., Palvimo, J.J., Raunio, H., Närvänen, A., Peräkylä, M., Juvonen, R.O., Honkakoski, P.,

Laatikainen, R., Pulkkinen, J.T. Preclinical pharmacology of FL442, a novel nonsteroidal androgen receptor modulator. *Mol. Cell Endocrinol*. **387**, 8-18 (2014).

33. Liu, W., Zhou, J., Geng, G., Lin, R., Wu, J.H. Synthesis and in vitro characterization of ionone-based compounds as dual inhibitors of the androgen receptor and NF-κB. *Invest. New Drugs*. **32**, 227-234 (2014).
34. Nagamine, N., Shirakawa, T., Minato, Y., Torii, K., Kobayashi, H., Imoto, M., Sakakibara, Y. Integrating statistical predictions and experimental verifications for enhancing protein-chemical interaction predictions in virtual screening. *PLoS Comput. Biol*. **5**, e 1000397 (2009).
35. Kawamura, T., Fujimaki, T., Hamanaka, N., Torii, K., Kobayashi, H., Takahashi, Y., Igarashi, M., Kinoshita, N., Nishimura, Y., Tashiro, E., Imoto, M. Isolation and structure elucidation of a novel androgen antagonist, arabilin, produced by Streptomyces sp. MK756-CF1. *J. Antibiot*. **63**, 601-605 (2010).
36. Tashiro, E., Imoto, M. Chemical biology of compounds obtained from screening using disease models. *Arch. Pharm. Res*. **38**, 1651-1660 (2015).
37. Fujimaki, T., Saito, S., Imoto, M. Arabilin overcomes resistance to AR-targeted therapy. *J. Antibiot*. Accepted (2016).
38. Kakinuma, K., Hanson, C. A., Rinehart, K. L. Jr. Spectinabilin, a new nitro-containing metabolite isolated from Streptomyces spectabilis. *Tetrahedron* **32**, 217–222 (1976).
39. Ui, H., Shiomi, K., Suzuki, H., Hatano, H., Morimoto, H., Yamaguchi, Y., Masuma, R., Sunazuka, T., Shimamura, H., Sakamoto, K., Kita, K., Miyoshi, H., Tomoda, H., Omura, S. Verticipyrone, a new NADH-fumarate reductase inhibitor, produced by Verticillium sp. FKI-1083. *J. Antibiot*. **59**, 785–790 (2006).

40. Igarashi, Y., Yu, L., Ikeda, M., Oikawa, T., Kitani, S., Nihira, T., Bayanmunkh, B., Panbangred, W. Jomthonic acid , a modified amino acid from a soil-derived Streptomyces. *J. Nat. Prod.* **75**, 986-990 (2012).

41. Bax, Ad., Farley, K. A., Walker, G. S. Increased HMBC Sensitivity for Correlating Poorly Resolved Proton Multiplets to Carbon-13 Using Selective or Semi-selective Pulses. *J. Magn. Reson.* **119**, 134-138 (1996).

42. Kwon, H.C., Kauffman, C.A., Jensen, P.R., Fenical, W. Marinomycins A-D, antitumor-antibiotics of a new structure class from a marine actinomycete of the recently discovered genus "marinispora". *J. Am. Chem. Soc.* **128**, 1622-1632 (2006).

43. Trost, B.M., Belletire, J.L., Godleski, S., McDougal, P.G., Balkovec, J.M., Baldwin, J.J., Christy, M.E., Ponticello, G.S., Varga, S.L., Springer, J.P. On the use of the O-methylmandelate ester for establishment of absolute configuration of secondary alcohols. *J. Org. Chem.* **51**, 2370-2374 (1986).

44. Scott, D.R., Bruce, N.R., Timothy, I.R. Configurational Assignment of Polyene Macrolide Antibiotics Using the [^{13}C]Acetonide Analysis. *Acc. Chem. Res.* **31**, 9-17 (1998).

45. Murata, M., Naoki, H., Matsunaga, S., Satake, M., Yasumoto, T. Structure and Partial Stereochemical Assignments for Maitotoxin, the Most Toxic and Largest Natural Non-Biopolymer. *J. Am. Chem. Soc.* **116**, 7098-7107 (1994).

46. Yu, L., Trujillo, M.E., Miyanaga, S., Saiki, I., Igarashi, Y. Campechic acids A and B: anti-invasive polyether polyketides from a soil-derived Streptomyces. *J. Nat. Prod.* **77**, 976-982 (2014).

47. Yabuuchi, T., Kusumi, T., Phenylglycine methyl ester, a useful tool for absolute configuration determination of various chiral carboxylic acids. *J. Org. Chem.* **65**, 397-404 (2000).

48. Kwon, H.C., Kauffman, C.A., Jensen, P.R., Fenical, W. Marinisporolides, polyene-polyol macrolides from a marine actinomycete of the new genus Marinispora. *J. Org. Chem.* **74**, 675-684 (2009).

49. Mizokami, A., Saiga, H., Matsui, T., Mita, T., Sugita, A. Regulation of androgen receptor by androgen and epidermal growth factor in a human prostatic cancer cell line, LNCaP. *Endocrinol. Jpn.* **39**, 235-243 (1992).

Acknowledgements

本研究は慶應義塾大学理工学部教授 井本正哉博士のご指導の下に行いました。終始親身にご指導ご高配賜りましたことを謹んで感謝の意を表します。

また、本研究を遂行するにあたり、多大なるご指導ご助言をいただきました慶應義塾大学理工学部専任講師 田代悦博士に深く感謝の意を表します。

本論文の執筆にあたり、ご指導ご助言をいただきました慶應義塾大学理工学部教授 佐藤智典博士、慶應義塾大学理工学部教授 末永聖武博士、慶應義塾大学理工学部准教授 犀川陽子博士に厚く御礼申し上げます。

学部 **4** 年生から博士課程 **3** 年生までの **6** 年間を通して、多大なるご指導ご鞭撻賜りました富山県立大学工学部 五十嵐康弘博士に厚く御礼申し上げます。

本研究を行うにあたり、多くのご指導ご激励頂きました慶應義塾大学理工学部ケミカルバイオロジー研究室卒業生 藤巻貴宏博士に心より御礼申し上げます。

Antarlide 類の生産菌である放線菌 **BB47** 株を供与していただきました、**Mahidol** 大学 **Watanalai Panbangred** 博士に深く御礼申し上げます。

Antarlide 類の構造解析を行うにあたり、ご指導ご助言をいただきました微生物化学研究所 澤竜一博士に深く御礼申し上げます。

AR レポータープラスミドを供与していただきました、がん化学療法センター分子生物治療研究部部長 清宮啓之博士に深く御礼申し上げます。

また、様々な場面でサポートしていただきましたケミカルバイオロジー研究室秘書 梅崎秀香さん、神奈川大学理学部研究員 渡部多恵子さんに深く御礼申し上げます。また、博士課程 **3** 年間切磋琢磨し励まし合った同期の井岡秀二君、四方雄貴君、溝谷優治君に厚く御礼申し上げます。また、ケミカルバイオロジー研究室の諸先輩方ならびに同期の皆様、池田拓慧君、今辻紗也佳さん、井上剛志君、加藤航君、濱村祐輝君をはじめ後輩の皆様に感謝致します。

最後に、研究生活を暖かく見守り支えてくれた家族に心より感謝致します。